Expedition 390/393 summary[1]

R.M. Coggon, D.A.H. Teagle, J.B. Sylvan, J. Reece, E.R. Estes, T.J. Williams, G.L. Christeson, M. Aizawa, E. Albers, C. Amadori, T.M. Belgrano, C. Borrelli, J.D. Bridges, E.J. Carter, T. D'Angelo, J. Dinarès-Turell, N. Doi, J.D. Estep, A. Evans, W.P. Gilhooly III, L.J.C. Grant, G.M. Guérin, M. Harris, V.M. Hojnacki, G. Hong, X. Jin, M. Jonnalagadda, M.R. Kaplan, P.D. Kempton, D. Kuwano, J.M. Labonte, A.R. Lam, M. Latas, C.M. Lowery, W. Lu, A. McIntyre, P. Moal-Darrigade, S.F. Pekar, C. Robustelli Test, C.M. Routledge, J.G. Ryan, D. Santiago Ramos, A. Shchepetkina, A.L. Slagle, M. Takada, L. Tamborrino, A. Villa, Y. Wang, S.Y. Wee, S.J. Widlansky, K. Yang, W. Kurz, M. Prakasam, L. Tian, T. Yu, and G. Zhang[2]

Contents

Core descriptions

Supplementary material

References (RIS)

Abstract

The South Atlantic Transect (SAT) is a multidisciplinary scientific ocean drilling experiment designed to investigate the evolution of the ocean crust and overlying sediments across the western flank of the Mid-Atlantic Ridge. This project comprises four International Ocean Discovery Program expeditions: fully staffed Expeditions 390 and 393 (April–August 2022) built on engineering preparations during Expeditions 390C and 395E (October–December 2020 and April–June 2021, respectively) that took place without science parties during the height of the Coronavirus Disease 2019 (COVID-19) pandemic. Through operations along a crustal flow line at ~31°S, the SAT recovered complete sedimentary sections and the upper ~40–340 m of the underlying ocean crust formed at a slow- to intermediate-spreading rate at the Mid-Atlantic Ridge over the past ~61 My. The sediments along this transect were originally spot cored more than 50 y ago during Deep Sea Drilling Project Leg 3 (December 1968–January 1969) to help verify the theories of seafloor spreading and plate tectonics.

The SAT expeditions targeted six primary sites on 7, 15, 31, 49, and 61 Ma ocean crust that fill critical gaps in our sampling of intact in situ ocean crust with regard to crustal age, spreading rate, and sediment thickness. Drilling these sites was required to investigate the history, duration, and intensity of the low-temperature hydrothermal interactions between the aging ocean crust and the evolving South Atlantic Ocean. This knowledge will improve the quantification of past hydrothermal contributions to global biogeochemical cycles and help develop a predictive understanding of the impacts of variable hydrothermal processes and exchanges. Samples from the transect of the previously unexplored sediment- and basalt-hosted deep biosphere beneath the South Atlantic Gyre are essential to refine global biomass estimates and examine microbial ecosystems' responses to variable conditions in a low-energy gyre and aging ocean crust.

The transect, located near World Ocean Circulation Experiment Line A10, provides records of carbonate chemistry and deepwater mass properties across the western South Atlantic through key Cenozoic intervals of elevated atmospheric CO_2 and rapid climate change. Reconstruction of the history of the deep western boundary current and deepwater formation in the Atlantic basins

will yield crucial data to test hypotheses regarding the role of evolving thermohaline circulation patterns in climate change and the effects of tectonic gateways and climate on ocean acidification.

During engineering Expeditions 390C and 395E (5 October–5 December 2020 and 6 April–6 June 2021, respectively), a single hole was cored through the sediment cover and into the uppermost rocks of the ocean crust with the advanced piston corer and extended core barrel systems at five of the six primary proposed SAT sites. Reentry systems with casing were then installed either into basement or within 10 m of basement at each of those five sites.

Expedition 390 (7 April–7 June 2022) conducted operations at three of the SAT sites, recovering 700 m of core (77% recovery) over 30.3 days of on-site operations. Sediment coring, basement coring, and wireline logging were conducted at two sites on ~61 Ma crust (Sites U1556 and U1557), and sediment coring was completed at the 7 Ma Site U1559. During Expedition 390, more than 1.2 km of sediments was characterized, including 793 m of core collected during Expeditions 390C and 395E at Sites U1556, U1557, and U1559 as well as Expedition 395E Site U1561, which was cored on thinly (<50 m) sedimented ~61 Ma crust. The uppermost ~342 and ~120 m of ~61 Ma ocean crust was cored at Sites U1556 and U1557, respectively. Geophysical wireline logging was achieved at both sites, but the basement hole at Site U1556 was not preserved as a legacy hole because of subsidence of the reentry cone below the seafloor. At Site U1557, the drill bit was deposited on the seafloor prior to downhole logging, leaving Hole U1557D available for future deepening and establishing a legacy borehole for basement hydrothermal and microbiological experiments.

Expedition 393 (7 June–7 August 2022) operated at four sites, drilling in 12 holes to complete this initial phase of the SAT. Complete sedimentary sections were collected at Sites U1558, U1583, and U1560 on 49, 31, and 15 Ma crust, respectively, and together with 257.7 m of sediments cored during earlier operations, more than 600 m of sediments was characterized. The uppermost ocean crust was drilled at Sites U1558, U1560, and U1583 with good penetration (~130 to ~204 meters subbasement); however, at the youngest ~7 Ma Site U1559, only ~43 m of basement penetration was achieved in this initial attempt. Geophysical wireline logs were achieved at Sites U1583 and U1560 only. Expeditions 390 and 393 established legacy sites available for future deepening and downhole basement hydrothermal and microbiological experiments at Sites U1557, U1560, and U1559 on 61, 15, and 7 Ma crust, respectively.

Highlights of the SAT expeditions include (1) recovering abundant altered glass, hydrothermal veins, complex breccias, and a wide range of alteration halos in the volcanic sequences of the uppermost ocean crust formed at 7–61 Ma, indicating low-temperature hydrothermal processes and exchanges between seawater and basalts across the western flank of the southern Mid-Atlantic Ridge for millions to tens of millions of years; (2) documenting extended redox gradients from both the seafloor and the sediment/basement interface that indicate significant subsurface fluid flow and may support a diversity of microorganisms and metabolisms; and (3) recovering an almost complete stratigraphic record of the Cenozoic (including the Paleocene/Eocene Thermal Maximum and other key climate events) composed of nannofossil oozes with varying amounts of clay indicating the shoaling and deepening of the calcite compensation depth.

1. Introduction

During the multidisciplinary South Atlantic Transect (SAT) experiment, comprising International Ocean Discovery Program (IODP) Expeditions 390 and 393, supported by preparatory engineering Expeditions 390C and 395E, a transect was drilled along a crustal flow line at ~31°S across the western flank of the southern Mid-Atlantic Ridge. The principal aims of the SAT expeditions are to investigate the hydrothermal evolution of the aging ocean crust, characterize the nature and variation of sediment- and basement-hosted microbial communities with increasing substrate age, and investigate the paleoceanographic evolution of the South Atlantic Ocean, including the responses of the deep ocean and subtropical gyre to changing global climate. The SAT expeditions revisited an area first cored in 1968, when Deep Sea Drilling Project (DSDP) Leg 3 accomplished one of the great achievements of scientific ocean drilling by recovering sediments from a transect

of spot cored holes across the South Atlantic Ocean between ~28° and 30°S (Figure F1). This coring demonstrated that basal sediment age increases with distance from the ridge axis, which provided definitive proof for the theory of seafloor spreading (Scientific Party, 1970). By revisiting the Leg 3 transect region, the SAT expeditions have been designed to take advantage of dramatic advances in drilling technology and analytical capabilities since the earliest days of scientific ocean drilling to address many high priority scientific objectives. Although the great majority of SAT expedition operations were successful, some of our drilling challenges will be familiar to the earliest seafloor explorers aboard the *Glomar Challenger*.

Despite more than 50 y of scientific ocean drilling since Leg 3, major gaps remain in our observations of the evolving Earth system. These gaps include drill cores of ocean crust of different ages formed across a representative range of spreading rates, virtually unexplored biogeographic microbial provinces, and continuous samples of key intervals in Earth's climate history, changing ocean chemistry, or magnetic field. Transects of drill holes that sample both the sediment cover and the uppermost ocean crust in a particular ocean basin can provide essential knowledge of how interconnected processes have evolved over Earth's history and responded to changes in external drivers such as atmospheric CO_2 concentrations, evolving marine life, oceanic gateways, or major ocean currents. Transects that sample tens of millions of years of ocean crust formed at the same mid-ocean ridge (MOR) segment can provide important information about the timing, duration, and intensity of hydrothermal exchange. However, sampling both the sediment and the underlying basaltic basement in a specific ocean region has rarely been undertaken in a systematic manner, and the few transects previously accomplished cover relatively short intervals of recent Earth history (e.g., Juan de Fuca Ridge, 0–3.5 Ma [Shipboard Scientific Party, 1997; Expedition 301 Scientists, 2005; Expedition 327 Scientists, 2011], and Costa Rica Rift, 0–7 Ma [Shipboard Scientific Party, 1983, 1985]).

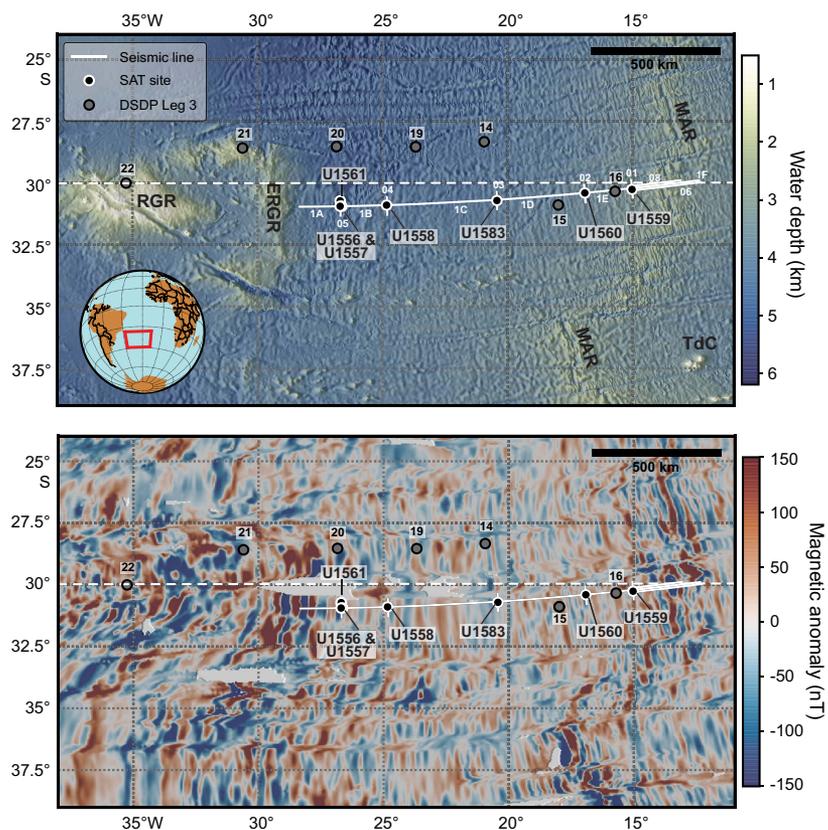**Figure F1.** SAT study region. Top: bathymetry (Ryan et al., 2009) of South Atlantic Ocean. Inset shows regional setting. Bottom: magnetic anomalies (Meyer et al., 2017). Solid lines = CREST seismic reflection profiles (Reece et al., 2016; Reece and Estep, 2019), dashed line = WOCE Line A10. MAR = Mid-Atlantic Ridge, RGR = Rio Grande Rise, ERGR = eastern Rio Grande Rise, TdC = Tristan da Cunha.

Comparison of predicted and observed conductive heat flow through the ocean crust reveals that, on average, a discernible conductive heat flow deficit exists out to 65 Ma in ocean crust formed at the full range of spreading rates (e.g., Von Herzen, 1959; Lister, 1972; Stein and Stein, 1994) (Figure **F2**). This requires that out to this age, there is significant advection by seawater-derived hydrothermal fluids from the cooling of the oceanic lithosphere. However, seafloor heat flow measurements are sparse and show large ranges even within small regions (e.g., Hole 504B region; Langseth et al., 1988; Mottl et al., 1983, 1985; Mottl and Gieskes, 1990; Shipboard Scientific Party, 1993b). Basement hydrologic flow can occur in crust of all ages if sufficient hydrologic heads can be established because crustal age is only one of a suite of interlinked parameters that influence the duration, depth, and intensity of off-axis hydrothermal fluid flow, including basement topography; volcanic stratigraphy and flow morphology; and sediment type, thickness, and completeness of basement blanketing (e.g., Fisher and Harris, 2010). Although simple relationships may not exist between crustal age, fluid flow, crustal properties, thermal and chemical exchange, and biological activity (cf. Kardell et al., 2019, 2021; Christeson et al., 2020), the potential for such relationships has not yet been investigated in a systematic aging transect of tens of millions of years duration.

The SAT drilling project was developed through IODP Proposal 853 (853-Pre, 853-Full1, 853-Full2, and 853-Add), which originated following discussions at two workshops that built on ideas originally developed at the Magma, Melting, Fluids and Life workshop (Southampton, July 2009; **https://usoceandiscovery.org/past-workshops-old/melting-magma-fluids-and-life-workshop-for-scientific-ocean-drilling**) that strongly influenced the IODP Science Plan for 2013–2023 for ocean drilling "Illuminating Earth's Past, Present, and Future" (**https://usoceandiscovery.org/wp-content/uploads/2016/05/Workshop_MMFL_Report.pdf**). To prioritize the 14 challenges in the 2013–2023 Science Plan and identify new approaches for more efficient planning of drilling expeditions, United States scientists met at the Building U.S. Strategies for 2013–2023 Scientific Ocean Drilling workshop (Denver, Colorado; April 2012). This workshop identified and adapted a
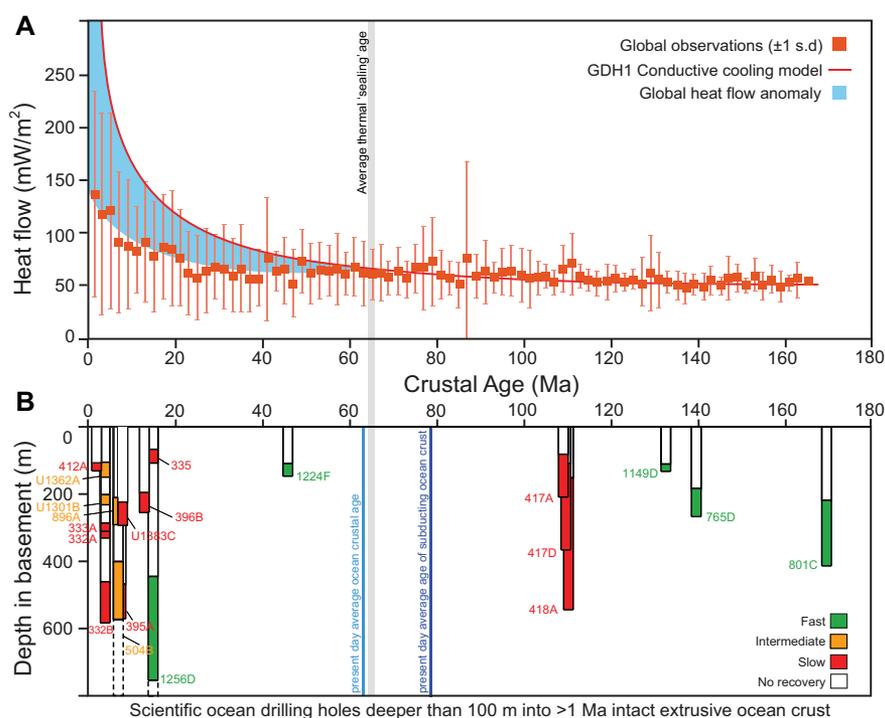
Figure F2. A. Observed and predicted conductive heat flow. Discrepancy between observed and predicted heat flow (blue area) indicates hydrothermal circulation persists across ridge flanks for ~65 My on average (modified from Stein and Stein, 1994). B. Compilation of all scientific ocean drilling holes prior to SAT that penetrate >100 m into intact upper (basaltic) ocean crust vs. crustal age, excluding holes drilled in seamounts, oceanic plateaus, back-arc basement, hydrothermal mounds, or passive continental margins (after Michibayashi et al., 2019). Colors show crustal spreading rate, and colored proportion of cored interval indicates average core recovery. Dashed lines = two holes that penetrated through entire upper ocean crust into underlying sheeted dikes.

key strategy described in Science Plan Challenge 10 to drill crustal age transects that provide opportunities to combine diverse scientific objectives (**http://usoceandiscovery.org/wp-content/uploads/2016/05/Workshop_BuildingUSStrategies_Report.pdf**). This concept was further developed during the Transect Drilling During Transits workshop (College Station, Texas [USA]; November 2013), which was convened to explore opportunities for multidisciplinary drilling transects exploiting likely drill ship transits to maximize the scientific output in relation to cost and time (**http://usoceandiscovery.org/wp-content/uploads/2016/05/Workshop_TransectDrilling_Report.pdf**). At this workshop, the South Atlantic was identified as a region where multiple Science Plan challenges could be addressed by drilling an age transect of sediment–basement holes. Consequently, the SAT expeditions were designed to recover complete sediment sections and the uppermost ~250 m of basaltic ocean crust produced between ~7 and 61 Ma at the slow- to intermediate-spreading Mid-Atlantic Ridge, returning to the Leg 3 transect region to achieve the following objectives:

- Quantify the timing, duration, and extent of ridge flank hydrothermal fluid-rock exchange;
- Investigate sediment- and basement-hosted microbial community variation with substrate composition and age; and
- Investigate the responses of Atlantic Ocean circulation patterns and the Earth's climate system to rapid climate change, including elevated atmospheric CO_2 during the Cenozoic.

The initial target depth of the SAT expeditions of 250 m of ocean crust penetration is not sufficient to constrain the full depth extent of low-temperature hydrothermal seawater-basalt exchange (e.g., Shipboard Scientists, 2003b; Alt, 2004), but deeper coring will require longer operational time. Consequently, basement drilling at the SAT sites was planned to establish scientific ocean drilling legacy holes with reentry cones and deep casing into or near to the oceanic volcanic rocks.

Expeditions 390 and 393 were delayed because of the Coronavirus Disease 2019 (COVID-19) pandemic. However, engineering and sediment coring operations during Expeditions 390C and 395E (Estes et al., 2021; Williams et al., 2021), which sailed without science parties, cored initial sediment sections and installed reentry cones and casing systems at five of the six proposed sites to maximize science operations during fully staffed Expeditions 390 and 393. The SAT expeditions targeted six primary sites on 7, 15, 31, 49, and 61 Ma ocean crust (Figure **F1**) to fill critical gaps in our sampling of intact in situ ocean crust with regards to crustal age, spreading rate, and sediment thickness (Figures **F2**, **F3**; Table **T1**).

These sections of upper ocean crust will enable us to quantify the magnitude and duration of low-temperature chemical exchange with the overlying oceans; investigate the impact of changing
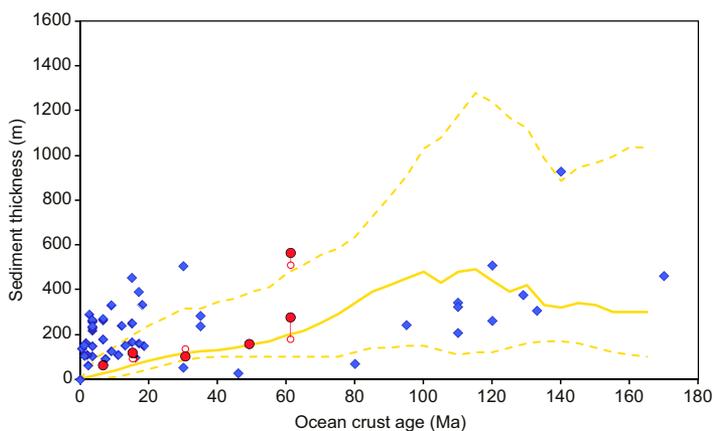
Figure F3. Sediment cover vs. crustal age, Expedition 390 and 393 sites. Solid circles = observed sediment thickness; open circles = expected sediment thickness; diamonds = sediment thicknesses at all scientific ocean drilling holes that cored >100 m into basement in intact ocean crust and tectonically exposed lower crust/upper mantle; solid line = global average sediment thickness vs. age (25 My moving average of median sediment thickness of 5 Ma binned global compilation of sediment thickness vs. lithospheric age of Spinelli et al. [2004]); dashed lines = 25 My moving average of 25th and 75th percentiles of 5 Ma binned data.

Table T1. Summary of SAT site operations achieved during Expeditions 390C, 395E, 390, and 393. **Download table in CSV format.**

Site	Proposed site	Proposed primary/ alternate site	Expedition	Hole	Latitude	Longitude	Water depth (m)	Age (Ma)	Half spreading rate (mm/y)
U1559	SATL-13A	Primary	390C, 390, 393	U1559B	30°15.6336′S	15°02.0941′W	3055	6.6	17.0
U1560	SATL-25A	Primary	395E, 393	U1560B	30°24.2057′S	16°55.3702′W	3723	15.2	25.5
U1583	SATL-33B	Primary	393	U1583F	30°42.6175′S	20°26.0336′W	4210	30.6	24.0
U1558	SATL-43A	Primary	390C, 393	U1558D	30°53.7814′S	24°50.4822′W	4334	49.2	19.5
U1556	SATL-53B	Primary	390C, 395E, 390	U1556B	30°56.5244′S	26°41.9472′W	5002	61.2	13.5
U1557	SATL-56A	Alternate	390C, 395E, 390	U1557D	30°56.4651′S	26°37.7892′W	5011	60.7	13.5
U1561	SATL-55A	Alternate	395E	U1561A	30°43.2902′S	26°41.7162′W	4910	61.2	13.5

				APC/XCB-cored hole			
Site	Proposed site	Hole	Expedition	Site survey predicted sediment thickness (m)	Observed sediment thickness (m)	Actual average sediment accumulation rate (m/My)	Total penetration (m)
U1559	SATL-13A	U1559A	390C	50	64.0	9.70	66.2
U1560	SATL-25A	U1560A	395E	104	120.2	7.91	122.5
U1583	SATL-33B	U1583C	393	138	106.0	3.46	107.5
U1558	SATL-43A	U1558A	390C	148	158.9	3.23	163.9
U1556	SATL-53B	U1556A	390C	180	278.0	4.54	283.8
U1557	SATL-56A	U1557B	390C	510	564.0	9.29	574.0
U1561	SATL-55A	U1561A	395E	126	46.0	0.75	49.0

		Installed reentry system			RCB-cored hole							
Site	Proposed site	Hole	Expedition	Casing shoe depth (mbsf)	Hole	Expedition	Top cored interval (mbsf)	Bottom cored interval (mbsf)	Cored interval thickness (m)	Recovered length (m)	Average recovery (%)	Sediment/basement interface depth (mbsf)	Basement penetration (m)
U1559	SATL-13A	U1559B	390C	55.3	U1559B	393	58.9	107.9	42.9	12.8	26	65.0	42.9
U1560	SATL-25A	U1560B	395E	122.0	U1560B	393	124.0	314.0	190.0	74.8	39	123.0	190.0
U1583	SATL-33B	U1583F	393	Free-fall funnel	U1583F	393	101.0	239.5	138.5	45.7	33	109.7	129.8
U1558	SATL-43A	U1558D	390C	146.1	U1558D	393	150.0	370.3	220.3	100.8	46	166.8	203.5
U1556	SATL-53B	U1556B	390C	284.2	U1556B	390	291.0	633.2	342.2	191.87	56	291.3	341.9
U1557	SATL-56A	U1557D	390C/395E	571.6	U1557D	390	575.6	684.7	109.1	71.28	65	564.8	119.9
U1561	SATL-55A												

ocean conditions on hydrothermal exchange; determine the critical thermal, hydrogeologic, chemical, and microbial transitions across the ridge flank; and evaluate hydrothermal contributions to global biogeochemical cycles. Coring during Expeditions 390 and 393 also sampled the sedimentary and upper crustal deep biosphere along the transect, allowing exploration of the microbial ecosystems' responses to variations in habitat conditions in a low-energy gyre and aging ocean crust. Sediments recovered during the SAT expeditions include Cenozoic stratigraphic sections required to investigate the Earth system's past responses to high atmospheric CO_2 and temperatures and better predict the impacts of projected future anthropogenic increases in atmospheric CO_2. The transect also provides a paleoceanographic record near World Ocean Circulation Experiment (WOCE) Line A10, enabling reconstruction of the history of the deep western boundary current and the sources of deepwater formation in the Atlantic basins.

2. Background

2.1. Opening of the South Atlantic Ocean and the regional geology of the South Atlantic Transect

The SAT expeditions operated in the Leg 3 transect region at ~31°S in the South Atlantic Ocean (Figure **F1**). To provide additional context for the SAT, here we summarize the major events forming the ocean basin between South America and Africa, including a description of the morphology and hydrothermal activity of the modern southern Mid-Atlantic Ridge crest at ~31°S.

Despite the importance of the South Atlantic Ocean in the development of concepts of continental drift, seafloor spreading, paleobathymetry and ocean circulation (e.g., Wegener, 1912; Bullard et al., 1965; Sclater and McKenzie, 1973; Pérez-Díaz and Eagles, 2017b; Müller et al., 1997, 2008a), the magnetic timescale (e.g., Cande et al., 1988), and ocean plateau and hot spot volcanism (e.g., Weaver et al., 1987; O'Connor and Duncan, 1990), many aspects of the geology of this region, especially the spreading ridge–formed ocean crust, remains relatively unexplored (Batiza et al., 1989; Michael et al., 1994; Zhang et al., 2020). There remains only partial coverage of the southern Mid-Atlantic Ridge axis with modern high-resolution bathymetry, and mapping of the western flank of the Mid-Atlantic Ridge is restricted to a narrow band of the Crustal Reflectivity Experiment Southern Transect (CREST) geophysical survey (Reece et al., 2016; Reece and Estep, 2019). Few scientific ocean drilling holes have penetrated more than a meter or so into rocks formed by ocean spreading, although other types of volcanic rocks have been recovered by drilling and dredging from targets related to hot spot trails (Homrighausen et al., 2019, 2020) including the Walvis Ridge (e.g., Sager et al., 2021; IODP Expedition 391) and the Rio Grande Rise to the west of the SAT (Hoyer et al., 2022). To date, the 2013 SoMARTherm survey (Devey, 2014) of the modern southern Mid-Atlantic Ridge during Cruise MSM25 of the research vessel (R/V) *Maria S. Merian* in 2013 remains the most detailed investigation of the southern Mid-Atlantic Ridge from 25° to 33°S and related hydrothermal activity.

2.1.1. Opening of the South Atlantic Ocean

Opening of the Southern Atlantic Ocean was initiated from the south with the beginning of seafloor spreading and separation (~138 Ma) of the Falklands Plateau and North Georgia Rise from southern Africa along the Falklands-Agulhas Fracture Zone leading to the formation of early deep basins that evolved to become the modern Argentine and Cape Basins (Torsvik et al., 2009; Pérez-Díaz and Eagles, 2017b). Continental rifting at midlatitudes (~25–40°S) was initiated about 142 Ma (Torsvik et al., 2009) coinciding with subaerial Parana-Etendeka magmatism. The oldest marine magnetic anomalies are ~125 Ma at these midlatitudes (Pérez-Díaz and Eagles, 2017b), and by 110–100 Ma seafloor spreading had propagated north toward the Gulf of Guinea. This spreading developed mostly shallow (<500 m) basins with high-salinity waters and strong evaporation leading to the deposition of evaporites. By 100 Ma, regions of the Rio Grande Rise and Walvis Ridge deepened to >1500 m in places and probably allowed a shallow water connection with the nascent tropical South Atlantic Ocean (Pérez-Díaz and Eagles, 2017b). A deepwater connection to the Southern Ocean was established by 100 Ma. Although an incipient equatorial gateway developed by ~100 Ma, this region probably existed as a series of disconnected pull apart basins separated by structural highs until the start of Campanian (~84 Ma; Pérez-Díaz and Eagles, 2017b).

From ~120 to 80 Ma, the Rio Grande Rise and Walvis Ridge formed above the Tristan-Gough mantle plume principally while it was below or close to the southern Mid-Atlantic Ridge (Homrighausen et al., 2019; Western Rio Grande Rise ~87–80 Ma; Hoyer et al., 2022). From 80 to 60 Ma, seafloor spreading and several major ridge jumps separated the Western Rio Grande Rise and the Walvis Ridge (O'Connor and Duncan, 1990). The approximately north-south–trending tholeiitic Eastern Rio Grande Rise and corresponding counterparts on the African plate were formed by plume interactions with the Mid-Atlantic Ridge between 83 and 70 Ma (O'Connor and Duncan, 1990; Hoyer et al., 2022). Subsequently, normal spreading resumed directly to the east of the Eastern Rio Grande Rise between 30° and 34°S (O'Connor and Duncan, 1990). Minor alkali volcanism (51–46 Ma) on the South American plate around and proximal to the Rio Grande Rise resulted from lithospheric rifting (Hoyer et al., 2022). By this time, the Tristan-Gough Plume was located below the African plate, and more recent magmatic events related to this system occur on that plate (Homrighausen et al., 2019, 2020). The initial magmatism from the prebreakup Parana-Etendeka large igneous provinces to the substantial foundations of the Rio Grande Rise and Walvis Ridge have enriched mantle (EM1) affinities, and the endurance of this magmatism is indicative of a deep mantle plume source related to the Tristan-Gough Hotspot (Homrighausen et al., 2019, 2020; Hoyer et al., 2022). Deep ambient mantle and High U/Pb ratio (HIMU) components contribute to younger features on the Walvis Ridge and other southeastern Atlantic seamount chains (e.g., Discovery and Richardson seamounts; Homrighausen et al., 2019, 2020).

From the early Campanian (80 Ma), full intermediate water connections between major ocean basins in the South Atlantic have existed. However, subsidence of the Rio Grande Rise and Walvis Ridge was only sufficient to allow deepwater circulation from between the Campanian (80 Ma) to mid-Paleocene (~60 Ma) times, with the latter time most consistent with recent paleobathymetry studies (e.g., Pérez-Díaz and Eagles, 2017b, and references therein). Throughout the Tertiary the South Atlantic has continued to widen and deepen with concurrent subsidence of major igneous bathymetric barriers such as the Rio Grande Rise and Walvis Ridge with retention of some compartmentalization of the major South Atlantic Ocean basins until after 40 Ma and only limited deepwater connections such as the Vema Gap between the eastern Rio Grande Rise and the South American continental margin.

The formation of the Drake Passage (33–30 Ma) and Tasmanian Gateway (e.g., Lawver and Gahagan, 2003) at a similar time led to the establishment of the Antarctic Circumpolar Current and eventually Antarctic Bottom Water (AABW), with many of the features of modern Atlantic circulation in place by the mid-Miocene (Pérez-Díaz and Eagles, 2017b, and references therein).

2.1.2. Modern southern Mid-Atlantic Ridge at ~30°S

To date, the 2013 SoMARTherm survey (Devey, 2014) remains the only comprehensive survey of the midlatitudes of the southern Mid-Atlantic Ridge. A total of 16 ridge segments were identified along the southern Mid-Atlantic Ridge between ~13°S and 33°30′S, and 15 were completely surveyed with a variety of techniques, including high-resolution bathymetry. These north-northwest (318° to 328°)–trending segments vary between 55 and 220 km in length (average = 118 km) and most, although not all, present well-defined axial valleys typical of classic slow-spreading ridges between 4 and 25 km wide. Many segments have substantial volcanic edifices indicating the loci of the most recent igneous activity. Transform offsets between segments, both dextral and sinistral, offset the axial valleys by 9 to 220 km, but most typically ~60 km.

The present-day Mid-Atlantic Ridge axis at 30°–32°S, Segment 3 of Devey (2014), is a ~100 km long well-defined 323°-trending axial valley, 5–7 km across, bounded by inward-facing faults with up to 250 m normal displacement (Devey, 2014). This segment is bounded by a minor (~16 km) sinistral offset to the south and a 22 km dextral offset to the north (Christeson et al., 2020). High-resolution bathymetric coverage on this segment is not comprehensive except between 29°50′ and 30°10′S where the ridge was crossed by the CREST seismic experiment during the SAT site survey (Reece et al., 2016; Reece and Estep, 2019; Kardell et al., 2019; Estep et al., 2021; Christeson et al., 2020). The segment deepens to the north to ~3800 meters below sea level (mbsl) where the axial valley meets the eastward-stepping transform fault. Toward the middle of the segment is a central ~45 km long, north-south–trending axial high that rises to 2800 mbsl. The moderately dipping, faulted western flank of the axial high contrasts with the more gently dipping but hummocky surface of its eastern flank, which has been interpreted to be a faulted axial volcanic ridge (Devey, 2014). South of the central axial high there are a large number of flat-topped seamounts.

An estimated half-spreading rate of ~16 mm/y (Kardell et al., 2019) suggests that rocks formed in the ridge spend ~500 ky in the axial valley before being uplifted by the bounding normal faults and subsiding on the ridge flanks. Outside the present-day axial valley, a well-developed subparallel ridge-basin seafloor texture is established, regularly dotted with small seamounts. This texture is more strongly developed on the western flank than on the eastern flank. Sediment-filled basins, 2 to 4 km across, developed within 100 km of the ridge axis on both flanks (Figure **F4**).

There are relatively few hydrothermal vents identified along the whole southern Mid-Atlantic Ridge, and there has been little detailed investigation of hydrothermal systems south of 14°S (Beaulieu et al., 2015). Two active hydrothermal vents have been inferred from seawater anomalies between 29° and 32°S; however, water column indicators have not been confirmed, and the sources of these anomalies remain unknown (Schmid et al., 2019). Neither of these potential hydrothermal sites are in the zero-age segment of the SAT (Segment 3 of Devey, 2014).

Crustal accretion along the northern Mid-Atlantic Ridge is complex in places, and there are significant regions where spreading is accommodated by amagmatic extension by detachment faults that exhume sections of deep lithosphere to form oceanic core complexes (OCCs; Mallows and

Searle, 2012) with a characteristic domal structure. However, the 2013 SoMARTherm survey (Devey, 2014) found no OCCs between 25° and 33°S. This finding, combined with the relatively well defined marine magnetic anomalies on the southern Mid-Atlantic Ridge flanks (Meyer et al., 2017; Perez-Diaz and Eagles, 2017a), is consistent with accretion of intact magmatic crust. Because the ~31°S SAT follows a crustal flow line through a relatively long spreading segment away from major transform faults, a Penrose-type stratigraphy of lavas overlying dikes and gabbros is predicted (Penrose Conference Participants, 1972) to have been accreted along the transect.

2.1.3. Pioneering drilling of the southern Mid-Atlantic Ridge flanks during DSDP Leg 3

The transformative efforts of Leg 3 proved the value of scientific ocean drilling and established a legacy for Earth sciences that continues more than five decades later (e.g., 2050 Science Framework; Koppers and Coggon, 2020). During Leg 3, ten sites were drilled in the equatorial and South Atlantic Ocean between Senegal and Brazil (The Shipboard Scientific Party, 1970), including seven sites along a transect across the southern Mid-Atlantic Ridge that penetrated basement volcanic rocks (Sites 14–20; Figure F1). The basal sediment ages are within a few million years of the inferred magnetic anomaly ages, which are consistent with a half-spreading rate of ~20 mm/y since 76 Ma. Recovery in the cored intervals was typically high (>98%), but the sediments were only spot cored, and there are significant gaps between cored intervals (The Shipboard Scientific Party, 1970). The cores recovered along the Leg 3 transect make up an almost continuous Lower Cretaceous to Pleistocene composite stratigraphic section (The Shipboard Scientific Party, 1970). All sites yielded calcareous sediments with calcareous nannoplankton and planktic foraminifera. Basalts (0.05–2 m penetration) were recovered from each site, and they comprise variably altered extrusive rocks with common glass and some calcium carbonate veins.
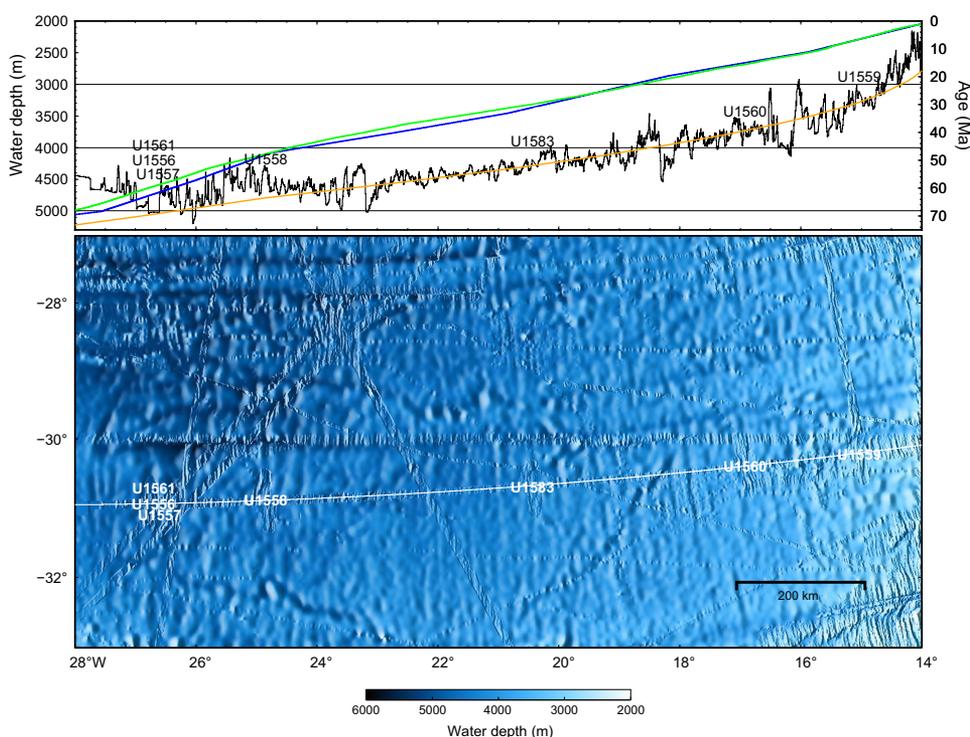
Figure F4. Bathymetry of western flank of southern Mid-Atlantic Ridge. Top: exaggerated bathymetric profile (black line; left scale) along SAT superimposed on depth predicted from simple plate cooling model (orange line; Marty and Cazenave, 1899) assuming ridge crest is ~2500 m depth and adjusting age to latitude. Other cooling models (e.g., Korenaga and Korenaga, 2008) yield similar curves, although classic Parsons and Sclater (1977) predicts deeper oceans with age. Green line = age model (right scale) for South Atlantic of Pérez-Díaz and Eagles (2017a), blue line = age model for South Atlantic of Seton et al. (2020). Bottom: SAT drill sites superimposed on regional and limited high-resolution bathymetry (Ryan et al., 2009) including west–east track of CREST site survey cruise (Reece et al., 2016).

2.2. Geologic setting of the South Atlantic Transect

The SAT expeditions occupied a transect of new sites in the Leg 3 region selected to (1) target basement formed along the same crustal flow line at similar spreading rates (~13–25 mm/y half rate; Table T1) and (2) recover sections of slow-spreading crust of comparable ages to the ocean crust reference sections in DSDP Hole 504B on the Costa Rica Rift (7 Ma; Shipboard Scientific Party, 1993a) and Ocean Drilling Program (ODP) Hole 1256D on the Cocos plate (15 Ma; Shipboard Scientific Party, 2003b; Expedition 309/312 Scientists, 2006; Expedition 335 Scientists, 2012), which are located in intermediate- and superfast-spreading crust, respectively. The site locations were chosen to optimize the recovery of material required to achieve our multidisciplinary objectives. Thick sediment cover is typically targeted by scientific ocean drilling to maximize the resolution of paleoceanographic records. Thick sediment sequences are also often required to install the seafloor infrastructure required for deep subseafloor drilling. This has led to a bias in DSDP/ODP/Integrated Ocean Drilling Program/IODP sampling of in situ upper ocean crust (for depths >100 m into basement) toward regions with anomalously thick sediment (Figure F3). Rapid deposition of sediment in such areas soon after the crust is formed seals the volcanic rocks of the ocean crust from bottom seawater, resulting in anomalously hot basement temperatures, and may result in premature cessation of hydrothermal circulation. Consequently, the SAT sites target locations where the sediment cover is close to the global average for their crustal ages (Spinelli et al., 2004; Olson et al., 2016; Straume et al., 2019) (Figure F3), even though this decision reduces the resolution of the paleoceanographic records. However, because seafloor roughness is greater in slow-spreading ocean basins than in fast-spreading basins (Spinelli et al., 2004; Kardell et al., 2019; Christeson et al., 2020), there are significant variations in sediment thickness and the continuity of sediment blanketing along the SAT. Indeed, the concept of an average sediment thickness is perhaps not useful in regions where significant proportions of the crust have little or no sediment. Volcanic rocks crop out at all ages along the transect (Estep et al., 2019), and these topographic variations (Figure F4) likely impact the crustal hydrogeology, and hence the conductive heat flow (Figure F5). Consequently, Expedition 390 occupied two sites on 61 Ma crust to investigate the variability in duration and extent of hydrothermal alteration due to basement topography at a given crustal age: Site U1556, which is blanketed by 278 m of sediment, and Site
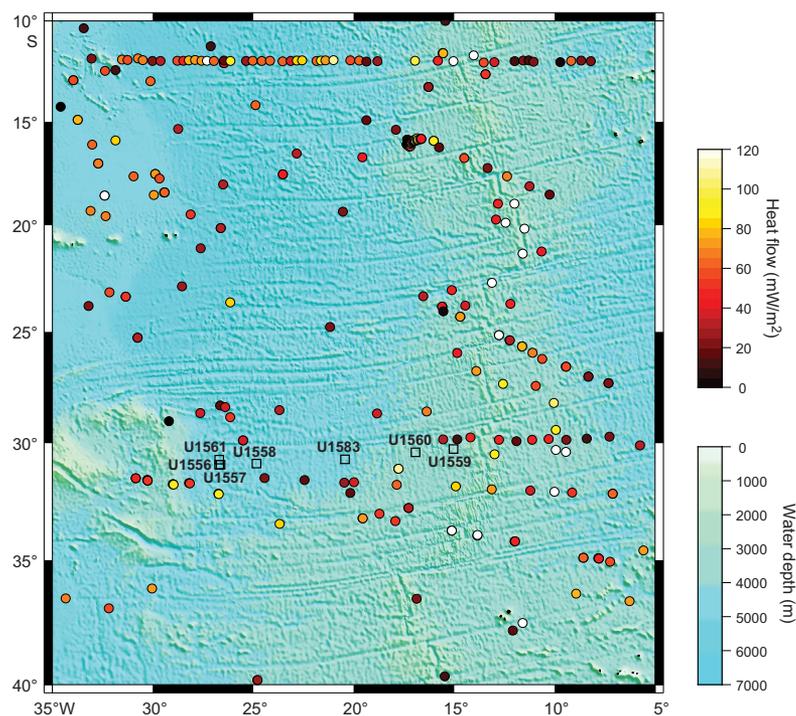
Figure F5. Map of South Atlantic Ocean showing conductive heat flow measurements in vicinity of SAT drill sites. Heat flow data from Fuchs et al. (2021). ETOPO1 bathymetry data from Amante and Eakins (2009).

U1557 in a more thickly sedimented (564 m) portion of the same local sediment basin (Figure **F6B**). Site U1557 also provides a higher resolution paleoceanographic record at this oldest crustal age. An additional short hole was drilled on 61 Ma crust (Site U1561) during Expedition 395E. The sediment sections cored at the 61 Ma sites cover key Paleogene hyperthermals, including the
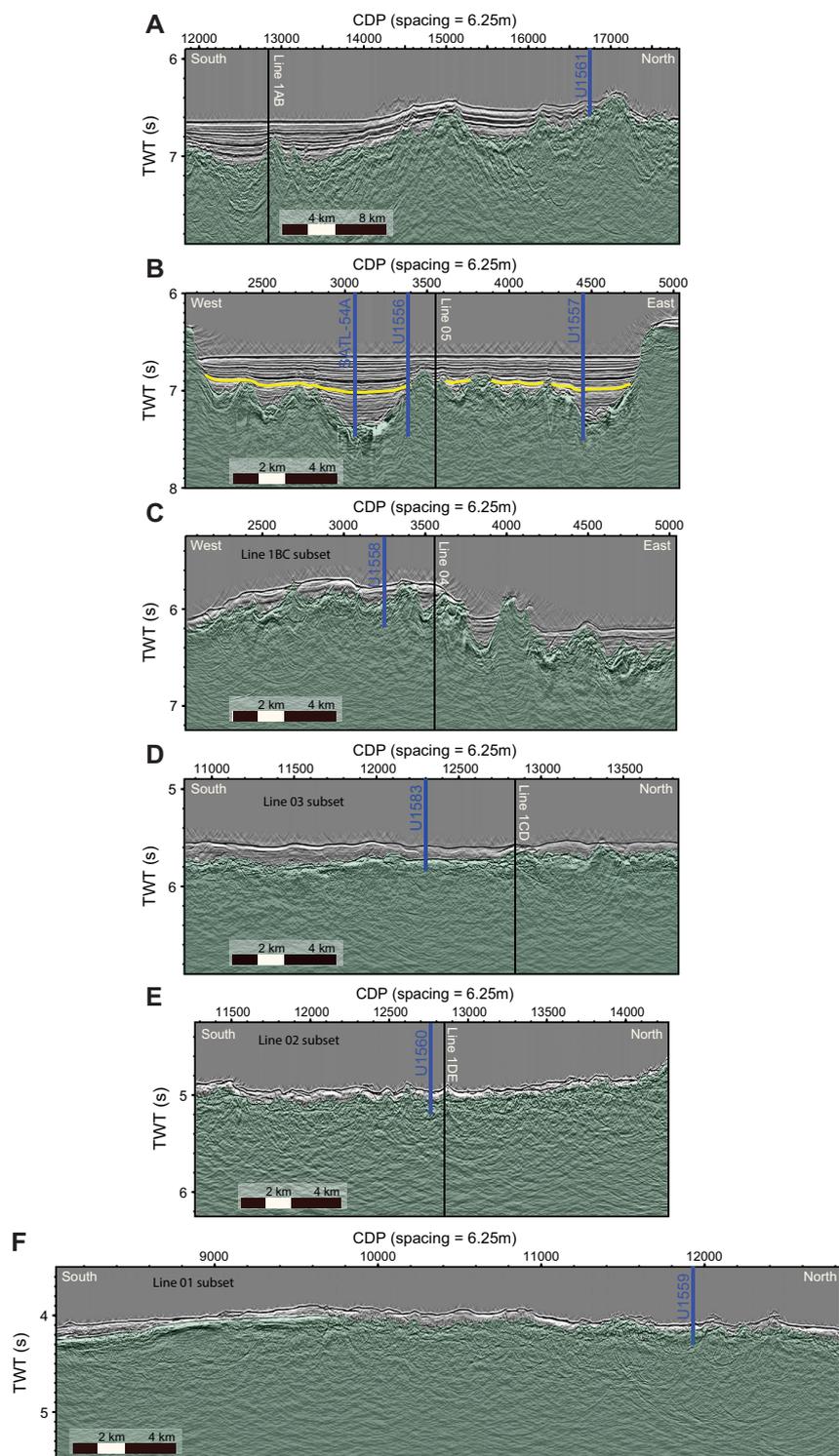
Figure F6. Seismic reflection profiles for SAT sites occupied during Expeditions 390C, 395E, 390, and 393. Site U1557 was relocated from proposed Site SATL-54A, given thicker than expected sediment cover at Site U1556 and consequent reinterpretation of seismic data for this area, to ensure casing could be installed to basement at Site U1557 without exceeding maximum deployable casing string length of ~600 m in that water depth (~5 km).

Paleocene/Eocene Thermal Maximum (PETM). The underlying basement records the cumulative hydrothermal alteration of the uppermost crust across the entire SAT.

Following Expedition 390 operations, Expedition 393 was then freed to target the younger sites that form the age transect across the western flank of the Mid-Atlantic Ridge. The 7 Ma site (U1559) provides the young end-member for investigating the evolution of hydrothermal and microbiological systems with crustal age and allows comparison with similar aged intermediate-spreading rate crust from Hole 504B (Shipboard Scientific Party, 1993a). The 31 Ma (Site U1583) and 49 Ma (Site U1558) sites fill critical gaps in our ocean crust and deep biosphere sampling with respect to basement age and major changes in ocean chemistry (Coggon et al., 2010). The 15 Ma site (U1560) was chosen for comparison to superfast-spreading rate crust from Hole 1256D (Shipboard Scientific Party, 2003b; Expedition 309/312 Scientists, 2006; Expedition 335 Scientists, 2012).

2.3. Seismic studies and site survey data

The SAT is located along a crustal flow line at ~31°S where fracture zones are far apart and magnetic lineations are clear (Figure F1). The CREST cruise aboard the R/V *Marcus G. Langseth* conducted a detailed geophysical survey across the western Mid-Atlantic Ridge flank along this crustal flow line (Reece et al., 2016). The CREST survey included a 1500 km multichannel seismic reflection profile from the ridge crest to the Rio Grande Rise spanning 0–70 Ma crust, two shorter ridge-crossing profiles spanning 0–7 Ma crust, and five ridge-parallel profiles at 6.6, 15, 31, 49, and 61 Ma. Ocean-bottom seismometer profiles were acquired coincident with the ridge-parallel profiles. Gravity, magnetics, multibeam bathymetry, and backscatter data were also acquired.

Kardell et al. (2019) calculated ages and spreading rates from magnetic data acquired during the CREST cruise (Figure F7). Ages of the six primary SAT sites are estimated at 6.6, 15.2, 30.6, 49.2, 60.7, and 61.2 Ma with half-spreading rates of 17.0, 25.5, 24.0, 19.5, 13.5, and 13.5 mm/y, respectively (Table T1). If a half-spreading rate of 20 mm/y is used to define the transition between slow- and intermediate-spreading rates (Perfit and Chadwick, 1998), then the SAT sites formed at slow- to intermediate-spreading rates.

Seismic imaging along the CREST transect shows an abundance of unsedimented or thinly sedimented, exposed basement outcrops that may allow the ingress and egress of seawater and ridge flank hydrothermal fluids at all crustal ages from 0 to 65 Ma. This suggests that the crust is never fully sealed by sediment at these ages (Estep et al., 2019) and that there may be long-lived and ongoing connection between the oceans and uppermost basaltic crust with implications for biogeochemical exchanges and subsurface microbial activity. This is in strong contrast to recent hydrogeologic and hydrothermal alteration research in the Pacific that has focused on regions and sites with thick continuous sediment blankets and few outcrops of volcanic rocks (e.g., Juan de Fuca Ridge [Hutnak et al., 2006; Fisher and Harris, 2010] and eastern equatorial Pacific [Langseth et al., 1983, 1988; Mottl, 1989; Mottl et al., 1983; Hutnak et al., 2008]).
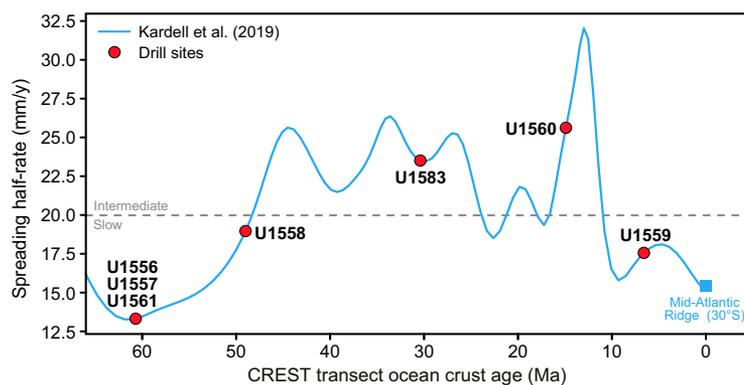

Figure F7. Ages and spreading rates along CREST transect. Blue line = cubic interpolation of rates calculated from table S3 in Kardell et al. (2019), red circles = estimated values at SAT drill sites.

Seismic Layer 2A exhibits relatively slow seismic velocities but a steep gradient of increasing velocities with depth (e.g., Houtz and Ewing, 1976) and is generally interpreted to correspond to the porous and permeable uppermost igneous portion of the ocean crust. In the SAT region, based on seismic velocities, Layer 2A is imaged in crust from the Mid-Atlantic Ridge crest out to 48 Ma crust but is not present in older crust toward the Rio Grande Rise (Estep et al., 2019). Along the CREST SAT survey line, velocities at the top of basement increase rapidly from 2.4 km/s at 0 Ma to 4.2 km/s at 6 Ma and then continue to increase gradually to 4.9 km/s at 58 Ma (Kardell et al., 2019). The presence of unsedimented basement outcrops, persistent imaging of Layer 2A, and continued velocity increase at the top of basement are consistent with fluid circulation within the upper crust that continues to at least 48–58 Ma (Estep et al., 2019; Kardell et al., 2019, 2021). The seismic transect ends just east of the eastern margin of the Rio Grande Rise, which may have affected the thermal history of the lithosphere and the structure of the crust at the western end of SAT.

The SAT sites were all positioned in localized sedimentary basins imaged on the seismic reflection profiles with unsedimented basement ridges within 1–2 km of most sites (Figure **F6**). Actual sediment thicknesses at the SAT sites increased with crustal age from 57 m at ~7 Ma Site U1559 to 278 and 565 m at ~61 Ma Sites U1556 and U1557, respectively. However, Site U1561, which is also located on 61 Ma crust, is close to an exposed ridge and consequently encountered only 46 m of sediment before reaching the ocean crust.

3. Scientific objectives

3.1. Objective 1 (primary): quantify the timing, duration, and extent of ridge flank hydrothermal fluid-rock exchange.

Hydrothermal circulation at MORs and across their vast ridge flanks influences tectonic, magmatic, and microbial processes on a global scale; is a fundamental component of global biogeochemical cycles of key elements and isotopes (e.g., O, S, Mg, Fe, Li, B, Tl, and ^{87}Sr); and facilitates geologic CO_2 sequestration within the ocean crust (e.g., Alt and Teagle, 1999). The chemical and isotopic composition of seawater reflects the dynamic balance between riverine inputs from the continents, burial of marine sediments, and hydrothermal exchanges with the ocean crust (e.g., Palmer and Edmond, 1989; Vance et al., 2009). Ocean crust is young and chemically relatively homogeneous compared to continental crust, and its chemical exchanges with seawater are limited to a few relatively well known reactions. Consequently, hydrothermal contributions to ocean chemistry are simpler to reconstruct than riverine inputs (Coggon and Teagle, 2011; Davis et al., 2003; Vance et al., 2009; Antonelli et al., 2017). Knowledge of the rates and magnitudes of hydrothermal exchanges will help us to decipher the changing global conditions responsible for past variations in seawater chemistry such as mountain building, changes in seafloor spreading rate, large igneous province emplacement, changing climate, and evolution of biological systems. Building this knowledge requires ocean basin–wide transects across ridge flanks with different hydrogeologic histories.

Conductive heat flow deficits indicate that, on average, hydrothermal exchange persists at low temperatures (generally ≪100°C) to 65 Ma on the ridge flanks (Stein and Stein, 1994; Figures **F2**, **F8**). Given the vast extent of the ridge flanks, the hydrothermal fluid flux through them is many orders of magnitude greater than that through high-temperature (~400°C) axial systems (Mottl, 2003) and is likely important for elements for which fluid-rock exchange occurs at low temperatures (e.g., Mg, K, S, Li, B, C, and H_2O). Hydrothermally altered ocean crust provides a time-integrated record of geochemical exchange with seawater manifested through changes in its chemical and isotopic composition, mineral assemblages, and physical properties (e.g., porosity, permeability, and seismic velocities). The intensity of seawater-basalt exchange depends on the crustal age, architectural and thermal history, sediment cover, and spreading rate. Consequently, hydrothermal contributions to global geochemical cycles depend on the global length of slow-, intermediate-, and fast-spreading ridges and the age-area distribution of the ridge flanks, which have varied significantly throughout the Phanerozoic (Müller et al., 2008b). However, the impact of these variations on geochemical cycles is uncertain because the magnitude and spatial and

temporal distribution of crust-seawater hydrothermal exchanges are poorly quantified. For example, the role of MOR spreading in controlling past atmospheric CO_2 and hence climate remains controversial (Alt and Teagle, 1999; Berner et al., 1983; Gillis and Coogan, 2011; Staudigel et al., 1989) because of uncertainties regarding the rate, extent, and duration of hydrothermal $CaCO_3$ precipitation due to our sparse sampling of intermediate-age ocean crust (Figure **F8**). The hydrothermal carbonates that sequester CO_2 in the ocean crust also record the composition of the fluids from which they precipitate (Coggon et al., 2004) and provide an exciting opportunity to develop medium-resolution records of past ocean chemistry (e.g., Mg/Ca and Sr/Ca) (Coggon and Teagle, 2011; Coggon et al., 2010; Rausch et al., 2013), which integrates past changes in major Earth system processes such as plate tectonics, mountain building, and climate. However, this approach is limited by sparse sampling of ocean crust of a variety of ages.

Knowledge of the controls on the extent, rate, and duration (Coogan et al., 2016; Harris et al., 2014) of natural CO_2 sequestration along the SAT will assist efforts to assess the feasibility of geo-engineered CO_2 sequestration within the ocean crust (e.g., Goldberg et al., 2008; Marieni et al., 2013). The permeable upper ocean crust is of particular interest because it constitutes a vast potential reservoir for CO_2 trapping in areas where the crust is isolated from the oceans by low-permeability sediments (Marieni et al., 2013) or permanent storage through carbonate mineralization (Matter et al., 2016).

Drilling experiments on the Juan de Fuca Ridge flank were a key investigation of hydrothermal evolution across a ridge flank but were restricted to young (<3.6 Ma), intermediate-spreading (29 mm/y half-spreading rate), heavily sedimented crust (Shipboard Scientific Party, 1997; Expedition 301 Scientists, 2005; Expedition 327 Scientists, 2011). There is a dearth of holes in 20–140 Ma
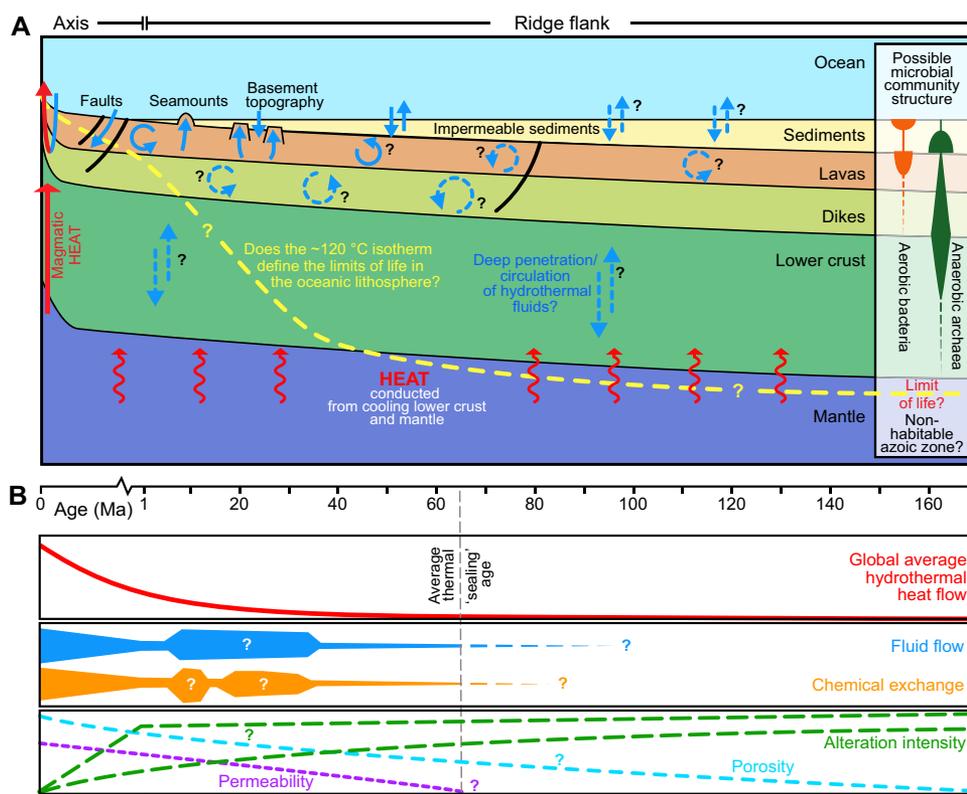
Figure F8. A. Schematic architecture of MOR flank (not to scale) illustrating parameters that may influence intensity and style of hydrothermal alteration and hypothetical trajectory of 120°C isotherm with crustal age. Arrows = heat (red) and fluid (blue) flow. B. Calculated global hydrothermal heat flow anomaly, which decreases to 0 by 65 Ma on average, and hypothetical variations in fluid flow and chemical exchange and crustal properties that could be measured to investigate intensity and style of ridge flank hydrothermal circulation (e.g., porosity, permeability, and two possible scenarios for alteration intensity). (After Coggon and Teagle, 2011; Expedition 335 Scientists, 2012; and an original figure by K. Nakamura, AIST.)

intact in situ MOR crust and no significant penetrations (>100 m) of 46–110 Ma crust (Figure **F2**; Expedition 335 Scientists, 2012). Consequently, the critical thermal, hydrogeologic, chemical, and microbial transitions across the ridge flanks remain unknown (Figure **F8**). Our current sampling of in situ upper ocean crust (>100 m) is biased toward areas with anomalously thick sediment for their crustal ages (Figure **F3**). The majority of holes in ocean crust older than 35 Ma penetrate intermediate- or fast-spreading rate crust. The recovery of uppermost basement sections along the SAT across slow- to intermediate-spreading Mid-Atlantic Ridge crust was planned to address these sampling gaps with respect to age, spreading rate, and sediment thickness. In addition, knowledge of the controls on the extent, rate, and duration of natural CO_2 sequestration along the SAT will assist in assessing the properties and processes that govern the flow and storage of carbon in the subseafloor.

The hydrothermal alteration of thinly sedimented slow- to intermediate-spreading ocean crust recovered along the SAT will be investigated using a combination of petrologic and geochemical analyses, radiometric dating, and detailed quantitative core logging of rock types, alteration features, and veins integrated with continuous wireline geophysical data with the following aims:

- To determine the nature, rates, magnitudes, distribution, and duration of hydrothermal alteration across the ridge flank;
- To investigate the effect of titanomagnetite/titanomaghemite alteration on the magnetic anomaly signal to elucidate its origin;
- To compare hydrothermal alteration of the uppermost slow- to intermediate-spreading crust with crust of similar ages produced at faster spreading ridges (e.g., Holes 504B and 1256D);
- To evaluate the effect of changes in global spreading rates and the age-area distribution of the seafloor on hydrothermal contributions to global biogeochemical cycles; and
- To investigate signatures of changing ocean chemistry in the hydrothermal record and develop medium-resolution records of past ocean chemistry using hydrothermal minerals (following Coggon et al., 2010).

Shipboard description and analyses combined with detailed postexpedition research will allow us to address the following hypotheses:

- Hydrothermal chemical exchange persists beyond 20 My of crustal formation.
- Basement topography and sedimentation history affect the rate and duration of hydrothermal alteration.

3.2. Objective 2 (primary): investigate sediment- and basement-hosted microbial community variation with substrate composition and age.

Scientific ocean drilling has revealed that microorganisms, including Archaea, Bacteria, viruses, and eukaryotic fungi and protists are present, intact, and metabolically active in uncontaminated deep subsurface sediment and basalt. Knowledge about subseafloor microbial communities has grown exponentially since the initial microbiological investigations by DSDP in the 1980s, but only ~4% of ODP/Integrated Ocean Drilling Program/IODP sites have been sampled, documented, or archived for microbiological purposes (Figure **F9**) (Kallmeyer et al., 2012; Orcutt et al., 2014). Determining microbial community composition and physiological capabilities along the SAT will provide insights into the role of microbes in mineral alteration, hydrocarbon formation, and global biogeochemical cycles.

In sediments, the number of microbial cells present is estimated to equal that in the entire oceanic water column (Kallmeyer et al., 2012). However, the amount of biomass stored in the deep subsurface remains contentious because microbial cell abundance in subseafloor sediment varies by ~5 orders of magnitude (Figure **F9**) with significant geographic variation in the structure of subseafloor communities (Inagaki et al., 2006). Most studies have focused on relatively high biomass continental shelf systems (Inagaki and Orphan, 2014). Recent efforts, including Integrated Ocean Drilling Program Expeditions 329 (South Pacific Gyre; Expedition 329 Scientists, 2011) and 336 (North Pond; Expedition 336 Scientists, 2012), investigated lower biomass sedimentary systems

underlying oceanic gyres. Crucially, no data have been collected from the South Atlantic Gyre (Figure **F9**). Hence, postexpedition analyses of the cores recovered during the SAT expeditions will refine the global biomass census and improve our understanding of the global carbon cycle.

The presence or absence of oxygen in marine sediments has profound implications for the quantity, diversity, and function of microbial communities. Oxygen penetration depth varies between oceanic regions and settings, ranging from only a few millimeters in areas with high rates of microbial respiration, such as on continental shelves, to the entire sediment column in extremely low biomass sediments, such as the relatively thin sediments beneath the South Pacific Gyre (D'Hondt et al., 2015). Extrapolation of an observed global relationship between oxygen penetration and sedimentation rate and thickness indicates South Atlantic Gyre sediment may be oxic to basement (D'Hondt et al., 2015). During Leg 3, oxygen was not measured, but pore water sulfate was detected near the basement. However, sediment organic carbon concentrations along the SAT are intermediate to those of North Pond, where oxygen penetrated tens of meters below seafloor and nitrate was present to basement, and Nankai Trough, where oxygen was depleted by 3 meters below seafloor (mbsf) and sulfate was depleted by 19 mbsf (Figure **F10**; Expedition 336 Scientists, 2012; Tobin et al., 2009; Orcutt et al., 2013; Reese et al., 2018). These results indicate that oxygen is unlikely to extend to the basement at sites along the SAT, contrary to model predictions (D'Hondt et al., 2015), and that the classical redox succession of oxygen respiration followed by nitrate reduction, potentially followed by metal reduction, may be present. However, oxygen may be reintroduced at the bottom of the sediment column because of oxygenated fluid flow from the uppermost volcanic basement, which is the case at North Pond (Expedition 336 Scientists, 2012). The recovery of the sediment package across the South Atlantic Gyre allows us to investigate the relationships between oxygen penetration, biomass, and carbon limitation of microbial activity.

Drilling allows us to compare the phylogenetic diversity, functional structure, and metabolic activity of South Atlantic Gyre communities with results from previously studied regions. By exploiting the variations in sediment carbon composition expected across the subsiding MOR flank, we can examine the response of autotrophy versus heterotrophy to carbonate chemistry. Additionally, previous studies of the sedimentary deep biosphere have explored community diversity based on site-to-site or downhole (age) comparisons, often implicitly assuming a similar "starter community" that colonized the seafloor and whose structure and function subsequently changed in response to evolving geochemical conditions or burial depth. However, recent work suggests energy limitation may preclude replication (Lever et al., 2015; Lomstein et al., 2012) and thus limit
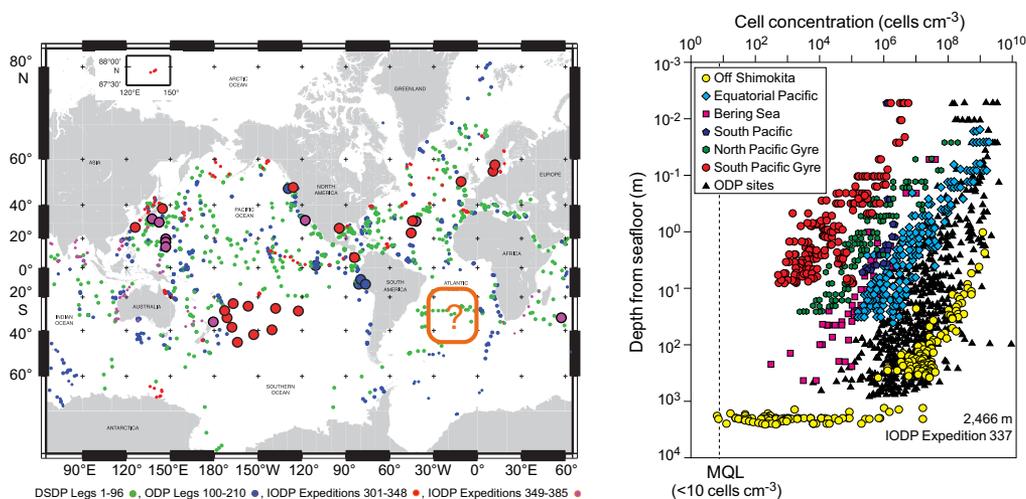
Figure F9. Left: global distribution of scientific ocean drilling sites. Larger circles = where microbiological samples were taken. Right: microbial cell abundance vs. depth, revealing >5 orders of magnitude variation in biomass-depth trends, depending on geographic origin of samples (after D'Hondt et al., 2019). MQL = minimum quantifiable limit. The South Atlantic represents a crucial gap in knowledge (orange box with question mark), and SAT samples will be used to groundtruth models of biomass density in subsurface sediments and basement predicted from current biomass database. Note that symbol colors between diagrams are not related because they are derived from different sources.

community changes. The SAT age-transect approach allows us to test this assumption directly by investigating the impact of burial depth and chemical zonation on sediment of the same age and hence the same starter community.

Given the dearth of basement holes in ocean crust of intermediate age before the SAT expeditions, it is no surprise that there were no microbiological samples across the critical ridge–flank transitions in basement properties that may affect microbial communities prior to the SAT expeditions (Figure **F8**). Most of the biological alteration of subseafloor basalts is thought to occur within 20 My of crustal formation (Bach and Edwards, 2003). However, microbiological investigations of oceanic basement have focused on young (<10 Ma) crust (Jungbluth et al., 2013; Lever et al., 2013; Mason et al., 2010; Orcutt et al., 2011) or older (>65 Ma) lava associated with hotspot volcanism along the Louisville Seamount Trail (Expedition 330 Scientists, 2012; Sylvan et al., 2015). Basement outcrops that penetrate the relatively impermeable sediment provide permeable conduits that facilitate subseafloor fluid circulation in older basement (Wheat and Fisher, 2008). Fluid flow across the sediment/basement interface can produce redox gradients that provide recharge of depleted electron acceptors (e.g., oxygen and nitrate) to basal sediments, as observed above 3.5 and 8 Ma ocean crust on the Juan de Fuca Ridge flank (Engelen et al., 2008) and at North Pond (Orcutt et al., 2013), respectively. However, the extent and duration of fluid flow through this interface across the ridge flanks remains unknown (Figure **F8**). The recovery of the uppermost basaltic basement from 7 to 61 Ma along the SAT enables us to determine whether microbial populations are indeed present in basement older than 20 Ma where hydrothermal flow persists across the ridge flanks and to investigate the nature, extent, and duration of communication between the sedimentary and crustal biosphere for the first time.

The SAT expeditions were designed to sample subseafloor populations of Bacteria, Archaea, viruses, and microbial eukaryotes in both the sedimentary and upper crustal ecosystems across the aging Mid-Atlantic Ridge flank, quantify their biomass by cell enumeration, identify them
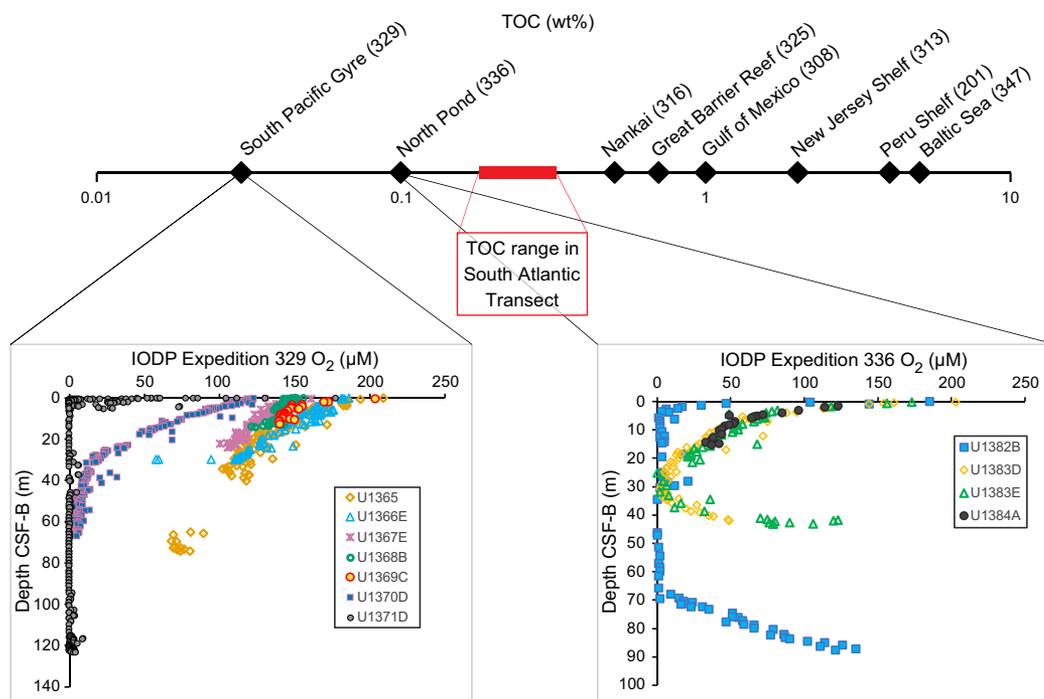
Figure F10. Comparison of predicted range of TOC for SAT study area with other areas where scientific ocean drilling has conducted microbiological investigations (data from Andrén et al., 2015; Shipboard Scientific Party, 2003a; Expedition 329 Scientists, 2011; Expedition 336 Scientists, 2012; Expedition 308 Scientists, 2006; Tobin et al., 2009; Expedition 313 Scientists, 2010; Expedition 325 Scientists, 2011). SAT drill sites have higher TOC than South Pacific Gyre, where oxygen penetrated to basement, and North Pond, where oxygen penetrated tens of meters into the seafloor in Holes U1383D, U1383E, and U1384A, but lower than Nankai Trough, where pore water oxygen was consumed <5 m below seafloor, based on pore water Mn concentrations.

using molecular biology methods, measure the stable isotopic composition (C, N, and S) of sediment and basement to relate processes to geochemistry, measure their metabolic activities using a variety of incubation assays, and resolve their physiological adaptations with omics-based approaches with the following aims:

- To evaluate cell abundance and community activity in the low-energy subseafloor biosphere of the South Atlantic Gyre and refine estimates of global subseafloor sedimentary microbial abundance;
- To resolve model predictions about the depth of oxygen penetration into sediment from overlying seawater and into the bottom of the sediment package from oxygenated fluid in basement;
- To evaluate the role of subseafloor microbes in sediment biogeochemistry and basement alteration and hence global biogeochemical cycles; and
- To investigate how aging of the ocean crust influences the composition of the crustal biosphere, particularly the effects of changing oxidation state and permeability on microbial abundance, diversity, and function.

The SAT samples will also allow us to test the following hypotheses:

- South Atlantic Gyre microbial communities share membership and function with both oligotrophic sediments, like those found at North Pond, and open-ocean systems with higher organic matter input, such as Nankai Trough, given the intermediate organic carbon content of the SAT sites.
- Microbial community structure and diversity depends on the starter community (and hence sediment age) rather than subsequent selection driven by burial or chemical zonation.
- Crustal biomass decreases with increasing basement age, and communication between the sedimentary and crustal biosphere ceases with the cessation of hydrothermal flow and sealing of the basement.
- Microbial diversity increases within subseafloor basalts with basement age as previously demonstrated in basalts exposed on the seafloor (Lee et al., 2015; Santelli et al., 2009).

3.3. Objective 3 (secondary): investigate the responses of Atlantic Ocean circulation patterns and the Earth's climate system to rapid climate change, including elevated atmospheric CO_2 during the Cenozoic.

Climate change due to anthropogenic CO_2 emissions poses significant and imminent threats to global society and the biosphere. Knowledge of past ocean circulation patterns and temperatures is essential to understand the operation of Earth's climate system and required to improve the efficacy of numerical models in simulating intervals of high pCO_2. High pCO_2 intervals are commonly characterized by relatively shallow lysocline and calcite compensation depths (CCDs) resulting in poor preservation of calcareous microfossils used to generate paleoceanographic records and reconstruct past climates. This problem can be overcome by coring sediment deposited on basement slightly older than the targeted sediment age that accumulated prior to thermal subsidence of the seafloor below the CCD. More continuous composite stratigraphic sequences can be obtained by drilling multiple sites along a crustal age transect, a strategy successfully employed during ODP Leg 199 (Shipboard Scientific Party, 2002) and Integrated Ocean Drilling Program Expedition 320/321 (Pälike et al., 2012). The Walvis Ridge depth transect sampled during ODP Leg 208 demonstrated the dynamic nature of the Cenozoic CCD and lysocline in the eastern South Atlantic (Shipboard Scientific Party, 2004) and the value of redrilling DSDP transects to collect more complete records of Earth's history. Although spot cored, Leg 3 sites in the western South Atlantic demonstrated moderate to excellent carbonate preservation along the SAT (Scientific Party, 1970) and the area's suitability for high-resolution paleoclimatic and paleoceanographic reconstructions through key intervals of rapid climate change (Cramer et al., 2009; Zachos et al., 2001, 2008), including the PETM and other short-lived hyperthermals, early and middle Eocene climatic optima, the onset of Antarctic glaciation across the Eocene–Oligocene transition (EOT), multiple Oligocene and the Miocene glaciation events (Oi and Mi events), the Miocene climatic

optimum and Monterey Carbon Excursion, the Middle Miocene climate transition, Pliocene warmth, and the onset of Northern Hemisphere glaciation. Figure **F11** illustrates the intervals that we expected to recover across the SAT, based on estimated basement ages (cf. Figure **F12**, which illustrates the intervals actually recovered during the SAT expeditions).

Global ocean circulation transfers heat and nutrients around the globe, both influencing and responding to changes in Earth's climate system (Broecker, 1991; Stommel, 1961; Wunsch, 2002). The western intensification of ocean currents means that by characterizing western portions of major ocean basins using drilling transects, records of deepwater mass properties and thus the development of modern thermohaline circulation can be reconstructed. The western South Atlantic is the main northward flow path of AABW and southward flow path of North Atlantic Deep Water (NADW) and their precursor water masses. Consequently, the SAT expeditions provide complementary data needed to constrain the evolution of thermohaline circulation patterns and climate change as the Drake Passage and Southern Ocean opened, the northern NADW gateway opened, and the Tethys Ocean became restricted to thermohaline circulation. In particular, the SAT cores will assist in establishing how high-latitude sea surface (and hence deep ocean) temperatures and the CCD varied in response to $p\text{CO}_2$ changes and ocean acidification (Barker and Thomas, 2004; Barrera et al., 1997; Billups, 2002; Bohaty et al., 2009; Cramer et al., 2009; Frank and Arthur, 1999; Kennett and Stott, 1991; Scher and Martin, 2006; Thomas et al., 2003; Wright et al., 1991). Together the complementary records from western North Atlantic sediments (Integrated

Figure F11. Composite deep-sea benthic foraminiferal $\delta^{13}\text{C}$ and $\delta^{18}\text{O}$ records show both gradual and abrupt changes in global climate during the Cenozoic; key events are highlighted by vertical bars (modified from Westerhold et al., 2020). Red and blue "climate stripes" = departure from average Cenozoic temperature in 100 ky time bins (red = warmer than average, blue = colder than average). SAT samples record a rich paleoceanographic record of these changes. Bottom bars show present water depths of SAT sites and intervals of Cenozoic climate history they expected to sample. Deepest sites were expected to contain carbonate-rich sediment (blue) in older part, deposited when site was closer to ridge crest and shallower than CCD, transitioning up to poorly preserved carbonate sediment (light blue) or carbonate-poor sediment (brown) in younger part as each site subsided below CCD. Sites on younger ocean crust were expected to recover younger carbonate-rich sediment. Together, these sites represent a megasplice of the last 61 My of Earth's climate history from an understudied region of the ocean.

Ocean Drilling Program Expedition 342; Norris et al., 2014) and the SAT will provide an exceptional record of the evolution of Atlantic overturning circulation through the Cenozoic.

A novel, direct way to compare paleoceanographic reconstructions of past high pCO_2 to modern conditions is to recover sediments along transects of water column data collected by the WOCE. The SAT constitutes a "paleo-WOCE" line following the western portion of WOCE Line A10 (Figure **F13**), providing access to paleoceanographic records of southern- and northern-sourced deep and bottom waters. We will test models of bipolar deepwater evolution (e.g., Borrelli et al., 2014; Cramer et al., 2009; Katz et al., 2011; Tripati et al., 2005) using stable and radiogenic isotope analyses of sediments recovered from these key western South Atlantic sites.

The Walvis Ridge depth transect (Shipboard Scientific Party, 2004) revealed a dramatic 2 km shoaling of the CCD during the PETM due to the acidification of the ocean from massive carbon addition followed by a gradual recovery (Figure **F14**) (Zachos et al., 2005; Zeebe et al., 2008). Given chemical weathering feedbacks, the recovery of the CCD should have resulted in a transient overdeepening of the CCD (Dickens et al., 1997). Collectively, the SAT sites will provide additional data for reconstructing changes in the position of the lysocline and CCD in the western South Atlantic that are essential for constraining the timing of gateway events and the history of Northern Component Water (NCW) and Southern Component Water (SCW), which were the precursors to NADW and AABW, and the nature of Atlantic basin responses to climate change relative to the Pacific.
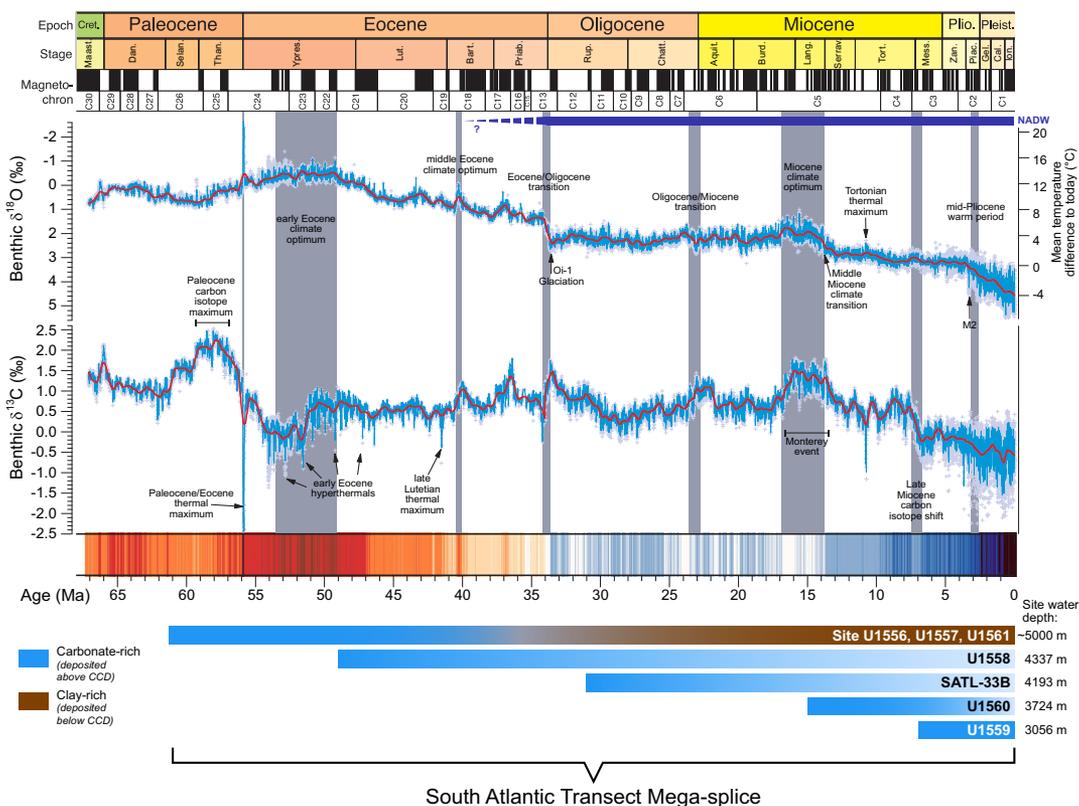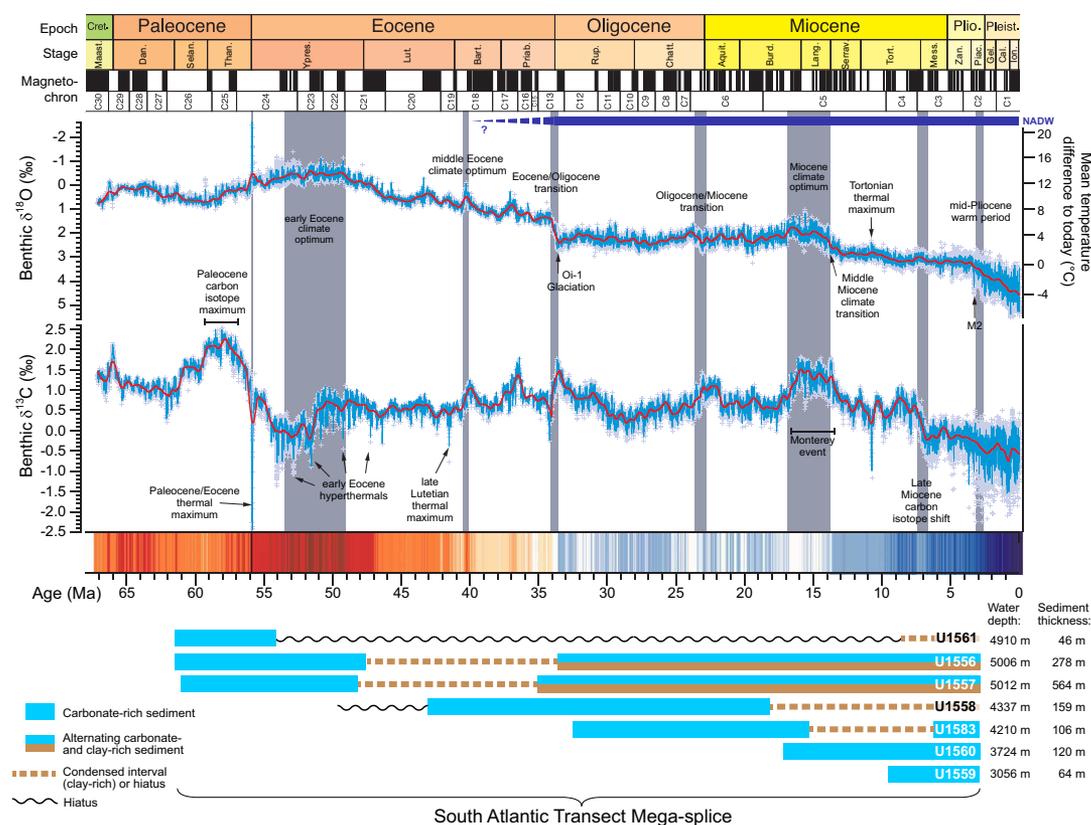

Figure F12. Composite deep-sea benthic foraminiferal $\delta^{13}C$ and $\delta^{18}O$ records show both gradual and abrupt changes in global climate during the Cenozoic; key events are highlighted by vertical bars (modified from Westerhold et al., 2020). Red and blue "climate stripes" = departure from average Cenozoic temperature in 100 ky time bins (red = warmer than average, blue = colder than average). Bottom bars show present water depth of SAT sites and intervals of Cenozoic climate history they sampled. Deepest sites comprise carbonate-rich sediment (blue) in older part, deposited when site was closer to ridge crest and shallower than CCD, transitioning up to carbonate-poor sediment (brown) in younger part as each site subsided below CCD. Sites on younger ocean crust recovered younger carbonate-rich sediment. Together, these sites represent a megasplice of the last 61 My of Earth's climate history from an understudied region of the ocean.

Microfossils provide a critical archive of ocean and climate history, including long-term changes (e.g., early Eocene warmth, Cenozoic cooling, and Pliocene warmth) and abrupt events (e.g., early Paleogene hyperthermals and multiple glaciation events). The SAT expeditions were designed to recover complete sedimentary sections along paleo-WOCE Line A10, exploiting the thermal subsidence of the ocean crust along the transect to provide material for high-resolution proxy records including benthic and planktic foraminiferal geochemistry, micropaleontological assemblages, orbitally tuned age models, neodymium isotopes, and alkenone $\delta^{13}C$ and boron isotope $p\text{CO}_2$ reconstructions with the following aims:

- To reconstruct the evolution of deepwater masses over the past 61 My to assess contributions of NCW and SCW in the early Paleogene western South Atlantic (Kennett and Stott, 1990), document the influence of the openings of the Drake and Tasman Passages on South Atlantic deepwater circulation, and reconstruct the overall development of modern thermohaline circulation;
- To provide high-resolution constraints on CCD and carbonate chemistry changes of the deep western Atlantic, particularly during transient hyperthermals and other intervals of global warmth;
- To reconstruct the Cenozoic history of the South Atlantic subtropical gyre by monitoring proxies of productivity and paleobiogeography of plankton, rates of speciation/extinction relative to the equatorial zone and higher latitudes, and changes in biodiversity and subtropical ecosystem dynamics; and
- To evaluate the response of subtropical planktic and benthic biota to changing environmental conditions such as global warming, ocean acidification, or fertility patterns during intervals of rapid climate change through the Cenozoic.
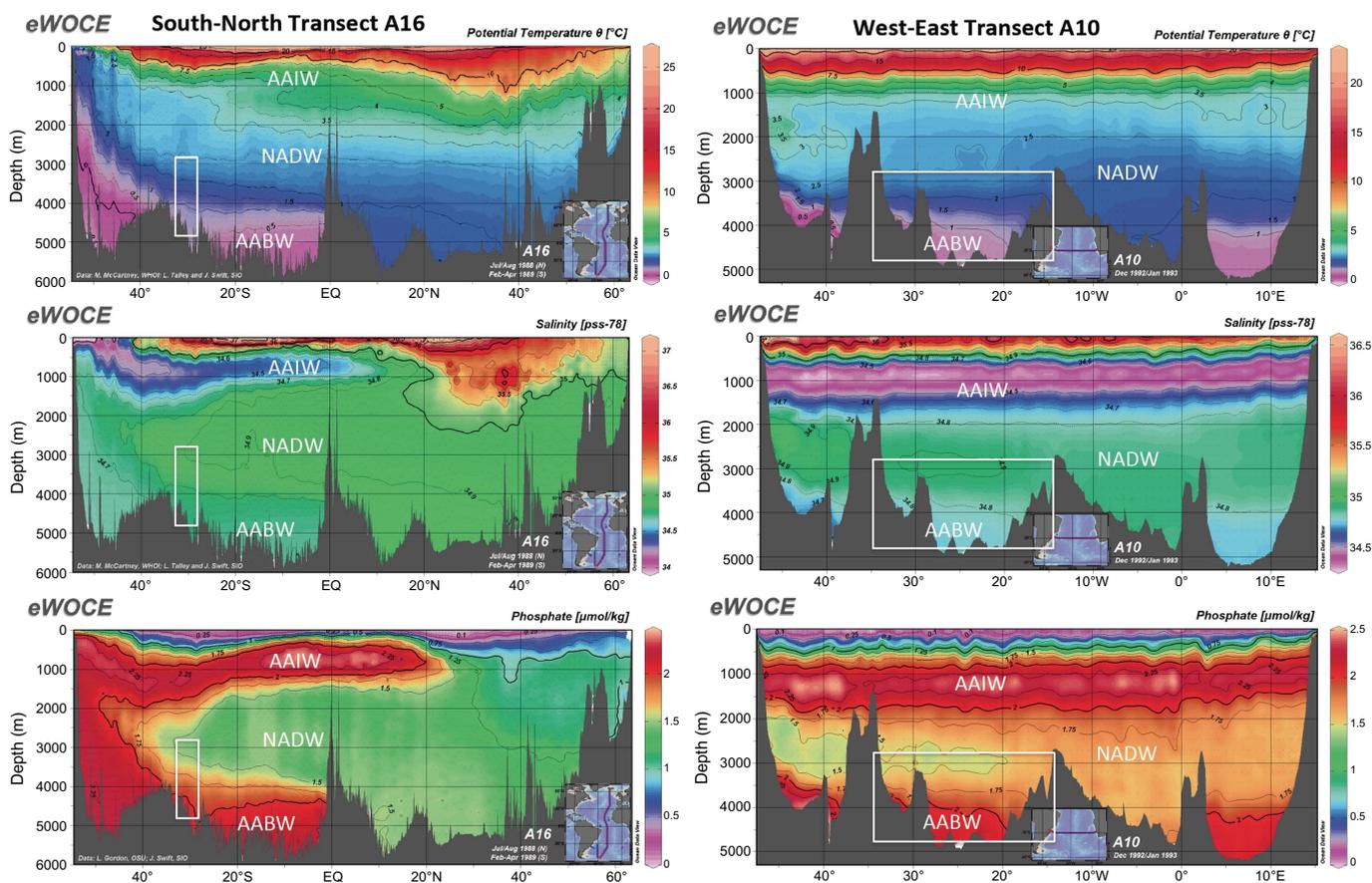
Figure F13. WOCE (top) temperature, (middle) salinity, and (bottom) phosphorus profiles along (left) south–north Transect A16 through (right) western South Atlantic Basin and west–east Transect A10 at 30°S close to location of SAT (data from WOCE; **http://www.ewoce.org**). Rectangles show approximate coverage of SAT. AAIW = Antarctic Intermediate Water.

The recovered sediment sections will also allow us to test the following hypotheses:

- Low-latitude sites were potential sources of deepwater formation at times of global warmth and high atmospheric pCO$_2$.
- The strength of the coupling between the climate and the carbon cycle varied through the Cenozoic.
- The lysocline and CCD responded differently on the western side of the Mid-Atlantic Ridge compared to the Walvis Ridge record due to changing deep/bottom water sources, gateway configurations, and flow paths.
- The subtropical gyre cut off the delivery of heat to Antarctica as the Antarctic Circumpolar Current developed through the late Eocene–Oligocene.

3.4. Connections to the 2050 Science Framework

Given its multidisciplinary essence, the SAT campaign will advance the full spectrum of the 2050 Science Framework including each of the seven interconnected Strategic Objectives (SOs) and five Flagship Initiatives (FIs) (Koppers and Coggon, 2020). For example, SAT Objective 1 explores hydrothermal alteration and fluid-rock exchange during crustal aging through the recovery of upper crustal sections (>100 m) along a crustal age transect. This aspect of the project directly
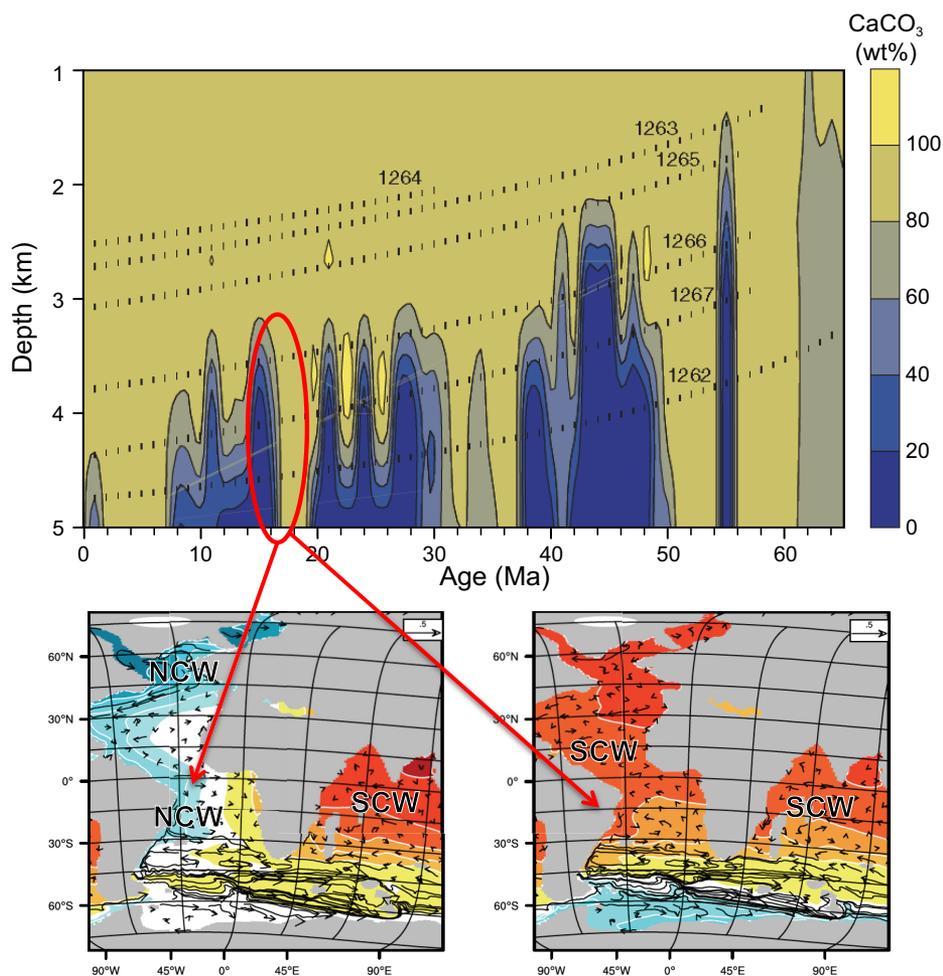
Figure F14. Top: carbonate in depth transect recovered during Leg 208 on Walvis Ridge, eastern South Atlantic (Shipboard Scientific Party, 2004). Position of lysocline and CCD were dynamic during Cenozoic related to changing deepwater circulation, productivity, and ocean acidification associated with PETM. Bottom: modeled relative water mass age during mid-Miocene climatic optimum (Coggon et al., 2020). Red oval = correlative changes in carbonate chemistry on Walvis Ridge. Colors represent benthic "age," which is a δ^{13}C-like tracer; red = old water, blue = young water. Left: mode with NCW on. Right: NCW off. The SAT, near 31°S, is expected to capture changes in these two modes of deepwater formation.

relates to the 2050 Science Framework SO2 The Oceanic Life Cycle of Tectonic Plates and SO6 Global Cycles of Energy and Matter, as well as FI2 Probing the Deep Earth. Documenting the impact of fluid-rock exchange on the composition and physical properties of the crust as a function of its age provides insights into key properties of old crust entering subduction zones, such as hydration state, seismic velocity, and strength, to inform studies of hazards generated along convergent plate margins (SO7 Natural Hazards Impacting Society and FI3 Assessing Earthquake and Tsunami Hazards).

Quantifying the abundance and diversity of microbial life in ocean crust and the overlying nutrient-limited sediment environments (SAT Objective 2) will help determine the impact of biological activity in geochemical cycles and improve our understanding of the limits of life in the lithosphere. This knowledge will contribute to SO1 Habitability and Life on Earth, SO6 Global Cycles of Energy and Matter, and FI5 Exploring Life and its Origins. SAT Objective 3 investigates the responses of Atlantic Ocean circulation patterns and the Earth's climate system to rapid climate change. This objective relates to SO3 Earth's Climate System, SO4 Feedbacks in the Earth System, and SO5 Tipping Points in Earth's History, as well as FI1 Ground Truthing Future Climate Change and FI4 Diagnosing Ocean Health by examining the ocean's past responses to climate events, including hyperthermals, changes in oxygenation, and acidification, to look ahead to future impacts on Earth's climate and ecosystems.

The SAT project also embraced new technologies and approaches to core description and objective quantification of recovered cores through the analysis of high-resolution images of external core surfaces and the application of machine learning approaches (e.g., Enabling Element 4 Technology Development and Big Data Analytics). The ambitious operational goals of the SAT project align with the 2050 Science Framework and emphasize, as stated in the framework, that achieving these scientific objectives "requires continued developing of drilling, coring, logging, observatory, and laboratory tools and techniques." Overall, the mission of the 2050 Science Framework for scientific ocean drilling is to guide "multidisciplinary subseafloor research into the interconnected processes that characterize the complex Earth system and shape our planet's future." The breadth of the interrelated science addressed by the SAT project exemplifies such investigation of the interconnected Earth by IODP.

4. Operational strategy

The original operational strategy for Expeditions 390 and 393 is described in detail in the *Scientific Prospectus* (Coggon et al., 2020) and was updated in the *Scientific Prospectus Addendum* (Coggon et al., 2022b) following the completion of engineering Expeditions 390C and 395E. In brief, the SAT intended to drill six sites located at five different crustal ages (~7, 15, 31, 49, and 61 Ma), with two of the sites located in the same localized sedimentary basin on 61 Ma crust where significant basement topography results in variable sediment thickness (estimated to be ~180 and 640 m thick at proposed Sites SATL-53B and SATL-54A, respectively, prior to drilling; Table T1). At each of the six sites, we planned the following operations to achieve our scientific objectives and establish legacy boreholes for future basement experiments:

- Recover a complete sediment section by coring three advanced piston corer (APC)/extended core barrel (XCB) sediment holes at each crustal age to allow compilation of complete paleoceanographic records across core breaks in the sediment sections using stratigraphic correlation and to provide sufficient material for whole-round microbiological and pore water sampling,
- Recover the sediment/basement interface using the XCB system,
- Install a drill-in reentry cone and casing to ~5 meters subbasement (msb),
- Core to ~250 msb, and
- Collect wireline geophysical logging data through the basement sections.

4.1. Sediment coring strategy

The original operations plan included three sediment holes at each crustal age, to allow compilation of complete paleoceanographic records across core breaks in the sediment sections using

stratigraphic correlation and provide sufficient material for whole-round microbiological and pore water sampling (Coggon et al., 2020). This was to be achieved by triple coring the sediments at the 7, 15, 31, and 49 Ma sites using the APC system unless drilling conditions required a switch to the XCB system. To optimize the drilling operations that were achievable during Expeditions 390 and 393, triple coring of the sediment section on 61 Ma crust was planned to comprise an APC hole to refusal (estimated to occur at 250 mbsf depending on drilling conditions) at Proposed Site SATL-54A followed by XCB coring to basement (~639 mbsf) and two APC/XCB holes to basement at Proposed Site SATL-53B (originally estimated to be at 180 mbsf; Table **T1**). This sediment coring strategy was designed to optimize the drilling operations that could be achieved during Expeditions 390 and 393 with the sedimentary coring at Proposed Sites SATL-53B and SATL-54A completed using a single pipe trip because they are only 1.2 nmi apart. Given uncertainty regarding the sediment thickness and to ensure that the sediment/basement interface was well sampled at all crustal ages, we planned to use the XCB system to sample the lowermost sediments and uppermost <10 m basement in all sediment holes.

4.2. Depth of basement drilling

To fully quantify the extent and duration of ridge flank hydrothermal exchange, we required our sampling of the upper basement to be as representative as possible of the entire extrusive crust. A systematic downward decrease in the extent of oxidative hydrothermal alteration is not observed through all previously drilled upper crustal sections (Shipboard Scientific Party, 2003b), and the permeability of the extrusive crust is highly heterogeneous and not always greatest at the top of the basement (Becker et al., 2013; Shipboard Scientific Party, 2003b). Commonly, fluid flow in the upper crust is channeled along specific horizons of enhanced permeability (Harris et al., 2015; Neira et al., 2016). At many drill sites globally, the fluid temperature–depth distribution recorded by hydrothermal carbonate veins, typically one of the last hydrothermal phases to form, indicates the circulation of cool (<100°C) ridge flank fluids through at least the upper 300 m (Coggon et al., 2010). If there is a depth limit to off-axis fluid circulation, sufficient basement drilling is required to establish what it is and how it varies across the ridge flanks; therefore, we aimed to achieve the maximum possible basement penetration in the time available. Consequently, our target was to core ~250 m into the uppermost basaltic ocean crust at each site along the transect.

4.3. Basement coring and wireline logging strategy

At each of the six primary sites, we planned to install a standard "drill-in" reentry cone system with 13⅜ inch casing (Coggon et al., 2020). The reentry cone systems were designed with 13⅜ inch casing to allow for future installation of a narrower 10¾ inch casing string across the sediment/basement interface (and deeper into basement) to stabilize this region of the holes if they are reoccupied during any future drilling investigations. Following installation of the reentry cone system, we planned to deploy two rotary core barrel (RCB) bits in each hole, with an anticipated basement penetration of ~250 m at each site. The planned wireline logging operations included deployment of the advanced piston corer temperature tool (APCT-3), the triple combo tool with the Ultrasonic Borehole Imager (UBI), and at least two passes of the Formation MicroScanner (FMS) at each site.

5. Preexpedition engineering and coring operations

SAT Expeditions 390 and 393 were originally scheduled for October–December 2020 and April–June 2021, respectively. In 2020 and 2021, the global COVID-19 pandemic resulted in the postponement of several IODP expeditions, including Expeditions 390 and 393, primarily because science parties were unable to travel to board the R/V *JOIDES Resolution*. In response, the ship was used to conduct preparatory work for postponed expeditions that did not require a science party aboard but could be carried out by the ship's crew and a team of technicians from the *JOIDES Resolution* Science Operator (JRSO). Two of these expeditions (390C and 395E) were in service of the SAT drilling project to reduce the operational risks and expedite basement drilling during the postponed Expeditions 390 and 393 by coring one hole through sediment to basement and installing a cased reentry system <5 m into basement in a second hole at each of the six

proposed primary SAT sites. Capturing the sediment/basement contact along the SAT was critical to document chemical exchange, alteration, and microbiological processes across this interface. The operational plans for the engineering expeditions therefore included using the XCB system with a polycrystalline diamond compact (PDC) cutting shoe to core the lowermost sediments and up to 10 m into the underlying igneous rocks in each APC/XCB hole to determine the thickness of the sediment cover and to recover this critical boundary for future sampling and study. The assumption was that this system would provide cleaner recovery of the interface by causing only minimal disturbance and yielding high recovery compared to RCB coring systems. All RCB basement coring was deferred to Expeditions 390 and 393.

5.1. Expedition 390C operations

During Expedition 390C, which sailed in October–December 2020 (Estes et al., 2021), the sediment section at four of the SAT sites (U1556–U1559) was cored. The contact with basalt was slightly deeper than estimated at all sites (Table **T1**), likely because of a slight underestimation of the in situ seismic velocities. At 61 Ma Site U1556, basalt was encountered at 278 mbsf, significantly deeper than expected (180 mbsf). If the sediment had also been thicker than expected (640 m) at proposed Site SATL-54A ~2.5 km west of Site U1556, the casing length required would have exceeded the drill string weight limit for the water depth (~5 km). Therefore, alternate proposed Site SATL-56A was drilled as Site U1557 instead. This site is ~6.5 km east of Site U1556 in the same localized sedimentary basin, where the basement contact was estimated to be at 510 mbsf and encountered at 564 mbsf.

The reentry systems were to be installed using the Dril-Quip running tool, which permits later extension of casing. However, there were difficulties installing casing into basement with this system (Estes et al., 2021) as had been reported during previous operations using the Dril-Quip system (e.g., Fryer et al., 2018). The release mechanism does not work when the casing string weight cannot be fully removed from the running tool, which can happen when the base of casing is in basement. Therefore, at Sites U1558 (49 Ma) and U1559 (7 Ma), casing was installed to ~10 m above basement. The thick (564 m) sediment cover at 61 Ma Site U1557 required multiple casing strings to reach basement; a reentry system with the first (16 inch) casing string was installed to 60 mbsf in Hole U1557D during Expedition 390C. The extra time taken for troubleshooting reentry system installations during Expedition 390C meant they could not be completed at all sites, and a second engineering expedition was planned. IODP Expedition 395P (February–April 2021) was given the go-ahead by the *JOIDES Resolution* Facility Board to complete the reentry system installations without a science party. Unfortunately, Expedition 395P did not leave port in Cape Town, South Africa, because of COVID-19 cases among the staff and crew in the port call hotel and on the ship. Expedition 395P operations were instead deferred to Expedition 395E.

5.2. Expedition 395E operations

Expedition 395E (April–June 2021; Williams et al., 2021) completed additional SAT preparatory work at Sites U1556, U1557, and U1560. Following installation of reentry systems at Sites U1556 and U1560 using the hydraulic release tool (HRT) and extension of the casing at Site U1557 into basement, there was insufficient time to core and install a reentry system at proposed Site SATL-33B (on 31 Ma crust). Instead, a single APC/XCB hole was cored at an alternate site adjacent to Sites U1556 and U1557, overlying 61 Ma crust (Site U1561; proposed Site SATL-55A; Figure **F6A**; Table **T1**). Proposed Site SATL-33B was the only primary SAT site at which no operations were conducted prior to Expeditions 390 and 393.

6. Expedition 390C and 395E principal results

Because there was no shipboard science party on the ship during engineering Expeditions 390C and 395E, no cores were described during the expeditions. Instead, the Expedition 390C and 395E cores are considered part of the joint Expeditions 390 and 393 and were described in detail by the expeditions' shipboard science parties in combination with new cores recovered from each site. Although a range of physical properties and chemical analyses were conducted during Expeditions

390C and 395E, sediment microbiological sampling was not possible. Core catcher samples were collected for distribution to the Expedition 390 and 393 micropaleontologists, and these allowed the development of preliminary biostratigraphic age models on shore ahead of Expeditions 390 and 393. A summary of the engineering expedition shipboard data is provided in the Expedition 390C and 395E *Preliminary Reports* (Estes et al., 2021; Williams et al., 2021), but all data generated during the preexpedition engineering operations along with the descriptions of the Expedition 390C and 395E cores made during Expeditions 390 and 393 are combined with the results of Expeditions 390 and 393 and presented in the relevant site chapters. The Expedition 390C and 395E geochemical data provided a valuable guide for chemical and microbiological sampling during Expeditions 390 and 393.

7. Revised Expedition 390 and 393 operational strategy

The successful installation of five of the six planned reentry systems along the SAT prior to Expeditions 390 and 393 significantly decreased the operational risk of the SAT expeditions. The time savings due to operations already completed were partially offset by the need to sail to and from Cape Town, South Africa, rather than from Cape Town to Montevideo, Uruguay, for Expedition 390 and from Montevideo to Montevideo for Expedition 393. These lengthier voyages added additional transit time to both expeditions. Extra time was also required to recore the thicker than expected sediments. The operations plans for the rescheduled Expeditions 390 and 393 were revised to account for these changes (Coggon et al., 2022b; Table **T2**; Figure **F15A**). The revised Expedition 390 operations plan included a fourth APC/XCB hole at 7 Ma Site U1559, where the sediment cover is <70 m, to provide additional material for microbiological sampling. The revised plans also included additional time for basement coring at the highest priority site, U1556, which has experienced the full history of ridge flank hydrothermal exchange across the SAT, with a new target depth of 350 msb. The failure of one of the electromagnetic brakes on the drawworks during Expedition 390 resulted in a premature curtailment of science operations and early return to Cape Town to enable repairs (Coggon et al., 2022a). Consequently, Expedition 393 operational plans were further refined to enable basement coring at the youngest (6.6 Ma) Site U1559 (Tables **T2**, **T3**; Figure **F15B**).

Table T2. SAT expeditions hole summary. * = between casing shoe at 122 mbsf and hole total depth at 124 mbsf (determined during Expedition 395E). DSF = drilling depth below seafloor. NA = not applicable. (Continued on next page.) **Download table in CSV format.**

Hole	Proposed SATL site	Latitude	Longitude	Age (Ma)	Half spreading rate (mm/y)	Approximate distance from ridge (km)	Water depth (m)	Penetration DSF (m)	Drilled interval (m)	Cored interval (m)	Recovered length (m)	Recovery (%)
390C-U1556A	53B	30°56.5244'S	26°41.9472'W	61.2	13.5	1250	5006	283.8	NA	283.8	243.8	85.9
395E-U1556B	53B	30°56.5244'S	26°41.9472'W	61.2	13.5	1250	5002	291.0	291.0	NA	NA	0.0
390-U1556B	53B	30°56.5244'S	26°41.9472'W	61.2	13.5	1250	5002	633.2	291.0	342.2	191.9	56.1
390-U1556C	53B	30°56.5406'S	26°41.9472'W	61.2	13.5	1250	5006	280.3	NA	280.3	283.8	101.3
390-U1556D	53B	30°56.5514'S	26°41.9472'W	61.2	13.5	1250	5003	9.5	NA	9.5	9.7	101.8
390-U1556E	53B	30°56.5622'S	26°41.9472'W	61.2	13.5	1250	5003	43.1	NA	43.1	43.3	100.5
							Site U1556 totals:	1249.9	582.0	958.9	772.5	74.2
390C-U1557A	56A	30°56.4549'S	26°37.7912'W	60.7	13.5	1243	5012	9.5	NA	9.5	9.6	101.4
390C-U1557B	56A	30°56.4547'S	26°37.7775'W	60.7	13.5	1243	5012	574.0	NA	574.0	414.9	72.3
390C-U1557C	56A	30°56.4646'S	26°37.7897'W	60.7	13.5	1243	5012	3.0	3.0	NA	NA	0.0
390C-U1557D	56A	30°56.4651'S	26°37.7892'W	60.7	13.5	1243	5011	64.2	64.2	NA	NA	0.0
395E-U1557D	56A	30°56.4651'S	26°37.7892'W	60.7	13.5	1243	5011	576.6	516.6	NA	NA	0.0
390-U1557D	56A	30°56.4651'S	26°37.7892'W	60.7	13.5	1243	5011	684.7	NA	109.1	71.3	65.3
							Site U1557 totals:	1271.2	583.8	692.6	495.9	39.8
390C-U1558A	43A	30°53.7728'S	24°50.4970'W	49.2	19.5	1067	4337	163.9	NA	163.9	138.7	84.6
390C-U1558B	43A	30°53.7707'S	24°50.4843'W	49.2	19.5	1067	4337	161.1	161.1	NA	NA	0.0
390C-U1558C	43A	30°53.7761'S	24°50.4942'W	49.2	19.5	1067	4337	162.7	162.7	NA	NA	0.0
390C-U1558D	43A	30°53.7814'S	24°50.4822'W	49.2	19.5	1067	4334	150.0	150.0	NA	NA	0.0
393-U1558D	43A	30°53.7814'S	24°50.4822'W	49.2	19.5	1067	4334	370.2	NA	220.2	100.8	45.8
393-U1558E	43A	30°53.7922'S	24°50.4822'W	49.2	19.5	1067	4337	9.5	NA	9.5	10.0	105.0
393-U1558F	43A	30°53.7923'S	24°50.4757'W	49.2	19.5	1067	4337	177.2	3.0	174.2	164.3	94.3
							Site U1558 totals:	1044.6	476.8	567.8	413.8	47.1
390C-U1559A	13A	30°15.6335'S	15°2.0942'W	6.6	17.0	130	3056	66.2	NA	66.2	58.0	87.6
390C-U1559B	13A	30°15.6336'S	15°2.0941'W	6.6	17.0	130	3055	58.9	58.9	NA	NA	0.0
393-U1559B	13A	30°15.6336'S	15°2.0941'W	6.6	17.0	130	3055	107.9	NA	49.0	12.8	26.2
390-U1559C	13A	30°15.6506'S	15°2.0911'W	6.6	17.0	130	3058	60.9	NA	60.9	56.8	93.3
390-U1559D	13A	30°15.6593'S	15°2.0906'W	6.6	17.0	130	3058	59.4	NA	59.4	43.6	73.4
							Site U1559 totals:	294.4	58.9	235.5	171.2	56.1
395E-U1560A	25A	30°24.2064'S	16°55.3718'W	15.2	25.5	315	3724	122.5	NA	122.5	119.0	97.2
395E-U1560B	25A	30°24.2057'S	16°55.3702'W	15.2	25.5	315	3724	124.0	124.0	NA	NA	0.0
393-U1560B	25A	30°24.2057'S	16°55.3702'W	15.2	25.5	315	3723	316.2	NA	192.2	74.8	38.9
393-U1560C	25A	30°24.2005'S	16°55.3703'W	15.2	25.5	315	3724	129.3	2.0	127.3	122.8	96.4
							Site U1560 totals:	568.0	126.0	442.0	316.6	58.1
395E-U1561A	55A	30°43.2902'S	26°41.7162'W	61.2	13.5	1250	4910	48.9	NA	48.9	45.4	92.9
395E-U1561B	55A	30°43.2902'S	26°41.7162'W	61.2	13.5	1250	4910	9.5	NA	9.5	9.6	101.4
395E-U1561C	55A	30°43.2902'S	26°41.7162'W	61.2	13.5	1250	4910	9.5	NA	9.5	10.2	107.4
							Site U1561 totals:	67.9	0.0	67.9	65.2	100.5
393-U1583A	33B	30°42.6060'S	20°26.0340'W	30.6	24.0	652	4210	9.1	NA	9.1	9.1	100.4
393-U1583B	33B	30°42.6062'S	20°26.0341'W	30.6	24.0	652	4210	9.4	NA	9.4	9.4	99.8
393-U1583C	33B	30°42.6011'S	20°26.0343'W	30.6	24.0	652	4215	107.5	NA	107.5	110.2	102.5
393-U1583D	33B	30°42.6288'S	20°26.0340'W	30.6	24.0	652	4210	9.5	NA	9.5	10.0	105.7
393-U1583E	33B	30°42.6285'S	20°26.0340'W	30.6	24.0	652	4210	105.2	NA	105.2	105.2	100.0
393-U1583F	33B	30°42.6175'S	20°26.0336'W	30.6	24.0	652	4210	239.5	101.0	138.5	45.8	33.1
							Site U1583 totals:	480.2	101.0	379.2	289.7	90.2
							South Atlantic Transect totals:	4976.2	1928.5	3343.9	2524.8	66.6

Table T2 (continued).

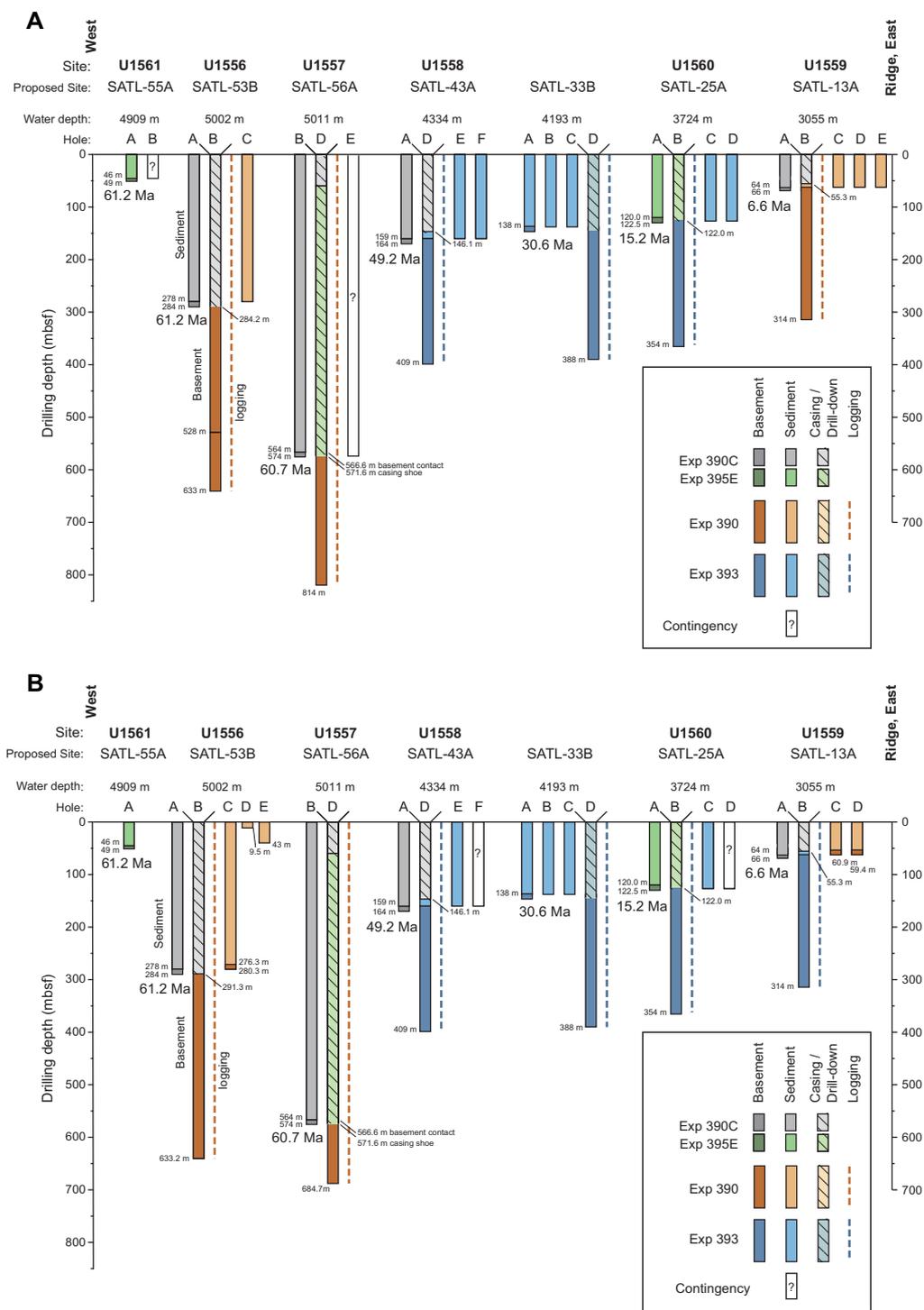| Hole	Proposed SATL site	Total cores (N)	APC cores (N)	HLAPC cores (N)	XCB cores (N)	RCB cores (N)	Depth to basement DSF (m)	Interval of recovered sediment/basement interface (cm)	Cores described during expedition	Start date	Start time (UTC) (h)	End date	End time (UTC) (h)	Time on hole (h)	Time on hole (days)
390C-U1556A	53B	33	16	0	17	0	278.3	30X-4, 72.5	390	28 Oct 2020	0130	01 Nov 2020	0310	97.7	4.07
395E-U1556B	53B	0	0	0	0	0	286.2	NA	NA	05 May 2021	0630	11 May 2021	0000	137.5	5.73
390-U1556B	53B	58	0	0	0	58	291.0	2R-1, 29.5	390	21 Apr 2022	2135	07 May 2022	0205	364.6	15.19
390-U1556C	53B	32	16	0	16	0	276.3	30X-CC, 31	390	07 May 2022	0205	10 May 2022	1720	87.4	3.64
390-U1556D	53B	1	1	0	0	0	NA	NA	390	10 May 2022	1720	10 May 2022	1920	1.9	0.08
390-U1556E	53B	5	5	0	0	0	NA	NA	390	10 May 2022	1920	11 May 2022	1330	18.2	0.76
Site U1556 totals:		129	38	0	33	58								707.3	29.5
390C-U1557A	56A	1	1	0	0	0	NA	NA	390	01 Nov 2020	0740	01 Nov 2020	1345	6.0	0.25
390C-U1557B	56A	66	11	0	55	0	564.0	63X-2, 87	390	01 Nov 2020	1345	09 Nov 2020	0110	179.5	7.48
390C-U1557C	56A	0	0	0	0	0	NA	NA	NA	09 Nov 2020	0110	09 Nov 2020	1835	17.5	0.73
390C-U1557D	56A	0	0	0	0	0	NA	NA	NA	09 Nov 2020	1835	12 Nov 2020	0808	61.4	2.56
395E-U1557D	56A	0	0	0	0	0	566.6	NA	NA	29 Apr 2021	2130	04 May 2021	1645	115.3	4.80
390-U1557D	56A	13	0	0	0	13	NA	NA	390	11 May 2022	1330	19 May 2022	0420	182.9	7.62
Site U1557 totals:		80	12	0	55	13								562.6	23.4
390C-U1558A	43A	19	11	0	8	0	158.9	18X-CC, 27	393	12 Nov 2020	1630	15 Nov 2020	0610	61.7	2.57
390C-U1558B	43A	0	0	0	0	0	155.9	NA	NA	15 Nov 2020	0610	18 Nov 2020	1900	84.7	3.53
390C-U1558C	43A	0	0	0	0	0	158.9	NA	NA	18 Nov 2020	1900	21 Nov 2020	0956	62.9	2.62
390C-U1558D	43A	0	0	0	0	0	NA	NA	NA	21 Nov 2020	0956	23 Nov 2020	2256	61.0	2.54
393-U1558D	43A	38	0	0	0	38	166.8	4R-1, 0	393	28 Jun 2022	0035	05 Jul 2022	0524	172.8	7.2
393-U1558E	43A	1	1	0	0	0	NA	NA	393	25 Jun 2022	1130	26 Jun 2022	0515	17.8	0.74
393-U1558F	43A	23	9	9	5	0	176.0	24X-CC, 16	393	26 Jun 2022	0515	28 Jun 2022	0035	43.4	1.81
Site U1558 totals:		81	21	9	13	38								504.2	21.0
390C-U1559A	13A	9	4	0	5	0	64.0	8X-CC, 13	390	25 Nov 2020	1640	26 Nov 2020	2120	28.6	1.19
390C-U1559B	13A	0	0	0	0	0	NA	NA	NA	26 Nov 2020	2120	28 Nov 2020	1715	43.9	1.83
393-U1559B	13A	12	0	0	0	12	65.0	3R-1, 9	393	20 Jun 2022	0630	23 Jun 2022	1230	78.0	3.25
390-U1559C	13A	7	6	0	1	0	59.0	NA	390	21 May 2022	1650	22 May 2022	1255	20.2	0.84
390-U1559D	13A	8	6	0	2	0	57.4	7X-CC, 9	390	22 May 2022	1255	23 May 2022	1740	28.8	1.2
Site U1559 totals:		36	16	0	8	12								199.4	8.3
395E-U1560A	25A	16	11	0	5	0	120.2	15X-CC, 0	393	22 Apr 2021	0230	24 Apr 2021	1515	60.7	2.53
395E-U1560A	25A	0	0	0	0	0	123.0*	NA	NA	24 Apr 2021	1515	28 Apr 2021	0000	80.6	3.36
393-U1560B	25A	40	0	0	0	40	123.0*	NA	393	19 Jul 2022	0124	28 Jul 2022	2355	238.6	9.94
393-U1560C	25A	17	10	5	2	0	129.0	18X-2, 0	393	28 Jul 2022	2355	30 Jul 2022	1926	43.4	1.81
Site U1560 totals:		73	21	5	7	40								423.4	17.6
395E-U1561A	55A	9	6	0	3	0	46.2	6H-CC, 21	390	11 May 2021	0345	13 May 2021	1145	55.9	2.33
395E-U1561B	55A	1	1	0	0	0	NA	NA	390	11 May 2021	0345	13 May 2021	1145	55.9	2.33
395E-U1561C	55A	1	1	0	0	0	NA	NA	390	11 May 2021	0345	13 May 2021	1145	55.9	2.33
Site U1561 totals:		11	8	0	3	0								167.8	7.0
393-U1583A	33B	1	1	0	0	0	NA	NA	393	06 Jul 2022	0324	06 Jul 2022	1615	13.0	0.54
393-U1583B	33B	1	1	0	0	0	NA	NA	393	06 Jul 2022	1615	06 Jul 2022	1800	1.7	0.07
393-U1583C	33B	13	12	0	1	0	106.0	13X-1, 0	393	06 Jul 2022	1800	07 Jul 2022	1540	21.6	0.9
393-U1583D	33B	1	1	0	0	0	NA	NA	393	07 Jul 2022	1540	07 Jul 2022	1730	1.9	0.08
393-U1583E	33B	12	12	0	0	0	NA	NA	393	07 Jul 2022	1730	10 Jul 2022	0430	59.0	2.46
393-U1583F	33B	28	0	0	0	28	109.7	3R-1, 0	393	10 Jul 2022	0430	18 Jul 2022	0845	196.3	8.18
Site U1583 totals:		56	27	0	1	28								293.5	12.2
South Atlantic Transect totals:		466	143	14	120	189								2858.2	119.1

Figure F15. A. Engineering and coring operations completed during Expeditions 390C and 395E and planned SAT operations prior to Expedition 390. B. A modified to show operations completed during Expeditions 390C, 395E, and 390 and planned operations for Expedition 393. (Continued on next page.)
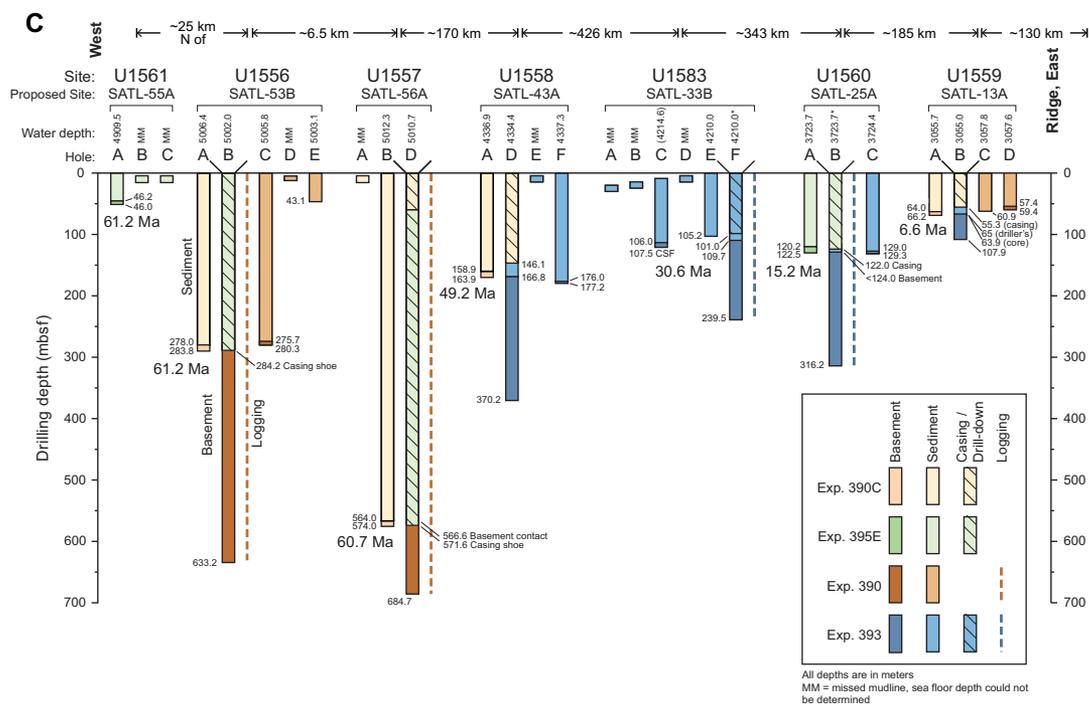
Figure F15 (continued). C. Operations completed during SAT Expeditions 390C, 395E, 390, and 393. MM = missed mudline.

Table T3. Comparison of SAT proposed targets with operational achievements at end of Expedition 393. Proposed objectives: * = achieved, † = mostly achieved, ‡ = partially achieved, ** = not achieved. NA = not applicable. (Continued on next page.) **Download table in CSV format.**

Site information	Sediment coring (coring system, expedition-hole)	Basement depth (msb)	Wireline operations	Legacy installations
Site U1559 (proposed Site SATL-13A); 6.6 Ma				
Proposal/*Scientific Prospectus* 2020	3× APC to basement	250	2× FMS + triple combo + UBI	Reentry cone case near basement
Expeditions 390C and 395E	390C-U1559A†	250	2× FMS + triple combo + UBI	390C-U1559B
Scientific Prospectus Addendum 2022				*
Revised operational plan May 2022	390-U1559C, 390-U1559D*	250	2× FMS + triple combo + UBI	*
Achieved—end of Expedition 393	*	43**	No logging**	*
Site U1560 (proposed Site SATL-25A); 15.2 Ma				
Proposal/*Scientific Prospectus* 2020	3× APC to basement	250	2× FMS + triple combo + UBI	Reentry cone case near basement
Expeditions 390C and 395E	395E-U1560A†	250	2× FMS + triple combo + UBI	395E-U1560B*
Scientific Prospectus Addendum 2022	2× APC			*
Revised operational plan May 2022	1× APC	150	2× FMS + triple combo + UBI	*
Achieved—end of Expedition 393	393-U1560C†	193†	2× FMS + triple combo + UBI‡	*
Site U1583 (proposed Site SATL-33B); 30.6 Ma				
Proposal/*Scientific Prospectus* 2020 Expeditions 390C and 395E	3× APC to basement	250	2× FMS + triple combo + UBI	Reentry cone case near basement
Scientific Prospectus Addendum 2022	3× APC	250	2× FMS + triple combo + UBI	Reentry cone case near basement
Revised operational plan May 2022	2× APC	250		Free-fall funnel
Achieved—end of Expedition 393	393-U1583C, 393-U1583E‡	129.8‡	1× FMS + triple combo‡	393-U1583F**
Site U1558 (proposed Site SATL-43A); 49.2 Ma				
Proposal/*Scientific Prospectus* 2020	3× APC to basement	250	2× FMS + triple combo + UBI	Reentry cone case near basement
Expeditions 390C and 395E	390C-U1558A	250		390C-U1558B*
Scientific Prospectus Addendum 2022	2× APC	250		*
Revised operational plan May 2022	1× APC	175		*
Achieved—end of Expedition 393	393-U1558F‡	203.5†	No logging**	Reentry system destroyed**
Site U1557 (proposed Site SATL-56A); 61.2 Ma				
Proposal/*Scientific Prospectus* 2020	APC/XCB to basement	250	2× FMS + triple combo + UBI	Reentry cone case near basement
Expeditions 390C and 395E	390C-U1557B*			390C/395E-U1557D*
Scientific Prospectus Addendum 2022		247		*
Revised operational plan May 2022				*
Achieved—end of Expedition 390		118‡	Triple combo‡	*

Table T3 (continued).

Site information	Sediment coring (coring system, expedition-hole)	Basement depth (msb)	Wireline operations	Legacy installations
Site U1556 (proposed Site SATL-53B); 61.2 Ma				
Proposal/*Scientific Prospectus* 2020	APC/XCB to basement	250	2× FMS + triple combo + UBI	Reentry cone case near basement
Expeditions 390C and 395E	390C-U1556A*			395E-U1556B*
Scientific Prospectus Addendum 2022		350		*
Revised operational plan May 2022	1× APC/XCB			*
Achieved—end of Expedition 390	390C-U1556A, 390-U1556C, and 390-U1556E*	353*	*	Reentry system lost**
Site U1561 (proposed Site SATL-55A); 61.2 Ma				
Proposal/*Scientific Prospectus* 2020	Alternative site 1× APC	NA	NA	NA
Expeditions 390C and 395E	395E-U1561A*			
Scientific Prospectus Addendum 2022				
Revised operational plan May 2022				
Achieved—end of Expedition 390	395E-U1561A*			

8. South Atlantic Transect drill sites

The SAT drilled during Expeditions 390C, 395E, 390, and 393 comprises the following seven sites from youngest to oldest:

- Site U1559 (proposed Site SATL-13A; Expeditions 390C, 390, and 393) is located nearest to the Mid-Atlantic Ridge on 6.6 Ma crust formed at a half-spreading rate of 17 mm/y and overlain by ~64 m of sediment. This site provides a comparison to young intermediate-spreading rate ocean crust drilled in reference Hole 504B (6.9 Ma; spreading rate of 36 mm/y; 275 m of sediment).
- Site U1560 (proposed Site SATL-25A; Expeditions 395E and 393) is located on 15.2 Ma crust formed at 25.5 mm/y and overlain by ~120 m of sediment. This site provides a comparison to reference superfast-spreading rate ocean crust at Site 1256 (15 Ma; spreading rate of 220 mm/y; 250 m of sediment).
- Site U1583 (proposed Site SATL-33B; Expedition 393) is located on 30.6 Ma crust formed at 24 mm/y and overlain by ~106 m of sediment.
- Site U1558 (proposed Site SATL-43A; Expeditions 390C and 393) is located on 49.2 Ma crust formed at 19.5 mm/y and overlain by ~159 m of sediment.
- Site U1557 (proposed Site SATL-56A; Expeditions 390C, 395E, and 390) is located on ~60.7 Ma crust formed at 13.5 mm/y and overlain by ~564 m of sediment.
- Site U1556 (proposed Site SATL-53B; Expeditions 390C, 395E, and 390) is located on 61.2 Ma crust ~6.5 km west of Site U1557 in the same localized sedimentary basin and has a sediment thickness of ~278 m.
- Site U1561 (proposed alternate Site SATL-55A; Expeditions 395E and 390) is located on ~61.2 Ma crust ~25 km north of Site U1556 and has a sediment thickness of ~46 m.

9. Site summaries

9.1. Site U1556

9.1.1. Background and objectives

Site U1556 is in the western South Atlantic Ocean ~1250 km west of the Mid-Atlantic Ridge at a depth of ~5000 mbsl (Figures **F1**, **F16**). Site U1556 was previously occupied during engineering Expeditions 390C and 395E, during which the sediment succession and uppermost <6 m of basement were cored with the APC/XCB system (Hole U1556A). A reentry system with casing that extends almost to the sediment/basement interface was installed in Hole U1556B. The main objectives for visiting Site U1556 during Expedition 390 were to (1) core a second hole with the APC/XCB system to recover the complete sediment succession (via stratigraphic correlation with Hole U1556A) and sample the sediment/basement interface and (2) core 350 m into basement with the RCB system in Hole U1556B (Figure **F15A**). Sediment and interface cores provide

samples that address the microbiological, geochemical, and paleoceanographic objectives of the SAT expeditions, and basement cores provide material that addresses the petrologic, geochemical, and microbiological objectives of the SAT expeditions.

Site U1556 is located 6.7 km west of Site U1557 with basement predicted to have formed at ~61.2 Ma at a half-spreading rate of ~13.5 mm/y. Ocean crust at these sites is the oldest of all sites drilled during the SAT expeditions. The mineralogy and extent of alteration of the basement rocks at Site U1556, changes in physical properties such as porosity, and the composition of the microbial communities will be compared to the same characteristics at the other sites along the transect to investigate the nature of crustal aging and the development of hydrothermal circulation in upper ocean crust formed at slow- to intermediate-spreading rate MORs. The sedimentary cover at Site U1556 is about half as thick as at Site U1557, and contrasts between these closely spaced sites will allow exploration of the blanketing effect of sediment of different thicknesses on hydrothermal circulation.

9.1.2. Operations

Site U1556 was first visited during engineering Expedition 390C, with the goal of coring a single APC/XCB hole to basement for gas safety monitoring and installing a reentry system with casing through sediment to ~5 m into basement; however, failure of the subsea camera system prevented installation of the reentry system at Site U1556. Engineering Expedition 395E returned to Site U1556 and installed a HRT reentry system with 284.2 m of 10¾ inch casing in Hole U1556B (Table **T1**). Casing did not extend into basement in Hole U1556B because of thicker than expected sediment locally, resulting from either a shallower seafloor or deeper basement compared to nearby Hole U1556A.

9.1.2.1. Transit

During Expedition 390, *JOIDES Resolution* completed its 2296 nmi voyage from Cape Town, South Africa, to Site U1556 on 20 April 2022, arriving at 2330 h (UTC + 2 h). Overall, the vessel averaged 11.1 kt and took 8.6 days to complete the transit.

9.1.2.2. Hole U1556B

Operations at Site U1556 started with reentry in Hole U1556B and basement coring with the RCB system. Reentry was made at 0405 h on 22 April 2022, and the hole was washed down to 291.0 mbsf, where the bit contacted a hard layer. This depth is deeper than the 286.2 mbsf hole bottom observed during Expedition 395E; whether this discrepancy is due to subsidence of the reentry system, tidal variation in water depth, or another factor remains undetermined. During the first reentry, we observed that the cone was below the sediment surface, making this reentry and
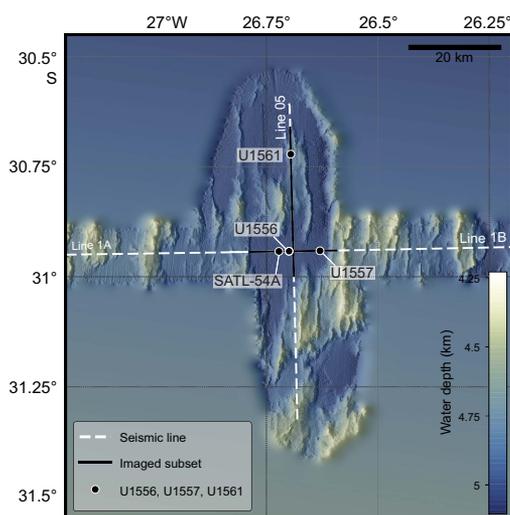

Figure F16. Sites U1556, U1557, and U1561 bathymetry (Christeson and Reece, 2020). Seismic reflection profiles were acquired during CREST cruise (Reece et al., 2016).

subsequent reentries challenging. Poor recovery and low penetration rates led to the decision to primarily drill half-length cores in Hole U1556B.

Coring progressed smoothly from Cores 390-U1556B-2R through 28R, at which time the bit had completed 61 h of drilling time and we conducted a bit change. Core 35R experienced high pump pressures (>2400 pounds per square inch [psi]), and the core barrel was retrieved so that we could attempt to restore circulation. The deplugger tool was deployed, and several mud sweeps were run, which successfully returned circulating pressure to normal coring values. Core 59R was the last core for the hole. The RCB bit, having completed 78 h of drilling time without failure, was dropped at the bottom of the hole using the mechanical bit release (MBR). We then pulled out of the hole, setting the pipe depth to 41 mbsf to prepare for logging operations. This hole was not preserved as a legacy hole because of the subsidence of the reentry cone. RCB drilling in Hole U1556B overall advanced 342.2 m to 633.2 mbsf and recovered 191.87 m of basement material (56%; Table **T2**; Figure **F15B**). Microbial contamination tracer was pumped with the drilling fluid throughout RCB coring in Hole U1556B.

To assist with logging, the hole was cleaned by pumping twice the hole's volume of seawater. The triple combo logging tool string, including tools for measuring natural gamma radiation (NGR), borehole diameter, formation density, resistivity, and magnetic susceptibility (MS), was lowered until it tagged hole bottom. Tool string telemetry failed after only a few meters of logging, and the string was pulled back to the surface and recovered. The Hostile Environment Natural Gamma Ray Sonde (HNGS) was identified as the issue, and a spare tool was substituted into the string. The second attempt at logging was successful. Two additional tool strings were then run: the UBI and Accelerator Porosity Sonde (APS) tool string, and the FMS tool string, which logged two upward passes. Following completion of logging, the ship was repositioned 30 m south of Hole U1556B to prepare to drill Hole U1556C. Hole U1556B used 16.2 days of operational time in total (Table **T2**).

9.1.2.3. Holes U1556C, U1556D, and U1556E

Three APC/XCB sediment holes were cored at Site U1556 during Expedition 390: Hole U1556C was cored to 280.3 mbsf, Hole U1556D was terminated after a missed mudline core, and Hole U1556E resampled the top 43.1 m of sediment for microbiology and geochemistry objectives (Table **T2**; Figure **F15B**). In Hole U1556C, coring progressed through Core 390-U1556C-30X, which recovered basalt fragments in the core catcher. Overall, Cores 1H–30X penetrated to 276.3 mbsf and recovered 281.74 m of sediment (102%). Cores 31X and 32X advanced another 4 m into basement to 280.3 mbsf, recovering 2.07 m (52%). APC cores in Hole U1556C (Cores 1H–16H) were collected using nonmagnetic core barrels and oriented for paleomagnetic research using the Icefield MI-5 core orientation tools. Formation temperature measurements were made while collecting Cores 4H, 7H, 10H, and 13H using the APCT-3 tool. In Hole U1556E 40 m south of Hole U1556C, coring progressed through Core 390-U1556E-5H in a water depth of 5003.1 m, achieving a final hole depth of 43.1 mbsf and recovering 43.33 m (100.5%). Cores from Hole U1556E were not oriented, and no temperature measurements were made. APC/XCB coring in Holes U1556C–U1556E took 4.5 days of operations time overall (Table **T2**).

9.1.3. Principal results

Site U1556 cores comprise two sedimentary units as well as 13 basement units, identified on the basis of macro- and microscopic visual observations combined with mineralogical analyses (by X-ray diffraction [XRD] for sediment), color reflectance, and MS data. The units are numbered from the top of the hole, with units in the sedimentary section designated by Roman numerals and basement units designated by Arabic numerals; subunits are designated with letters. The sediment/basement interface was recovered at three different depths below seafloor in Holes U1556A–U1556C. Differences in basement depth are likely attributable to basement topography and subsequently different sediment thicknesses but may also be due to differences in seafloor height. For stratigraphic correlation across holes and reporting, basement was defined at 290.29 mbsf based on the first occurrence of basalt in Hole U1556B, the hole with the reentry system and casing where we conducted basement drilling.

9.1.3.1. Sediments

9.1.3.1.1. Sedimentology

In the five holes cored at Site U1556, a mixture of biogenic and siliciclastic sediments were recovered (Figure **F17**). The former typically consists of pinkish white or light gray calcareous nannofossil ooze that is lithified to chalk downhole. Variable but minor amounts of foraminifera are present throughout. Siliciclastic sediment consists of silty clays that range from brown/dark brown where carbonate is absent to reddish brown where the carbonate content is higher. Two lithologic units (I and II) are defined based on a combination of visual observations of sedimentologic characteristics, microscopic examination of smear slides and bulk mineralogical analysis by XRD, integrated with MS, and color reflectance observations. Lithologic Unit I is composed of ~235 m of upper Oligocene to Pleistocene sediments, mainly silty clay and calcareous nannofossil ooze. Lithologic Unit II is composed of ~42 m of Paleocene or Eocene sediments, predominantly nannofossil-rich calcareous chalk or calcareous nannofossil chalk. Differences in mineral assemblages are relatively small with increasing burial depth within the respective silty clay and ooze/chalk phases. Below the sediment/basement interface is a transitional unit that comprises both pelagic sedimentary material and volcanic clasts where the sediment matrix is composed of calcareous chalk with clay.

9.1.3.1.2. Biostratigraphy

Calcareous nannofossil and planktic foraminifera biostratigraphy was performed on core catcher samples recovered from Hole U1556A (collected during Expedition 390C and examined on shore) and at a higher resolution (utilizing both core catchers and additional samples from the working half of each core) from Hole U1556C. Additional calcareous nannofossil and planktic foraminifera samples were taken from Hole U1556A archive halves and Hole U1556C working halves to refine the biostratigraphic zonation. Calcareous nannoplankton are present in the oozes and chalks but are mostly absent from the clays; planktic and benthic foraminifera are also mostly absent from the clays and have variable abundance in the nannofossil oozes of Unit I, in which they commonly comprise depauperate assemblages of mostly very small specimens (Figure **F18**).

Sedimentation rates appear to be relatively continuous from the Holocene through the early Oligocene (Figure **F19**). A ~44 m thick condensed interval or unconformity composed of dark brown pelagic clay spans the early Oligocene to early Eocene at Site U1556. Below this unconformity, the Eocene extends from ~216 to 266 m core depth below seafloor, Method B (CSF-B). Eocene assemblages contain significant reworking of Paleocene calcareous nannofossils and foraminiferal taxa that appear to be principally or entirely sourced from the middle Paleocene planktic foraminifera Zone P4a and calcareous nannoplankton Zones NP5/CNP8–CNP7, including a coherent slump deposit that contains an entirely Paleocene assemblage. Increasing reworking downhole makes precise age determinations difficult, but the middle Eocene (likely below planktic foraminifera Zone E5 and calcareous nannofossil Zones NP11/CNE3) unconformably overlies the middle Paleocene in the lowermost part of the sediment section, representing an interval of missing time spanning at least 5 My and up to 10 My. Samples directly above the in-place Paleocene sediments contain an increased proportion of benthic foraminifera and broken planktic foraminifera. Samples below the Paleocene–Eocene unconformity are middle Paleocene in age (planktic foraminifera Zone P4a and calcareous nannofossil Zones NP5/CNP8–CNP7).

To constrain the age of basement at Site U1556, samples were taken as close to the sediment/basement interface as possible and comprise the same middle Paleocene assemblages of planktic foraminifera and calcareous nannofossils. A thin section from a sediment lens in the deepest core in Hole U1556B (~633 m CSF-B) recorded a planktic foraminifera assemblage in Zone P4a. This suggests that the entire 341 m sequence of basalt cored at Site U1556 must have been erupted within 220 ky, or between 60.54 and 60.76 Ma (based on the global calibration for the duration of Zone P4a by Gradstein et al., 2020) because sediments at the sediment/basement interface and at the bottom of the basement were deposited within the same planktic foraminifera zone.

Benthic foraminifera indicate that Site U1556 was at lower bathyal depths in the Paleocene and early Eocene before subsiding to its present abyssal depth by the Pliocene. Subsidence likely occurred even earlier, but the lack of benthic foraminifera in the intervening samples makes a precise determination impossible.

Figure F17. Stratigraphic summary of representative sediment holes at each Expedition 390 site, Holes U1556C, U1557B, U1561A, and U1559C. For epoch, see Figure F19. a* (red–green) is smoothed with 100 point moving average. cps = counts per second. NGR and magnetic susceptibility (point source) are plotted on CSF-B depth scale.

Sieved residues from Site U1556 contain varying abundances of broken fish debris (most abundant in pelagic clays), siliceous microfossils (diatoms, radiolarians, and sponge spicules), and authigenic manganese (Mn) oxide. Siliceous material is most common in the Pliocene–Pleistocene and then again in the middle Oligocene. Mn oxides are primarily found in the Neogene.

9.1.3.1.3. Paleomagnetism

Paleomagnetic investigation of Site U1556 sediments included remanence analysis of cores split during engineering Expedition 390C alongside Expedition 390 analyses of the archive halves of Sections 390C-U1556A-30X-1 through 30X-4 (the portion of Core 30X above basement) and Cores 390-U1556C-1H through 30X, 390-U1556D-1H, and 390-U1556E-1H through 5H on the superconducting rock magnetometer (SRM) and 59 discrete sediment samples primarily from Hole U1556C. We use these data to establish a magnetostratigraphy for the sediment package at Site U1556, which will be refined with additional analysis postexpedition. All three Expedition 390 holes display clear polarity reversals that can be tied to Hole U1556A for magnetostratigraphic correlation. Furthermore, Hole U1556C recovered material from depth intervals that were not recovered in Hole U1556A, including near the base of the sediment package, which will allow better constraint of the basal age.

Anisotropy of magnetic susceptibility (AMS) and bulk susceptibility were measured on all discrete cubes. AMS is routinely used as a petrofabric proxy to determine the preferred alignment of the magnetic mineral assemblage under an external field, and bulk susceptibility is used to determine the concentration of magnetic material present. Likewise, all cubes were alternating field (AF) demagnetized, up to 190 mT in some instances. Stepwise demagnetization characterizes, to a first order, the dominant magnetic mineral assemblage and allows determination of the characteristic remanent magnetization (ChRM) of the sample, which reflects the magnetic field direction at or soon after sediment deposition and aids in the magnetostratigraphic interpretation. Acquisition of isothermal remanent magnetization (IRM) and backfield IRM experiments were performed on a subset of discrete samples to characterize the magnetic mineral assemblage. Both the AF demag-
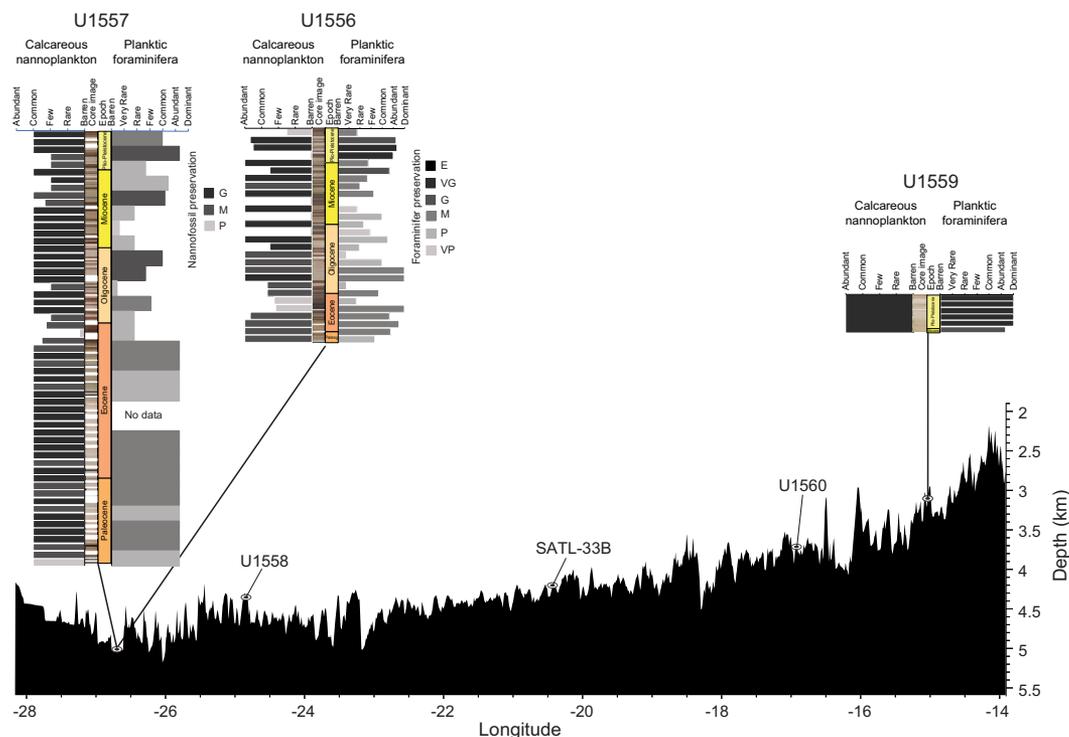

Figure F18. Summary of calcareous nannoplankton and planktic foraminifera abundance and preservation across the SAT and plotted in 10 m thick bins (except Site U1557 foraminifera, which are binned at 20 m because of sample resolution) and shown above seafloor bathymetry measured during CREST cruise (Reece and Estep, 2019), Expedition 390. Preservation: E = excellent, VG = very good, G = good, M = moderate, P = poor, VP = very poor.

netization and IRM experiments suggest the presence of titanomagnetites/titanomaghemites of various oxidation states and/or grain sizes. Of the 59 discrete sediment samples, 49 samples had orthogonal vector plots (OVPs) "clean" enough to contribute to defining the ChRM, and only 28 samples gave maximum angular deviation angles of less than 15°.

9.1.3.1.4. Sediment age model and mass accumulation rate

The age model for Site U1556 was constructed using calcareous nannoplankton and planktic foraminifera bioevents and paleomagnetic reversal datums from Hole U1556C, which is the best recovered hole at Site U1556 and the most densely sampled for biostratigraphy. Overall, the sediment section ranges in age from middle Paleocene to Holocene, with a ~10 My unconformity/condensed interval spanning the middle Eocene to earliest Oligocene and a ~5 My unconformity spanning the middle Paleocene to early Eocene. Overall sedimentation rates average 0.58 cm/ky from the early Oligocene to Holocene (0–32.1 Ma) and 0.36 cm/ky in the early Eocene between the unconformities (46.7–53.6 Ma; Figure F19). Mass accumulation rates at Site U1556 are generally highest from the Late Miocene to Holocene (up to 1.01 $g/cm^2/ky$) and in the early Oligocene (up to 1.3 $g/cm^2/ky$) and tend to covary with carbonate accumulation rate, indicating that sedimentation is primarily driven by pelagic carbonate production. Organic carbon accumulation rates are very low at Site U1556, with a maximum value of 0.003 $g/cm^2/ky$, in the early Eocene.

9.1.3.1.5. Physical properties and downhole measurements

Physical properties characterization of the sediment section at Site U1556 was based on cores and in situ downhole measurements from Holes U1556A and U1556C and wireline logging data from Hole U1556B. Whole-round core-based measurements included NGR (sensitive to the abundance of minerals containing radioisotopes of K, U, and Th), bulk density from gamma ray attenuation
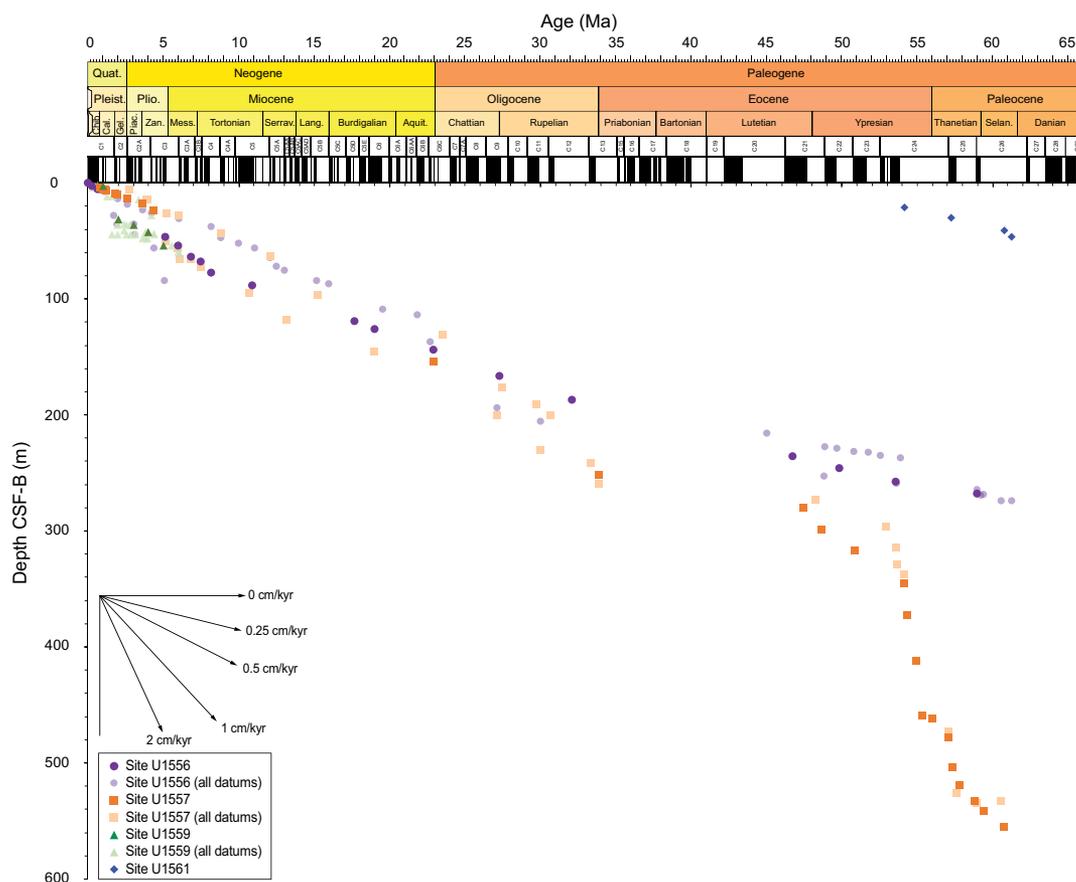

Figure F19. Age-depth plots, Expedition 390. Lighter symbols = all biostratigraphic and magnetostratigraphic datums, darker symbols = datums used to construct age-depth models at each site. Inset to interpret sedimentation rates for the age transect is also shown.

(GRA), MS (an indicator of the concentration of magnetic minerals), and *P*-wave velocity. Discrete measurements of moisture and density (MAD; to estimate grain density and porosity), thermal conductivity, triaxial *P*-wave velocity, and rheological properties (shear and compressional strength) were made on samples from working-half sections. Trends in the physical properties and downhole logging data generally correlate well with lithologic units.

NGR values are generally low and vary from 6 to 20 counts/s in calcareous nannofossil ooze/chalk and moderate with variability up to 65 counts/s in silty clay (Figure **F17**). Spectral gamma data from wireline logging show clearly defined intervals of lower and higher values, consistent with the presence of alternating ooze/chalk and silty clay, respectively. At Site U1556, spectral gamma ray logs show that the NGR signal comes largely from the radioactive isotopes of potassium and thorium, with additional contributions from uranium in the higher gamma ray, silty clay layers. Sediment lithologic unit boundaries coincide with sharp changes in NGR, as well as MS. MS values are low (0–60 instrument units [IU]) in carbonate-dominated lithologies and high (up to 250 IU) in silty clays (Figure **F17**). Bulk density and *P*-wave velocity generally increase with depth in the sedimentary section, which is consistent with a compaction trend. Both are generally locally anticorrelated with natural gamma ray and MS, indicating that oozes and chalks are denser with higher velocities than silty clay lithologies. Discrete porosity values in sediments decrease downhole, with some variation that is likely related to lithology but also to drilling disturbance in XCB cores. Mean thermal conductivity in sediments ranges 0.8–1.5 W/(m·K).

Eight successful downhole temperature measurements were made in sediments at Site U1556 with the APCT-3 tool. Measurements were made while drilling Cores 4H, 7H, 10H, and 13H in both Holes U1556A and U1556C, extending temperature data to 123 mbsf. Linear temperature profiles varied between the two holes, with a geothermal gradient of 15°–36°C/km.

Data from cores recovered using the APC/XCB system in Holes U1556A, U1556C, U1556D, and U1556E were correlated to produce a near-continuous shipboard splice for the upper 195.6 m core composite depth below seafloor (CCSF). The correlation is primarily based on changes in MS, NGR, and density in cores from Holes U1556A and U1556C that correspond to lithologic variations between silty clay and nannofossil ooze/chalk. Hole U1556D and U1556E stratigraphy can be correlated to fill gaps in the upper ~40 mbsf of the splice generated between Holes U1556A and U1556C. The composite depth scale will facilitate future sampling at higher resolution. Deeper than 195 m CCSF, physical properties records from Holes U1556A and U1556C are consistent and can be tentatively correlated, but the construction of a detailed composite section is not possible.

9.1.3.1.6. Sedimentary and pore water geochemistry

During the sediment drilling in Holes U1556A, U1556C, and U1556E, interstitial water (IW) samples were extracted via squeezing. For APC coring, IW whole-round samples were taken at a frequency of two per core during Expedition 390 (Hole U1556C) and one per core during Expedition 390C (Hole U1556A). One IW sample per core was taken during XCB drilling. Sampling frequency of the squeezed IW increased to two per core within 40 m above the basement. Rhizon IW samples were taken from Holes U1556C and U1556E for postexpedition research. Shipboard analyses of the squeezed IW from Holes U1556A and U1556C include pH, salinity, alkalinity, major cations and anions (sodium, calcium, magnesium, potassium, chloride, and sulfate) using ion chromatography (IC), major and minor elements using inductively coupled plasma–atomic emission spectroscopy (ICP-AES), nutrients (phosphate and ammonium), and sulfide on the spectrophotometer. Carbonate and total carbon measurements were then conducted on the squeeze cake and selected samples from the working half. The remaining IW and squeeze cake were distributed to scientists for postexpedition research. Dissolved oxygen in IW was also measured in Holes U1556C and U1556E using optical oxygen sensors, with a resolution of ~1–5 m.

Data generated from Hole U1556A and U1556C IW samples are very similar. They both show a strong redox gradient in the top ~100 m, with decreasing sulfate and increasing dissolved manganese and ammonium concentrations consistent with organic carbon respiration. Below ~260 m CSF-B in both holes, sulfate concentrations increase, and dissolved manganese concentrations are minimal (Figure **F20**). Maxima in silica concentrations at ~5 and ~150 m CSF-B may reflect biogenic silica dissolution. Carbonate contents vary depending on lithology (up to ~93 wt% in the

carbonate ooze/chalk and often <1 wt% in the silty clay), whereas the organic carbon concentrations are all less than 1 wt%.

9.1.3.1.7. Microbiology

Microbiological sediment samples were collected from Holes U1556C (Cores 390-U1556C-1H through 31X) and U1556E (Cores 390-U1556E-1H through 5H). Samples destined for physiology experiments were processed in the anaerobic chamber in the walk-in cold room, whereas samples destined for postexpedition cell counts and nucleic acid analysis were conducted at room temperature between two KOACH air-filtering units to mitigate contamination. This dual setup allowed faster sample processing. To test for potential microbial contamination, drilling fluid was collected during coring of Hole U1556C on 9 May 2022 and Hole U1556E on 10 May. During postexpedition research, DNA will be extracted from these samples to create a database of potential contaminants for comparison with cored samples.

9.1.3.2. Volcanic rocks

9.1.3.2.1. Igneous petrology

In Hole U1556B, 342.3 m of igneous rock, including breccias, was cored after the igneous basement was reached at 291.4 mbsf. The igneous rock succession consists predominantly of pillow lavas, with thin intervals of either more massive lava flows or larger pillows, all punctuated by periodic occurrences of breccias (Figure **F21**). The igneous sequence was divided into 13 lithologic units based on changes in petrographic type and phenocryst assemblage. The lithologic units were grouped into three overarching stratigraphic sequences (A: Sections 390-U1556B-2R-2 through 38R-2; B: interval 38R-3 through 54R-3, 130 cm; and C: interval 54R-3, 130 cm, through 59R-4; Figure **F22**). The uppermost 5.1 and 4.7 m of the igneous sequence at Site U1556 were also recovered in Holes U1556A and U1556C, respectively.

The uppermost igneous basement, and the top of Stratigraphic Sequence A, comprises a 11.7 m thick sedimentary breccia (Lithologic Unit 1), which probably represents talus deposits of volcaniclastic debris transported downslope via a gravity flow. Beneath this is a series of sparsely to moderately olivine phyric basalt pillow lava flows interspersed with volcanic breccias in Lithologic Units 2–11. The breccias contain clasts of chilled pillow margins and variably altered glass, but the proportions of sedimentary matrix and carbonate cement vary significantly between breccia units. Lithologic Unit 12, which has six subunits, corresponds to Stratigraphic Sequence B. It consists of a series of aphyric to very sparsely olivine (micro)phyric basalts that are highly altered. Lithologic Unit 11 is noteworthy in that it records intrusive relationships between the lavas of Stratigraphic Sequences A and B. Stratigraphic Sequence C corresponds to Lithologic Unit 13, which is a highly
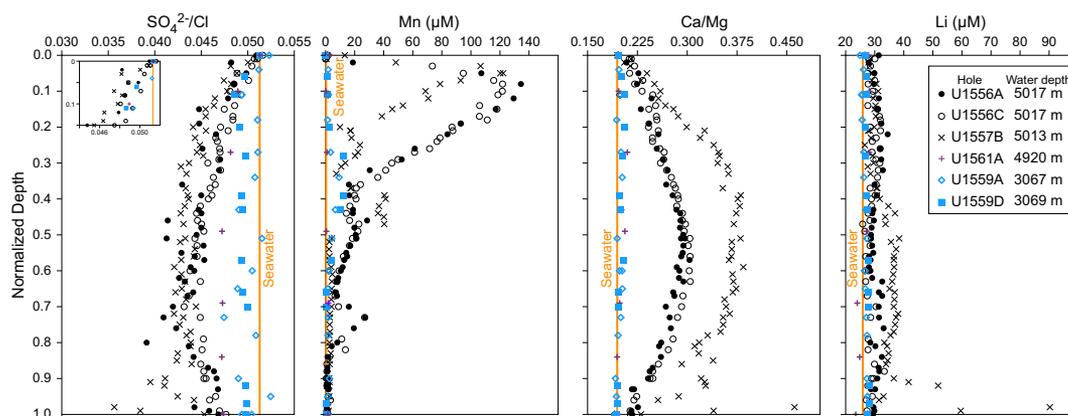

Figure F20. IW chemistry along SAT, Expedition 390. Orange lines = standard seawater values (SO_4^{2-}/Cl = 28 mM/546 mM, Mn = 0.36 µM, Ca/Mg = 10.27 mM/52.7 mM, Li = 25.9 µM) taken from Monterey Bay Aquarium Research Institute (MBARI) Periodic Table of Elements in the Ocean (**https://www.mbari.org/know-your-ocean/periodic-table-of-elements-in-the-ocean**). Sediment depths were normalized to maximum sediment thickness of each hole to compare variations in IW chemical profiles (0 = near mudline, 1 = near basement). Inset on SO_4^{2-}/Cl plot shows depth dependent decrease in ratios in all holes between 0 and 0.15 normalized depth.

plagioclase-olivine-clinopyroxene phyric basalt that contains cognate inclusions interpreted as cumulates formed in a magma chamber.

9.1.3.2.2. Alteration petrology

All the rocks recovered from Site U1556 are altered to some degree. Alteration manifests as a wide range of styles and extents from slight to moderate background alteration all the way to almost complete oxidation and replacement of groundmass and phenocrysts. The pattern of this alteration is strongly spatially controlled at the scale of individual sections and is primarily related to the locations of veins and the chilled margins of igneous flows/pillows which have provided free surfaces for fluid-rock interactions (Figures **F21**, **F22**). The overall degree of alteration broadly increases downhole and is closely related to the igneous stratigraphy and emplacement style of the basalts. Altogether, 5000 veins and vein networks, 600 intervals of breccia cement, and 320 occurrences of filled vesicles were recorded in Hole U1556B. The most abundant fill phases include smectite clays, carbonate, Fe oxyhydroxides, and zeolites. A range of different alteration styles characterize the cores and, together with cross-cutting relationships, indicate a potentially prolonged sequence of alteration under a variety of conditions both oxidative and more reducing.

9.1.3.2.3. Paleomagnetism

Discrete cube samples for paleomagnetic analysis were collected from representative basalts recovered from Hole U1556B, targeting both fresher basalts and those with varying extents and styles of alteration. Both AF demagnetization of the natural remanent magnetization (NRM) and acquisition of IRM indicate a variety of coercivities for the ferromagnetic phases present in samples, requiring fields up to 190 mT to fully demagnetize NRM. The contributing ferromagnetic minerals cannot be determined without additional shore-based work. Most samples carry a well-defined single-component remanence with positive inclinations (reversed polarity) compatible with the rock age. An additional component of negative inclination was observed in brecciated
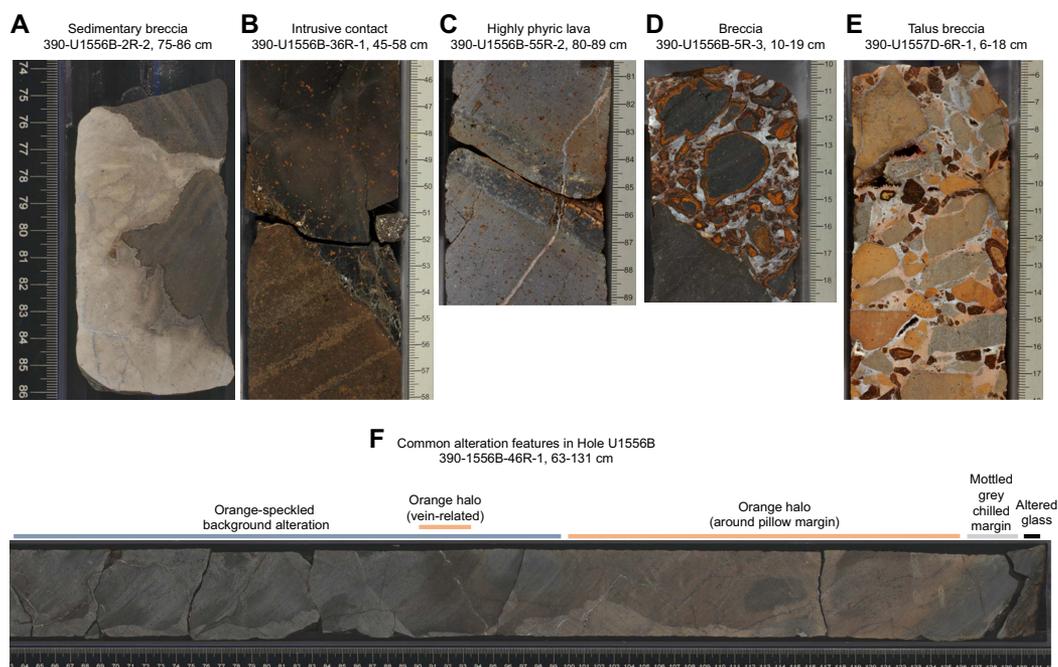

Figure F21. Representative samples of uppermost basement rocks, Sites U1556 and U1557. A. Sedimentary breccia from sediment/basement interface: fragments of basaltic lava in micritic limestone matrix. B. Moderately olivine phyric basalt (Stratigraphic Sequence A; upper half of image) in which olivine is highly altered to distinctive orange-brown, intrudes an older, intensely altered pillow basalt (Stratigraphic Sequence B; lower half of image). C. Chilled margins of highly plagioclase-olivine-clinopyroxene phyric basalts (Stratigraphic Sequence C). D. Hyaloclastite breccia with carbonate cement. E. Talus breccia comprising gray, brown, and orange clasts of altered basalt and altered glass cemented by a zeolite ± micritic or microsparry calcite. F. Common alteration types and their typical spatial relationship in sequence from chilled margin (right) to interior of large pillow (left), typically including altered glass, a mottled gray cryptocrystalline to variolitic zone, orange halos paralleling pillow margin and along veins, and orange speckled background interior.

orange rocks and some oxidized basalt samples that likely represents a component acquired upon alteration (Figure F23). Because analyzed samples are saturated or close to saturation at the maximum field applied during IRM acquisition (1.2 T), maghemitization of original magnetite-titanomagnetite minerals is suspected. Suitable half-core pieces (greater than about 15–20 cm long) from the archive halves have also been measured on the SRM. Finally, a subset of samples was subjected to thermal demagnetization up to 580°C (the temperature used to define magnetite by a loss in magnetization). These data confirm the results of both the AF demagnetization and IRM analyses.

9.1.3.2.4. Physical properties and downhole measurements

Basement physical properties were determined primarily from cores and downhole logging data from Hole U1556B, with additional information from the deepest cores from Holes U1556A and U1556C which extended several meters into basement. Measurements on whole-round and split half sections were compared with each other and with downhole measurements from Hole U1556B for lithostratigraphic characterization and integration of core description and borehole data. In addition to the standard whole-round and discrete measurements, high-resolution 3-D exterior images were also taken from ~170 m of hard rock whole-round cores using the DMT CoreScan3.

In the basement interval of Site U1556, NGR data show distinct variations that correspond well with the three main stratigraphic igneous units. NGR values range 0–60 counts/s in the upper-most Stratigraphic Sequence A. Between 504 and 529 m CSF-B, mean NGR increases, which corresponds to a transitional zone in basement in which both Stratigraphic Sequence A and B appear together. Below 529 m CSF-B in Stratigraphic Sequence B, NGR decreases and varies between 7
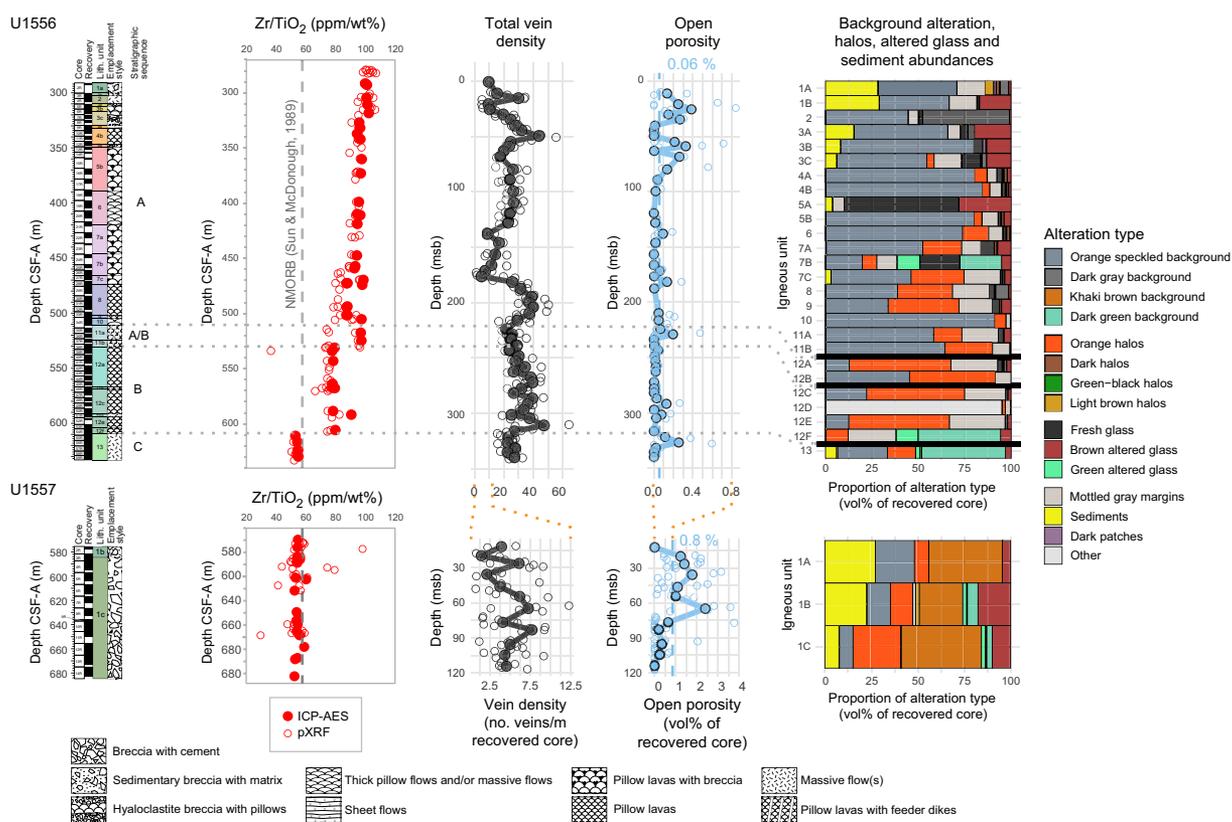

Figure F22. Expedition 390 basement core description summary. Core recovery and igneous stratigraphy are based on Holes U1556B and U1557D. Zr/TiO$_2$ shows enriched geochemical signatures in Stratigraphic Sequences A and B at Site U1556 (all geochemical data measured during Expedition 390 are shown; vertical dashed line = composition of N-MORB [Sun and McDonough, 1989] for reference). Note that some pXRF data from Holes U1556A and U1557B plot shallower than top of basement in Holes U1556B and U1557D. Total vein density and open macroscale porosity (vertical dashed line = mean as a proportion of all recovered rock, open circles = calculated by section, solid circles = calculated by core, dotted red lines = tie lines indicating differences in *x*-axis scales for the two holes). Summary of relative proportion of alteration types recorded for each igneous unit (thick black lines = boundaries between major stratigraphic sequences).

and 25 counts/s. At 609 m CSF-B, NGR decreases abruptly and remains low to the base of the drilled interval, all within Stratigraphic Sequence C. Gamma ray from wireline logging shows similar trends, and sharp changes in these data are associated with igneous lithologic subunit contacts. MS in the basement interval ranges 0 to >800 IU, generally increasing with depth in basement. A sharp increase in MS coincides with the change from Stratigraphic Sequence B to C at 609 m CSF-B. Bulk density generally decreases downhole, and discrete sample data indicate that the majority of basalt samples have higher density, lower porosity, and higher *P*-wave velocity than hyaloclastite samples. Electrical resistivity and porosity data from wireline logging are both sensitive to formation porosity and show clear distinctions between the more massive basalt flows, which have higher density and resistivity and lower porosity, and the hyaloclastite intervals, which have lower density and resistivity and higher porosity. Thermal conductivity in basement cores ranges 1.0–1.7 W/(m·K), with lower conductivity generally associated with hyaloclastite samples and higher conductivity with basalt samples.

9.1.3.2.5. Igneous geochemistry

For the Hole U1556B basement cores, representative samples were taken from the freshest portions of each lithologic subunit to obtain a downhole record of the primary magmatic composi-
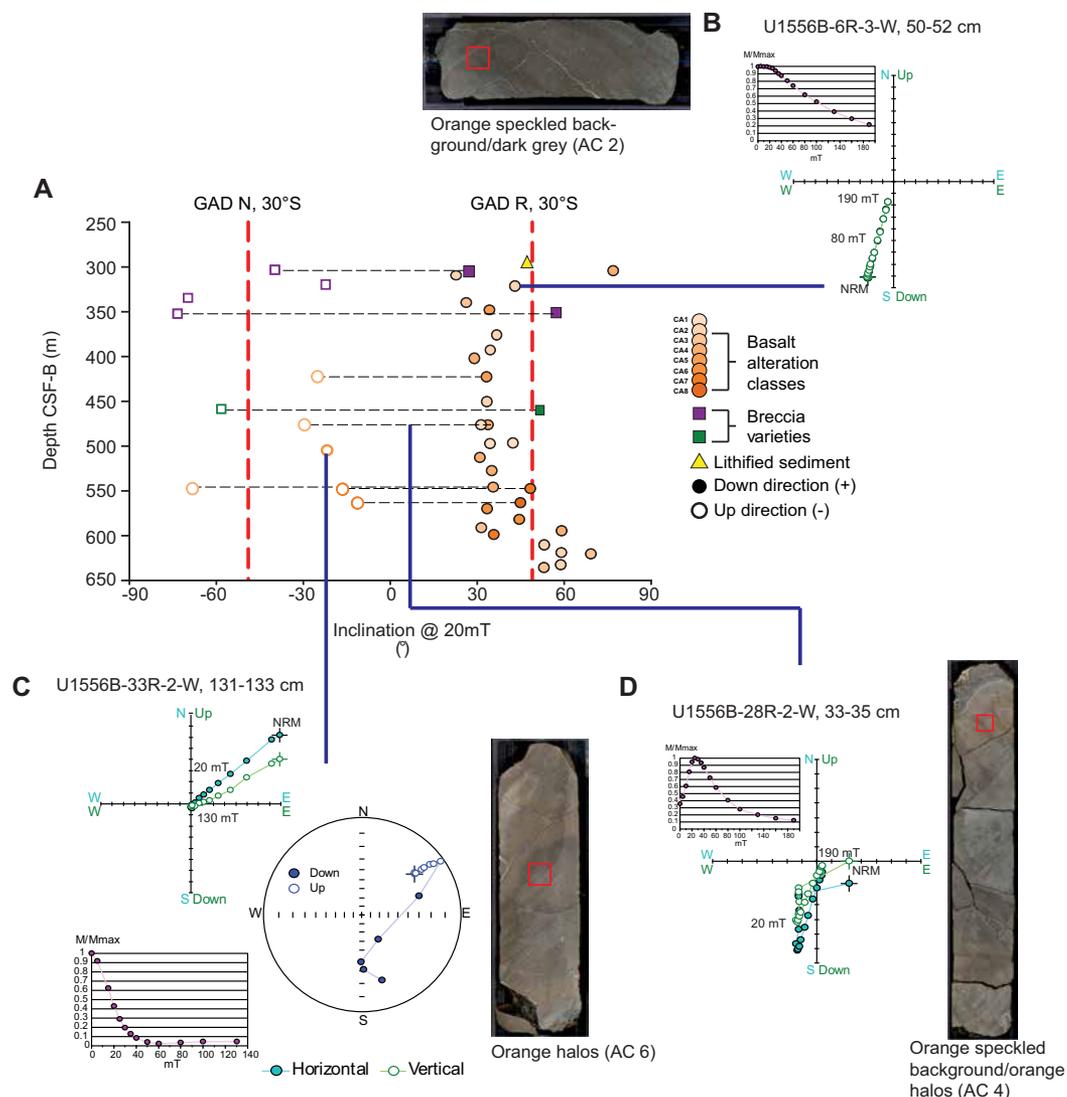

Figure F23. Stepwise demagnetization OVPs, decay AF plot, and discrete sample locations of representative samples of different alteration classes (ACs) along with (A) ChRM and (B–D) overprint inclinations, Hole U1556B (B: no overprint, C: completely overprinted, D: partially overprinted).

tions. These samples were supplemented with additional basalt samples with different styles and extents of alteration that were considered homogeneous at the scale of sampling to make a preliminary investigation of the alteration effects on elemental abundances. Additionally, lithified sediments, primarily micritic limestone, were sampled from the matrix of sedimentary breccias. Combined, a total of 45 samples were taken for loss on ignition (LOI) and bulk rock geochemical analysis via ICP-AES from Hole U1556B. The 45 samples also included 3 paired basalt samples, with each pair sampling different portions of a single lava flow that display different styles or extents of alteration to investigate the effects of alteration on the bulk rock composition. LOI varies between 0.2 and ~4 wt%, indicating that all selected samples are at least partially altered, with higher LOI suggesting more alteration. Most basalt samples are categorized as basalt and trachybasalt with a transition to lower concentrations for incompatible elements at the bottom of the hole. Comparison of the paired samples suggest addition of Al_2O_3, Na_2O, K_2O, Ba, and Zn with increased degree of alteration. High field strength element ratios (e.g., Zr/TiO_2) show a transition from normal mid-ocean-ridge basalt (N-MORB) at the bottom of the hole to ocean-island basalt (OIB) at the top of the hole (Figure **F22**).

9.1.3.2.6. Microbiology

Approximately one microbiological whole-round sample per 10 m advance in Hole U1556B was collected and preserved for shore-based analysis. Before processing the whole rounds, they were imaged using the Foldio lightbox/turntable system (Figure **F24**). All sampling was done within the KOACH system, a portable air filtration unit that creates a particle-free area for low-contamination sampling. Sample handling was conducted using an ethanol-washed steel rock box and chisels.

Postexpedition research on samples from these microbiology whole rounds will include cell counts; analysis of community DNA, RNA, and lipids; single-cell genomics; stable and radioisotope incubation experiments; and generation of enrichment cultures. To test potential contamination of whole rounds by drilling fluid, we collected inner and outer rock chips containing perfluorocarbon tracer (perfluoromethyldecalin [PFMD]) from each whole round. Preliminary analysis of PFMD samples analyzed via gas chromatography–electron capture detector (GC-ECD) indicated no intrusion of drilling fluid in most samples.

9.2. Site U1557

9.2.1. Background and objectives

Site U1557 is in the western South Atlantic Ocean ~1250 km west of the Mid-Atlantic Ridge at a depth of ~5000 mbsl (Figures **F1**, **F16**). Site U1557 was previously occupied during engineering Expeditions 390C and 395E, during which the sediment succession and uppermost <6 m of basement were cored with the APC/XCB system in Hole U1557B and a reentry system was installed with casing that extends into the uppermost basement in Hole U1557D. The main objectives of revisiting Site U1557 during Expedition 390 were to (1) core up to 250 m into basement with the RCB system in Hole U1557D to collect material that addresses the petrologic, geochemical, and microbiological objectives of the SAT expeditions and (2) collect wireline geophysical logging data through the basement section (Figure **F15A**).

Site U1557 is located 6.7 km east of Site U1556, with basement predicted to have formed at ~60.7 Ma, slightly younger than the 61.2 Ma age calculated for Site U1556, at a half-spreading rate of ~13.5 mm/y. Ocean crust at these sites is the oldest that was drilled during the SAT expeditions. The mineralogy and extent of alteration of the basement rocks at Site U1557, physical properties such as porosity, and composition of the microbial communities will be compared to the same characteristics at the other sites along the transect to investigate crustal aging and the development of hydrothermal circulation in the upper ocean crust formed at slow- to intermediate-spreading rate MORs. The sedimentary cover at Site U1557 is about twice as thick as at Site U1556, and contrasts between these closely spaced sites will allow exploration of the blanketing effect of sediment of different thicknesses and basement topography on hydrothermal circulation.

Site U1557 was first visited during engineering Expedition 390C, with the goal of coring a single APC/XCB hole to basement for gas safety monitoring and installing a reentry system with casing
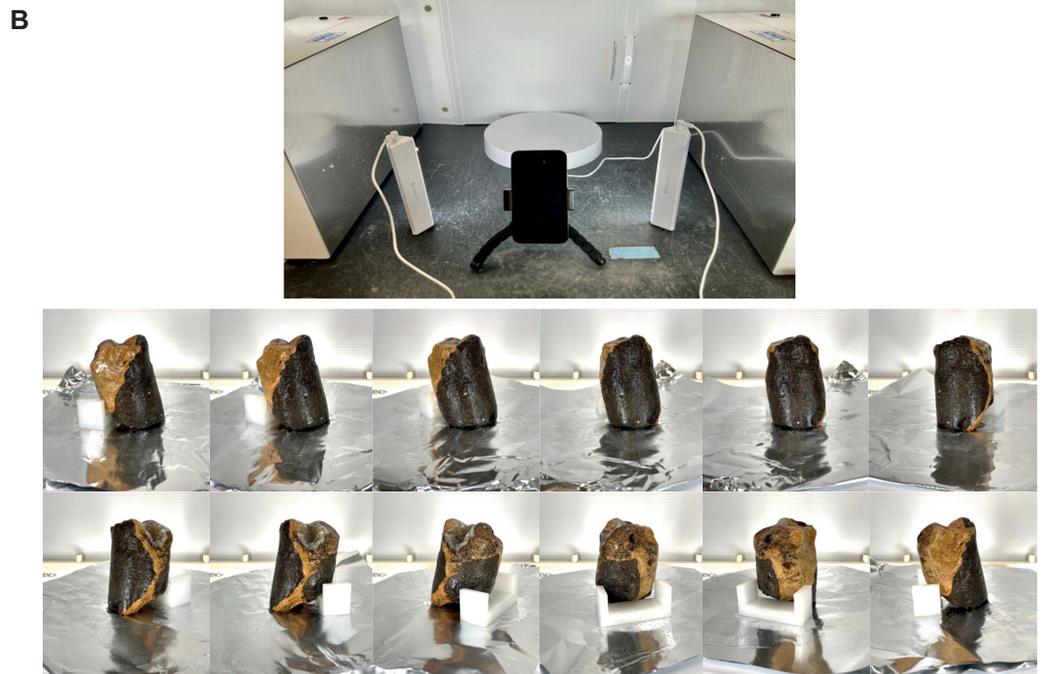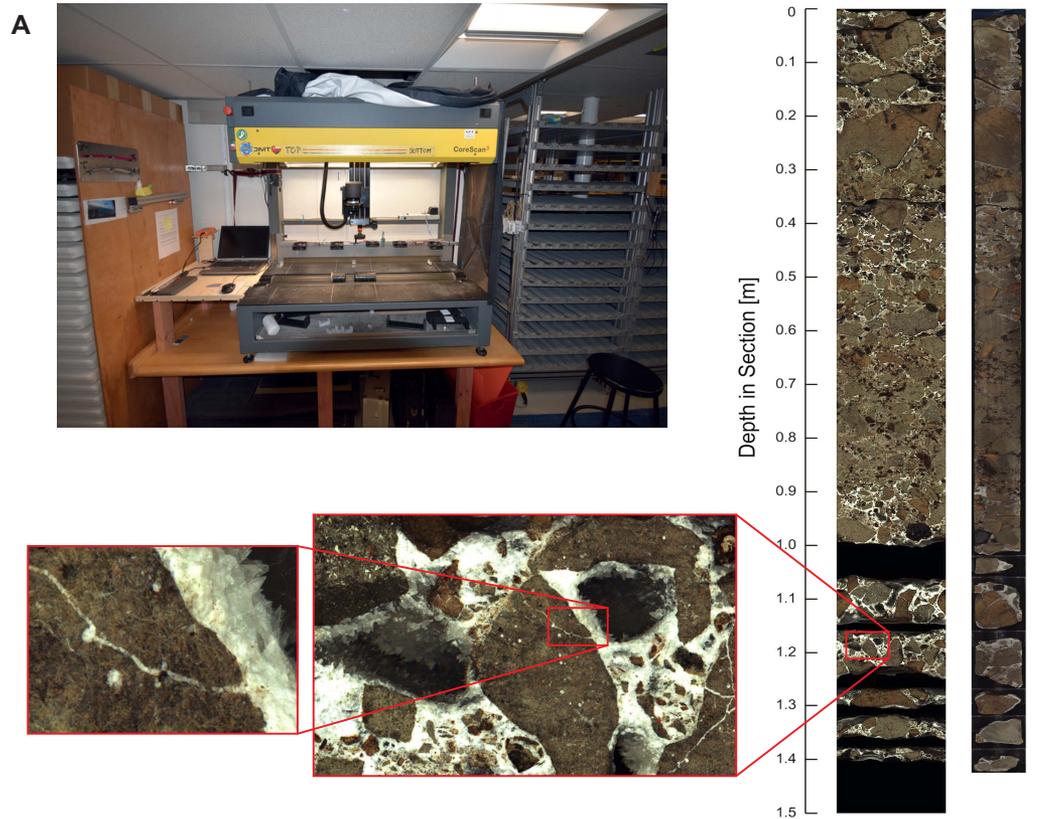
Figure F24. A. DMT CoreScan3 workstation with example of 3-D high-resolution image created using novel methods developed during Expedition 390. B. Foldio workstation with rotating stage and camera positioned to take multiple time-lapsed images of core pieces as it rotates that were taken to preserve information on pieces fragmented for microbiological sampling.

through sediment to ~5 m into basement. After a missed mudline in Hole U1557A, Hole U1557B penetrated to 574.0 mbsf, contacting basement at 564.0 mbsf, with an overall recovery of 414.94 m of sediment as well as the sediment/basement interface (72%). In Hole U1557C, a jet-in test determined that we would not be able to jet in the Dril-Quip reentry system and five joints of 16 inch casing prior to drilling a 10¾ inch casing string into basement. Instead, the reentry system and 16 inch casing were drilled in to Hole U1557D. The casing could not be extended during Expedition 390C because of a subsea camera system failure; Expedition 395E returned to the site, installing casing to 571.6 mbsf with the hole reaching 576.6 mbsf (Table **T1**).

9.2.2. Operations

9.2.2.1. Transit
Expedition 390 arrived at Site U1557 on 12 May 2022 after moving over from Site U1556 in dynamic positioning (DP) mode.

9.2.2.2. Hole U1557D
We reentered Hole U1557D with the bottom-hole assembly (BHA) for RCB coring and began operations. Core 390-U1557D-2R was the first core recovered in this hole, from below the two drilled intervals completed during Expeditions 390C and 395E. Coring continued smoothly through Core 8R; Core 9R had advanced only 1 m when we had to pull out of the hole to wait on weather. After 1.5 days waiting on weather, we continued coring from 637.1 mbsf, with Core 10R. Core 14R was the final core for the site and advanced to 684.7 mbsf; after its recovery, we began tripping out of the hole to drop the bit on the seafloor and reenter the hole for logging. Excluding Cores 2R, 3R, and 9R, all cores were full length. A mud sweep was pumped after every core following Core 5R. Penetration rates were <2.5 m/h throughout the hole. In total, coring in Hole U1557D during Expedition 390 advanced 109.1 m and recovered 71.28 m (65%; Table **T2**; Figure **F15B**).

After dropping the bit on the seafloor using the MBR, we reentered the hole to log with the triple combo tool string. The string included tools for measuring NGR, borehole diameter, formation density, resistivity, and MS. Two upward passes covering the basement section of the hole were completed and then the sediment section of the hole was logged through casing while the tools were pulled back to surface. The logging tools were recovered, and we departed Site U1557 to transit to Site U1559. Operations time at Site U1557 totaled 7.6 days during Expedition 390.

9.2.3. Principal results
During Expedition 390, the science party described APC/XCB cored material as well as the sediment/basement interface from Holes U1557A and U1557B, collected during Expedition 390C. An additional 109.1 m of basement was cored in Hole U1557D during Expedition 390. Both sediment and basement results are summarized here. The cores recovered at Site U1557 comprise two sedimentary units overlying a single basement unit, identified on the basis of macro- and microscopic visual observations combined with mineralogical analyses by XRD, color reflectance, and MS data. The units are numbered from the top of the hole, with units in the sedimentary section designated by Roman numerals and basement units designated by Arabic numerals; subunits are designated with letters. The sediment/basement interface was recovered at 564.8 mbsf in Hole U1557B; installation of casing into basement in Hole U1557D prevented recovery of the interface in that hole. The interface depth was therefore defined as the shallowest recovered occurrence of basalt in Hole U1557B.

9.2.3.1. Sediments

9.2.3.1.1. Sedimentology
The sedimentary column at Site U1557 is composed of two units: alternating silty clays and nannofossil ooze (Lithologic Unit I; Eocene–Holocene; ~290 m thick) overlying nannofossil/calcareous chalk deposits (Unit II; Paleocene–Eocene; ~275 m thick; Figure **F17**). The contact between Units I and II is marked by the first substantial (>25 m thick) deposit of siliciclastic sediments (dark brown silty clays) at the EOT. The color of the sediment primarily reflects its lithologic characteristics; sediments composed mainly of nannofossil ooze/chalk are generally pinkish white or light gray, whereas silty clays range from brown/dark brown where carbonate is absent to reddish brown where the carbonate content is higher. In addition to the major lithologies

(nannofossil ooze/chalk and silty clay), several minor local sedimentologic features are observed, including greenish white foraminifera-rich layers/lenses (especially at the contact between silty clays and nannofossil ooze intervals), microstructural deformation (faulting and folding), and a unique clay-bearing layer (<0.8 m thick; identified as the PETM interval; Figure **F25**) in the thick sequence of nannofossil chalk of Unit II.

9.2.3.1.2. Biostratigraphy

The ~564.8 m thick sedimentary succession of pelagic ooze, chalk, and clay in Hole U1557B ranges in age from Pleistocene to middle Paleocene. Planktic and benthic foraminifera and calcareous nannoplankton are present in varying abundance in the oozes and chalks but are mostly absent from the clays (Figure **F18**). Preservation and abundance of calcareous nannoplankton and planktic foraminifera are better in the Paleocene and Eocene than in the Oligocene and Neogene. Sedimentation is continuous from the early Oligocene to Pleistocene (Figure **F19**). A 12.94 m thick condensed interval or hiatus composed of dark brown pelagic clay and spanning the middle Eocene to early Oligocene occurs in Cores 390C-U1557B-29X through 31X. Below this hiatus/condensed interval, sedimentation again appears to be continuous, although there are significant gaps in core recovery and some evidence for reworking in the early Eocene. We interpret a prominent reddish brown clay in Core 50X to represent the PETM based on the occurrence of the calcareous nannofossil genus *Rhomboaster*, which is characteristic of the PETM interval, as well as sedimentologic and physical properties data indicating a significant drop in carbonate content (Figure **F25**). These observations are strong evidence that a complete PETM section was recovered in Section 50X-3. Below this hyperthermal event, continuous sedimentation is observed

Figure F25. Summary of physical properties in Section 390-U1557B-50X-3, inferred to contain sediments deposited during PETM. Stars = locations of samples taken for nannofossil analyses, 1–14 = locations of closely spaced lithologic descriptions, yellow lines = two intervals for which close-up images are provided on right. Magnetic susceptibility is from point source. Photomicrographs show *Rhomboaster calcitrapa* (top: plane-polarized light, bottom: cross-polarized light).

through to the sediment/basement interface. A sample taken directly above basement (Sample 63X-2, 78–80 cm; 564.15–564.17 m CSF-B) was assigned to planktic foraminifera Zone P4a (between 60.54 and 60.76 Ma) and calcareous nannofossil Zones NP5/CNP7 (between 60.76 and 61.27 Ma), both of which are in good agreement with the projected crustal age of ~60.7 Ma at Site U1557. No samples were analyzed from the limestone-basalt breccia that characterizes the transition from pelagic sediment to basement.

9.2.3.1.3. Paleomagnetism

The sediment package at Site U1557 was cored in Holes U1557A and U1557B during engineering Expedition 390C, during which most cores were split, and remanence measurements were made using the SRM. The NRM of core sections was measured prior to applying three AF steps (5, 10, and 20 mT), where the remanence was measured after each step. Measurements were made at 2 cm intervals. Because the working halves of Site U1557 cores were not on the ship during Expedition 390, no discrete samples were taken from the majority of the sediment sequence. The sediment/basement interface cores from Hole U1557B were split and analyzed during Expedition 390, with the archive halves run on the SRM and two discrete samples collected from the interface.

Measured inclinations for Hole U1557B cluster around –52.2° and 49.8°. The inclinations for Hole U1557A are slightly shallower than (but within error of) the inclination expected for this latitude for a geocentric axial dipole (GAD; ±49.1° at 30°S), whereas those for Hole U1557B are in good agreement with GAD inclination. For all sites, MS and intensity correlate well with lithologic variations—high values correspond to the silty clays and lower values correspond to the biogenic carbonates. The remanence intensities for the sediment at Site U1557 are relatively strong for pelagic material. Throughout Lithologic Units I and II in Hole U1557B, intensity averages are on the order of 10^{-2} A/m for both the NRM and 20 mT intensity. Unit I intensities are roughly twice what they are for Unit II. Three intervals of normal polarity are identified in Core 390C-U1557A-1H that we correlate to the Brunhes, Jaramillo, and Cobb Mountain Chrons, respectively. Similar normal polarity intervals are also identified in the uppermost cores of Hole U1557B. Unfortunately, the depth of the Brunhes/Matuyama chron boundary in Hole U1557B is only an estimate because the sediment interval that contained the transition from normal to reversed polarity was not recovered.

A smooth demagnetization curve and an interpretable OVP were observed for the lithified sediment sample from the sediment/basement interface, whereas the nonlithified sediment returned spurious results. The magnetic field direction of the lithified discrete sediment sample (inclination = ~37°; declination = ~128°) calculated from the ChRM using principal component analysis (PCA) between 30 and 60 mT is lower than that expected for a GAD at this latitude (30°S). This result cannot be accounted for by magnetic secular variation and is likely due to inclination shallowing because of compaction by the overlying sediment column. Analysis of further discrete samples should help elucidate this inclination discrepancy. The median destructive field (MDF) and coercivity spectra for this sample suggest a magnetite-like phase is the dominant magnetic carrier.

9.2.3.1.4. Age model and mass accumulation rate

The most obvious feature of the age model for Site U1557 is a large hiatus or condensed interval spanning the early Oligocene to middle Eocene. This interval also separates the relatively low sedimentation rates of the Holocene to the Oligocene with the high sedimentation rates of the Eocene and Paleocene. Sedimentation rates average 0.77 cm/ky in Unit I (except in the condensed interval, Subunit IE, which has a sedimentation rate of 0.17 cm/ky and would bring the overall Unit I average down to 0.57 cm/ky) and 2.24 cm/ky in Unit II (Figure **F19**). The highest sedimentation rate (11.53 cm/ky) occurs in the late Paleocene of Unit II. Mass accumulation rates at Site U1557 are primarily driven by carbonate accumulation, with periods of CCD shoaling resulting in less carbonate dilution of eolian dust flux. A surprising result at Site U1557 is the elevated organic carbon content. Total organic carbon (TOC) values as high as 3 wt% are generally not expected in a mid-latitude gyre setting, and the organic carbon accumulation rate suggests that the Paleocene and Eocene were characterized by high organic carbon production and preservation, with a peak near 0.1 $g/cm^2/ky$. The general correspondence of high organic carbon accumulation rates with high carbon accumulation rates indicates overall high productivity in surface waters during this time interval.

9.2.3.1.5. Physical properties and downhole measurements

Physical properties characterization of the sediment section at Site U1557 is based on cores and in situ downhole measurements from Holes U1557A and U1557B. Whole-round core-based measurements include NGR (sensitive to the abundance of minerals containing radioisotopes of K, U, and Th), bulk density from GRA, MS (an indicator of the abundance of magnetic minerals), and *P*-wave velocity. Trends in the physical properties recorded downhole in Hole U1557B correlate with lithologic units.

NGR values in Unit I show high-frequency variability between 7 and 50 counts/s reflecting the alternating carbonate and silty clay layers (Figure **F17**). In contrast, Unit II is characterized by uniformly lower NGR, with a mean of 6 counts/s. Similar trends are present in MS data, which alternate between ~40–50 and 100–150 IU in Unit I and are generally less than ~50 IU and less variable in Unit II, reflecting the more uniform, carbonate chalk-dominated lithology (Figure **F17**). In Unit II, concomitant abrupt increases in NGR and MS suggest short-lived possible carbonate dissolution events, likely associated with shoaling of the CCD at the time of deposition of these sediments. Bulk density and *P*-wave velocity generally increase with depth in the sedimentary section, which is consistent with carbonate lithologies being denser than the silty clays and an overall compaction trend.

Data from cores recovered using the APC/XCB system in Holes U1557A and U1557B are correlated based on changes in bulk density, MS, NGR and luminosity (L*) data. The lack of correspondence in the physical properties between Cores 390C-U1557A-1H and 390C-U1557B-1H, suggests at least 4.1 m is missing from the top of Core 390C-U1557A-1H, which was a missed mudline core. A shipboard splice for the upper 15 m CCSF at Site U1557 is produced with a small splice gap between the bottom of Core 390C-U1557B-1H and the top of Core 390C-U1557A-1H.

Three downhole temperature measurements were made in Hole U1557B using the APCT-3 tool, and a geothermal gradient of 34°C/km is calculated, similar to the reported upper range at Site U1556. A total of 60 thermal conductivity measurements yield an average of 1.4 ± 0.25 W/(m·K) with a discernible downhole increase to 1.6 W/(m·K) near the sediment/basement interface. Using temperature and thermal conductivity measurements, a heat flow of 48 W/m^2 for Hole U1557B is calculated.

9.2.3.1.6. Sedimentary and pore water geochemistry

Approximately 565 m of sediment was cored in Hole U1557B during Expedition 390C, with headspace gas and IW whole rounds taken once per core. A total of 61 IW samples were squeezed under a laboratory atmosphere. During Expedition 390C, shipboard IW analyses included pH, salinity, alkalinity, major cations and anions (sodium, calcium, magnesium, potassium, chloride, and sulfate) using IC, major and minor elements using ICP-AES, and nutrients (phosphate and ammonium). Carbonate and TOC were then analyzed on the squeeze cakes. Depth profiles of redox-sensitive elements in Hole U1557B suggest dissolved oxygen depletion in the upper ~100 m. We observed decreasing sulfate concentrations, a dissolved Mn peak, and increasing ammonium associated with organic carbon decay. Increasing sulfate concentrations combined with Mn concentrations near the limit of detection below 280 mbsf may suggest input of oxygenated fluids from basement (Figure **F20**). A sharp change in measured alkalinity, as well as calcium, magnesium, boron, and lithium concentrations near the bottom of the hole (~540 mbsf), could also be associated with basement fluid flow. Elevated dissolved Si concentrations at ~3 and ~150 mbsf may be indicative of biogenic silica dissolution at those depths.

9.2.3.2. Volcanic rocks

9.2.3.2.1. Igneous petrology

Two holes at Site U1557 recovered basement rocks in the form of sedimentary breccia (Figure **F21**). In Hole U1557B, 9.5 m of sedimentary breccia was cored after basement was reached at 564.8 mbsf. Expedition 390 cored 109.1 m of basement in Hole U1557D, recovering sedimentary breccia throughout the cored interval of the hole. The breccia consists of a range of basaltic clast types derived predominantly from pillow lavas. The clasts are all moderately to highly altered, obscuring many aspects of primary igneous lithology. Therefore, for the purposes of macroscopic core description, we have distinguished between altered glass and basalts (cryptocrystalline to

microcrystalline) and grouped the basalts into three categories based on color that broadly reflect different degrees of alteration: gray, brown, and orange. In general, gray basalts are the least altered and most diverse lithologically; they range from cryptocrystalline to microcrystalline and from aphyric to highly plagioclase-olivine-clinopyroxene phyric, although aphyric is most common. Brown and orange basalts are typically aphyric to sparsely plagioclase or olivine phyric. In addition, orange basalts are associated with textures indicative of an origin in a pillow chilled margin. With few exceptions, basaltic glass is completely altered throughout the core. Although some variation in clast lithology is observed downhole, systematic variations were not identified, and the entire sequence of rocks recovered has been defined as a single lithologic unit. It has been divided into three lithologic subunits based on variations in breccia matrix and cement.

9.2.3.2.2. Alteration petrology

Alteration of the breccias at Site U1557 is variable, with evidence of alteration prior to brecciation and redeposition, as well as overprinting alteration in the breccia pile itself. The overall range of alteration is very similar in color, extent, and mineralogy to the alteration observed at Site U1556 ~6.5 km away, with the major difference at Site U1557 being that clasts of variable alteration have been fragmented and juxtaposed in a breccia where they are further altered in situ (Figure **F22**). Veins are rare, with only ~300 logged and just under 50 occurrences of vesicles recorded in total. Most of the logged mineral fill consists of breccia cements. The interclast space of the breccias is filled with pelagic sediment, fine-grained igneous material (glass and basalt), carbonate, and/or authigenic zeolite "sediment," with open porosity common throughout much of the hole. The volume proportion of open porosity and cement decreases downhole.

9.2.3.2.3. Paleomagnetism

Progressive AF demagnetization of basement split-core sections and discrete samples are used to characterize the paleomagnetic signal and resolve the magnetization components recorded in Site U1557 cores. The NRM of core sections was measured at 2 cm intervals on the SRM. Three AF steps (5, 10, and 20 mT) were applied, and the remanence was measured after each step. Discrete sampling was accomplished for Hole U1557D with 13 discrete cubes (8 cm³) collected across the 14 recovered cores from sufficiently big clasts that displayed diverse grades of alteration. Here, we use these data to primarily characterize the magnetic mineral assemblage. AMS was measured on all collected discrete samples to characterize the magnetic fabric. Acquisition of IRM and backfield IRM experiments were performed on two representative discrete samples.

Histograms of the inclinations measured on the SRM suggest that the inclinations in Hole U1557D sweep the full spectrum of values from −90° to 90° and cluster around 7°. This is much shallower than the inclination expected for this latitude for a GAD (±49.1° at 30°S). This large departure from that GAD inclination is likely a function of sampling the large clasts from the sedimentary breccia, which should produce randomly oriented directions if the ChRM was blocked before clast emplacement. Every discrete breccia sample displayed stable demagnetization data of a single component that describes a straight line to the origin, which defines the ChRM. Inclinations from the calculated ChRM directions verify the inclinations measured from the SRM. Additionally, all discrete samples gave maximum angular deviation angles <15°. IRM and backfield IRM experiments illustrate the "softness" of the ferromagnetic assemblage. The coercivity of remanence (B_{cr}) values are around 20 mT, the S ratios are equal to 1, and the SRM_{100}/SIRM ratios are 0.99 and 1, respectively, in the two studied samples. These values are indicative of the presence of soft ferromagnetic phases as remanence carriers likely dominated by either titanomagnetite or titanomaghemite. AMS indicated the presence of both oblate (planar) and prolate (linear) ellipsoids with no consistent directions or particular distribution along the basement rock package.

The "conglomerate test" was employed to test whether the clasts' ChRM was blocked prior to their emplacement in the sedimentary breccia or reset at a later stage. ChRM directions plot randomly about a stereonet, indicating the conglomerate test was passed and that the ChRM of the clasts has been stable since before their incorporation in the clastic rock. However, the soft nature of the ferromagnetic assemblage suggests that the actual measured components may represent an earlier remagnetization, resulting from alteration (maghemitization) of the original magnetic component on the parent rocks. This result suggests no secondary alteration events that affected magnetization took place between clast emplacement and core retrieval.

9.2.3.2.4. Physical properties and downhole measurements

Basement physical properties were determined primarily from cores and downhole logging data from Hole U1557D, with additional information from the deepest cores from Hole U1557B, which extended several meters into basement. Measurements on whole-round and split half sections were compared with downhole measurements from Hole U1557D for lithostratigraphic characterization and integration of core description and borehole data. In addition to the standard whole-round and discrete measurements, high-resolution 3-D exterior images were also taken from ~70 m of hard rock whole-round cores using the DMT CoreScan3.

In the basement interval of Site U1557, NGR, MS, and GRA bulk density from core data show no obvious trends with depth in basement. NGR ranges from 0 to ~30 counts/s, MS ranges 0–800 IU, and GRA clusters around ~2.5 g/cm³. Bulk density, porosity, and *P*-wave velocity from discrete samples show good agreement with the alteration described for the basalt clasts in the breccia. Additionally, discrete samples show the breccia matrix porosity increases with depth, whereas the *P*-wave velocity of the matrix samples decreases with depth. Electrical resistivity from wireline logging is sensitive to formation porosity and qualitatively agrees with the trends seen in the discrete samples. Thermal conductivity in basement cores ranges 1.1–1.8 W/(m·K) and qualitatively appears to decrease with depth in agreement with the discrete sample porosity and wireline resistivity data.

9.2.3.2.5. Igneous geochemistry

For the Hole U1557B and U1557D basement cored during Expeditions 390C and 390, respectively, representative samples were taken from the least macroscopically altered basaltic clasts in the sedimentary breccia to obtain a downhole record of the primary magmatic compositions. Lithology of clasts includes aphyric basalt, yellow-brown phyric basalt, and equigranular basalt. Additional basalt samples with different styles of alteration were chosen to investigate alteration effects on elemental abundances. A total of 20 samples were selected from Hole U1557D and 1 sample was taken from Hole U1557B for LOI and bulk rock geochemical analysis using ICP-AES. LOI varies between 0.09 and ~3.85 wt%, with higher LOI in Hole U1557D samples indicating more alteration. Because of the high degree of alteration, traditional classification methods, such as total alkalis versus silica, cannot be applied. Based on high field strength element ratios (e.g., Zr/TiO_2; Figure **F22**), the rocks can be classified as N-MORBs. Alteration leads to enrichment in some transition metals (e.g., TiO_2, Fe_2O_3, Sc, and V) and large-ion lithophile elements (e.g., Na_2O, K_2O, and Ba) with lower MgO concentrations.

9.2.3.2.6. Microbiology

Microbiology sampling in basement at Site U1557 during Expedition 390 was focused on exploring evidence for life in basement using microscopy, culture-based approaches, and culture-independent approaches. No microbiology samples were collected from Hole U1557B, which was drilled during Expedition 390C, because there were no scientists on the ship to process the ephemeral microbiology samples. For Hole U1557D, sampling efforts were focused on collecting a single whole-round core sample from each 9.5 m advance that would be processed and subsampled for different analyses. The aim was to generate a suite of samples that were representative of the different rock types and alteration styles that compose the basement stratigraphy of the site. In total, 12 whole-round samples (8–15 cm long) were collected for microbiological analysis. The lithology of all samples collected was sedimentary breccia.

A total of 12 samples were processed for cell counts, shore-based DNA (polymerase chain reaction [PCR] amplicon-based and metagenomes), and/or RNA (PCR amplicon-based and/or metatranscriptomes) analyses; 8 samples were preserved for single-cell genomics; and 7 samples were collected for lipid analysis. Microbial isolation experiments were initiated for Samples 390-U1557D-5R-5, 37.5–48.5 cm, and 7R-3, 0–9.5 cm, on petri dishes with 1/10 ZoBell Marine Agar enrichment media. This media selects for heterotrophic marine microorganisms and is commonly used to isolate new microorganisms. Samples 6R-3, 39–49 cm, and 8R-3, 52–63 cm, were used to initiate stable isotope probing experiments to determine proportions of the microbial community that use specific carbon and nitrogen compounds. Three samples of drilling fluid were collected from a pipe on the rig floor during coring operations in Hole U1557D: during coring of Cores 2R

(586 mbsf), 11R (645 mbsf), and 14R (676 mbsf). Samples were collected for cell counts and shore-based molecular biology analysis to determine the microorganisms present in drilling fluid.

9.3. Site U1561

9.3.1. Background and objectives

Site U1561 is in the western South Atlantic Ocean ~1250 km west of the Mid-Atlantic Ridge at a depth of ~5000 mbsl (Figures **F1**, **F16**). Site U1561 was only occupied during engineering Expedition 395E, during which the sediment succession and uppermost <5 m of basement were cored with the APC/XCB system (Hole U1561A), but the sediment and sediment/basement interface acquired enhance petrologic, paleoceanographic, and chemical investigations as part of the SAT. Site U1561 is located 24 km north of Site U1556. The basement at Sites U1556 and U1561 is predicted to have formed at ~61.2 Ma at a half-spreading rate of ~13.5 mm/y. Ocean crust at these sites is the oldest that was drilled during the SAT expeditions. The mineralogy and extent of alteration of the basement rocks at Site U1561 and their physical properties such as porosity will be compared to the same characteristics at the other sites along the transect to investigate the crustal aging and the development of hydrothermal circulation in the upper ocean crust formed at slow- to intermediate-spreading rate MORs. The sedimentary cover at Site U1561 is substantially thinner than at Sites U1556 and U1557 and will provide information on sediment accumulation patterns and pore water chemical profiles of this local area. Contrasts between these closely spaced sites will allow exploration of the blanketing effect of sediment of different thicknesses on hydrothermal circulation. Basement topography between the sites may also affect circulation; Site U1561 appears to sit on a local high.

9.3.2. Operations

Site U1561 was visited during Expedition 395E. Following reentry system installation at Site U1556 and the extension of casing into basement at Site U1557, the remaining 2.5 days of operations time was used to core a single hole at an alternate SAT site on ~61 Ma crust. Holes U1561B and U1561C were missed mudline cores, where seafloor depth was uncertain because of a malfunction of the 3.5 kHz precision depth recorder (PDR) signal and a discrepancy between the reading from the 12.5 kHz signal and what was indicated in the *Scientific Prospectus* (Coggon et al., 2020) as the estimated water depth. These single-core holes were curated as Holes U1561B and U1561C despite being cored before Hole U1561A. Hole U1561A was spudded at 2335 h on 11 May 2021, with Core 395E-U1561A-1H recovering 6.7 m. Core 6H encountered hard rock at 46.2 mbsf, bending the APC cutting shoe. We switched to the XCB system for capturing the sediment/basement interface; however, Core 7X was empty. Cores 8X and 9X advanced to 48.9 mbsf and recovered 2.39 m. Overall, Cores 1H–9X recovered 45.4 m (93%; Table **T1**).

9.3.3. Principal results

During Expedition 390, the science party described APC/XCB cored material as well as the sediment/basement interface from Holes U1561A–U1561C, collected during Expedition 395E. The cores recovered at Site U1561 compose two sedimentary units overlying a single basement unit, identified on the basis of macro- and microscopic visual observations combined with mineralogical analyses by XRD, color reflectance, and MS data. The units are numbered from the top of the hole, with units in the sedimentary section designated by Roman numerals and basement units designated by Arabic numerals; subunits are designated with letters. The sediment/basement interface was recovered at 46.5 mbsf in Hole U1561A; the interface is defined as the shallowest recovered occurrence of basalt in the hole, even though drilling parameters indicate a hard layer at 46.2 mbsf that was not recovered.

9.3.3.1. Sediments and volcanic rocks

9.3.3.1.1. Sedimentology and igneous petrology

In the three holes cored at Site U1561, the sedimentary column consists of two main lithologies and hence units: silty clays and calcareous nannofossil ooze (Figure **F17**). Unit I is ≤24 m thick and composed mainly of reddish brown silty clay with a variable amount of zeolite. Some organic-rich spots occur in Unit I. Unit II (Paleocene–Eocene) is ~24 m thick; it is mainly composed of light yellowish calcareous nannofossil ooze and hosts a variable abundance of foraminifera. The bound-

ary between Units I and II is a gradational transition, defined by a reduction in the proportion of siliciclastic material down through a <75 cm interval. Unit II was only recovered in Hole U1561A. Units I and II contain <5 wt% and >90 wt% calcite, respectively, and differences in mineral assemblages are relatively small with increasing burial depth within the silty clay and ooze lithologies, respectively.

Basalts collected from the sediment/basement interface are aphyric and were emplaced as a pillow lava flow. Analysis by portable X-ray fluorescence (pXRF) suggests that the basalts are chemically similar to the alkali basalts at the top of the basement section of Hole U1556B. Chilled contacts between pillows contain brecciated and altered glass interlaid with pinkish gray to white sediment, which contains fossil foraminifera.

9.3.3.1.2. Biostratigraphy

Calcareous nannofossil biostratigraphy was performed on core catcher samples with additional toothpick samples taken from the archive halves of split sections from Hole U1561A (collected during Expedition 395E). Site U1561 comprises a ~45 m thick sedimentary sequence of pelagic clay and calcareous ooze that is dated to the Paleocene and early Eocene, with the lowermost samples equivalent in age to the oldest assemblages observed at nearby Sites U1556 and U1557. Calcareous nannoplankton are absent from the clays of Unit I but abundant in the ooze that characterizes Unit II and are moderately preserved throughout the carbonate sequence (Figure **F18**). A hiatus or extremely condensed interval of up to ~5 My recorded between the late Paleocene and earliest Eocene is also observed at Site U1556 at the westernmost end of the SAT. The sample taken directly above the basement interface at Site U1561 is assigned to Zones NP4/CNP7–CNP6, agreeing with the predicted basal age (~61.2 Ma) and correlating to nearby Sites U1556 and U1557. Planktic foraminifera data are not yet available for this site.

9.3.3.1.3. Paleomagnetism

Paleomagnetic results from Site U1561 include data collected using the SRM. Because only the archive halves were available shipboard during Expedition 390, analyses of discrete sediment samples could not be conducted. During Expedition 395E, the NRM of core sections was measured at 2 cm intervals. Three AF steps (5, 10, and 20 mT) were applied, and the remanence was measured after each step. Paleomagnetic inclinations after the 20 mT demagnetization step are bimodal, reflecting intervals of reversed and normal polarity during sediment deposition, and conform well to the expected GAD for this site latitude (49.1° at 30°S). However, reversed polarity inclinations in selected intervals from Hole U1561A are somewhat steeper than the expected 49.1° inclination. This may reflect steeper inclinations in the interval below 26 m CSF-B that are of uncertain origin, but are perhaps due to drilling disturbances. Basement rocks from Cores 395E-U1561A-8X and 9X consistently provide positive (reversed) inclinations compatible with the GAD field at the site latitude and their expected age of 61.2 Ma in the Selandian (Paleocene) in Chron C26r.

9.3.3.1.4. Physical properties and downhole measurements

Physical properties characterization of the sediment section at Site U1561 is based primarily on cores from Hole U1561A with additional data provided by one core from Hole U1561B and one core from Hole U1561C. Whole-round core-based measurements include NGR, bulk density from GRA, MS, and *P*-wave velocity. Discrete measurements included MS on split-core section halves and thermal conductivity. Formation temperature was also measured at 35.2 m CSF-B with the APCT-3 tool.

Both NGR and MS exhibit two general downhole trends at Site U1561 (Figure **F17**). Initially, both are relatively high (~35 counts/s and ~110 IU, respectively) from the seafloor to ~24 m CSF-B. Below ~24 m CSF-B, both NGR and MS are relatively low (~5 counts/s and ~40 IU, respectively) to the sediment/basement interface at ~45 m CSF-B. The trends in NGR and MS are reflective of the dominant lithologies: carbonate ooze from the seafloor to ~24 m CSF-B and silty clay from ~24 m CSF-B to the sediment/basement interface (Figure **F17**). Bulk density and *P*-wave velocity both increase downhole from ~1.4 g/cm³ and ~1500 m/s, respectively, at the seafloor to ~1.8 g/cm³ and ~1550 m/s, respectively, at the sediment/basement interface.

Stratigraphic correlation was completed using the cores from Hole U1561A and Cores 395E-U1561B-1H and 395E-U1561C-1H to create a splice that is mostly complete, with only 3 small gaps, to ~42 m CCSF and a larger gap between ~42 and ~48 m CCSF.

The one downhole temperature measurement of 8.19°C was used along with a calculated mudline temperature and the thermal conductivity of the cored sediment to estimate conductive heat flow at Site U1561 at 227.56 mW/m^2. This heat flow is higher than expected, but the calculation from only two temperature data points increases uncertainty.

9.3.3.1.5. Sedimentary and pore water geochemistry

IW samples were collected at a frequency of one per core in Cores 395E-U1561A-1H through 6H for a total of 7 water samples including the mudline. During Expedition 395E, shipboard IW analyses included pH, salinity, alkalinity, major cations and anions (sodium, calcium, magnesium, potassium, chloride, and sulfate) using IC, major and minor elements using ICP-AES, and nutrients (phosphate and ammonium). Carbonate and TOC were then analyzed on the squeeze cakes. The pore waters at Site U1561 have Br/Cl molar ratios (~1.5 × 10^{-3}) that are consistent with seawater. Sodium has a similar shape profile to Br and Cl. Sulfate concentrations decrease from ~29.6 mM in the mudline sample to 26.5 mM in the upper 22 m of sediment and then remain stable through the rest of the sediment column. Dissolved manganese concentrations are low in all samples; dissolved iron is likewise low, but, notably, this site is the only one sampled thus far as part of the SAT where iron was detected at all. Carbonate content varies with lithology, with an average of 0.25 ± 0.06 wt% (±1σ, n = 3) in Unit I (silty clay) and 85.9 ± 4.6 wt% (±1σ, n = 3) in Unit II (calcareous nannofossil ooze or clayey nannofossil ooze).

9.4. Site U1558

9.4.1. Background and objectives

Site U1558 is located ~1067 km west of the Mid-Atlantic Ridge at 30°53.78′S, 24°50.48′W in 4334 m of water (Figures **F1**, **F26**). The basement at Site U1558 was predicted to have formed at ~49.2 Ma at a half-spreading rate of 19.5 mm/y (Kardell et al., 2019) (Figure **F7**). The site is located on CREST Seismic Line 1B/1C at Common Depth Point (CDP) 3252 about 3.4 km west of CREST crossing Line 04 (Figures **F1**, **F6C**, **F26**) where a reflector at ~5.94 s two-way traveltime (TWT) was interpreted to be the top of basement, estimated to be at 148 mbsf and observed at 158.9 mbsf (Figure **F6C**).

Site U1558 was previously occupied in November 2020 during Expedition 390C (Figure **F15A**) with objectives to confirm the depth to basement by coring, conduct gas safety measurements,
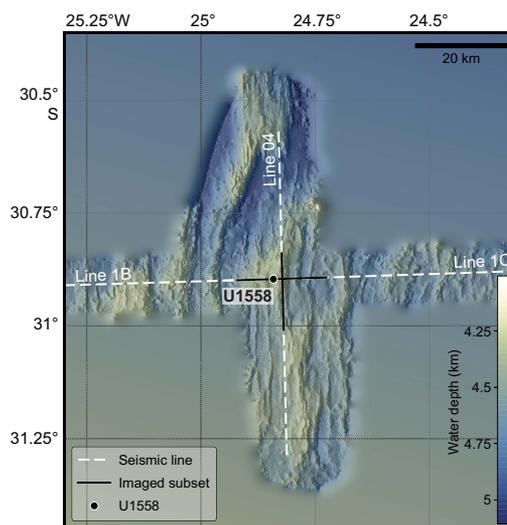

Figure F26. Site U1558 bathymetry (Christeson and Reece, 2020). Seismic reflection profiles were acquired during CREST cruise (Reece et al., 2016).

and set a reentry system consisting of a reentry cone and 13⅜ inch casing (Estes et al., 2021). Hole U1558A was cored by the APC and XCB systems to 163.9 mbsf (Figure **F15C**), finding the sediment/basement contact at 158.9 mbsf. Holes U1558B and U1558C marked unsuccessful attempts to drill in and release the reentry system using the Dril-Quip running tool. While lowering the reentry system for Hole U1558D, the reentry cone and mudskirt became detached from the casing and fell to the seafloor the right way up and within a few meters of the intended location. The drill bit and casing assembly was lowered through the cone and was drilled into Hole U1558D, setting the casing shoe at 146.1 mbsf and the base of the hole at 150.0 mbsf.

The original operational objectives of Expedition 393 at Site U1558 were to core a single APC/XCB hole to basement and to core and log ~250 m of basement volcanic rocks in Hole U1558D.

At 49.2 Ma, Site U1558 is the second oldest location of the SAT and will be compared to older and younger crustal material cored at Expedition 390/393 sites. Science objectives at Site U1558 are to (1) investigate the history of the low-temperature hydrothermal interactions between the aging ocean crust and the evolving South Atlantic Ocean and quantify past hydrothermal contributions to global geochemical cycles, (2) collect samples of the sediment- and basalt-hosted deep biosphere beneath the low-productivity South Atlantic Gyre that will be used to refine global biomass estimates and investigate microbial ecosystems' responses to variable conditions, and (3) construct paleoceanographic records of carbonate chemistry and deepwater mass properties across the western South Atlantic Ocean through key Cenozoic intervals of elevated atmospheric CO_2 and rapid climate change.

9.4.2. Operations
During Expedition 393, three holes were cored at Site U1558. Hole U1558E consisted of one APC core, which missed the mudline. Hole U1558F was cored by the APC and XCB systems to 177.2 mbsf (Figure **F27**), with the sediment/basement contact at 176.0 mbsf. In Hole U1558D, the sediment/basement contact was found at 166.8 mbsf and the volcanic sequence was cored by the RCB system to 370.2 mbsf (203.4 msb) (Figure **F28A**). Unfortunately, while withdrawing the bit out of Hole U1558D to prepare for wireline logging, the reentry cone and some casing were pulled out the seafloor by the BHA, ending operations in that hole. The cased SAT holes were intended to be legacy holes for potential future deepening or other operations, but this is no longer possible at this site. This damage also precluded wireline logging of the volcanic sequences.

9.4.2.1. Transit
The ship completed the 508 nmi transit from Site U1559 to Site U1558 in 46.5 h (1.9 days), arriving on site at 1125 h on 25 June 2022. The ship was switched to DP mode, beginning operations at Site U1558.

9.4.2.2. Hole U1558E
An APC/XCB BHA was assembled and deployed to 4321 m below rig floor (mbrf). A pipe "pig" was circulated down through the drill pipe to remove any rust from the extra ~1300 m of pipe required to reach the seafloor at Site U1558, compared to the shallower Site U1559 drilled previously. Heavy weather and sea conditions delayed the start of coring in Hole U1558E by 3 h, waiting for the ship's heave to subside. The ship was positioned 20 m south of Hole U1558D. At 0440 h on 26 June, Core 393-U1558E-1H penetrated 9.5 m and recovered 9.97 m (105%), but there was no mudline. Therefore, Hole U1558E was terminated at 0515 h.

9.4.2.3. Hole U1558F
The ship was offset 10 m east of Hole U1558E (50 m southeast of Hole U1558A), and at 0610 h on 26 June 2022 we started Hole U1558F (Figure **F27**). Coring started with the full-length APC and a seafloor depth of 4337.3 mbsl was established based on the mudline in Core 393-U1558F-1H. After Core 3H was drilled ahead by 3 m in an effort to offset gaps in the stratigraphy recovered from Expedition 390C Hole U1558A. APC coring continued to Core 393-U1558F-10H at 86.9 mbsf, where 80,000 lb of overpull was required to free the barrel, marking APC refusal depth. All full-length APC cores were oriented and the APCT-3 tool was deployed on Cores 3H, 6H, and 10H. Unfortunately, the advance in Core 10H was overdrilled by 4.7 m and core is missing from

Hole U1558F from 82.2 to 86.9 mbsf. The half-length APC (HLAPC) system was deployed for Cores 11F–19F. Core 19F at 129.2 mbsf needed to be freed by drilling over the core barrel, marking HLAPC refusal depth. The XCB coring system was deployed from Cores 20X–24X. The driller noted a formation change at 176.0 mbsf, and drilling was terminated at 177.2 mbsf, approximately 1.2 meters into volcanic rocks. Cores 1H–24X penetrated from 0 to 177.2 mbsf and recovered 164.3 m (94%). The drill string was recovered to the ship, and the drill bit cleared the rotary table at 0035 h on 28 June, ending Hole U1558F.

9.4.2.4. Hole U1558D

We then made up the RCB BHA with a new TransCo C-4 RCB bit and following a slip and cut, lowered it down to Hole U1558D, where a reentry system had been installed in November 2020 during Expedition 390C (Figure **F15A**). Guided by the subsea camera video feed, the ship maneuvered over the hole. At first the bit entered the center of the cone but soon met resistance and did not pass down into the casing and had to be pulled back above the cone. The second attempt was successful and the bit reentered Hole U1558D at 1505 h. We lowered the bit to the depth of the existing hole, 150 mbsf, and started coring at 1845 h. The existing hole is designated as drilled interval 390C-U1558D-11. Cores 393-U1558D-2R and 3R penetrated from 150 to 166.5 mbsf and recovered 3.27 m (20%) of sediment. The sediment/basement contact was determined to be at 166.8 mbsf based on an abrupt slowing of the rate of penetration at that depth while starting to drill Core 4R. Coring continued, at first alternating between full and half cores based on the rate of penetration and core recovery, and from Core 16R switching exclusively to half-length cores. Perfluorocarbon tracer was run on all cores. Core 39R reached a healthy 203.4 m into volcanic rock, and coring was stopped to enable wireline logging. Basement Cores 4R–39R sampled from 166.8 to 370.2 mbsf and recovered 97.53 m of core (~48% recovery) and took 5.0 days to drill.
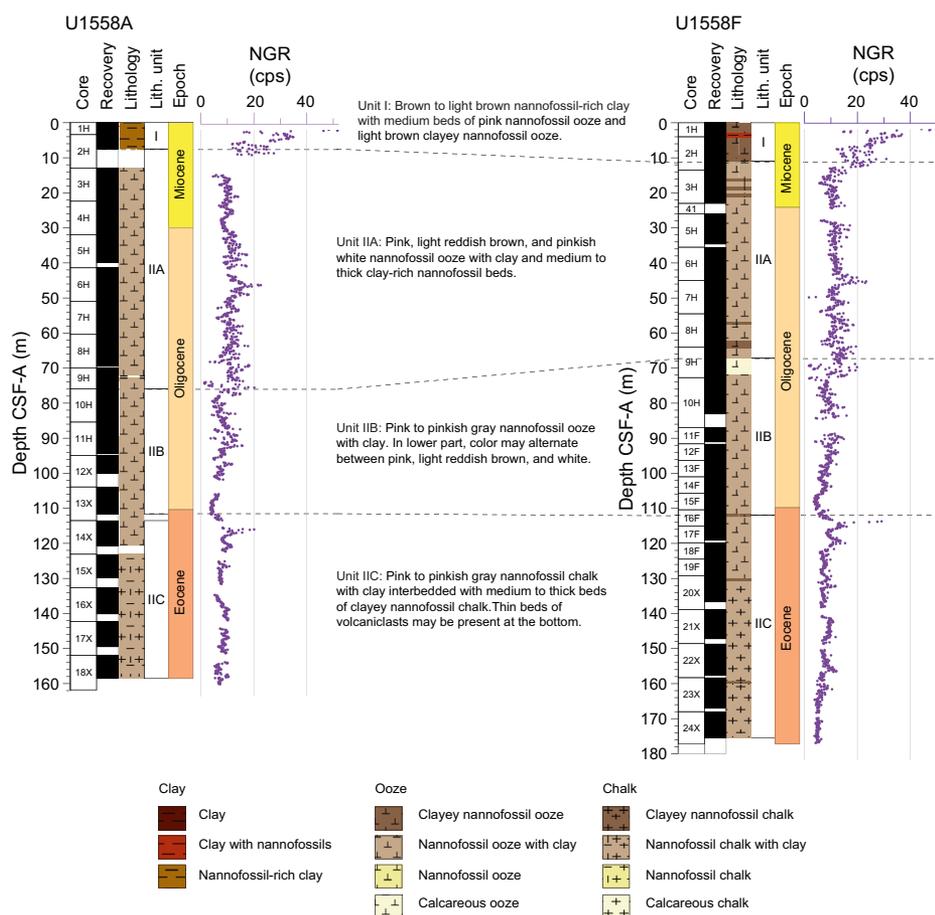
Figure F27. Lithostratigraphic summary of sediment units and correlation of full sediment sequences, Holes U1558A and U1558F. Dashed lines = correlation between units. cps = counts per second.

At 0330 h on 4 July 2022, we set back the top drive and pulled the bit up to 126.3 mbsf, observing 20,000 lb drag. At 0445 h we deployed the subsea camera to observe the bit release and guide reentry, in preparation for downhole logging. We pulled the bit out of the hole to 4317 mbsl, 17 m above seafloor. However, at 0615 h the drill pipe was observed by the subsea camera to be still inside the reentry cone, with the cone much higher up than it should be. The extra weight on the drill string confirmed that the cone and some, perhaps all, casing had been pulled out of the hole by the BHA. From 0730 to 0830 h, we attempted unsuccessfully to free the casing by pushing into the seafloor. We raised the camera back up to the ship and from 1030 to 1100 h we attempted to free the drill string from the casing by rotation. During this process, a weight decrease of 30,000 lb was observed on the hook load indicator, showing that at least part of the casing had come free. The subsea camera was deployed again and at 1345 h we observed that the cone had fallen away and that some of the BHA drill collars appeared to be bent, but the casing hanger and casing cross-over were still attached. The decision was made to retrieve the drill string and deal with any casing at the surface. When the drill string reached surface, the casing hanger and casing were no longer attached and must have fallen away while being raised. The bit cleared the rotary on the rig floor at 0215 h on 5 July. We disassembled the BHA and examined it for damage and set aside the bottom three drill collars, one of which was slightly bent. We then secured the rig floor for transit and raised the thrusters, ending operations in Hole U1558D and at Site U1558. The original operations plan had included running three downhole logging tool strings in Hole U1558D, but this could not be undertaken. Unfortunately, Hole U1558D is no longer a legacy hole for potential future operations. At 0530 h on 5 July, we started the 227 nmi transit to Site U1583.
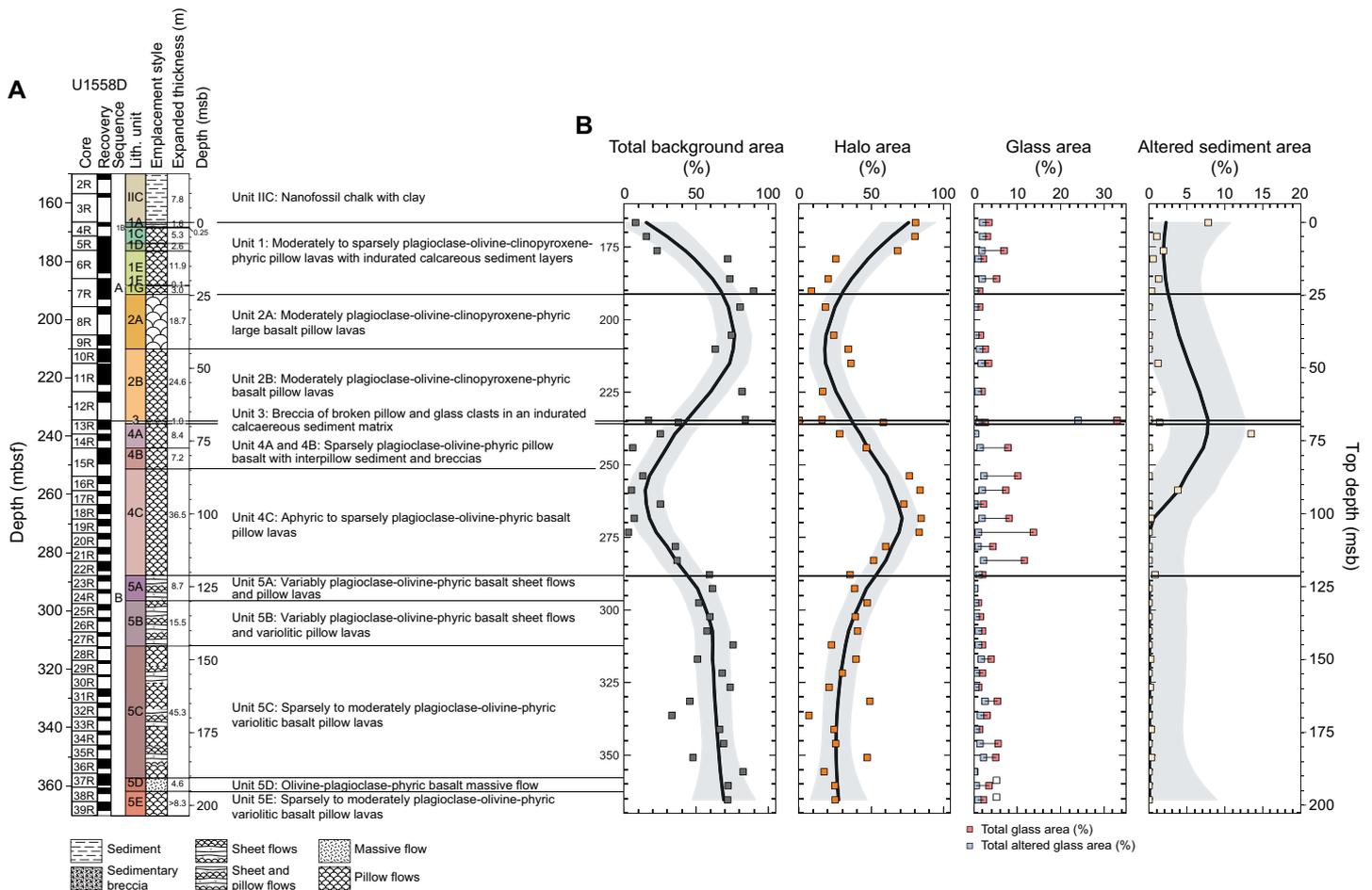
Figure F28. A. Stratigraphic column for igneous basement, Hole U1558D. Unit contact depths and thicknesses are expanded to account for <100% recovery. B. Area abundance of background alteration, alteration halos, fresh and altered glass, and altered sediment. Data are plotted at individual core level. Depths are CSF-A and plotted at top of cored interval. Black trend lines = locally weighted nonparametric regression (LOWESS), gray shading = 2σ of mean.

9.4.3. Principal results

Site U1558 targeted 49.2 Ma upper ocean crust along the SAT. A near-complete sedimentary sequence was recovered from the combination of Holes U1558A and U1558F (Figure **F27**), and uppermost basement rocks were recovered in both holes as well as Hole U1558D. Hole U1558D advanced 203.7 m into basement and recovered a volcanic sequence of moderately altered plagioclase ± olivine ± clinopyroxene phyric pillow lavas and sheet and massive flows with abundant interlava intervals of indurated calcareous sediment (Figure **F28A**).

9.4.3.1. Sediments

9.4.3.1.1. Sedimentology

A near-complete 159–176 m thick sequence of siliciclastic and biogenic sediments was recovered from two sediment holes cored at Site U1558 (Holes U1558A and U1558F), principally comprising brown Early Miocene nannofossil-rich clay overlying pinkish middle Eocene to Early Miocene nannofossil ooze and chalk with clay and foraminifera (Figure **F27**).

Two lithologic units (I and II) are defined at Site U1558. Lithologic Unit I is composed of up to 10.11 m of Pleistocene to Early Miocene, brown and reddish brown nannofossil-rich clay containing varying amounts of foraminifera and sponge spicules and subordinate nannofossil ooze with clay and foraminifera. Lithologic Unit II is composed of up to 165.32 m of middle Eocene to Early Miocene biogenic sediments consisting primarily of pink, pinkish white, pinkish gray, and light brown nannofossil ooze and chalk with varying amounts of clay and foraminifera. Unit II is subdivided into three subunits based on their composition (clay, $CaCO_3$, and foraminifera content) and color. Differences in constituent mineral assemblages between the units and with increasing burial depth are relatively subtle. There is a discernible increase in $CaCO_3$ content with concomitant decrease in clay content downhole. In lower portions of the sediment section, nannofossil ooze is moderately consolidated and is termed chalk. Overall, clay content decreases downhole.

9.4.3.1.2. Biostratigraphy and age-depth model

Calcareous nannofossil and planktic foraminiferal biostratigraphy of sediments recovered at Site U1558 were performed primarily on core catcher samples from Expedition 390C Hole U1558A and Expedition 393 Hole U1558F, examined both on shore and on board *JOIDES Resolution* during Expedition 393.

The mudline sample from Hole U1558A lacks microfossils, preventing an age determination. The mudline sample from Hole U1558F contains Pleistocene planktic foraminifera, whereas calcareous nannofossil assemblages are a predominantly modern assemblage with some Miocene and Paleogene taxa present, indicating some degree of reworking and mixing.

Biostratigraphic analyses indicate that Miocene sediments occur above 22.27 m CSF-B in Hole U1558A and above 13.50 m CSF-B in Hole U1558F. This corresponds to Lithologic Unit I and the uppermost part of Subunit IIA. Oligocene-aged sediments occur between 31.85 and 108.90 m CSF-B in Hole U1558A and between 28.83 and 110.40 m CSF-B in Hole U1558F. Thus, most of Lithologic Subunits IIA and IIB are Oligocene.

The Eocene/Oligocene boundary is inferred to occur within the lowermost part of Lithologic Subunit IIB (at 108.90 m CSF-B in Hole U1558A and at 109.45 m CSF-B in Hole U1558F), close to the Subunit IIB/IIC transition. Eocene sediments are approximately 48.41 m thick in Hole U1558A and 50.4 m thick in Hole U1558F, corresponding to Lithologic Subunit IIC.

The most accurate determination of the age of the sediment/basement interface comes from core catcher samples from Sections 390C-U1558A-18X-CC and 393-U1558F-24X-CC, both of which contained *Reticulofenestra umbilicus*, suggesting that sediments near the sediment/basement interface are not older than 42.72 Ma. Planktic foraminiferal assemblages in Sample 393-U1558F-24X-CC indicate a minimum basement age of 42.6 Ma. These results combined indicate that the first sediments deposited at this site are almost 6.5 My younger than 49.2 Ma, the age estimated for ocean crust at Site U1558 (Kardell et al., 2019).

Calcareous nannofossil and planktic foraminiferal bioevents, in conjunction with paleomagnetic data, allowed for comprehensive hole age-depth models and calculation of linear sedimentation

rates (LSRs). LSRs range 0.38–1.09 cm/ky in Hole U1558A and 0.34–1.8 cm/ky in Hole U1558F. Apart from the condensed sedimentation of Unit I, the lowest sedimentation rates occur in the late Oligocene and Early to Middle Miocene, as well as across the EOT. The highest LSRs occur at the base of the holes, in the middle Eocene, and throughout the Oligocene.

9.4.3.1.3. Sedimentary and pore water geochemistry

Samples from Holes U1558A and U1558F were analyzed for IW and sediment geochemistry and, in the case of Hole U1558A, for headspace gas. IW geochemical data from U1558F is consistently higher for sulfate, Na, Mg, and Cl concentrations and lower for Sr than those in Hole U1558A. When applying a mudline correction and adjusting Hole U1558A values to expected mudline values, elemental concentrations in Hole U1558A show excellent agreement with data from Hole U1558F. Variations in pore water Ca, Mg, and Sr concentrations and Sr/Ca ratios observed in both holes are consistent with authigenic carbonate formation and recrystallization of a high-Mg calcite phase during sediment diagenesis. Dissolution of biogenic silica, weathering of detrital silicates, and/or ion exchange between sediment and pore waters may explain the sharp increases in fluid B, Li, Si, and K concentrations relative to the mudline in Unit I (nannofossil-rich clay) in both holes (Figure **F29**). The pH of Hole U1558A IW is consistent with local seawater pH, with lower values recorded in Hole U1558F. Alkalinity was conversely higher in Hole U1558F and reached seawater values within Subunit IIC (nannofossil chalk with clay and volcaniclastics). Calcium carbonate contents in clay-rich Lithologic Unit I are lower compared to the underlying nannofossil oozes, as expected. The SO_4 minima in both holes roughly coincide with a spike in Mn concentrations and are likely controlled by organic matter remineralization.

9.4.3.1.4. Paleomagnetism

Paleomagnetic measurements were undertaken to determine the magnetic polarity stratigraphy and constrain the magnetic mineralogy of sedimentary units at Site U1558. Continuous measurements of the remanent magnetization were conducted on sediment cores from Hole U1558F and the sediment/basement interface in Hole U1558D using the SRM at a resolution of 2 cm. Remanent magnetization before and after progressive AF demagnetization of three steps (5, 10, and 20
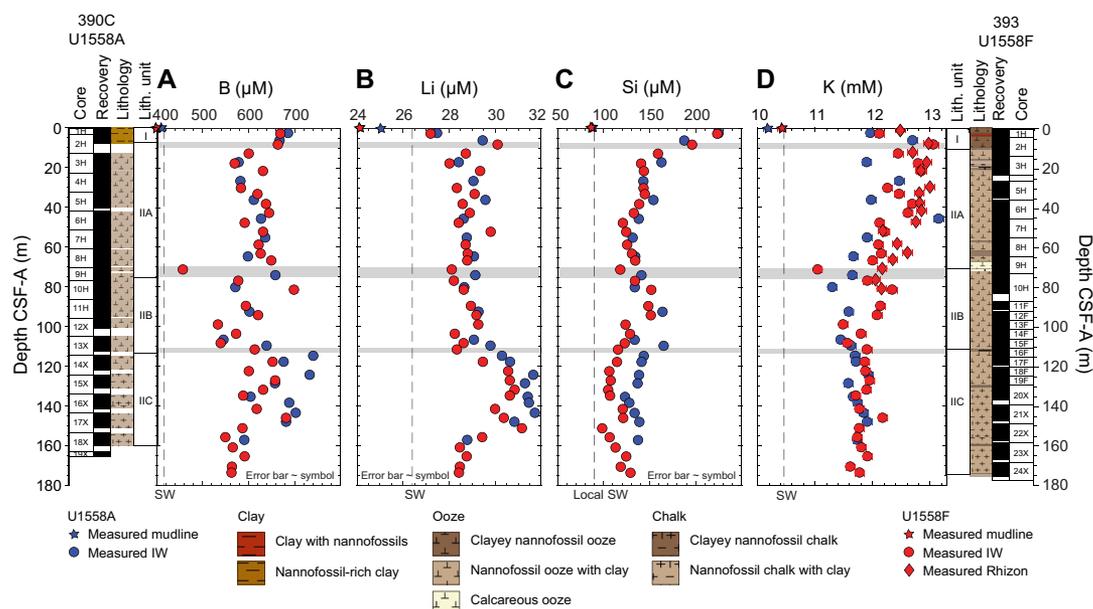

Figure F29. (A) Boron, (B) lithium, (C) silicon, and (D) potassium, Holes U1558A and U1558F. Significant increases in B, Li, Si, and K relative to mudline in Unit I (nannofossil-rich clay) likely result from dissolution of biogenic silica, weathering of detrital silicates, and/or ion exchange between sediment and pore waters. Second increase in B and Li coincides with higher clay contents and lower $CaCO_3$ at Subunit IIB (nannofossil chalk with clay)/IIC (nannofossil chalk with clay and volcaniclastics) boundary. Although Si decreases with depth in both holes, K virtually does not change in Subunit IIC. Smectite-to-illite transformation and alteration of underlying ocean crust may also affect concentrations of these elements. Seawater (SW) reference values for B, Li, and K correspond to International Association for the Physical Sciences of the Oceans (IAPSO) standard composition; local Si concentration is sourced from Sarmiento et al. (2007).

mT fields) were measured during this process. Discrete measurements including AMS and AF demagnetization were conducted on a total of 38 cube samples. IRM acquisition experiments were performed on eight selected samples, which is about two per lithologic unit.

The SRM results from Hole U1558F and the sediment/basement interface in Hole U1558D, along with data obtained from Hole U1558A during Expedition 390C, were used to define the magneto-stratigraphy for the entire sediment sequence at Site U1558. Viscous overprints are almost completely removed at 20 mT demagnetization to reveal characteristic components. The distribution of inclination values is bimodal in both Holes U1558A and U1558F with peaks near ±56° in Hole U1558A and +60° and −51° in Hole U1558F. These values are steeper than indications expected at 30°S in the GAD (±49.1°). SRM data record clear polarity reversals for most of the sedimentary sequence in both Holes U1558A and U1558F, giving confidence in the correlation to the geomagnetic polarity timescale (GPTS). Some intervals near the top of each hole reveal indistinct polarities due to core gaps and drilling disturbances. All collected discrete samples were subjected to AF demagnetization up to 100 mT to derive the ChRM. A total of 35 of the measured samples revealed well-defined ChRMs with maximum angular deviations between 1.9° and 14.8°. The inclination of ChRM components mostly coincide with those shown in the SRM data, providing robustness to the results. The proposed correlation with the current GPTS (Gradstein et al., 2020) has the Chattian/Rupelian boundary (28.1 Ma; Gradstein et al., 2020) within Subunit IIA (~56 m CSF-B in Hole U1558F) and the Oligocene/Eocene boundary at ~110 m CSF-B, near the base of Subunit IIB.

Rock magnetic experiments were conducted on eight samples and reveal the dominance of low-coercivity minerals throughout the cores with no significant variations among different lithologic unit/subunits. AMS measurements mainly reveal a subhorizontal magnetic foliation with neutral to oblate ellipsoidal shapes typical of sedimentary fabric.

9.4.3.1.5. Physical properties

Characterization of the sediment physical properties at Site U1558 was primarily based on cores from Hole U1558F supplemented by measurements from Hole U1558A. Whole-round, section-half, and discrete measurements were considered together to characterize the petrophysical signatures for the different lithologic units. All archive halves were imaged using the X-ray logger (XMAN). A correlation framework and splice were developed for Site U1558 that considers NGR, GRA, MS, and magnetic inclination from each hole. The correlation resulted in an almost continuous spliced record to 207 m CCSF, although a cumulative total of ~12 m of core gap still persists in the splice section. Stratigraphic correlation also highlighted ~2 m of lateral thickness variation between Holes U1558A and U1558F, with Hole U1558F having an expanded record relative to Hole U1558A.

Whole-round measurements of NGR range 2–50 counts/s through the sedimentary section in Hole U1558F. NGR is highest in the upper 10 m of the section, corresponding to the nannofossil-rich clay and ooze of Lithologic Unit I (mean NGR from Unit I in Hole U1558F = 24 ± 7 counts/s [±1σ]). An additional sharp peak in NGR (20–29 counts/s) occurs at the boundary between Subunits IIB and IIC in Holes U1558A and U1558F. In contrast, intervals dominated by carbonate ooze generally have low NGR (<15 counts/s). Pass-through magnetic susceptibility follows a similar downhole trend to NGR with an overall range of 0–145 IU) (mean = 32 ± 16 IU) in Hole U1558F. The highest values are associated with the clayey nannofossil-rich ooze of Unit I (ranges 18–118 IU; average = 70 ± 22 IU). Magnetic susceptibility is relatively low through Unit II, with peaks at ~65 m core depth below seafloor, Method A (CSF-A) (Subunit IIA), ~112 m CSF-A (Subunit IIB/IIC boundary), and from ~154 to 160 m CSF-A (Subunit IIC). The average GRA bulk density of whole-round cores is lowest in Unit I (mean = 1.6 ± 0.1 g/cm^3) compared to the other three subunits (mean = 1.8 ± 0.1 g/cm^3), and a similar trend is seen in bulk density from discrete samples. Porosity of discrete samples decreases with depth, from ~70% at the seafloor to ~50% close to the sediment/basement interface (173 m CSF-A). *P*-wave velocity measured on whole-round cores ranges 1.45–1.74 km/s (mean = 1.56 ± 0.03 km/s) and generally increases with depth. Compressional strength of the sediments increases with depth, whereas shear strength reaches maximum values (~52 kN/m^2) at 30 m CSF-A before decreasing downhole. Thermal conductivity values range 1–1.61 W/(m·K) throughout Hole U1558F (mean = 1.34 ± 0.14 W/[m·K]) and gradu-

ally increase downhole. The vertical conductive heat flow for Site U1558 was estimated to be 28–30 mW/m², which is lower than modeled heat flow values for ocean crust of this age, requiring significant regional hydrothermal advection of heat to make up the difference (cf. Kardell et al., 2021).

9.4.3.1.6. Microbiology

Microbiological analysis of samples from Hole U1558F will focus on microscopy and culture-based and culture-independent approaches to characterize microbial abundance, diversity, and activity in the sediments. One microbiology whole-round sample (5–10 cm long) was collected from each 9.5 m core and divided for shipboard and shore-based studies. Additional whole-round cores for specialized shore-based analyses were also taken. A number of microbiology analyses on sediment samples from Hole U1558F were initiated shipboard during Expedition 393. To study the extent of viral activity and dynamics between viruses and other microbial life (Bacteria and Archaea), virus-induced microbial mortality and prophage induction experiments were performed on subsamples taken from six microbiology whole-round cores throughout the sediment column. To study the microbial activity at the sediment/basement interface, ammonium enrichment incubation experiments were started with the deepest sediment cores at Site U1558 along with the uppermost basement samples.

9.4.3.2. Volcanic rocks

9.4.3.2.1. Igneous petrology

Hole U1558D drilled ~203 m of MOR basalts and intersected two distinct volcanic sequences separated by a ~1 m thick layer of indurated calcareous sedimentary breccia with volcanic debris possibly indicating a hiatus in volcanism at this site on the order of tens of thousands of years (Figure **F28A**). The upper Sequence A (166.55–234.64 mbsf) includes volcanic Units 1 and 2 that are moderately to highly plagioclase-olivine-clinopyroxene phyric microcrystalline basaltic lavas mostly emplaced as lava pillows of varying comfort (10–130 cm diameter). Extremely sparse but distinctive green clinopyroxene phenocrysts are a characteristic feature of the Sequence A volcanic rocks. In contrast, the underlying Sequence B (234.65–370.20 mbsf) lacks these green phenocrysts, and its uppermost unit contains abundant interflow sediments and breccias, suggestive of a buried seafloor horizon. This change in phenocryst assemblage indicates that some aspect of the magmatic system changed between eruptive sequences. However, lava geochemistry as assessed by Cr/Ti ratios measured directly on the cores by pXRF is relatively consistent downhole with little evidence for fractionated series, apart from Unit 4, which has higher Cr concentrations than the other lava units.

9.4.3.2.2. Alteration petrology

The alteration within Hole U1558D can be divided into four zones (Figure **F28B**). From the top of the volcanic sequence down to 179 mbsf within Unit 1, there is a dominance of brown halo alteration associated with pillow lava chilled margins. Between 179 and 234 mbsf (part way through Subunit 1E to the base of Subunit 2B), the second zone is distinguished by a decrease in the abundance of all halo types and gray background alteration and orange speckled background alteration of the pillow lavas dominate (Figure **F28B**). This shift from brown halo dominated to background alteration dominated is interpreted to represent a seafloor weathering overprint and suggests that the pillow lavas were exposed to open circulation of seawater for some period of time before becoming covered with sediment. The third zone (234–286 mbsf) is broadly associated with igneous Units 3 and 4 and is marked by the first appearance of orange-reddish yellow alteration within pillow lavas. This color likely represents the strongest alteration within Hole U1558D and is generally associated with alteration fronts developing from the glassy margins of individual pillows (Figure **F28B**). Macroscopically these orange-reddish yellow alteration fronts transition into the more ubiquitous brown halos seen throughout Hole U1558D. Some of the freshest volcanic glass is preserved where the groundmass alteration of the pillow lavas is strongest. The abundance of breccia and sediment at the top of this interval suggests that these rocks were also exposed to seawater for a significant duration before becoming covered by the overlying lava sequences. The fourth alteration zone is defined by the onset of mixed gray-brown background alteration that has a common but not unique association with variolitic textures. The orange-reddish yellow halos persist through this change in background alteration. Although there are some associations between the

igneous units and the different alteration zones, the onset of the key alteration features defining the zones do not generally follow igneous unit boundaries.

9.4.3.2.3. Igneous geochemistry

Representative samples were taken from the freshest portions of each volcanic subunit in Hole U1558D to obtain a downhole record of the primary magmatic conditions, along with one sample near the basalt/sediment contact. Additionally, four samples of breccia were taken to understand the basalt-sediment chemical exchanges that occurred as new lavas erupted and interacted with pelagic sediment. A total of 29 samples were measured for LOI and bulk rock geochemical analysis via ICP-AES. The unoxidized powders of these samples were also characterized for elemental abundances via pXRF to complement the direct core measurements. The Hole U1558D basalts are weakly to strongly altered, with variable MgO and CaO concentrations and elevated abundances of K_2O and Rb. Basaltic protolith compositions change downhole, with TiO_2 contents varying between 1 and 1.2 wt% from 160 to 290 mbsf, and then increasing to 1.3–1.5 wt% deeper than 290 mbsf. In terms of basaltic rock type, the freshest samples classify as olivine tholeiites per the Yoder and Tilley (1962) normative classification scheme as also displayed in the Zr/Y versus Zr tectonic discrimination plot (Figure **F30**; Pearce and Norry, 1979). K/Zr ratios, a broad measure of alteration extent, vary between 20 and 109 in Site U1558 basalts, averaging 44.5, much higher than fresh South Atlantic mid-ocean-ridge basalt (average = 7.4). Incompatible element concentrations are consistent with a similar depleted mid-ocean-ridge basalt (D-MORB) composition for lavas at Site U1558. The breccia fill materials, which are partly of sedimentary origin, vary widely in composition from very Ca-rich to Ca-poor, with the most Ca-poor samples showing the highest K_2O abundances.

9.4.3.2.4. Paleomagnetism

Paleomagnetic measurements were conducted on basement cores of Hole U1558D using the SRM at a resolution of 2 cm. Remanent magnetization before and after progressive AF demagnetization at 5, 10, and 20 mT fields were measured on pieces that are longer than 9 cm. Since the recovery rate varied greatly throughout the hole (11%–90%), there are clear differences in data resolution between cores. Rock magnetic experiments were performed on a total of 36 cube samples, targeting basalts of various degrees of alteration and one sample from the sedimentary breccia.

The SRM results mostly remove all viscous overprints and successfully reveal primary components at the 20 mT demagnetization step. These components mainly show a negative inclination which indicates a normal polarity, in agreement with the expected polarity for 49.2 Ma (Gradstein et al., 2020; Kardell et al., 2019) ocean crust, although positive inclinations were found in some
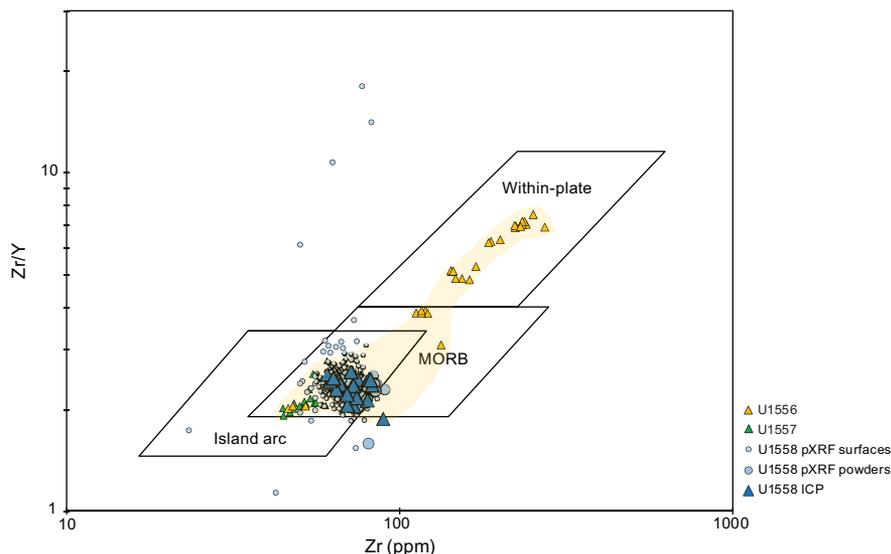

Figure F30. Zr/Y vs. Zr tectonic discrimination diagram from Pearce and Norry (1979) showing combined pXRF and ICP-AES data for Site U1558 basalts compared to data from Sites U1556, U1557, and U1559. MORB = mid-ocean-ridge basalt.

layers in the lower parts of the hole. The distribution of inclination values is heavily clustered around –55°, about 6° steeper than the angle expected in the GAD (±49.1° at 30°S).

A subset of 32 discrete samples was subjected to stepwise AF demagnetization up to 130 mT to derive the ChRM. The remaining 6 samples were stepwise thermally demagnetized up to 580°C. Discrete sample measurements mostly reveal well-defined ChRM with maximum angular deviation between 0.4° and 5.4°. IRM acquisition experiments conducted on 24 selected samples revealed saturation levels around 150–300 mT, implying that low-coercivity minerals such as titanomagnetite and/or maghemite are the main magnetic carriers (Figure **F31**). Slight variations in remanence intensity and MS occurred depending on the alteration degree. AMS measurements reveal a well-defined prolate fabric characterized by subhorizontal magnetic foliation.

9.4.3.2.5. Physical properties

Characterization of the basement physical properties at Site U1558 is primarily based on cores from Hole U1558D supplemented by information from Holes U1558A and U1558F where the uppermost basement was also recovered. Whole-round, section-half, and discrete measurements were considered together to characterize the petrophysical signatures for the different lithologic
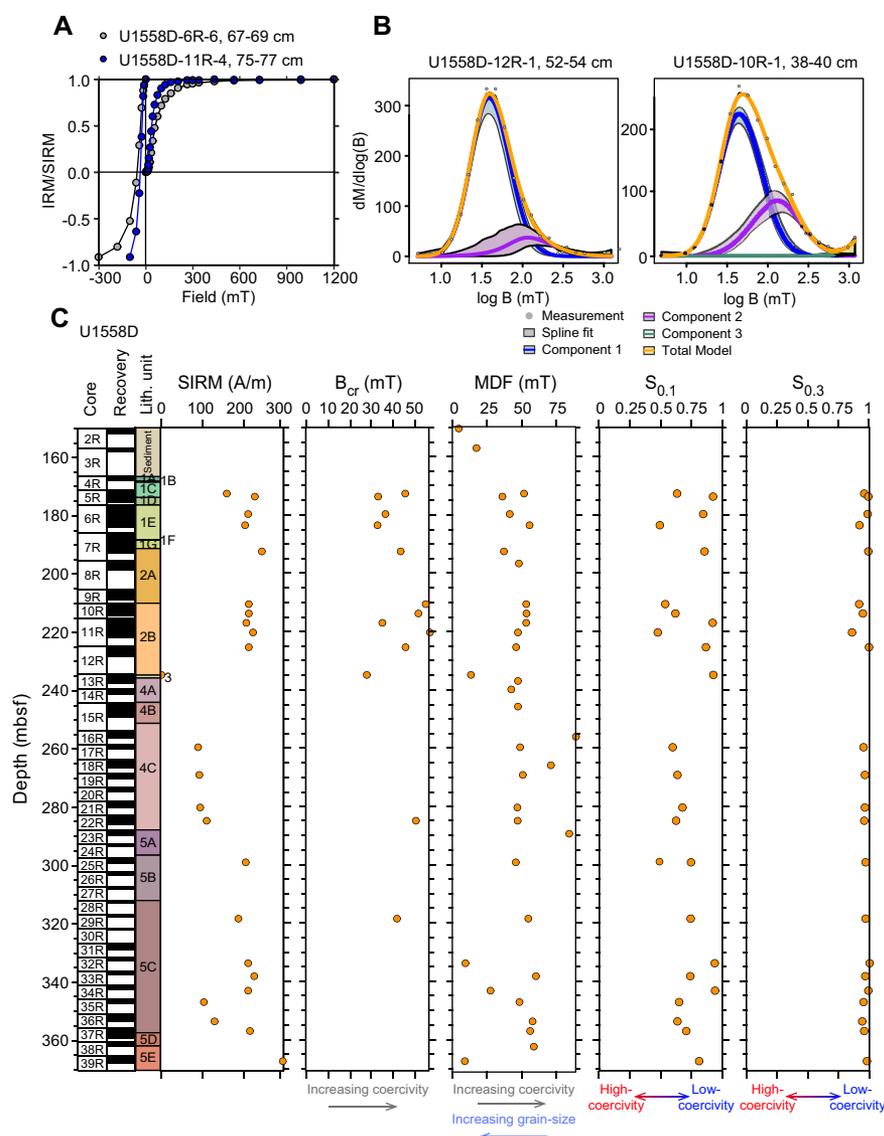
Figure F31. A. Curves of saturation IRM (SIRM) acquisition up to 1200 mT and backfield IRM truncated at −0.3 T for two representative samples of basement rock, Hole U1558D. B. Coercivity distribution and unmixing of IRM acquisition curves (Maxbauer et al., 2016). C. IRM acquisition: B_{cr} = coercivity of remanence, $S_{0.1}$ = IRM$_{100}$/SIRM, $S_{0.3}$ = S ratio.

units. All whole-round cores were imaged using an XMAN. About 72% of the recovered material was scanned using the DMT CoreScan3.

NGR in Hole U1558D ranges 0.1–11.6 counts/s with a mean of 4.0 counts/s. The highest NGR in this section is associated with an indurated calcareous sedimentary breccia (Volcanic Unit 3), although basalts in Subunits 4A and 4B also show elevated NGR. Discrete point magnetic susceptibility (MSP) measurements from section halves range 1–669 IU (mean 159 ± 88 IU [±1σ]). Units 1 and 2 have a higher mean MS than Units 4 and 5, with the lowest MS observed in the volcaniclastic sedimentary breccia Unit 3. A pronounced peak in MS is seen in Subunit 5D (massive flow).

To integrate petrophysical measurements with the observations of other groups, all discrete MAD samples were also used for paleomagnetic measurements, and, with the help of petrologists, all samples were classified according to key attributes such as grain size, alteration, or emplacement style. Discrete MAD measurements (bulk and grain densities and porosity) as well as *P*-wave velocity are affected by the alteration level in the 40 samples that were measured. Samples displaying higher levels of alteration such as those with strongly developed brown alteration halos, mixed gray-brown variolitic textures, or orange-reddish yellow colors generally have lower bulk and grain density, lower *P*-wave velocity, and higher porosity compared to less altered samples. There is no clear relationship between these physical properties and the igneous units. However, basalts emplaced as large pillow flows appear to have higher density and *P*-wave velocity and lower porosity compared to mixed sheet and pillow flows, with smaller pillow flows occupying an intermediate range of values. The average thermal conductivity measured in basement samples is 1.54 ± 0.14 W/(m·K) (*n* = 39 measurements). Combined with an estimated vertical conductive heat flow in sediments of 28–30 mW/m^2, this suggests a temperature gradient of about 20°C/km in the shallow basement at Site U1558 if the thermal regime is mostly conductive.

9.4.3.2.6. Microbiology

Microbiology sampling of volcanic rocks from Hole U1558D was focused on exploring evidence for life in the basement, especially at the sediment/basement interface, using microscopy and culture-based and culture-independent approaches. A total of 21 whole-round samples between 12 and 23 cm long were sampled to characterize microbiology in the variety of volcanic formations in Hole U1558D. After the contaminated exteriors of whole-round pieces were removed, the remaining material was split into subsamples that were prepared for different microbiology analyses. Experiments were started shipboard to study microbial activity at the sediment/basement interface using ammonium enrichment incubations. These incubations focused on the uppermost basement samples to correspond with the deep sediment column samples described above.

To determine the extent of contamination of microbiology samples, the perfluorocarbon tracer PFMD was injected into the drilling fluids during coring in Hole U1558F. Microbiologists then collected samples from both the exterior and interior of core intervals selected for microbiology analysis, as well as core catcher rubble, to quantify the presence of PFMD. PFMD was detected on a majority of the exterior samples, with an average concentration of 18 ppb/g and a median concentration of 10 ppb/g of rock when detected. The tracer was not detected in the interior microbiology samples, suggesting no to minimal drilling contamination of the samples.

9.5. Site U1583

9.5.1. Background and objectives

Site U1583 is located ~652 km west of the Mid-Atlantic Ridge at 30°42.6175′S, 20°26.0336′W (Hole U1583F) in 4210 m of water (Figure **F1**). The basement at Site U1583 was predicted to have formed at ~30.6 Ma at a half-spreading rate of 24 mm/y (Kardell et al., 2019; Christeson et al., 2020) (Figure **F7**). The site is located on the approximately north-south–trending (355) CREST seismic crossing Line 03 at CDP 12300 about 3.3 km south of the main east–west (085) CREST Seismic Line 1C/1D (Figures **F1**, **F6D**, **F32**). A reflector at ~5.73 s TWT was interpreted to be the top of basement, estimated to be at 138 mbsf and observed at 106 mbsf (Figure **F6D**).

Site U1583 is a new site that had not been previously occupied. The original operational objectives of Expedition 393 at Site U1583 were to core two APC/XCB holes to basement and to core and log

~250 m of basement volcanic rocks. At 30.6 Ma, Site U1583 is in the middle of the SAT and will be compared to older and younger sediments and igneous rocks cored during Expeditions 390 and 393. Science objectives at Site U1583 are to (1) investigate the history of the low-temperature hydrothermal interactions between the aging ocean crust and the evolving South Atlantic Ocean and quantify past hydrothermal contributions to global geochemical cycles, (2) collect samples of the sediment- and basalt-hosted deep biosphere beneath the low-productivity South Atlantic Gyre that will be used to refine global biomass estimates and investigate microbial ecosystems' responses to variable conditions, and (3) construct paleoceanographic records of carbonate chemistry and deepwater mass properties across the western South Atlantic Ocean through key Cenozoic intervals of elevated atmospheric CO_2 and rapid climate change.

While *JOIDES Resolution* was operating at Site U1583 at 1030 h on 6 July 2022, a tribute was held for Professor Dirk "Dick" Kroon, Regius Professor of Geology at the University of Edinburgh (Scotland), former IODP Science Evaluation Panel Co-Chair, and until recently Chair of the IODP Forum. Many colleagues from the international scientific ocean drilling community around the world joined the shipboard party in the minute's silence. A free-fall funnel labeled "Dick Kroon 1957–2022" was dropped over Hole U1583F to enable coring and wireline logging operations during Expedition 393.

9.5.2. Operations

9.5.2.1. Transit
At 0530 h on 5 July 2022 we started the 227 nmi transit to Site U1583. The transit took 21.5 h at an average speed of 10.6 kt and we arrived on site at 0300 h on 6 July.

9.5.2.2. Site U1583
The ship switched to DP mode at 0315 h on 6 July 2022, beginning operations in Hole U1583A. On site, we noted a 41 m seafloor depth discrepancy between the ship's PDR 12 kHz estimate of 4234 mbsl and the prospectus estimate from the preexpedition seismic survey of 4193 mbsl. Sea conditions were rough and ship heave was 3–4 m. The APC/XCB BHA was made up and lowered down to 4228.5 mbsl, 4.5 m above the PDR estimated depth.

9.5.2.3. Holes U1583A and U1583B
At 1545 h, we started Hole U1583A, but Core 393-U1583A-1H recovered 9.14 m of sediment, indicating that the bit was below the seafloor when the piston was shot, so the mudline depth could not be determined. At 1715 h, we started Hole U1583B at approximately the same geographic location with the drill bit 5 m shallower and similarly Core 393-U1583B-1H was full, recovering 9.38 m of sediment, so the mudline depth again could not be determined.
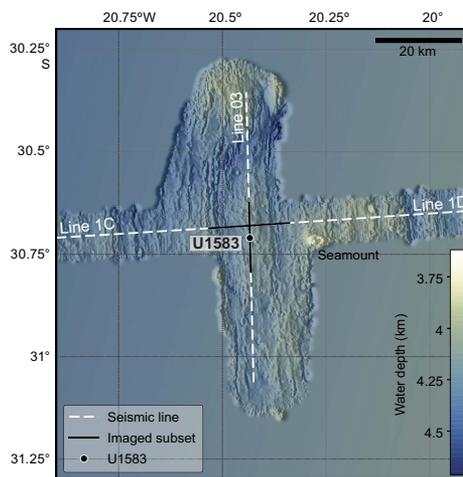

Figure F32. Site U1583 bathymetry (Christeson and Reece, 2020). Seismic reflection profiles were acquired during CREST cruise (Reece et al., 2016).

9.5.2.4. Hole U1583C

The bit was raised 10 m shallower than the Hole U1583B shooting depth to 4213.5 mbsl, and the ship moved 10 m to the north. At 1845 h, we started Hole U1583C (Figure **F33**), and Core 393-U1583C-1H recovered 8.5 m of sediment, giving an apparent mudline at 4214.6 mbsl. We did not know at the time that this core was also shot from below the mudline. Coring continued with the full-length APC system with the Icefield orientation tool run on each core. Temperature measurements were taken on Cores 4H, 7H, and 10H. Core 12H hit hard rock when it was fired, based on some damage to the cutting edge of the APC shoe. The basement contact was subsequently confirmed when the bit encountered hard formation 2 m below the top of the Core 12H at 104.5 mbsf. Core 12H recovered 8.02 m of sediment, an apparent 401% recovery, most of which was disturbed sucked-in sediment and is not in place. This basement depth was ~33.5 m shallower than expected from the site survey seismic interpretation of basement depth at ~138 mbsf. Cores 1H–12H penetrated from 0 to 104.5 mbsf and recovered 108.3 m (103%).

The XCB coring system was then deployed for Core 13X, which penetrated 3 m to 107.5 mbsf and recovered 1.9 m of fresh microcrystalline basalt (63%). The bit was then pulled out of the hole, clearing the seafloor at 1540 h on 7 July 2022, ending Hole U1583C.

9.5.2.5. Hole U1583D

We started Hole U1583D 50 m south of Hole U1583C and 20 m south of the preexpedition site coordinates, which we reserved to be the location for hard rock coring in Hole U1583F. All holes at this site are located on a north–south line because the site sits on the edge of a north-south–trending basin and the basement depth was anticipated to be more uniform in this direction compared to the east–west direction. Core 393-U1583D-1H recovered 10.04 m of sediment and the mudline depth could not be determined. Coring was terminated and Hole U1583D ended at 1730 h on 7 July 2022.

9.5.2.6. Hole U1583E

We raised the bit by 5 m to 4204.5 mbsl and at 1835 h we started Hole U1583E (Figure **F33**) in the same location as Hole U1583D. Core 393-U1583E-1H recovered 4.03 m of sediment, placing the mudline at 4210.0 mbsl. This seafloor depth was 24 m shallower than the PDR depth and 17 m deeper than depth predicted from the preexpedition seismic survey. The difference from the
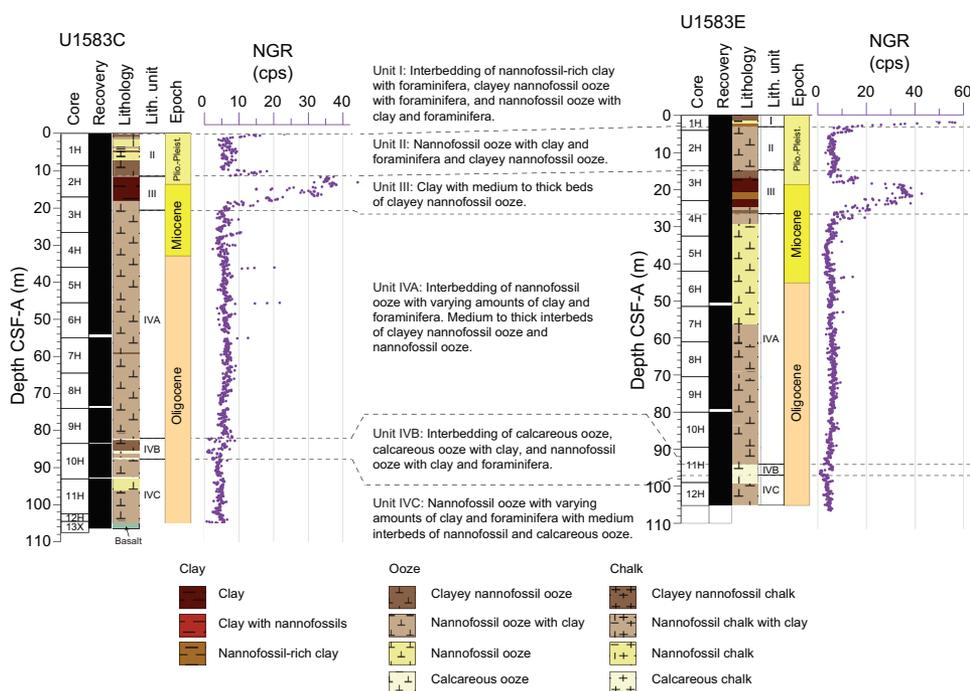

Figure F33. Lithostratigraphic summary of sediment units and correlation of full sediment sequences, Holes U1583C and U1583E. Dashed lines = correlation between units. cps = counts per second.

seismic survey depth is consistent with observations at Sites U1556–U1560 along the transect, where mudline seafloor depths are deeper by 8–21 m than the depth estimated from the seismic survey. While retrieving Core 393-U1583E-2H, the core winch weight indicator showed that the core barrel became detached from the core winch line. An overshot was made up using a core catcher and a RCB core barrel. The barrel was lowered and the APC core barrel was retrieved. Coring continued to Core 12H to a depth of 105.2 mbsf. All cores were full-length APC cores with the Icefield orientation tool run on all but two cores (3H and 4H). Temperature measurements were taken on Cores 3H and 8H.

After cutting Core 12H, the APC core barrel could not be pulled back into the BHA. From 1230 to 1545 h on 8 July we tried to free the barrel by pumping and washing over it, but it would not move. We decided to deploy the Kinley Cutter tool to cut the winch core line just above the APC corer. The Kinley Cutter was deployed at 1610 h and the hammer/actuator was deployed at 1640 h. However, based on the core winch line tension, the Kinley wireline cutter and crimper stopped before reaching the bottom of the drill string and cut part way down. Approximately 1560 m of core winch line was pulled up to the ship and we then started to raise pipe. The drill pipe was pulled out of the hole to a depth of 2562 mbrf when the severing tool was found in stand number 83. A second Kinley Cutter was deployed to sever the remaining core winch line from the sinker bar assembly. This was unsuccessful, and the rig crew continued to pull the drill string out of the hole, cutting and removing the remaining core winch line at each stand. The second severing tool was found at the top of stand 55. The rig crew continued to pull the drill string to surface, cutting and removing the core winch line as before. The bit reached the rig floor at 0435 h on 10 July, ending Hole U1583E. The rig floor team then disassembled the lower part of the BHA and found that the APC core barrel assembly had stuck in the landing saver sub because a shear pin had become wedged between the landing seat and the core barrel. The APC cutting shoe was undamaged, showing that it had not hit basement, and Core 12H recovered 6.1 m of sediment after its long trip to the surface. Cores 1H–12H penetrated from seafloor to 105.2 m and recovered 105.2 m (100%).

9.5.2.7. Hole U1583F
At 1000 h on 10 July we began assembling the RCB BHA with a C-7 bit and then lowered it down to 4174 mbsl, where we paused to slip and cut the drill line and pick up the top drive. At 0030 h on 11 July we started Hole U1583F (Figure **F34A**) and washed down through most of the sediment column to 101 mbsf (drilled interval 393-U1583F-11). Core 2R penetrated from 101.0 to 109.5 mbsf and recovered 6.4 m (76%) of clayey nannofossil ooze. At the start of drilling Core 3R a hard formation was noted by the drillers at 109.7 mbsf, and the formation was subsequently confirmed to be basalt. Coring continued to Core 8R at depth of 142.9 mbsf. With a hole in basement established, a free-fall funnel was deployed at 1450 h on 12 July to aid in reentry for downhole logging or for a bit change, which was still a possibility at the time. Coring continued with a typical RCB half-core advance of 4.8 m. To test for microbiological contamination PFMD tracer was run continuously in the drilling fluid until the supply was exhausted on Core 12R. From Core 12R there was up to 3 m of backfill in the hole after each core, and the drill string experienced high torque at times. It was uncertain if the fill resulted from cuttings not being completely cleared from the hole or if new material was falling down from the borehole wall. We ran 30–60 barrel mud sweeps after every core to flush out the cuttings. The last five cores (25R–29R) averaged only 7% recovery and the bit had been run for ~73 h of drilling time, so coring was terminated at 1230 h on 16 July after recovering Core 29R. Basement Cores 3R–29R penetrated from 109.5 to 239.5 mbsf and recovered 39.4 m (30%).

To prepare for wireline logging in Hole U1583F we ran a 75 barrel mud sweep and released the RCB bit at the bottom of the hole. We set the end of the pipe at 102.8 mbsf in sediment ~7 m above the basalt flow that forms the uppermost basement to avoid of the risk of dislodging rock pieces while the logging tools were below that depth. At 1730 h we began to rig up the triple combo logging tool string, consisting of NGR, neutron porosity, density, and electrical resistivity tools. Because of the hole conditions and ~3 m ship heave, which is high for logging, the density tool source and the magnetic susceptibility tool were not included in the tool string, and the density tool was used only for the caliper log of borehole diameter. The tool string was lowered down the pipe, but at ~540 mbsl it developed an electrical fault and had to be raised back to the ship. The

fault was found in the electrical resistivity tool (the lowermost tool of the tool string), which was then replaced with the backup resistivity tool.

We started to lower the triple combo from the rig floor again at 0045 h on 17 July. Logs were recorded on the downward pass, and the tool string reached to 237 mbsf, within 3 m of the bottom of the hole. Two logging passes were run in the open hole. During the first pass, the wireline heave compensator cut out about half-way up the open hole but logging continued to the top of basement. While descending for the second pass, the tool string encountered an obstruction at 182 mbsf and could not pass below it. We raised the triple combo to the rig floor, disassembled it, and assembled the FMS-sonic tool string. We lowered the FMS-sonic tool string down to 182 mbsf and made a logging pass up to the top of basement at 109.5 mbsf. At that point we found that the tool string could not go back down into basement, and overpull of approximately 8000 lb was observed when trying to pull the tool string back into drill pipe. After pumping to remove any potential obstruction, the tool string still could not enter the pipe. Finally, we rotated the pipe 180° and the tool string could be pulled in. When the tool string reached the rig floor, it was discovered that the FMS tool caliper arms had been damaged and one was missing. By midnight we had disassembled the FMS-sonic tool string, ending downhole logging operations at Hole U1583F. The difficult borehole conditions and continuing high heave did not allow for the planned logging with the UBI tool string. We raised the pipe from 102.8 mbsf, clearing seafloor at 0035 h on 18 July. The BHA reached the ship at 0645 h and was disassembled. The rig floor was secured for transit by 0840 h, and we raised the thrusters and began the transit to Site U1560.
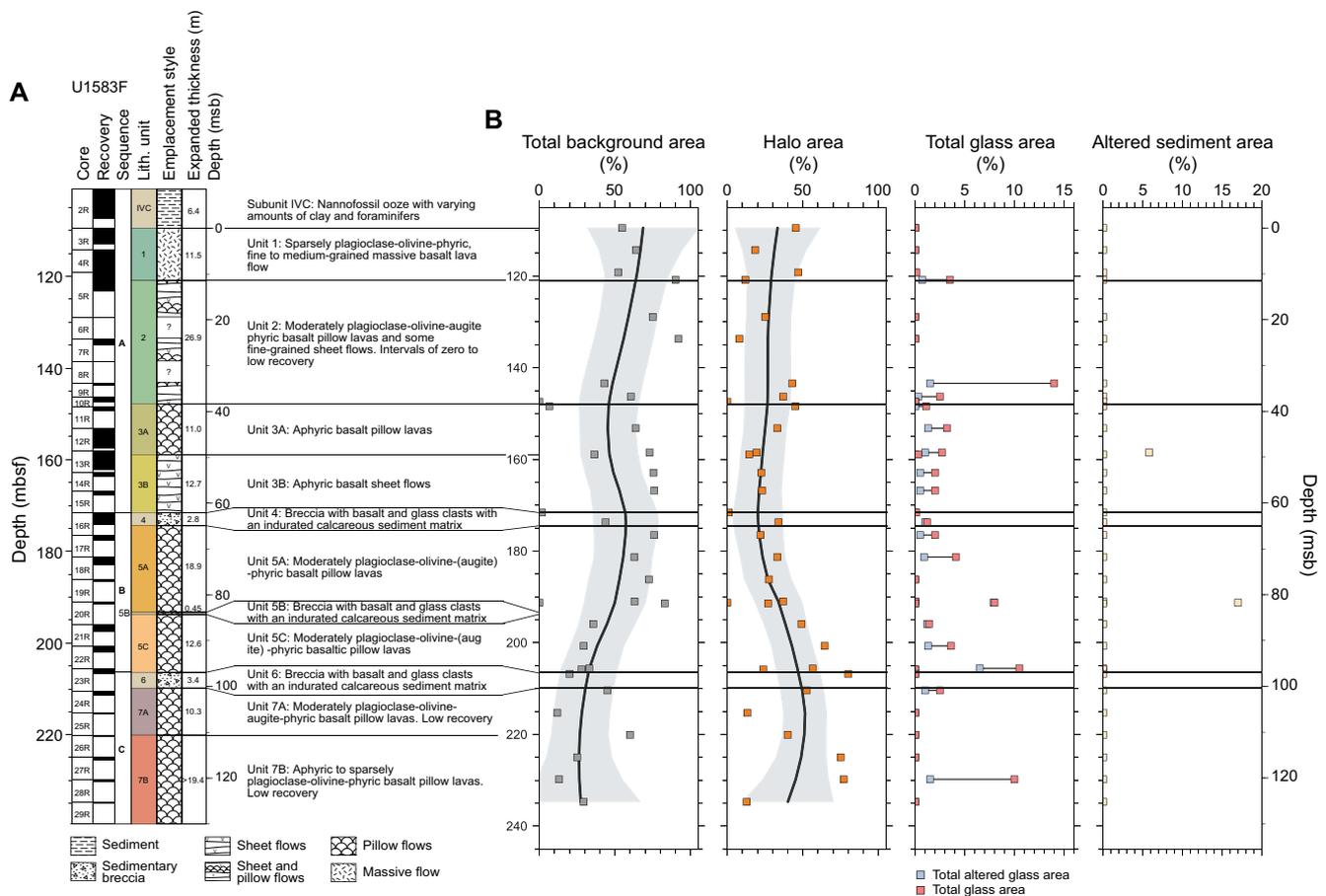

Figure F34. A. Stratigraphic column for igneous basement, Hole U1583F. Unit contact depths and thicknesses are expanded to account for <100% recovery. B. Area abundance of background alteration, alteration halos, fresh and altered glass, and altered sediment. Data are plotted at individual core level. Depths are CSF-A and plotted at top of cored interval. Black trend lines = locally weighted nonparametric regression (LOWESS), gray shading = 2σ of mean.

9.5.3. Principal results

Site U1583 targeted 30.6 Ma upper ocean crust along the SAT. A near-complete sedimentary sequence was recovered from the combination of Holes U1583C and U1583E (Figure **F33**), and uppermost basement rocks were recovered in Hole U1583C as well as Hole U1583F. Hole U1583F advanced to a total depth of 239.5 m (Figure **F15C**), ~130 m into volcanic rocks of the ocean crust and recovered >39 m of basalt lavas and breccias with a recovery rate of ~30%.

9.5.3.1. Sediments

9.5.3.1.1. Sedimentology

Drilling at Site U1583 recovered 108.3 m of sediment and 1.89 m of volcanic rock in Hole U1583C and 105.2 m of sediment in Hole U1583E (Figure **F33**). The cores recovered from Holes U1583A to U1583F record four major sedimentary lithologic units (I–IV). Biogenic sediments consist primarily of calcareous nannofossil ooze with varying amounts of clay and foraminifera. Intervals with siliciclastic sediments have abundant clays with variable nannofossil and foraminifera content. Lithologic Unit I, composed of 3 m of Pliocene/Pleistocene sediments consisting of interbedded nannofossil-rich clay with foraminifera and clayey nannofossil ooze, was only recovered in Hole U1583E. Lithologic Unit II is composed of up to 11.3 m of Pliocene/Pleistocene sediments, predominantly beds of nannofossil ooze with clay and foraminifera interbedded with beds of nannofossil ooze with clay. Unit III consists of up to 11.9 m of clay and nannofossil ooze with varying amounts of clay. Unit IV is divided into three subunits (IVA–IVC). Subunit IVA is up to 64.4 m thick and consists of nannofossil ooze with clay and varying amounts of foraminifera. Subunit IVB comprises up to 6.1 m of nannofossil ooze with clay and decimeter-thick beds of calcareous ooze. Subunit IVC is up to 24.4 m thick and consists of nannofossil ooze with clay and varying amounts of foraminifera.

9.5.3.1.2. Biostratigraphy and age-depth model

Calcareous nannofossil and planktic foraminiferal biostratigraphy of Site U1583 was performed primarily on core catcher samples examined on board *JOIDES Resolution* during Expedition 393. The mudline sample in Hole U1583E contains modern assemblages of planktic foraminifera and calcareous nannofossils. In contrast, the uppermost sediments in Hole U1583C contain a collection of recent to Late Pleistocene planktic foraminifera, accompanied by Early Pleistocene calcareous nannofossils, confirming that the mudline was missed in this hole.

Biostratigraphic analyses indicate that the Pliocene/Pleistocene boundary occurs above 11.1 m CSF-B in Hole U1583C and above 13.5 m CSF-B in Hole U1558E (Figure **F35**), which corresponds to the sequence of brown nannofossil-rich clays and pink nannofossil oozes (Lithologic Units I and II, respectively). Dark clay sediments (Lithologic Unit III) below the Pliocene–Pleistocene sediments are ~6.6 m thick in Hole U1583C and 11.8 m thick in Hole U1583E and represent a condensed interval spanning roughly ~9 My across the Miocene/Pliocene boundary (Figure **F35**).

Biostratigraphic data indicate early Middle Miocene sediments occur between 14.8 and 36.0 m CSF-B in Hole U1583C and between 23.0 and 42.0 m CSF-B in Hole U1583E (Figure **F35**). The Oligocene is ~71.5 m thick in Hole U1583C, and ~54.8 m thick in Hole U1583E, and corresponds to the sequence of calcareous and nannofossil oozes (combined Lithologic Unit IV).

The most accurate determination for the age of sediment/basement interface comes from the deepest sediment samples from Holes U1583C (Sample 393-U1583C-12H-CC, 12–17 cm) and U1583E (Sample 393-U1583E-12H-CC, 0–1 cm) that both contain *Sphenolithus distentus*, suggesting an age younger than 30.0 Ma (Figure **F35**). Planktic foraminiferal assemblages in the same two samples contain *Subbotina angiporoides* and record the disappearance of *Paragloborotalia opima*, suggesting an age older than 30.8 Ma. These results are generally in good agreement with the projected crustal age of ~30.6 Ma at Site U1583.

Calcareous nannofossil and planktic foraminiferal bioevents, in conjunction with paleomagnetic data, allowed for comprehensive hole age-depth models (Figure **F35**) and calculation of LSRs. LSRs range 0.13–4.08 cm/ky in Hole U1583C and 0.06–7.29 cm/ky in Hole U1583E. In both holes, the highest LSRs consistently occurred within the Oligocene, with values ranging 0.29–4.08 cm/ky

in Hole U1583C and 0.17–7.29 cm/ky in Hole U1583E. In contrast, the Neogene and Quaternary in both holes record the lowest sedimentation rates.

9.5.3.1.3. Sedimentary and pore water geochemistry

Samples from Site U1583 were mostly collected from Hole U1583C, with one additional water sample each from Holes U1583E (mudline) and U1583F (sediment/basement interface). Shipboard analyses included fluid chemistry, sediment geochemistry, and measurements of headspace gas. Pore fluid salinity is uniform at the seawater value (35) throughout Hole U1583C, although concentrations of Na, Cl, and Br are higher than in seawater below ~5 m CSF-A. Measured pH is uniformly (7.5 ± 0.1, 2σ, *n* = 13) lower than local bottom seawater between ~3 and 56 m CSF-A and gradually increases (up to 7.8) between ~60 and 100 m CSF-A. Alkalinity values are much more variable and show a number of inflection points, including increases at the boundaries between lithostratigraphic Units II (nannofossil ooze with clay and foraminifera) and III (clay with nannofossils and clayey nannofossil ooze; 2.0–2.5 mM) and between Subunits IVA (nannofossil ooze with clay and foraminifera) and IVB (calcareous and nannofossil oozes with clay and foraminifera; 2.2 to 2.5 mM). The transition from Units II to III is also marked by (1) an increase in Ca, Sr, and Sr/Ca and a decrease in Mg concentrations in pore fluids, consistent with the dissolution of biogenic carbonate and recrystallization of high-Mg inorganic calcite, and (2) significant increases in B (67%), Li (10%), Si (78%), and K (17%) concentrations, which are likely a result of diagenetic reactions involving detrital silicates and biogenic silica. The weak positive trend between SO_4 and Ca concentrations in Hole U1583C hints at a potential role for sulfate reduction within these sediments, which may also explain the concomitant downhole decrease in SO_4 and TOC content. NH_4 (3–17 µM) and Mn (0.63–2.86 µM) concentrations remain low throughout the sediment column, with the exception of two peaks observed in Unit III (clay with nannofossils and clayey nannofossil ooze) and Subunit IVB. Oxygen concentrations decrease between Unit II and Subunit IVA and reach a minimum value of 10.5 µM at ~22 m CSF-A before gradually increasing to 207.4 µM at ~99 m CSF-A. Calcium carbonate content is generally high throughout the hole, with the exception of Unit III, which has a difference of ~80 wt% between the top and bottom of the unit. Conversely, low TOC concentrations (<0.36 wt%) are measured in Hole U1583C and values gradually decrease toward the bottom of Subunit IVC (nannofossil ooze with clay and foraminifera),
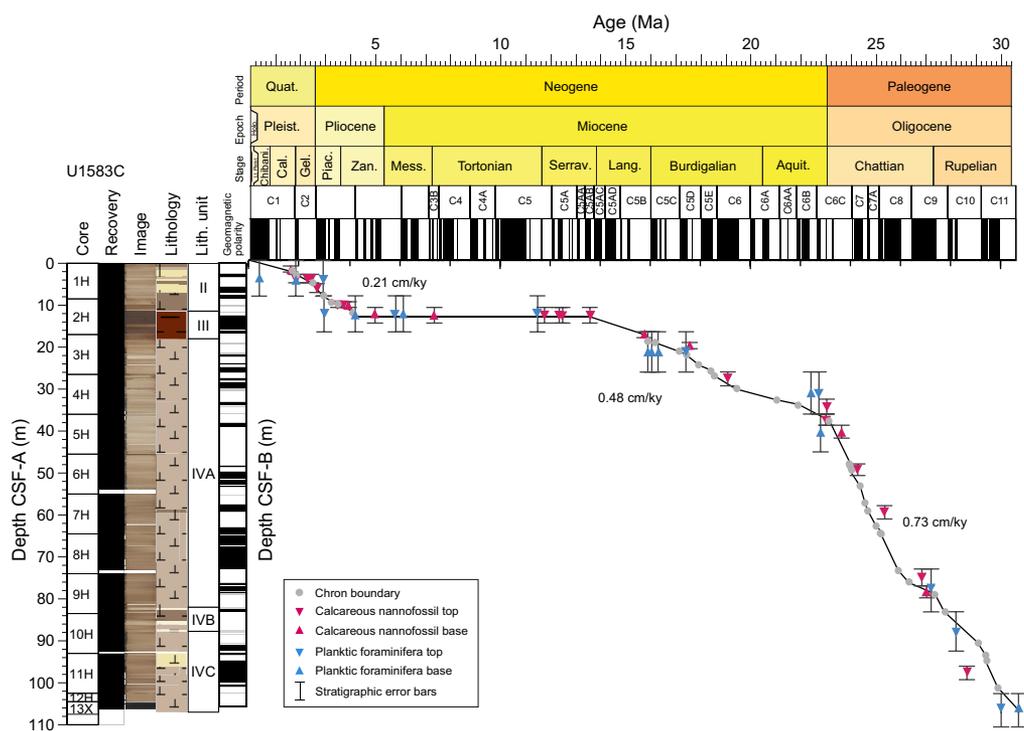

Figure F35. Age-depth model showing biostratigraphic and magnetostratigraphic datums, Hole U1583C. LSRs were averaged for Pleistocene, Pliocene, Miocene, and Oligocene.

consistent with organic matter oxidation. A spike in TOC is seen in Subunit IVB, which coincides with increases in SO_4, NH_4, and Mn geochemical profiles. In Hole U1583C, headspace gas measurements for methane, ethane, propane, and higher molecular weight hydrocarbons were below detection limits.

9.5.3.1.4. Paleomagnetism

Continuous measurements of remanent magnetization were conducted on sediment cores from Hole U1583C and Hole U1583E using the SRM at 2 cm intervals before and after progressive AF demagnetization of three steps (5, 10, and 20 mT fields). Discrete measurements including AMS and remanence after AF demagnetization were conducted on 25 cube samples. IRM acquisition experiments were performed on eight selected samples, which is at least one per lithologic unit. Paleomagnetic measurements provide constraint on the magnetostratigraphy for the entire sediment sequence at Site U1583.

Viscous overprints are almost completely removed at 20 mT demagnetization, and characteristic components can be observed at this stage. Inclination values of the revealed characteristic components (i.e., 20 mT inclination) show a bimodal distribution in both holes, where values are clustered around +57° and −54° in Hole U1583C and around +59° and −51° in Hole U1583E. Well-defined normal and reversed polarities in the 20 mT inclination are present in both Holes U1583C and U1583E, enabling age determinations by magnetostratigraphic correlations with polarity chrons in the GPTS. The topmost sediment sequence in Hole U1583E contains the Brunhes, Matuyama, and Jaramillo Chrons, which are absent in Hole U1583C. The Oligocene/Miocene boundary occurs within Subunit IVA at ~40 m CSF-A in Hole U1583C and at ~45 m CSF-A in Hole U1583E. Paleomagnetic results at the bottom of the sediment sequence, above the sediment/basement interface (between 100 and 110 m CSF-A), were placed in Chron C11r for Hole U1583C and Cr11.2n in Hole U1583E. The relative ages of those chrons agree with the estimated basement age of ~30.6 Ma (Kardell et al., 2019).

Discrete samples were subjected to AF demagnetization up to a maximum of 130 mT. Most of the samples reveal a single remanent magnetization component after the 5 mT AF demagnetization step with maximum angular deviation angles spanning from 2.2° to 14.8°. Inclinations of ChRM components calculated from discrete sample measurements are consistent with the values measured from the SRM.

Mineralogy-related measurements (IRM and AMS) were conducted on one to two discrete samples per each lithologic unit. IRM measurements reveal the dominance of low-coercivity minerals throughout the cored interval with no variations with depth or between lithologic units. AMS measurements show two different trends in the magnetic fabric with either a subvertical or a subhorizontal magnetic foliation. Samples showing subhorizontal magnetic foliation correspond to typical oblate sedimentary fabric. In contrast, the presence of samples characterized by a subvertical magnetic foliation might be related to either soft-sediment deformation or drilling disturbance.

9.5.3.1.5. Physical properties

Characterization of the sediment physical properties at Site U1583 was primarily based on cores from Hole U1583C, with additional information from Hole U1583E. Whole-round, section-half, and discrete measurements were considered together to characterize the petrophysical signatures for the different lithologic units. All archive halves were imaged using XMAN. A correlation framework and a semicontinuous splice was developed for the site that considers NGR, GRA, MS, and magnetic inclination from each hole.

Whole-round measurements of NGR range 1–42 counts/s through the sedimentary section in Hole U1583C. NGR is relatively low in the nannofossil ooze (Units II and IV; ~5 counts/s) and high in the clay-rich Unit III (15–42 counts/s; mean = 27 counts/s). MS ranges 1–126 IU and shows a downhole trend similar to the NGR record over the entire hole, with the highest values in Unit III (30–122 IU; mean = 78 IU). Bulk density based on GRA ranges 1.4–2.5 g/cm^3 over the interval measured and shows an overall gradual increase downhole due to increasing consolidation of sediments with depth. In MAD analyses, porosity shows an overall decreasing trend from 65% at the top of Unit II to 55% in the bottom of Subunit IVA then remains relatively constant through the

bottom of Hole U1583C, and bulk density generally follows the GRA record. *P*-wave velocity ranges 1.45–1.72 km/s with a mean value of 1.54 ± 0.03 km/s and increases downhole, which is likely due to sediment compaction. Shear strength is relatively uniform in nannofossil ooze with a value of 15–16 kN/cm² and shows its highest value of 42 kN/cm² in clay-rich Unit III. Compressional strength is scattered between 0.1 and 1.0 kg/cm² (mean = 0.6 ± 0.3 kg/cm²) throughout the sedimentary sections with no apparent downhole trend. Most samples have a thermal conductivity of ~1.3 W/(m·K), and the lowest measurements come from Unit III (0.93 W/[m·K]). The vertical conductive heat flow for Site U1583 was estimated to be 31 mW/m², based on three APCT-3 tool measurements and thermal conductivity. This value is lower than the modeled heat flow values for ocean crust of this age, requiring significant regional advection of heat by hydrothermal fluid circulation (cf. Kardell et al., 2021)

9.5.3.1.6. Microbiology

Microbiology sampling of sediments in Hole U1583C was focused on exploring evidence for microbial life using microscopy and culture-based and culture-independent approaches. One microbiology whole-round sample (5–10 cm long) was collected from each 9.5 m core. One additional sediment sample was taken from near the sediment/basement interface in Hole U1583F. A total of 13 routine microbiology whole rounds were taken and subsequently subsampled for different ship- and shore-based scientists, and an additional 33 whole rounds were taken for personal, specialized, shore-based analyses.

Two microbiology experiments were started shipboard during Expedition 393 on sediment samples from Site U1583. To study the extent of viral activity and dynamics between viruses and other microbial life (Bacteria and Archaea), virus-induced microbial mortality and prophage induction experiments were performed on subsamples taken from five microbiological whole-round cores throughout the sediment column. To study the microbial activity at the sediment/basement interface, ammonium enrichment incubation experiments were started with the deepest sediment cores in Holes U1583C and U1583F, along with the uppermost basement samples.

9.5.3.2. Volcanic rocks

9.5.3.2.1. Igneous petrology

Site U1583 was established above ~30.6 Ma ocean crust by Expedition 393, and Holes U1583C and U1583F recovered volcanic basement. The uppermost igneous rock encountered was an ~11 m thick massive basalt lava flow intersected by Holes U1583C and U1583F at 107.5 and 109.7 mbsf, respectively, some 30 m shallower than predicted by seismic site surveys (Kardell et al., 2019; Christeson et al., 2020). Only Hole U1583F advanced deeply into basement, reaching 239.6 mbsf (129.8 msb) with ~30% recovery (Figure **F34A**).

Hole U1583F intersected three volcanic sequences: A, B, and C with 62, 35, and 33 m expanded thicknesses, respectively, separated by two sedimentary breccia units (Units 4 and 6) with thicknesses estimated between 0.8 and 3.4 m (Figure **F34A**). The upper Sequence A (109.7–171.6 mbsf) consists of Unit 1, an 11 m thick massive lava flow, Unit 2, moderately plagioclase-olivine-augite phyric pillow lavas and sheet flows, and the aphyric Unit 3, which is markedly more primitive than all the other lavas in the hole. The middle Sequence B is capped by sedimentary breccia Unit 4 and consists of moderately plagioclase-olivine (± augite) phyric pillow basalts and another thin breccia horizon. The lower Sequence C is again capped by a sedimentary breccia (Unit 6) above sparsely to moderately plagioclase-olivine phyric pillow basalts that are chemically and lithologically similar to Sequence B.

Lava compositions assessed by pXRF downhole vary both gradationally and in a stepwise fashion across petrologically defined unit boundaries. Incompatible element concentrations and Zr/Ti ratios are consistent with a relatively primitive N-MORB-like lava composition at Site U1583. In contrast to the sequence stratigraphy defined by the presence of sedimentary breccias, pXRF measurements reveal that Unit 3 has a uniquely primitive composition in Hole U1583F, splitting the hole into three major chemostratigraphic units: Units 1 and 2, Unit 3, and Units 4–7.

9.5.3.2.2. Alteration petrology

Hole U1583F records fluid-rock reactions over the full range of spatial contexts expected for uppermost basement. The secondary minerals forming are predominantly various clay minerals, calcium carbonate, Fe oxyhydroxides, and zeolites that are consistent with reactions at low temperatures between basalt and seawater or seawater-derived ridge flank hydrothermal fluids. Within Hole U1583F it is possible to identify zones of alteration that have distinctive characteristics. The uppermost 70 m of the hole is characterized by the presence of green clay filling vesicles (in background and in alteration halos) and a generally low abundance of alteration halos (<30% of core surface); background alteration dominates (Figure **F34B**). This zone also hosts the most calcium carbonate, and carbonate abundance increases downhole through this zone. From 40 to 70 msb, complex multicolored halos that exhibit both diffuse and sharp halo sequences are variably mutually overprinting. These multihalos are best observed through the changing sequences of vesicle fillings. From 70 msb, green clay in vesicles is absent and the abundance of carbonate filled veins decreases. These changes are accompanied by an increased modal proportion of alteration halos, with the prominence of brown halos increasing downhole. From 95 msb halos are most commonly orange and there is a slight increase in carbonate veins.

9.5.3.2.3. Igneous geochemistry

For Hole U1583F basement cores, representative samples were taken from the freshest portions of each lithologic subunit to obtain a downhole record of the primary magmatic conditions, along with one sample near the sediment/basalt contact. In addition, one sample of the intercalated indurated calcareous sediment/breccia matrix was taken to better understand the sediment-basalt chemical exchanges that occurred as new lavas erupted. A total of 17 samples were measured for LOI and bulk rock geochemical analysis via ICP-AES. The unoxidized powders of these samples were characterized for elemental abundances via pXRF to complement additional pXRF measurements made directly on the cut core surfaces.

In terms of basaltic rock type, the freshest Site U1583 basalts classify as olivine tholeiites following the Yoder and Tilley (1962) normative classification scheme. Basalt compositions show variability downhole that is most evident in the pXRF surface data. TiO_2 contents vary between 1.3 and 1.5 wt%, consistent with a moderate amount of magmatic crystallization before eruption. The Hole U1583F basalts are moderately altered with elevated abundances of K_2O and Rb. K_2O shows a gradual increase downhole, from 0.1 wt% to as high as 0.48 wt%. K/Zr ratios are overall lower than seen in the older SAT sites, ranging to values similar to those seen at Site U1559 (≈6.6 Ma). MgO shows clear evidence for Mg removal from the rocks via seafloor weathering, with the lowest MgO samples clustered near horizons of volcano-sedimentary breccias, suggesting locally more intensive reactions with seawater.

9.5.3.2.4. Paleomagnetism

Continuous measurements of remanent magnetization were performed at a resolution of 2 cm on Hole U1583F basement cores using the SRM before and after progressive AF demagnetization at 5, 10, and 20 mT fields. Only core pieces longer than 9 cm were measured. Discrete magnetic measurements were performed on 20 cube samples taken predominantly from fresh background basalts with some samples displaying different styles and intensities of hydrothermal alteration.

The SRM results indicate that viscous overprints are mostly removed and primary components can be clearly observed at the 20 mT demagnetization step. The primary components predominantly show positive inclination, which indicates reversed geomagnetic polarity at this latitude (30°S). Inclination values are clustered around 45.4°, agreeing with the calculated GAD (±49.1°). Based on the age of the sediments at the sediment/basement interface, the basement at Site U1583 can be placed in reversed Chron C11r with a basal age of 30.59 Ma (Gradstein et al., 2020). However, in brecciated intervals some rocks present negative inclinations, suggesting either the extensive overprinting of the primary remanent magnetization by a secondary component or rotation of the clasts.

A subset of 20 discrete samples were subjected to AF demagnetization up to 190 mT step to isolate the ChRM. Discrete sample measurements mostly revealed well-defined ChRM with maximum angular deviations between 0.3° and 14.8°. A few samples show a more stable secondary compo-

nent, as the ChRM is revealed after the 25 mT step. Experiments to determine the magnetic mineralogy were conducted on a selected number of samples to define the possible relationships with igneous units and alteration types. Most of the samples show the dominance of low-coercivity minerals as titanomagnetite. A few altered basalts and the breccias do not reach saturation at the maximum applied field of 1200 mT, implying a significant contribution of high-coercivity minerals such as hematite. AMS measurements reveal different magnetic fabric shapes depending on the emplacement style of igneous units.

9.5.3.2.5. Physical properties
Whole-round, section-half, and discrete measurements characterize the petrophysical signatures for the different igneous units. In addition to these measurements, ~77% of the recovered material was scanned using the DMT CoreScan3 after identifying oriented core pieces with relatively cylindrical shapes. Selected archive-half sections with breccia were imaged using XMAN.

NGR in Hole U1583F is relatively low in the basalts (Unit 2, 3, 5, and 7), around 2 counts/s, and higher in the sedimentary breccias, 5.1 ± 2.7 counts/s in Unit 4 and 4.0 ± 1.5 counts/s in Unit 6. Discrete MSP range 1–2910 IU and are highest in the massive flows of Unit 1 (mean = 610) and sheet flows of Unit 3 (mean = 196). A total of 23 discrete sample cubes were used for *P*-wave velocity and MAD analyses and were described in terms of their alteration, emplacement style, and groundmass grain size. Bulk density ranges 2.05–2.90 g/cm^3 with the breccia samples having lower densities than the basalts. Breccias also have the lowest *P*-wave velocity and the highest porosity. Basalts with stronger alteration have higher porosity and lower *P*-wave velocity, bulk density, and grain density. Most basalt samples have a porosity <10%, although one sample of a strongly altered basalt from a brown halo has a porosity of 12.1%. *P*-wave velocity shows a general decreasing trend with depth in Hole U1583F and ranges 4.87–6.00 km/s. Lower *P*-wave velocity toward the bottom of the hole is likely driven by the higher prevalence of altered basalts in Units 5 through 7. Thermal conductivity in the basement at Site U1583 ranges 1.23–2.00 W/(m·K), with lowest values found in Units 4 and 6 (sedimentary breccias) and higher mean values of 1.6–1.7 W/(m·K) in basalt flows.

9.5.3.2.6. Downhole measurements
After completion of coring, two downhole logging tool strings were deployed in Hole U1583F (see operations, above). Sea state was marginal for logging (up to 3 m heave) and affected the operations. However, the logging data, in particular the resistivity log, are still of good quality (Figure **F36**) and will help constrain the major units identified in the volcanostratigraphy.

9.5.3.2.7. Microbiology
Microbiology sampling from volcanic rocks in Hole U1583F was focused on exploring evidence for life in the basement, especially at the sediment/basement interface, using microscopy and culture-based and culture-independent approaches. Nine whole-round samples (10–17 cm long) from Hole U1583F and one whole round sample (15 cm) from Hole U1583C, reflecting all the major igneous characteristics and units, were collected for microbiological analyses. Following careful removal of potentially contaminated core exteriors the remaining material was split into subsamples that were prepared for different microbiology analyses. Experiments were started shipboard to study microbial activity at the sediment/basement interface using ammonium enrichment incubations. These incubations focused on the uppermost basement samples to correspond with the deep sediment column samples described in the sediment section.

To determine the extent of contamination of microbiology samples, the perfluorocarbon tracer PFMD was injected into drilling fluids during Hole U1583F coring until the tracer ran out after Core 393-U1583F-12R. Microbiologists then collected samples from both the exterior and interior of core intervals selected for microbiology analysis, as well as core catcher rubble, to quantify the presence of PFMD. PFMD was detected from a majority of the exterior samples, with an average concentration of 46 ppb/g and a median concentration of 48 ppb/g of rock when detected. The tracer was not detected in the interior microbiology samples, suggesting no to minimal drilling contamination of the samples.

9.6. Site U1560

9.6.1. Background and objectives

Site U1560 is located ~315 km west of the Mid-Atlantic Ridge at 30°24.2057′S, 16°55.3702′W in 3724 m of water (Figure F1). The basement at Site U1560 was predicted to have formed at ~15.2 Ma at a half-spreading rate of 25.5 mm/y (Kardell et al., 2019) (Figure F7), which is the highest spreading rate in the study region. The site is located on the north-south–trending (356) CREST seismic crossing Line 02 at CDP 12770 about 0.4 km south of the main east–west (085) CREST Seismic Line 1D/1E (Figures F1, F6E, F37), where a reflector at ~5.07 s TWT was interpreted to be the top of basement, estimated to be at 104 mbsf and observed at ~120 mbsf (Figure F6E).

Site U1560 was previously occupied in April 2021 during Expedition 395E with objectives to confirm the depth to basement by coring, conduct gas safety measurements, and set a reentry system consisting of a reentry cone and 10¾ inch casing (Williams et al., 2021). Hole U1560A was cored using the APC and XCB systems to 122.5 mbsf (Figure F15A), finding the sediment/basement contact at 120.2 mbsf. The drill bit and casing assembly was drilled into Hole U1560B (Figure F15A), setting the casing shoe at 122.0 mbsf and the base of the hole at 124.0 mbsf. Although the drill bit showed signs of wear, the underreamer and casing were in excellent condition, and conse-
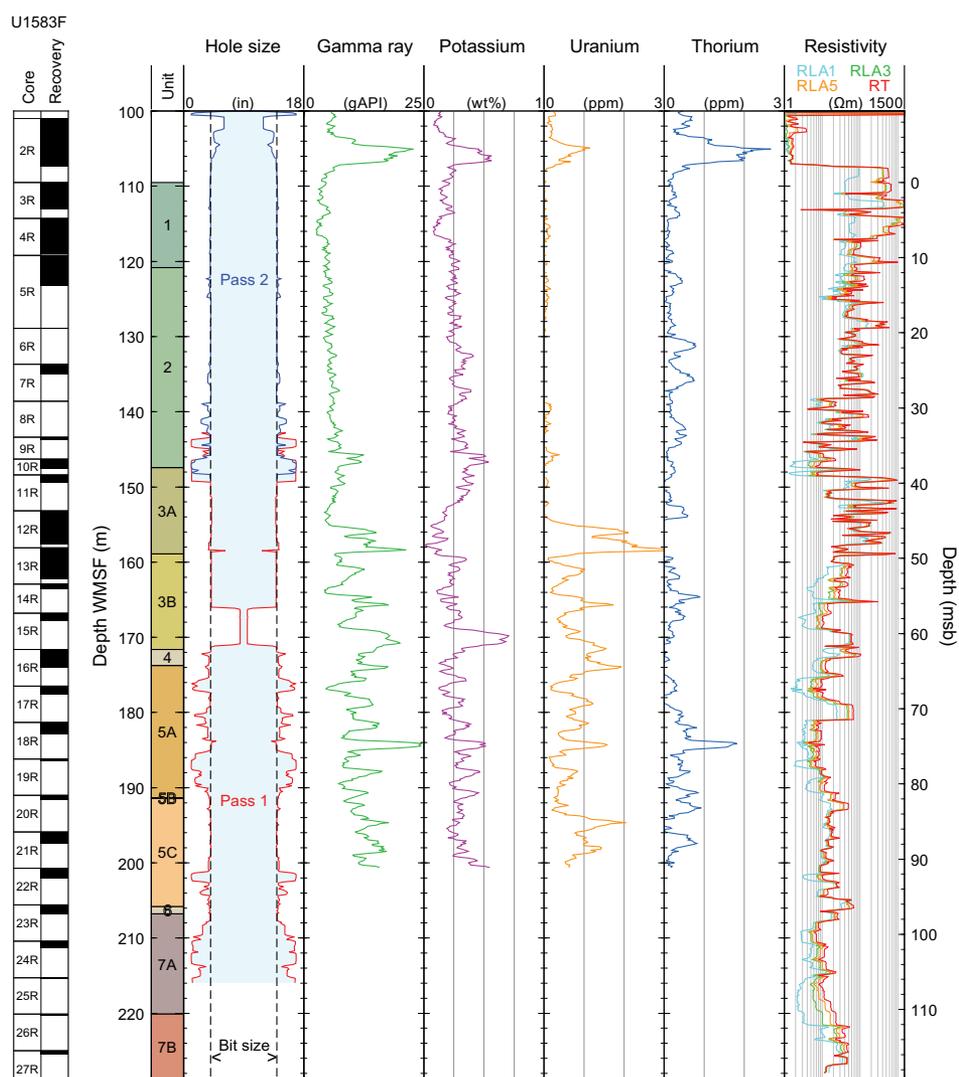
Figure F36. Summary of logging data recorded with triple combo logging string, Hole U1583F. Caliper is combination of two upward passes that were made. RLA1, RLA3, and RLA5 = apparent resistivity from Computed Focusing Modes 1, 3, and 5, respectively; RT = true resistivity.

quently the top of basement in Hole U1560B was defined to be between those depths (~123 mbsf). Ten barrels of 15 ppg cement was pumped with the intention to fill the base of the hole, and pipe to ~100 mbsf. Hole U1560C (Figures **F15C**, **F38**), drilled during Expedition 393, encountered volcanic rocks at 129 mbsf indicating significant basement topography over ~10 m.

The original operational objectives of Expedition 393 at Site U1560 were to core a single APC/XCB hole to basement (Hole U1560C) and to core and log ~250 m of basement volcanic rocks in Hole U1560B.
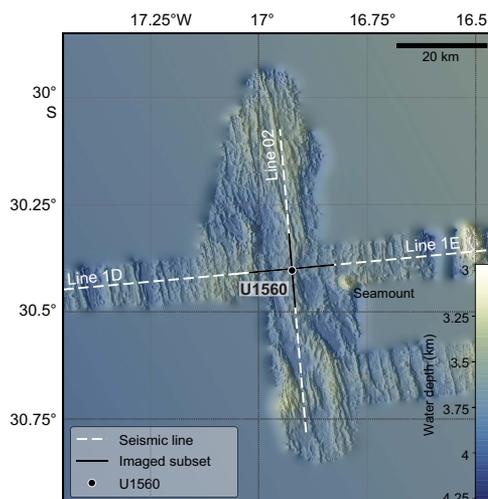
Figure F37. Site U1560 bathymetry (Christeson and Reece, 2020). Seismic reflection profiles were acquired during CREST cruise (Reece et al., 2016).
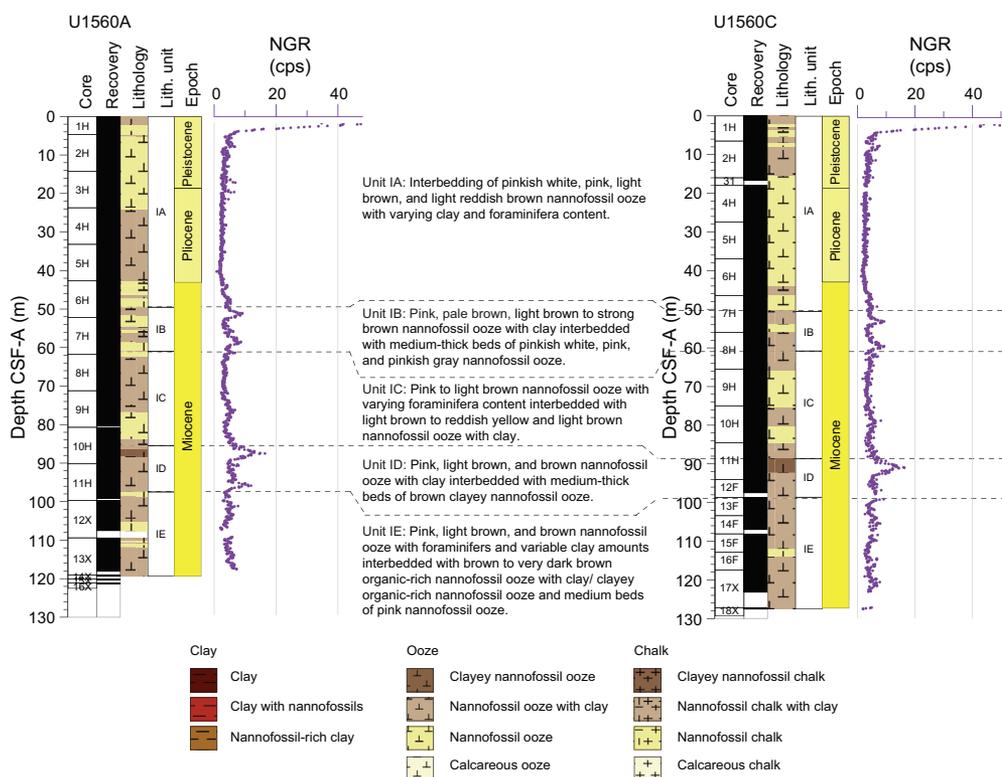
Figure F38. Lithostratigraphic summary of sediment units and correlation of full sediment sequences, Holes U1560A and U1560C. Dashed lines = correlation between units. cps = counts per second.

At 15.2 Ma, Site U1560 is the second to youngest location on the SAT and will be compared to older and younger crustal material cored at Expedition 390/393 sites. Site U1560 is of similar age but contrasting environment to the deep drilling at the superfast-spreading Hole 1256D (Wilson et al., 2006; Expedition 309/312 Scientists, 2006; Expedition 335 Scientists, 2012) on crust that formed at the East Pacific Rise during an episode of superfast-spreading rate in a region of high pelagic productivity and rapid sedimentation (Shipboard Scientific Party, 2003b).

Science objectives at Site U1560 are to (1) investigate the history of the low-temperature hydrothermal interactions between the aging ocean crust and the evolving South Atlantic Ocean and quantify past hydrothermal contributions to global geochemical cycles, (2) collect samples of the sediment- and basalt-hosted deep biosphere beneath the low-productivity South Atlantic Gyre that will be used to refine global biomass estimates and investigate microbial ecosystems' responses to variable conditions, and (3) construct paleoceanographic records of carbonate chemistry and deepwater mass properties across the western South Atlantic Ocean through key Cenozoic intervals of elevated atmospheric CO_2 and rapid climate change.

9.6.2. Operations

9.6.2.1. Transit
The ship completed the 187 nmi voyage to Site U1560 from Site U1583 in 16 h at an average speed of 11.3 kt, arriving at 0130 h on 19 July 2022.

9.6.2.2. Hole U1560B
At 0130 h on 19 July 2022, we lowered the thrusters and started operations in Hole U1560B (Figures **F15A**, **F39**). We assembled the RCB BHA with a new C-7 bit and lowered it down to 3714
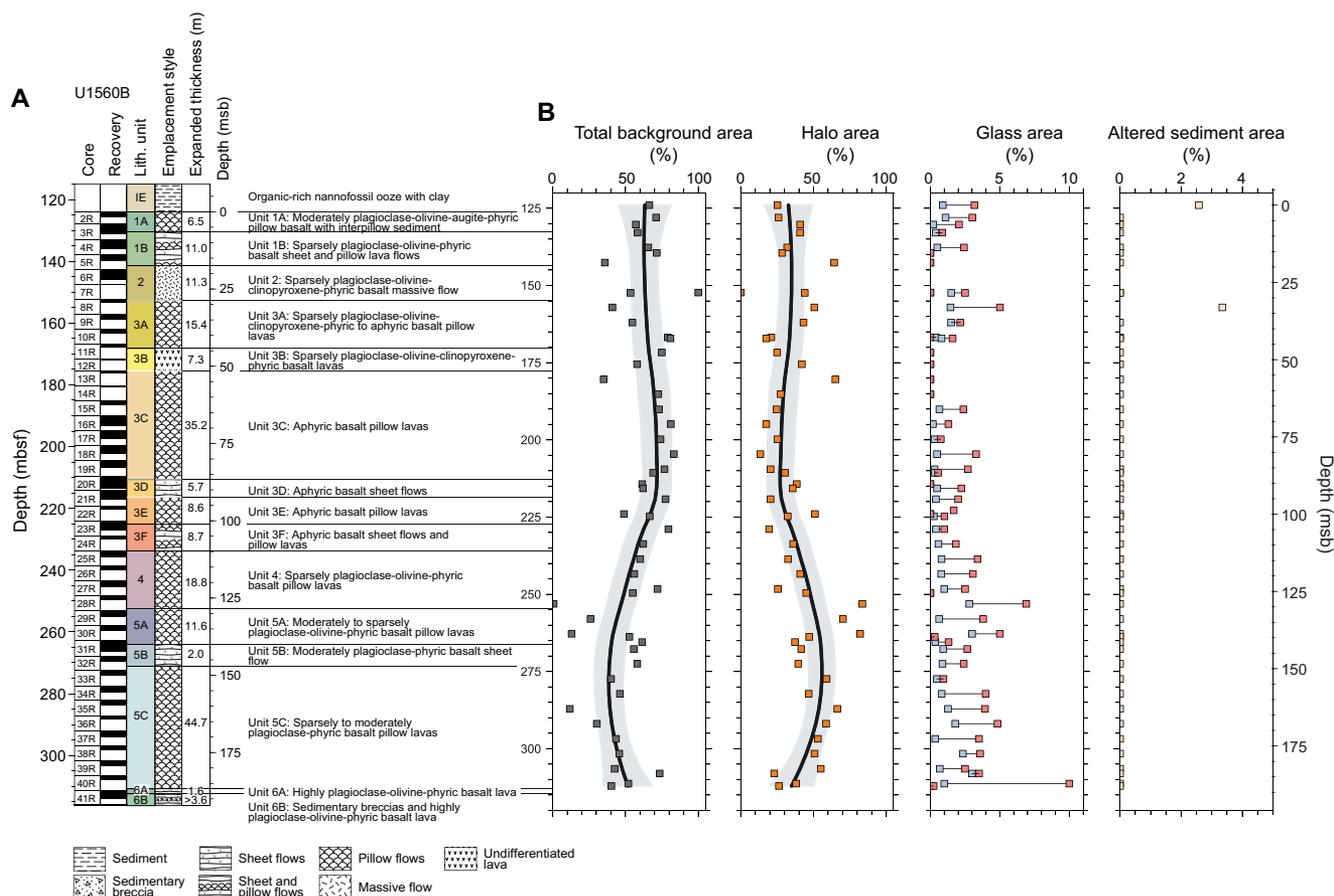

Figure F39. A. Stratigraphic column for igneous basement, Hole U1560B. Unit contact depths and thicknesses are expanded to account for <100% recovery. B. Area abundance of background alteration, alteration halos, fresh and altered glass, and altered sediment. Data are plotted at individual core level. Depths are CSF-A and plotted at top of cored interval. Black trend lines = locally weighted nonparametric regression (LOWESS), gray shading = 2σ of mean.

mbsl. Guided by the subsea camera images, we reentered Hole U1560B at 0920 h on 19 July and lowered the bit down to 124 mbsf, the base of the existing hole. No set cement was found by drilling except for a small 5 cm roller at the top of Core 393-U1560B-2R. A turbid greenish cloud issued from the reentry cone on reentry.

We started coring in Hole U1560B at 1215 h on 19 July. Cores 2R–21R penetrated volcanic basement from 124.0 to 219.2 mbsf, recovering 38.4 m (40%). Ship heave reached over 4 m at times, and up to 4 m of soft hole fill was reported between cores. Mud sweeps of 30–60 barrels were made after most cores to flush out cuttings and fill. All cores were half-length (4.8–4.9 m). After cutting Core 21R, the bit had 52.3 h of drilling time. It was still cutting in-gauge, good-recovery cores, but it would not last to the intended target depth, so at 2325 h on 22 July we started to raise the pipe to change to a new bit. There was 5,000–10,000 lb overpull at 128 mbsf (~5 msb), so the drillers rotated through this area to clear the tight spot. We deployed the subsea camera to observe the clean exit of the BHA from the reentry cone, and the bit cleared the seafloor at 0250 h on 23 July. The BHA was racked in the derrick, the used bit and MBR were removed, and a new MBR with a new C-7 bit and BHA were made up. At 1030 h we started lowering the new bit down to the seafloor.

We redeployed the subsea camera and reentered Hole U1560B at 1955 h. We found 1 m of soft fill, and at 0030 h on 24 July we restarted coring from 219.2 mbsf. Cores 393-U1560B-22R through 41R penetrated from 219.2 to 316.2 mbsf and recovered 36.35 m (37%). There were no problems with torque and a 30–60 barrel mud sweep was run after every core to flush out any cuttings. At 2320 h on 26 July 2022, the decision was made to stop coring to leave time for downhole logging and a sediment hole at this site.

With ship heave increasing through the day to an extent where it would have not only posed problems for the downhole logging tools but also provide poor quality data, it was decided not to drop the RCB bit on the seafloor for logging. Instead, we decided to change to an APC/XCB PDC bit and log through that, to give time for the heavy seas to subside, as forecasted. The narrower diameter of the PDC bit at 9⅞ inch compared to 11⁷⁄₁₆ inch for a typical APC/XCB roller-cone bit would allow the bit to reenter casing in Hole U1560B for downhole logging. The lockable float valve (LFV) would be locked open to allow the logging tools to pass through. The RCB bit was raised to the ship, clearing the seafloor at 0225 h on 27 July and the rig floor at 0905 h. The bit, MBR, and RCB parts of the BHA were removed and replaced with an APC/XCB BHA. The RCB bit had been used for 42.5 drilling hours and had some wear to the inner teeth but was otherwise in good condition.

From 1115 h we lowered the bit to the seafloor and deployed the subsea camera to guide reentry. At 1755 h we reentered Hole U1560B and set the bit at 27.7 mbsf in the casing for downhole logging. From 2025 h we assembled the triple combo downhole logging tool string, consisting of MS, electrical resistivity, density, neutron porosity, and natural gamma tools. During drilling, hole conditions had not caused excessive torque and no tight spots were encountered while raising the RCB bit, so the hole seemed to be in good condition for logging. Therefore, the density tool source and the magnetic susceptibility tool were included in the tool string, unlike operations in Hole U1583F. We lowered the triple-combo down the pipe and it reached the base of the hole, 316 mbsf, recording logging data down from the seafloor. The tool string completed one upward pass in open hole (316–122 mbsf) and a second pass from 316 mbsf through the open hole and casing to the seafloor. The triple combo was raised back to the ship, and the FMS-sonic tool string was assembled. At 0645 h on 28 July we started to lower it down the pipe. The bottom of the tool was kept 5 m off the bottom of the hole (311 mbsf) to prevent damage to the bottom part of the FMS tool. The tool made two upward passes in the open hole. After the second pass, one of the caliper arms would not fully close, remaining open by 0.2 inch and causing difficulty at first to bring the tool into the base of the BHA. However, after pumping to clear the hole and tool of potential debris we were able to bring the tool string to the surface without damage. We assembled the UBI tool string, and at 1545 h we lowered it down the pipe. This tool string also reached 311 mbsf and made two upward passes in the open hole and was back on the rig floor at 2245 h. We rigged down the Schlumberger logging equipment and started pulling the bit out of Hole U1560B, clearing the seafloor at 2355 h.

In summary, Cores 393-U1560B-2R through 41R penetrated from 124.0 to 316.2 mbsf (192.2 m of basement rocks), recovering 74.8 m (39%). Of the two C-7 RCB bits deployed in Hole U1560B, bit number one drilled for 52.3 h over a 95.2 m interval with 38.44 m of recovery (40%), and bit two drilled for 42.5 h over a 97.0 m interval recovering 36.35 m of basalt (38%). A total of 9.9 days (238.5 h) were spent on operations in Hole U1560B.

9.6.2.3. Hole U1560C

The ship was offset 10 m to the north in preparation for coring Hole U1560C (Figure **F38**). An XCB core barrel was deployed to close the LFV in the BHA, which had been set open for the previous day's downhole logging. The bit was set at 3721.7 mbsl, and at 0245 h on 29 July we started Hole U1560C. Core 393-U1560C-1H recovered 6.5 m of sediment, placing the mudline depth at 3724.7 mbsl. To correct the stratigraphic overlap with cores from Hole U1560A (Figure **F38**), cored in April 2021 during Expedition 395E, we drilled ahead by 2.0 m from 16.0 mbsf (drilled interval 393-U1560C-31). Cores 1H–15F penetrated from seafloor to 112.8 mbsf and recovered 111.9 m (101%) of nannofossil ooze with varying amounts of clay and foraminifera. APCT-3 tool measurements were made on Cores 5H, 8H, and 11H. While taking the Core 11H APCT-3 measurement, the APC core barrel became stuck in the formation and required three drillover attempts and 160,000 lb overpull to free it. The APC piston rods had twisted during the process, and as a result we switched over to HLAPC coring from Core 12F. The drill crew worked between cores to straighten the piston rods for the full-length tool.

After Core 16F reached 117.5 mbsf we switched to the XCB coring system in anticipation of reaching basement at approximately the depth it was found in Holes U1560A (120.2 mbsf) and U1560B (~123 mbsf). Basement was eventually encountered at 129.0 mbsf in Hole U1560C, 9.8 m deeper than in Hole U1560A. The two holes are only 10 m lateral distance apart, and the difference in basement depth reflects the rugged basement surface topography that is typical of slow- to intermediate-spreading rate ridges. Core 393-U1560C-18X drilled a further 0.3 m into the basement and recovered two ~5 cm pieces of basalt. It was the last core of the expedition. Cores 1H–18X cored from seafloor to 129.3 mbsf and recovered 122.75 m (96%). Nonmagnetic core barrels were used on all APC and HLAPC cores, and all full-length APC cores were oriented using the Icefield orientation tool.

From 0530 h on 29 July, the rig floor team coated the core line and then raised the bit to the ship, clearing the seafloor at 0900 h and the rig floor at 1655 h. The BHA was disassembled and stowed for transit, and 115 ft of drill line was slipped and cut. We raised the thrusters and started the transit to Cape Town at 1930 h.

9.6.3. Principal results

Site U1560 targeted 15.2 Ma upper ocean crust along the SAT. A complete sedimentary sequence comprising nannofossil ooze with varying amounts of clay and foraminifera was recovered from both Holes U1560A and U1560C (Figure **F38**), and uppermost basement rocks were recovered in both holes as well as in Hole U1560B. Hole U1560B advanced 192.2 m into basement and recovered a volcanic sequence of moderately to sparsely plagioclase ± olivine phyric pillow lavas and sheet and massive flows (Figure **F39A**). Most of the lavas show positive magnetic inclinations but negative inclinations for rocks from igneous Units 1 and 2 occur, hinting at a younger age for these flows. Core 393-U1560B-7R, directly beneath the fine-grained basalt massive flow of Unit 2, was without recovery. Preliminary wireline logs hint at elevated natural gamma readings suggesting the presence of strongly altered basalts that enjoyed prolonged direct exposure to ocean bottom waters at the southern Mid-Atlantic Ridge. The lowermost lavas in Hole U1560B are highly plagioclase-olivine-clinopyroxene phyric basalt lavas that include two tantalizing zones of sedimentary breccias comprising altered basalt and glass clasts in a matrix of indurated calcareous sediment, hyaloclastite, and zeolite.

9.6.3.1. Sediments

9.6.3.1.1. Sedimentology

Biogenic and minor amounts of siliciclastic sediments were recovered from Expedition 395E Hole U1560A and Expedition 393 Hole U1560C. Biogenic sediments consist primarily of nannofossil ooze with varying amounts of clay and foraminifera. Intervals with siliciclastic sediments include

rare to common clays with variable nannofossil and foraminifera content. A single sedimentary Lithologic Unit I was defined at Site U1560 and was divided into five subunits (Figure **F38**). Subunit IA extends from the top of the hole to 49.5 m CSF-A in Hole U1560A and to 51.3 m CSF-A in Hole U1560C. It is Pleistocene to Late Miocene pinkish white, pink, light brown, and rarely light reddish brown nannofossil ooze with variable amounts of clay and foraminifera. Subunit IB is Late Miocene and extends from 49.5 to 61.0 m CSF-A in Hole U1560A and from 51.3 to 61.2 m in CSF-A in Hole U1560C and comprises pink, pale brown, and light brown to dark brown nannofossil ooze with clay interbedded with 10–30 cm thick beds of pinkish white, pink, and pinkish gray nannofossil ooze. Subunit IC extends from 61.0 to 85.4 m CSF-A in Hole U1560A and from 61.2 to 89.3 m in CSF-A in Hole U1560C and consists of Late Miocene pink to light brown nannofossil ooze with varying foraminifera content interbedded with light brown to reddish yellow and light brown nannofossil ooze with clay. Subunit ID extends from 85.4 to 96.4 m CSF-A in Hole U1560A and from 89.3 to 98.9 m CSF-A in Hole U1560C. It consists of Late to Middle Miocene pink, light brown, and brown nannofossil ooze with clay interbedded with medium–thick beds of brown clayey nannofossil ooze. Subunit IE extends from 96.4 and 98.9 m CSF-A in Holes U1560A and U1560C, respectively, down to the sediment/basement interface. It consists of Middle Miocene pink, light brown, and brown nannofossil ooze with foraminifera and variable amounts of clay interbedded with brown to dark brown organic carbon–bearing nannofossil ooze with clay, brown to dark brown clayey organic carbon–bearing nannofossil ooze, and 10–30 cm thick beds of pink nannofossil ooze.

9.6.3.1.2. Biostratigraphy and age-depth model
Calcareous nannofossil and planktic foraminiferal biostratigraphy was performed primarily on core catcher samples recovered from Expedition 395E Hole U1560A and Expedition 393 Hole U1560C, examined both on shore and on board *JOIDES Resolution*. The mudline sample in Hole U1560C contains Late Pleistocene to recent planktic foraminifera, but ages based on nannofossils could not be determined due to contamination. Biostratigraphic analyses indicate that the Pliocene–Pleistocene occurs above 42.65 m CSF-B in Hole U1560A and above 43.24 m CSF-B in Hole U1560C, with the Pliocene/Pleistocene boundary located at 20.42 m CSF-B in Hole U1560A and at 20.56 m CSF-B in Hole U1560C. The Miocene/Pliocene boundary could not be determined precisely because index taxa were not observed for either nannofossils or foraminifera. However, the position of this boundary is approximated by a nearby nannofossil bioevent, base of *Ceratolithus cristatus* (5.08 Ma), which occurs at 42.65 m CSF-B in Hole U1560A and at 43.24 m CSF-B in Hole U1560C. Combined nannofossils and planktic foraminifera biostratigraphy indicates presence of Early to Middle Miocene sediments below 45.80 m CSF-B in Hole U1560A and below 46.45 m CSF-B in Hole U1560C.

The most refined estimate for the age of basement comes from the micropaleontological analysis of the thin section (Sample 393-U1560B-2R-1, 83–85 cm) taken from indurated calcareous interpillow sediments. The sample contained preserved planktic foraminifera tests and identified taxa included *Orbulina* spp., *Praeorbulina* spp., and *Trilobatus sicanus*. This provides a narrow 14.4–15.1 Ma age constraint, which agrees with the projected crustal age of ~15.2 Ma for Site U1560.

Calcareous nannofossil and planktic foraminiferal bioevents, in conjunction with paleomagnetic data, allowed for comprehensive hole age-depth models and calculation of LSRs. LSRs range 0.43–2.01 cm/ky in Hole U1560A and 0.29–2.24 cm/ky in Hole U1560C. In both holes, the highest LSRs occur throughout the Miocene–Pliocene interval, with values ranging 0.43–2.01 cm/ky in Hole U1560A and 0.49–2.16 cm/ky in Hole U1560C, whereas the lowest LSRs are recorded in the Pleistocene.

9.6.3.1.3. Sedimentary and pore water geochemistry
Samples from Holes U1560A and U1560C were analyzed for IW and sediment geochemistry (Figure **F40**). In addition, headspace gas was measured in Hole U1560A during Expedition 395E. IW geochemical data from Holes U1560A and U1560C show that Na, Cl, and Br increase in the upper ~20 m, remain uniform downhole for most of the section, and decrease to near seawater values in the lowermost ~25 m of Subunit IE. Measured pH is mostly uniform in both holes and remains within the range of local bottom seawater (7.6–7.8), with the exception of the upper ~40 m in Hole U1560A (pH varies from 7.7 to 7.8). Alkalinity profiles are mostly indistinguishable between the

two holes, and values remain uniformly higher than seawater between ~25 and 90 m CSF-A (~2.8–2.9 mM) before decreasing gradually toward near seawater values at the sediment/basement interface. In contrast to the small changes in the Ca and Mg pore water profiles, Sr concentrations and consequently Sr/Ca ratios vary significantly in both holes (~90–190 µM and ~8–17 µM/mM, respectively) (Figure **F40**), consistent with carbonate dissolution and recrystallization within the sediments. Increases in concentration relative to the mudline are observed for B (11%–13%), Li (2%–4%), Si (179%–215%), and K (7%–9%) at Site U1560, and all profiles behave similarly between Holes U1560A and U1560C. Silicate diagenesis within the sediment column, as well as chemical exchanges between sediment and basement, are likely responsible for the downhole variability observed in these elements. Sulfate concentrations in both holes show some variability in Subunit IA (~27–28 mM) but remain uniform below ~40 m CSF-A. Ammonium concentrations vary significantly between Holes U1560A (3.5–40.6 µM) and U1560C (7.5–20.3 µM), whereas Mn profiles are mostly similar (0.13–3.67 µM). Oxygen concentrations in Hole U1560C decrease in Subunit IA to near anoxic for much of the hole before increasing again to reach ~260 µM at the sediment/basement interface. Calcium carbonate is generally high in both holes, with lowest values in the lowermost ~10 m of each hole. TOC values in Hole U1560A are fairly uniform downhole (0.3 wt%), but concentrations in Hole U1560C are higher overall and gradually increase with depth (up to ~1.4 wt% near the top of Subunit IE). In Hole U1560C, TOC is low in the lowermost ~20 m of the sediment cover.

9.6.3.1.4. Paleomagnetism
Paleomagnetic measurements were conducted at 2 cm resolution on sediment archive-half sections from Holes U1560A and U1560C using the SRM. Remanent magnetization was measured before and after AF demagnetization steps at 5, 10, and 20 mT. Discrete measurements including AMS and AF demagnetization were conducted on a total of 26 (7 cm³ J-cube) samples. IRM acquisition experiments were performed on 10 selected samples, at least once per lithologic subunit. Paleomagnetic measurements were used to construct the magnetostratigraphy for the sediment package at Site U1560.
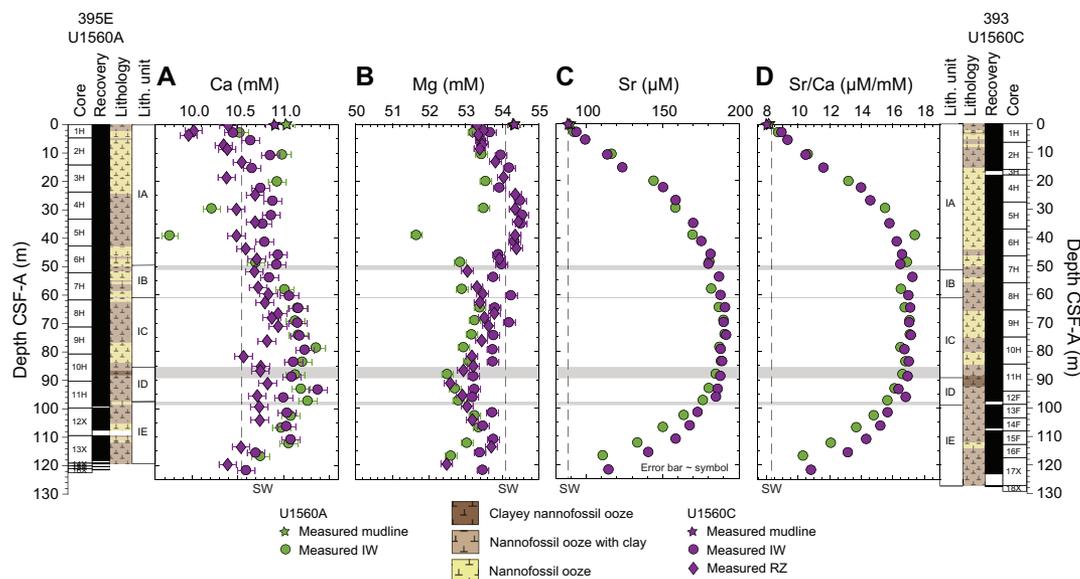

Figure F40. (A) Calcium, (B) magnesium, (C) strontium, and (D) Sr/Ca ratios, Holes U1560A and U1560C. Ca remains close to or above seawater (SW) value (dashed black line) throughout Holes U1560A (10.2–11.4 mM) and U1560C (10.5–11.4 mM), with good agreement between holes. Mg broadly decreases in Hole U1560A (54.3–52.6 mM at 0–116.86 m CSF-A), remaining less than SW throughout sediment column. In Hole U1560C, Mg increases in Subunit IA (53.7–54.5 mM; ~3–27 m CSF-A), decreases in Subunits IB–ID (54.6–53.2 mM; ~27 to ~90 m CSF-A), and increases slightly in Subunit IE (to 53.8 mM at 111.00 m CSF-A). In contrast to small changes observed in Ca and Mg profiles, Sr and Sr/Ca ratios vary significantly in both holes. Sr and Sr/Ca ratios increase in Subunit IA (Sr: ~90–180 µM; Sr/Ca: ~8–17 µM/mM), remain uniform throughout Subunits IB and IC (Sr: ~190 µM; Sr/Ca: ~17 µM/mM), and then decrease toward sediment/basement interface in both holes (Sr: ~110–115 µM; Sr/Ca: ~11 µM/mM). SW reference values correspond to International Association for the Physical Sciences of the Oceans (IAPSO) standard composition. RZ = Rhizon.

A single remanent magnetization component could be defined after cleaning the drilling overprint with the 5 mT AF demagnetization step. The distribution of the 20 mT inclination is generally bimodal in both holes. The values are clustered around ±46° in Hole U1560A, whereas clusters centered at +43° and −45° were measured in Hole U1560C. Despite the presence of few intervals with shallow inclinations, generally clear positive and negative polarities can be detected, allowing good preliminary correlation to polarity chrons in the GPTS. AF demagnetization of discrete samples up to a maximum of 160 mT isolate the ChRM with maximum angular deviation angles ranging 2.1°–14.0°. Inclinations from ChRM calculated for discrete samples confirm the values measured from the SRM used to construct the magnetostratigraphy. Preliminary ties to the GPTS reveals the Brunhes, Matuyama, and Jaramillo Chrons in the uppermost sediment column down to ~8 m CSF-A in both Holes U1560A and U1560C. The Pliocene/Pleistocene boundary is identified in Subunit IA at ~20 m CSF-A and the Miocene/Pliocene boundary at the bottom of Subunit IA in both holes. The base of the sediment column was placed in the Chron C5ADn (14.163–14.609 Ma, Gradstein et al., 2020), which agrees with the estimated basement age of ~15.2 Ma (Kardell et al., 2019).

Rock magnetic experiments were conducted on one to two samples per each lithologic subunit, revealing the dominance of low-coercivity minerals in the cores with no significant variations with depth or sediment type. AMS measurements reveal a well-defined oblate magnetic fabric characterized by a steeply inclined magnetic foliation, which might reveal deposition on a steep slope or subsequent tectonic tilting.

9.6.3.1.5. Physical properties

Characterization of the sediment physical properties at Site U1560 was primarily based on cores from Hole U1560C, with additional information from Expedition 395E Hole U1560A. A correlation framework and splice were developed for the site that considers NGR, GRA, MS, and magnetic inclination from each hole. The correlation resulted in an almost continuous spliced record to 138 m CCSF, with a total core gap of ~4 m.

Whole-round measurements of NGR range 1–52 counts/s but are mostly lower than 10 counts/s throughout Hole U1560C (mean = 5 ± 4 counts/s). A few peaks (10 and 20 counts/s) stand out in the middle portion of the sequence (within Subunit IB and at the boundary between Subunits IC and ID). In particular, peaks in Subunit IB reflect its clayey nannofossil ooze lithology. In both holes, the elemental concentrations of K and Th display trends that are similar to the NGR total counts. U shows the lowest concentration of the radioactive components. These well-defined features were used as tie points for stratigraphic correlation.

Whole-Round Multisensor Logger (WRMSL) MS mimics the NGR trends, ranging 1–60 IU, although it is scattered toward higher values in the lower Subunit IE, likely due to drilling disturbance caused by the XCB system. Discrete MSP shows a downhole trend similar to the WRMSL record, with some higher peaks in the upper Subunit IA. For both magnetic susceptibility measurements, the lower values are consistent with the nannofossil ooze. Bulk density based on GRA ranges 1.4–1.9 g/cm^3 over the interval measured and is uniform with depth. The highest density interval is recorded in the upper Subunit IC (60–65 m CSF-A), up to 1.9 g/cm^3, which also corresponds to a peak in *P*-wave velocity.

MAD analyses were performed on 25 discrete samples to measure porosity and density. Porosity shows a decreasing trend from ~70% to ~60% within the uppermost 15 m but stays relatively constant at ~60% to the bottom of Hole U1560C. There is a small interval with 45% porosity that corresponds to the highest bulk density at 106 m CSF-A, but the sedimentologic cause remains unclear. *P*-wave velocity data range 1.5–1.6 km/s with a mean of 1.53 ± 0.02 km/s and is invariant downhole other than an increase from 1.55 to 1.6 km/s in the uppermost 15 m.

Shear strength is relatively uniform in lower Subunit IA and Subunits IC–IE around values of 8–10 kN/cm^2, whereas higher values were measured in upper Subunit IA and the highest value was measured in Subunit IB (30 kN/cm^2). Compressional strength decreases from the seafloor to ~75 mbsf from 2.0 to 0.1 kg/cm^2 (mean = 1.1 ± 0.5 kg/cm^2), below which it shows a scattered trend around 1 kg/cm^2 to the sediment/basement interface. Most samples have a thermal conductivity of ~1.2 W/(m·K) with the highest measurements from Subunit IC (1.34 ± 0.02 W/[m·K]). Using the

thermal conductivity data and formation temperature measurements from Holes U1560A and U1560C, the vertical conductive heat flow for Site U1560 is estimated to be 22 mW/m^2.

9.6.3.1.6. Microbiology

Microbiology sampling in sediments at Site U1560 during Expedition 393 occurred in Hole U1560C and was focused on exploring evidence for microbial life in the sediments using microscopy and culture-based and culture-independent approaches. From Hole U1560C, one microbiology whole-round sample (5–10 cm long) was collected from each 9.5 m core. These whole-round samples were subsampled for different ship- and shore-based scientists. Additional personal whole-round cores for specialized shore-based analyses were also taken. A total of 14 routine whole rounds were taken and subsequently subsampled and an additional 35 whole rounds were taken for personal, shore-based analyses.

Multiple microbiology analyses were started shipboard during Expedition 393 on sediment samples from Site U1560. To study the extent of viral activity and dynamics between viruses and other microbial life (Bacteria and Archaea), virus-induced microbial mortality and prophage induction experiments were performed on subsamples taken from five MBIO whole-round cores throughout the sediment column. To study the microbial activity at the sediment/basement interface, ammonium enrichment incubation experiments were started with the deepest sediment cores in Hole U1560C, along with the uppermost basement samples.

9.6.3.2. Volcanic rocks

9.6.3.2.1. Igneous petrology

Expedition 395E Hole U1560A and Expedition 393 Holes U1560B and U1560C all recovered volcanic basement, but only Expedition 395E Hole U1560B penetrated deeply into basement. Expedition 393 cored from the Hole U1560B pilot bit depth at 124 mbsf and advanced a further 192.2 m to 316.2 mbsf, recovering ~75 m of basalt (~39% recovery) (Figure **F39A**). This recovery was generally sufficient for unit boundaries, lava types, and volcanic emplacement styles to be determined with confidence throughout most of the hole, although low to zero core recovery in critical parts of the sequence means some important transitions were not recovered (e.g., Core 393-U1560B-7R; 147–153 mbsf). Similarly, the extent of sedimentary breccias and other fragile or broken formations from throughout the hole remain uncertain. Some clarification may come from the careful analysis of drilling and wireline logging information and paleomagnetic conglomerate tests.

Hole U1560B recovered a volcanic sequence composed of six main volcanic and units, comprising 15 subunits (Figure **F39A**). Unit 1 directly underlies basal sedimentary Subunit IE and consists of sparsely to moderately plagioclase-olivine-phyric pillow lavas with some intervening sheet flows and interpillow sediments near the interface. Unit 2 is a sparsely plagioclase-olivine-augite-phyric massive flow with a fine- to medium-grained interior, 6–11 m thick depending on the unrecovered material in Core 393-U1560B-7R (see Figure **F39A**). Unit 3 consists mostly of pillow lavas with phenocryst abundances that grade from sparsely phyric to aphyric. Unit 3 is the most primitive of Hole U1560B in terms of Cr/Ti ratios. Unit 4 consists of sparsely plagioclase-olivine-phyric basalt pillow lavas, with a composition transitional between Unit 3 and Unit 5. Subunits 5A and 5C consist of moderately to sparsely plagioclase-olivine-phyric pillow lavas, separated by two to three sheet lava flows (Subunit 5B). Basalts in Unit 6 are highly plagioclase-olivine-clinopyroxene phyric and may provide a relatively fresh protolith for comparison with other, more strongly altered highly phenocryst-rich basalts recovered at other sites along the SAT. Hole U1560B ends in Subunit 6B, which contains highly plagioclase-olivine-clinopyroxene phyric lavas with two tantalizing sedimentary breccias of basalt and glass clasts in a matrix of indurated calcareous sediment and hyaloclastite.

Lava composition assessed by pXRF varies significantly downhole, with geochemical boundaries largely corresponding to the petrologically defined boundaries. Incompatible element concentrations and Zr/Ti ratios are mostly consistent with an N-MORB-like composition for the lavas at Site U1560, although higher Zr/Ti in Subunits 3A and 3B and Unit 6 nudge toward E-MORB and warrant further investigation. The recurring sequence of chemostratigraphic units, with a central primitive, aphyric lava unit as was noted for Sites U1558 and U1583 is also present at Site U1560.

9.6.3.2.2. Alteration petrology

Hole U1560B records fluid-rock reactions over the range of spatial contexts expected for uppermost basement, albeit with only limited recovery of breccias. The secondary minerals forming (predominantly various clays, carbonate, Fe oxyhydroxides, and zeolites) are consistent with reactions at low temperatures with seawater derived fluids. The uppermost 25 m of the igneous rocks in Hole U1560B are characterized by the presence of green clay filling vesicles in the background rocks and alteration halos in the massive flows as well as the low abundance of alteration halos (<20%) and few carbonate veins (Figure **F41**). From 25 to 250 msb, the proportion of halos remains similar, but orange halos dominate the overall halo abundance. This zone in Hole U1560B also hosts the most carbonate veins, whereas green clay is restricted to massive flows. From below 250 msb there is a marked increase in the abundance of brown halos of variable alteration intensity. The lowermost part of the hole (below 250 msb) is carbonate vein poor. but zeolite veins are more abundant than higher in the section. This overall change in dominant characteristics is in part controlled by the volcanic architecture of the upper crust, such as the association of green clay with massive flow, but also reflects hiatuses in volcanism that exposed parts of the crust to direct contact with seawater for prolonged periods of time as recorded by the brown halo zones.

9.6.3.2.3. Igneous geochemistry

For the Hole U1560B basement cores, representative samples were taken from the freshest portions of each lithologic subunit to obtain a downhole record of the primary magmatic conditions, along with one sample near the basalt/sediment contact. A sample of intercalated sediments-breccia fill was taken to better understand the basalt-sediment chemical exchanges that occurred as new lavas erupted. A total of 27 samples were measured for LOI and bulk rock geochemical
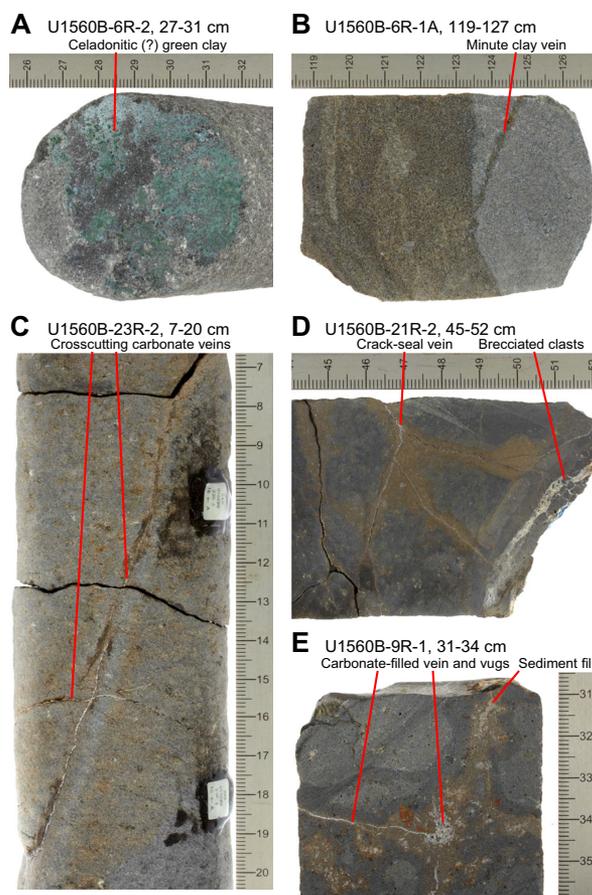

Figure F41. Vein types, Hole U1560B. A. Strong green vein, potentially composed of celadonite, on broken rock surface. B. Submillimeter-wide clay vein with brown halo. C. Several crosscutting narrow carbonate veins. D. Branched carbonate veins with crack-seal texture and wider carbonate vein in which brecciated fragment of host rock are floating. E. Carbonate-filled vein and vuggy space. Also note vein filled with metamorphosed sediment.

analysis via ICP-AES and powder pXRF to complement the huge number of direct pXRF analyses taken directly on the split-core surface.

Basalt compositions show strong variability downhole that is evident in both the pXRF surface data and in the ICP-AES data. In terms of basaltic rock type, the freshest Site U1560 samples classify as olivine tholeiites per the Yoder and Tilley (1962) normative classification scheme. TiO_2 contents vary between 1.3 and 1.7 wt%, consistent with moderate to large amounts of crystallization before eruption. The Hole U1560B basalts are moderately altered, with elevated abundances of K_2O and Rb, but lower abundances overall than seen at older sites. K_2O shows only a slight increase downhole, from 0.1 wt% to 0.33 wt%. K/Zr ratios, a measure of relative K enrichment, range from MORB-like values of 7–9, up to 24.6. MgO shows evidence for Mg removal from the rocks via seafloor weathering. The lowest MgO samples are clustered near unit boundaries, suggesting locally more intensive reactions with seawater.

9.6.3.2.4. Paleomagnetism

Paleomagnetic measurements were conducted on archive halves basement cores of Hole U1560B using the SRM at 2 cm intervals. Remanent magnetization before and after progressive AF demagnetization at 5, 10, and 20 mT fields was measured on pieces that are longer than 9 cm. Data resolution varied according to the core recovery rate in Hole U1560B (0%–84%). AF demagnetization and rock magnetic experiments were performed on cube samples, targeting representative levels of both fresh basalts and those with varying degrees and types of alteration.

NRM intensity of volcanic rocks at Site U1560 varies between 8.65 and 0.04 A/m, with the highest values detected in volcanic units and some rocks showing unexpectedly high MS values (8.65 A/m). The SRM results at 20 mT demagnetization step show mean intensity values around 0.95 A/m and mostly positive inclination, which agrees with the expected reversed polarity for a 15.2 Ma basement. However, negative inclinations were also observed at the top of the basement, suggesting a significant younger age for Subunit 1A to Unit 2. Overall, the 20 mT inclination values are clustered around 64°, significantly steeper than the expected values calculated based on the GAD (±49.1° at 30°S).

A total of 28 discrete samples were subjected to AF demagnetization up to 190 mT to isolate the ChRM, which is generally well defined with maximum angular deviations between 0.5° and 11.3°. Locally, a secondary component was detected in pillow lava units. Rock magnetic experiments in fresh basalts reveal the dominance of low-coercivity minerals such as magnetite or maghemite. In contrast, heavily altered samples are characterized by a mixture of high- and low-coercivity minerals. These samples also revealed the lowest MS and remanence intensity values. In addition, variations in magnetic mineral grain size were observed for units associated with different emplacement styles. The magnetic fabric of the volcanic rocks in Hole U1560B is mostly prolate, showing a subhorizontal magnetic foliation with no visible correlation with the emplacement style.

9.6.3.2.5. Physical properties and downhole measurements

Characterization of the basement physical properties at Site U1560 is primarily based on cores from Hole U1560B (for a total of 190 m), with additional information from Holes U1560A and U1560C, where only the uppermost basement was recovered. In Hole U1560B, NGR is 2.1 ± 0.7 (±1σ) counts/s and ranges 0.2–5.3 counts/s. The highest NGR is associated with sedimentary breccias, which have a mean NGR of 2.7 ± 1.3 counts/s. Basalts of all flow styles have lower mean NGR, between 1.8 and 2.1 counts/s. MSP ranges 0–2595 IU. Five prominent peaks in magnetic susceptibility are associated with relatively fresh, fine-grained holocrystalline massive and sheet basalt flows. These peaks in magnetic susceptibility are also apparent in the wireline logging data. A total of 33 discrete samples were used for MAD and *P*-wave velocity measurements, and these samples were characterized in terms of alteration, emplacement style, and groundmass grain size. Bulk density from MAD analysis ranges 2.08–2.89 g/cm³, with the lowest densities measured from breccia matrix and pillow lava chilled margins with thin sedimentary intercalations. These samples also display the lowest *P*-wave velocity and the highest porosity. *P*-wave velocity ranges 3.85–5.89 km/s in Hole U1560B and is highest in igneous Units 1 and 6 (mean ~5.7 km/s). Units 2, 3, and 4 have a mean *P*-wave velocity of ~5.4 km/s, but the lowest mean velocity was measured in

Unit 5 (5.0 ± 0.6 km/s). Porosity ranges 2.0%–35.5%, but basaltic samples that are not associated with a chilled margin generally show porosities < 10%. Thermal conductivity in the hole ranges 1.13–1.79 W/(m·K) with a mean of 1.63 ± 0.15 W/(m·K). There is a slight downhole increase in thermal conductivity from ~1.7 W/(m·K) at the top of the basement sequence to ~1.8 W/(m·K) at ~230 mbsf. Thermal conductivity values show two broad oscillations in the lower part of Hole U1560B, with relative minima at ~255 and 288 mbsf. Its overall trend mimics the *P*-wave pattern and is opposite to the porosity profile.

Three different wireline logging tool strings (triple combo with MS, FMS-sonic, and UBI) were run successfully through the basement section in Hole U1560B, reaching the bottom of the hole at every pass, and indicating overall good hole conditions. Some of the more outstanding features observed in the core measurements, such as high MS values associated with massive flows in Unit 2 and smaller peaks in deeper units, are clearly recognized in the logs, and the generally good agreement between the logs and core measurements provide robust constraints for the stratigraphy of intervals with incomplete recovery (Figure **F42**). Two full passes each with the FMS
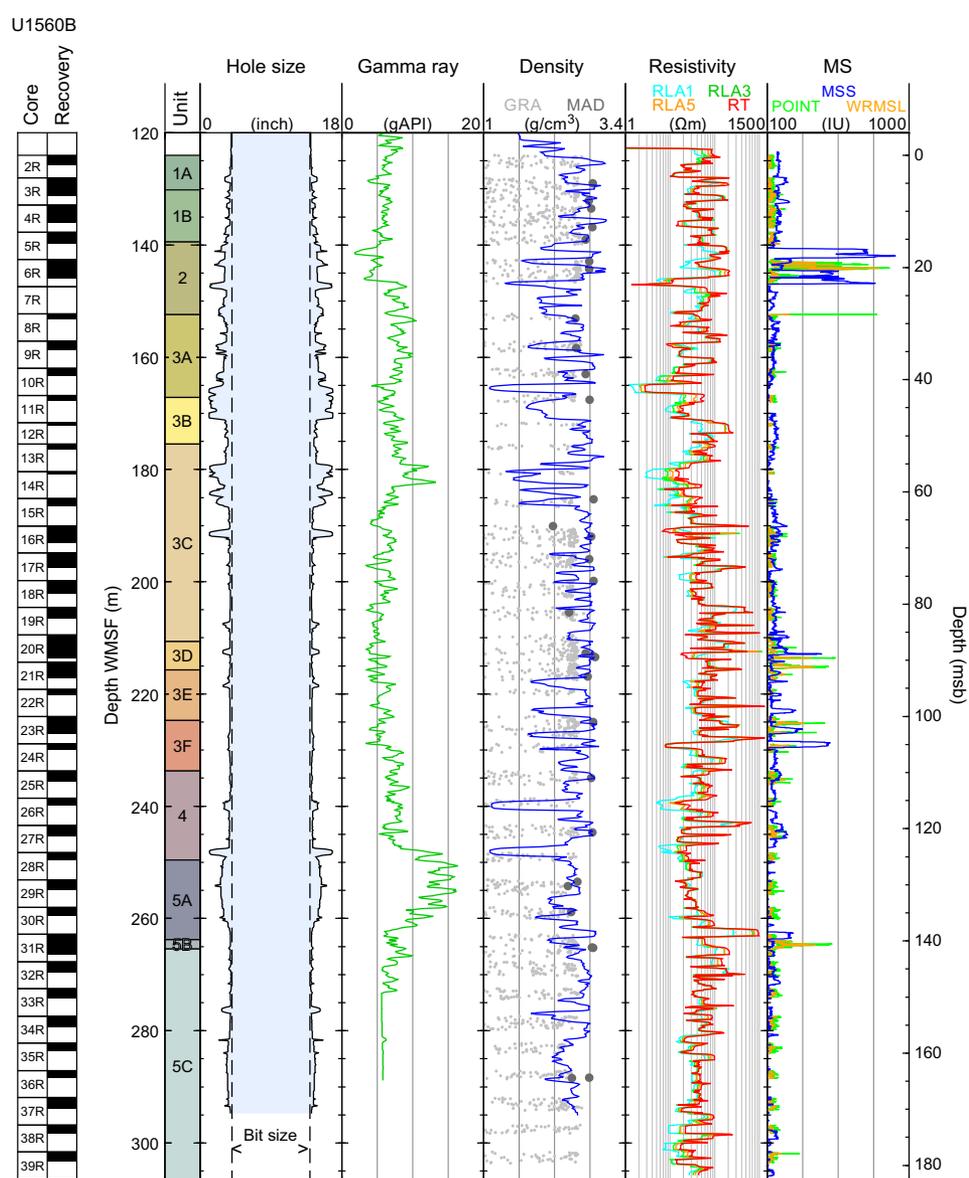

Figure F42. Summary of logging data recorded with triple combo logging string, Hole U1560B. RLA1, RLA3, and RLA5 = apparent resistivity from Computed Focusing Modes 1, 3, and 5, respectively; RT = true resistivity; MSS = Magnetic Susceptibility Sonde.

(high-resolution resistivity images of the borehole wall) and the UBI (360° acoustic images) may provide a comprehensive frame core log integration.

9.6.3.2.6. Microbiology

Microbiology sampling in volcanic rocks from Hole U1560B focused on exploring evidence for life in the basement, especially at the sediment/basement interface, using microscopy and culture-based and culture-independent approaches. A total of 18 whole-round samples (9–14 cm long) representing all characterized lithostratigraphic units were collected for microbiological analyses from Hole U1560B. After the exteriors of whole-round pieces were removed to avoid material contaminated during coring, the remaining material was split into subsamples that were prepared for different microbiology analyses. Experiments were started shipboard to study microbial activity at the sediment/basement interface using ammonium enrichment incubations. These incubations focused on the uppermost basement samples to correspond to the deep sediment column samples described in the sediment section.

9.7. Site U1559

9.7.1. Background and objectives

Site U1559 is located ~130 km west of the Mid-Atlantic Ridge at 30°15.63′S, 15°2.09′W in 3055 m of water (Figure **F1**). The basement at Site U1559 was predicted to have formed at ~6.6 Ma at a half-spreading rate of 17 mm/y (Figure **F7**). The site is located on CREST Seismic Line 01 at CDP 11923 between CREST crossing Lines 06 and 1E/1F (Figures **F1**, **F6F**, **F43**), where a reflector at ~4.15 s TWT was interpreted to be the top of basement, estimated to be at 50 mbsf (Figure **F6F**).

Site U1559 forms the young crustal end-member of the SAT and will be compared to older crustal material cored at Expedition 390/393 sites further from the ridge axis. The site is similar in age to Hole 504B in the eastern equatorial Pacific (6.9 Ma) that formed at an intermediate rate (36 mm/y half-spreading rate) and is covered by 275 m of sediment. Science objectives at Site U1559 are to (1) investigate the history of the low-temperature hydrothermal interactions between the aging ocean crust and the evolving South Atlantic Ocean and quantify past hydrothermal contributions to global geochemical cycles, (2) collect samples of the sediment- and basalt-hosted deep biosphere beneath the low-productivity South Atlantic Gyre that will be used to refine global biomass estimates and investigate microbial ecosystems' responses to variable conditions, and (3) construct paleoceanographic records of carbonate chemistry and deepwater mass properties across the western South Atlantic through key Cenozoic intervals of elevated atmospheric CO_2 and rapid climate change.
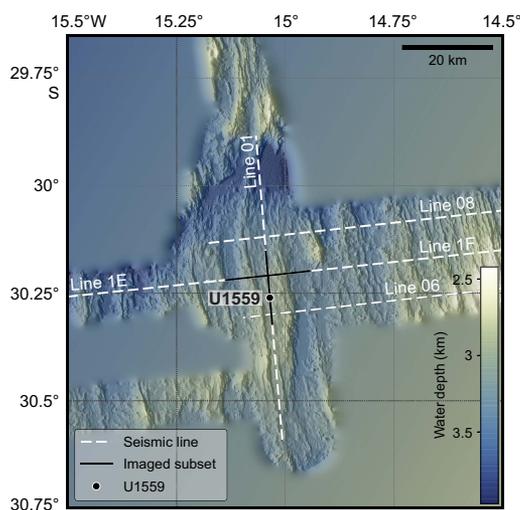

Figure F43. Site U1559 bathymetry (Christeson and Reece., 2020). Seismic reflection profiles were acquired during CREST cruise (Reece et al., 2016).

Site U1559 was first occupied in November 2020, when Expedition 390C cored Hole U1559A (Figure **F15A**) to a depth of 66.2 mbsf, contacting basement rocks at 63.9 mbsf, and drilled in a reentry system with 13⅜ inch casing in Hole U1559B (Figure **F15A**) to a depth of 55.3 mbsf, the hole itself extending to 58.9 mbsf. Expedition 390 revisited the site and cored Holes U1559C to 60.9 mbsf and Hole U1559D to 59.4 mbsf (Figure **F15B**). The plan for Expedition 390 was to core 250 m into basement with the RCB system in Hole U1559B and collect wireline geophysical logging data through the basement. However, failure of the forward electromagnetic drawworks brake caused operations to be cut short, and the ship returned to Cape Town early. Instead, the Hole U1559B basement objectives were postponed to Expedition 393. Expedition 393 reoccupied Hole U1559B (Figure **F15C**) but deepened it only 49.0 m into relatively fresh basaltic lava flows of the upper ocean crust and recovered 12.8 m of hard rock core. Very slow rates of drilling (<0.7 m/h, absolute; 0.8 m/h rotational) and low rates of recovery (~26%) may in part reflect heavy damage to the RCB bit even after a short duration of rotation (52.7 h) and are perhaps displayed in the commonly flared deformation of the basalt cores recovered.

9.7.2. Operations

9.7.2.1. Expedition 390 operations

9.7.2.1.1. Transit
The ship completed the approximately 2 day, 600 nmi voyage from Site U1557 to Site U1559 at 1818 h on 21 May 2022, and transitioned from cruise to DP mode to begin drilling operations.

9.7.2.1.2. Hole U1559C
Hole U1559C, located 30 m south of Hole U1559B, was spudded on 22 May 2022 using the APC/XCB system in a water depth of 3058.0 m. Cores 390-U1559C-1H through 6H advanced to 51.8 mbsf, recovering 52.08 m (100%). Because we expected to penetrate basement in the next core, we transitioned to using the XCB system. Core 7X encountered a hard layer at ~59 mbsf that was assumed to be the sediment/basement contact. However, no basement material was recovered in the core, only 4.82 m of sediment out of the 9.1 m advance (57%). We ended coring in Hole U1559C and pulled out of the hole to the seafloor at 1545 h, aiming for better recovery of the sediment/basement interface in Hole U1559D. All Hole U1559C APC cores were oriented; APCT-3 tool formation temperature measurements were made while collecting Cores 390-U1559C-4H, 5H, and 6H.

9.7.2.1.3. Hole U1559D
For Hole U1559D, the vessel was offset 20 m south. Cores 390-U1559D-1H through 6H advanced to 49.9 mbsf and recovered 42.01 m of sediment (84%). During drilling of Core 7X, we contacted a hard layer and recovered some small rubbly pieces of basement. Core 8X advanced 2 m to a final hole depth of 59.4 mbsf and recovered 0.37 m of material (18%). All Hole U1559D APC cores were oriented; perfluorocarbon microbial contamination tracer was pumped during the circulation of drilling fluid. In total, 2.0 days of expedition time was spent coring at Site U1559 (Table **T2**; Figure **F15B**).

During the pipe trip back to the surface after finishing operations in Hole U1559D, the bearings failed on the forward electromagnetic drawworks brake. The brake was disconnected from the drawworks and isolated. Tripping back to the surface was finished using the single remaining brake. However, it was not possible to continue operations at Site U1559, and the decision was made to end operations for Expedition 390.

9.7.2.2. Expedition 393 operations

9.7.2.2.1. Transit
JOIDES Resolution departed Repair Quay 3 in Cape Town, South Africa, on 11 June 2022, with the last line released at 0949 h. Just outside the harbor we stopped to test the 50 kVA uninterruptible power supply (UPS) system under different levels of electrical load before starting the sea voyage to Site U1559 at 1455 h. Much of the transit was completed at reduced speed due to rough seas and high winds, and at times the heading had to be adjusted. Sea conditions began to improve on 18 June, allowing the ship to increase to full speed for the final 2 days of the transit. The ship com-

pleted the 1713 nmi voyage in 7 days, 23 h, at an average speed of 9 kt. The ship's thrusters were lowered at 1220 h on 19 June, beginning operations in Hole U1559B.

9.7.2.2.2. Hole U1559B

An RCB BHA was made up and run to 3031 mbrf. The top drive was picked up and a pipe pig was pumped through the drill string to clean rust from the inside. The ship maneuvered for reentry into Hole U1559B (Figure **F15C**), which had been established and cased during Expedition 390C in November 2020. We reentered Hole U1559B at 0143 h on 20 June and washed to 58.9 mbsf, the bottom of the existing hole. Cores 393-U1559B-2R through 13R penetrated from 58.9 to 107.9 mbsf and recovered 12.82 m (26.2%). Core 2R had no recovery and drilled very quickly, indicating softer sediment above basalt. While drilling Core 3R the drillers encountered basement at a depth of approximately 65 mbsf. Coring proceeded through Core 11R with a rate of penetration of about 1 m/h. In Core 12R, penetration slowed to less than 0.5 m/h with decreasing recovery. After 9% recovery of distinctively undergauge poor quality core in Core 13R, it was decided to terminate coring and retrieve the bit to the ship. There was significant damage to the core guides and bit cones, some of which had been ground down to the bearings, creating a large 20 cm diameter hemispheroidal void where once were cones and cutting buttons. Similar damage had been seen during recent operations drilling young basalts during IODP Expedition 395C in Holes U1562B and U1554F. Recovery in Hole U1559B was low and penetration was slow in part because of the fresh and fractured hard young ocean floor basalts being drilled but also because the ~65 m of sediment cover meant that the BHA extended ~100 m above seafloor, limiting the weight that could be applied to the bit. However, serious bit damage was clearly an issue, probably for some days. Early diagnosis and identification of warning signs of this style of bit failure require investigation. The ship was secured for transit and switched from DP to cruise mode at 1232 h on 23 June, ending operations at Site U1559.

9.7.3. Principal results

9.7.3.1. Sediments

9.7.3.1.1. Sedimentology

In the three APC/XCB holes cored at Site U1559 during Expeditions 390C and 390, lithology is composed almost entirely of biogenic deposits of calcareous nannofossil ooze with foraminifera (Figure **F17**). Because of the uniform composition, only member-like subunits are defined, and they are numbered from the top of the hole. Subunit definitions are based on relatively small changes in color, sedimentary structures, bioturbation, and general appearance, combined with microscopic examination of smear slides, bulk mineralogical analysis by XRD, and physical properties data including MS and color reflectance. Subunit IA consists of pale brown calcareous nannofossil ooze with trace siliciclastic material; Subunit IB is similar but has a high foraminifera content (>25% bulk sediment volume). Both date to the Pleistocene. Subunits IC and ID are reversed in age, with Subunit IC consisting of white calcareous nannofossil ooze with foraminifera dating to the early Pliocene and Subunit ID consisting of a very pale brown ooze dating to the Late Pliocene. Subunit IE is Messinian to Late Pliocene in age and consists of a very pale brown calcareous nannofossil ooze with foraminifera enriched in *Discoaster* sp. Differences in mineral assemblages are relatively small downhole; all samples have a ~95 wt% carbonate composition. Below the sediment/basement interface in Holes U1559A and U1559D, a transitional unit comprises a mix of micritic limestone (lithified ooze) and basalt clasts.

9.7.3.1.2. Biostratigraphy, age model, and mass accumulation rate

The 50.95–62.47 m thick sedimentary succession at Site U1559 contains a Holocene to latest Miocene sequence of pelagic ooze. Calcareous nannoplankton and planktic and benthic foraminifera are diverse and abundant throughout, although preservation decreases directly above basement (Figure **F18**). A coherent Late Miocene assemblage in an otherwise Late Pleistocene sequence of samples in Holes U1559A and U1559C marks the presence of a 6–8 m thick slump or sequence of slumps in Holes U1559A and U1559C (~8–14 m CSF-B in Hole U1559A and ~6–14 m CSF-B in Hole U1559C). These out-of-place Miocene samples occur in an interval of noticeably lighter colors in the core and a coincident shift in physical properties (particularly *P*-wave velocity) that delimit the full extent of the slump(s) and allow the same interval to be identified in Hole U1559D (~8–14 m CSF-B). The Pleistocene extends well below the slumped interval to roughly 32 m CSF-

B in both Holes U1559A and U1559C. Below this level, multiple calcareous nannoplankton and planktic foraminifera datums occur within the same samples, indicating either very slow sedimentation or a series of short unconformities spanning the Pliocene that requires higher sampling resolution postexpedition to confirm.

The sediment/basement interface was recovered in Holes U1559A and U1559D and is inferred in Hole U1559C based on very slow XCB drilling rates, although no basalt was recovered. The depth of basement varies by more than 5 m between these three holes; in the shallower holes, biostratigraphic markers indicate a latest Miocene age of ~6.0 Ma, whereas the deepest hole contains datums that indicate that the sediment/basement interface there must be older than 6.8 Ma (broadly in line with the projected basement age of 6.6 Ma for this site). Sedimentation rates are high (1.97 cm/ky) in the Pleistocene at Site U1559 (and still 1.43 cm/ky when the 6–8 m slump is removed from the calculation). Assuming that the Pliocene is condensed and not truncated by hiatuses, sedimentation rates in the bottom of the hole are around 0.56 cm/ky (Figure **F19**). Benthic foraminifera indicate gradual subsidence below abyssal depths from the Miocene to the Holocene.

9.7.3.1.3. Paleomagnetism

Paleomagnetic investigation of Site U1559 sediments included remanence analysis of cores split during engineering Expedition 390C alongside Expedition 390 analyses of the archive halves of Core 390-U1559C-1H through Section 7X-4 and Core 390-U1559D-1H through Section 7X-1. Discrete sediment samples were taken from Sections 390C-U1559A-8X-2 and 8X-4, as well as from Holes U1559C and U1559D cored during Expedition 390 (26 samples total). These data were used to establish a magnetostratigraphy for the sediment package at Site U1559, which will be refined with additional analysis postexpedition. All discrete sediment cubes were AF demagnetized, in steps up to 190 mT. By demagnetizing samples in a stepwise fashion, we determine the ChRM of the sample, which reflects the magnetic field direction at or soon after sediment deposition and aids in magnetostratigraphic interpretation. Additionally, this demagnetization process helps to characterize, to a first order, the dominant magnetic mineral assemblage. IRM experiments contribute additional background information on the magnetic minerals present, such as coercivity, by "unmixing" the signal and using qualitative relationships between intensities at various field values.

Inclinations after 20 mT demagnetization measured from Holes U1559A, U1559C, and U1559D are bimodal, although histograms indicate significant contributions from inclinations between the two "peaks." Hole U1559A inclinations cluster around −53° and 43°. Inclinations for Hole U1559C cluster around −41° and 37° and are the shallowest inclinations at this site. Hole U1559D inclinations cluster around −53° and 34°. Except for the two negative modal inclinations in Holes U1559A and U1559D, most of these inclinations are much shallower than that expected for a GAD at this latitude (±49.1° at 30°S). A small number of the discrete sediment samples display noisy OVPs; of the 26 sediment samples, 20 samples had OVPs clean enough to contribute to defining the ChRM. Only 16 of these samples gave maximum angular deviation angles <15°, typically considered the cutoff for reliable magnetic field directions.

Because inclination data depict a clear polarity sequence for most intervals, the magnetostratigraphy for each hole can be confidently determined. Considering the estimated age of the basement (6.6 Ma) and the pattern of the polarity sequence retrieved at Site U1559, which mainly derives from Hole U1559C, a tie to the GPTS is proposed. The proposed correlation of the normal polarities at the base of Holes U1559A and U1559C to Miocene Chron C3An is compatible with the crustal age of the basement. MDFs, considered the field at which half of the NRM intensity remains, IRM up to 1.2 T, and backfield IRM experiments suggest that stable single-domain or fine pseudosingle-domain magnetite/titanomagnetite is the predominant magnetic mineral.

9.7.3.1.4. Physical properties and downhole measurements

Physical properties characterization of Site U1559 sediments is based on cores and in situ downhole measurements from Holes U1559A, U1559C, and U1559D. Whole-round core-based measurements include NGR, bulk density from GRA, MS, and *P*-wave velocity. Split-core section

measurements include MSP, *P*-wave velocity, MAD, thermal conductivity, and sediment shear and compressional strength.

NGR is relatively low throughout the carbonate-dominated sediments at Site U1559 (Figure **F17**). MS records high-frequency but low-amplitude variability, between 1 and 25 IU, reflecting only minor differences in the concentration of magnetic minerals in carbonates from the seafloor to the sediment/basement interface. Bulk density increases from ~1.3–1.4 g/cm^3 at the seafloor to ~1.7–1.8 g/cm^3 at the sediment/basement interface, with punctuated intervals of low bulk density likely a reflection of dislocated slumped sediments or slurries caused by drilling disturbance. *P*-wave velocity corresponds to bulk density, and both are likely associated with porosity changes downhole. Shear strength increases downhole, whereas compressional strength remains relatively constant with depth. Thermal conductivity varies between 1.091 and 1.284 W/(m·K) with no downhole trend, which is expected given the uniformity of the carbonate lithology observed in all three sediment holes. Using downhole temperature and thermal conductivity measurements, a geothermal gradient of 6.3°C/km and a heat flow of 7.73 mW/m^2 through the sediments were calculated. Calculated conductive heat flow is low for 6.6 Ma crust, which may suggest substantial advective heat loss via hydrothermal circulation.

Minor variations in MS and color reflectance data are used to correlate stratigraphy between holes, resulting in an almost continuous spliced record to the sediment/basement interface at 71.4 m CCSF. Three breaks exist in the shipboard splice where core gaps from all three holes coincide. Proximal to the sediment/basement interface, there is excellent correspondence in the stratigraphy, resulting in a robust alignment of the holes.

9.7.3.1.5. Sedimentary and pore water geochemistry

In addition to a mudline water sample, two whole-round samples per core were collected for IW squeezing and geochemical analyses from Holes U1559A (15 samples) and U1559D (13 samples). Rhizon samples were also taken for postexpedition research at an approximate frequency of one per section prior to splitting cores from Holes U1559C and U1559D. No Rhizon samples were taken from intervals with drilling disturbance visible through the core liner. Shipboard analyses of the squeezed IW from Holes U1559A and U1559D include pH, salinity, alkalinity, major cations and anions using IC, major and minor elements using ICP-AES, and nutrients (phosphate and ammonium) using a spectrophotometer. Carbonate and TOC measurements were conducted on squeeze cakes (Holes U1559A and U1559D) and discrete samples from the working half (Holes U1559C and U1559D). IW oxygen was measured in Hole U1559C and U1559D cores using Presens optical oxygen sensors at a resolution of ~1.5 m. Sulfate concentrations decrease immediately across the sediment/water interface; however, downcore concentrations are highly variable and do not indicate substantial sulfate reduction (Figure **F20**). Major cation (e.g., Ca, Mg, K, and Sr) concentrations are stable throughout the hole, but Ca and Sr show a gradual decline near the sediment/basement interface that coincides with an increase in Si. Sediment carbonate varies between ~86 and ~96 wt%, reflecting the calcareous nannofossil ooze lithology of all three holes, whereas the organic carbon content is low (<0.5 wt%).

9.7.3.1.6. Microbiology

Sediment microbiological samples were collected from Cores 390-U1559D-1H through 7X. Samples destined for experiments testing physiology were processed in the anaerobic chamber in the walk-in cold room; samples destined for postexpedition cell counts and nucleic acid analysis were processed at room temperature between two KOACH units to mitigate contamination. This dual setup allowed faster sample processing in the collected sediment sections compared to processing time at Site U1556. To test for microbial contamination of whole-round core samples from drilling fluid, we collected sediment samples containing perfluorocarbon tracer PFMD from each microbiology whole round. PFMD analyses demonstrate successful delivery of the tracer to the core exterior and limited penetration of tracer into core interiors, indicating minimal or no contamination during the coring process.

9.7.3.2. Volcanic rocks

9.7.3.2.1. Igneous petrology

Five lithostratigraphic units were identified comprising four main volcanic units and one thin sedimentary unit (Figure F44A). Those four volcanic units were further divided into seven subunits based on volcanic emplacement style and subtle changes in phenocryst assemblages. No brecciated rocks were recovered. The uppermost volcanic rocks are aphyric microcrystalline basalt sheet flows with some planar glassy margins and vuggy vesicular patches (Unit 1). These are underlain by sparsely plagioclase-phyric microcrystalline to fine-grained basalt pillow lavas (Subunit 2A) with common curved and planar glassy margins. Rare fresh olivine phenocrysts present from 73.9 mbsf (Subunit 2B) and the absence of curved glassy margins from 83.7 mbsf suggest the lowermost lavas of this unit are sheet flows (Subunit 2C). Unit 2 basalts are separated from Unit 4 basalts by a thin layer (~10 cm) of hydrothermally altered indurated calcareous sediment (Unit 3) with altered glass impregnated into both the upper and lower contact (~85.5 mbsf). The directly underlying lavas (Subunit 4A) are sparsely plagioclase-phyric microcrystalline to fine-grained basalt sheet flows containing rare olivine phenocrysts; the absence of glass and relatively coarse holocrystalline grain size suggest emplacement as a sheet flow. Unit 5 (~100.7 mbsf) comprises sparsely plagioclase-phyric microcrystalline to fine-grained basalt sheet and pillow flows with rare olivine and clinopyroxene phenocrysts. The relative abundance of olivine over plagioclase phenocrysts in the final recovered pieces distinguishes Subunit 5B (104.34 mbsf). Despite this variation, distinctive sparse macroscopic plagioclase phenocrysts are common to all the volcanic units apart from aphyric Unit 1. Together with only modest differences in geochemistry determined by pXRF analysis, this consistency suggests all of the igneous lithologic units at Site U1559 belong to a sin-
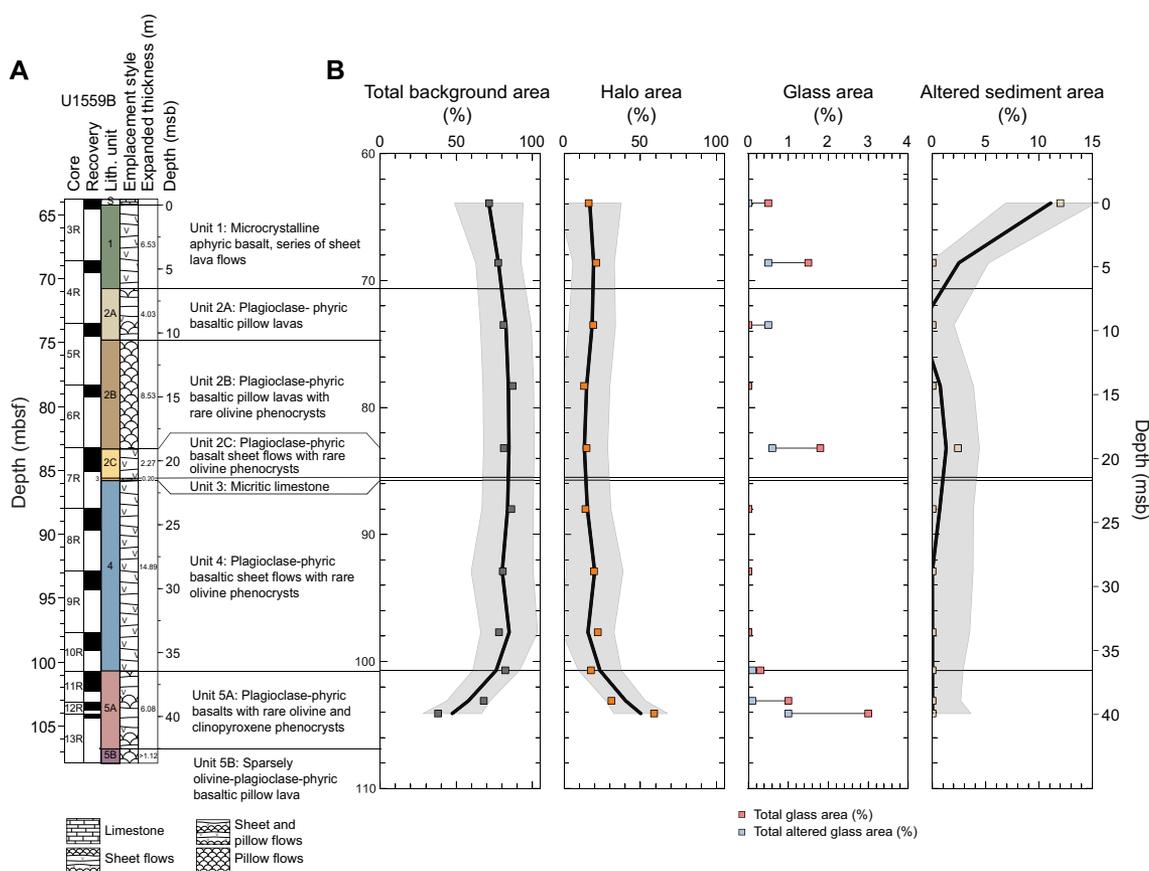

Figure F44. A. Stratigraphic column for igneous basement, Hole U1559B. Unit contact depths and thicknesses are expanded to account for <100% recovery. B. Area abundance of background alteration, alteration halos, fresh and altered glass, and altered sediment. Data are plotted at individual core level. Depths are CSF-A and plotted at top of cored interval. Black trend lines = locally weighted nonparametric regression (LOWESS), gray shading = 2σ of mean.

gle co-magmatic sequence of relatively N-MORB with subtle internal variations related to fractional crystallization and other magma chamber processes. The interpretation of significant intervals of sheet flows is somewhat atypical for a slow-spreading ridge. However, given the poor recovery, it is possible some sections of pillow basalts or breccia were not recovered. This potentially biased recovery must be carefully considered by subsequent studies seeking to compare hydrothermal exchange between this hole and others along the SAT.

9.7.3.2.2. Alteration petrology

Hydrothermal alteration in Hole U1559B is characterized by pervasive gray background alteration with a variety of different colored alteration halos throughout the cored interval (Figure **F44B**). The short penetration of Hole U1559B precludes separation of alteration zones with depth, but a downhole evolution in alteration halo types is present and the recovery of a more oxidized pillow lava fragment at the base of the hole indicates that seawater-basalt exchange continues below the bottom of the hole. All alteration is dominated by the formation of yellow-brown clay minerals that replace mesostasis and groundmass. Calcite replaces groundmass in some sections. Three halo types present show a downhole shift from mainly dark gray halos accompanied by orange-light brownish gray halos in the cores down to 92 mbsf to an increasing abundance of orange-gray halos below 92 mbsf (Igneous Units 1 and 2 and the uppermost part of Unit 4). The earliest stage of alteration is the formation of dark gray alteration halos around fractures and veins. This is followed by the formation of the orange-light brownish gray and orange-gray halos. Crosscutting relationships are rare, and the sequence of later alteration is determined by crack-seal textures in veins that suggest that early clay lined veins are reopened and filled with calcite.

9.7.3.2.3. Igneous geochemistry

Representative samples of basement cores from Hole U1559B were taken from the freshest portions of each lithologic subunit to obtain a downhole record of the primary magmatic conditions, along with one sample near the basalt/sediment contact. In addition, two Hole U1559B samples were prepared as matrix-matched check standards for use with direct core pXRF data collection throughout Expedition 393. Eight samples were measured for LOI and bulk rock geochemical analysis via ICP-AES. The unoxidized powders of these samples as well as powders of the reference billets of the two standards were also characterized for elemental abundances via pXRF. The Hole U1559B basalts are exceptionally uniform in their major element compositions: TiO_2 contents vary between 1.0 and 1.2 wt%, with high Cr (320–390 ppm) and low Ba (<1–6 ppm). In terms of basaltic rock type, they are olivine tholeiites per the Yoder and Tilley (1962) normative classification scheme. K/Zr ratios, which are a crude measure of alteration, are 10–18 in Hole U1559B samples, moderately higher than fresh South Atlantic MORB, which averages 7.4.

9.7.3.2.4. Paleomagnetism

Paleomagnetic measurements on basement cores from Hole U1559B were performed to characterize the magnetic signature and retrieve initial information regarding the magnetic mineralogy. Continuous measurements of the remanent magnetization were conducted using the SRM at 2 cm spacing. To avoid excessive noise and edge effects, we only measured pieces longer than 9 cm. Measurements of remanence were made before and after progressive AF demagnetization at steps of 5, 10, and 20 mT applied field strength. Measurements were also conducted on a total of 11 discrete cubes of 8 cm³ volume, which is one to two per core. Paleomagnetic experiments included AMS, remanence before and after AF or thermal demagnetization, and IRM acquisition.

Paleomagnetic SRM results reveal a clear principal component at 20 mT demagnetization. Inclination values of these components are predominantly positive, which indicates reversed polarity. The distribution of inclinations is approximately Gaussian with mean values around 38°, about 11° less than the GAD (±49.1°) at 30°S. Discrete sample measurements revealed clear ChRM that has inclinations similar to the SRM results. Discrete sample results confirm reversed polarity magnetization, which is in contrast to the normal polarity expected for the 6.6 Ma basement age at Site U1559 based on magnetic data collected during the CREST survey (Kardell et al., 2019). Considering the biostratigraphic datums at the sediment/basement interface, the crustal age is likely placed within the geomagnetic polarity Chron C3Ar (Gradstein et al., 2020), which is slightly older than the expected age for Site U1559. In addition, MDFs and IRM acquisition up to 1.2 T suggest that the dominant magnetic carriers are likely low-coercivity minerals (e.g., titanomagnetite and

maghemite). AMS measurements indicate a dominant prolate fabric for the majority of samples along with a well-defined subhorizontal magnetic foliation perhaps caused by flow emplacement. No systematic changes of the scalar parameters of AMS were found with depth in Hole U1559B.

9.7.3.2.5. Physical properties

Characterization of the basement physical properties at Site U1559 is primarily based on cores from Hole U1559B with additional information from Holes U1559A, U1559C, and U1559D. Whole-round, section-half, and discrete measurements were considered together to characterize the petrophysical signatures for the different volcanic units. In addition to these measurements, all whole-round cores were imaged using XMAN and ~30% of the recovered material was scanned using the DMT CoreScan3 after identifying oriented core pieces with relatively cylindrical shapes.

Many of the hard rock whole-round measurements are impaired by the small, discontinuous core pieces recovered from Hole U1559B. These measurements therefore often underestimate the true physical properties of the material. NGR in Hole U1559B is relatively low and consistent across units and ranges 0.2–2.1 counts/s (mean = 1.05 ± 0.36 counts/s [±1σ]). Pass-through MS measured on whole-round cores ranges 1–1054 IU (mean = 68.5 ± 112 IU). Discrete MSP measurements from section halves range 1–1636 IU (mean = 97.6 ± 199 IU). Peaks in magnetic susceptibility are associated with Lithologic Unit 3 (thin indurated calcareous sediment layer), the base of Unit 4 (sheet flow), and Subunit 5A (mixed sheet and pillow flows).

Discrete bulk density measurements using MAD range 2.79–2.90 g/cm^3 (Figure **F45**). Porosity is variable in Hole U1559B and ranges from 2.6% in the fine-grained sheet and pillow flows of Subunit 5A to 5.6% in the microcrystalline sheet flow of Unit 4 (Figure **F45**). *P*-wave velocity ranges from 5.46 km/s in Subunit 2A to 5.80 km/s in Unit 1 (mean = 5.63 ± 0.91 km/s) (Figure **F45**). The
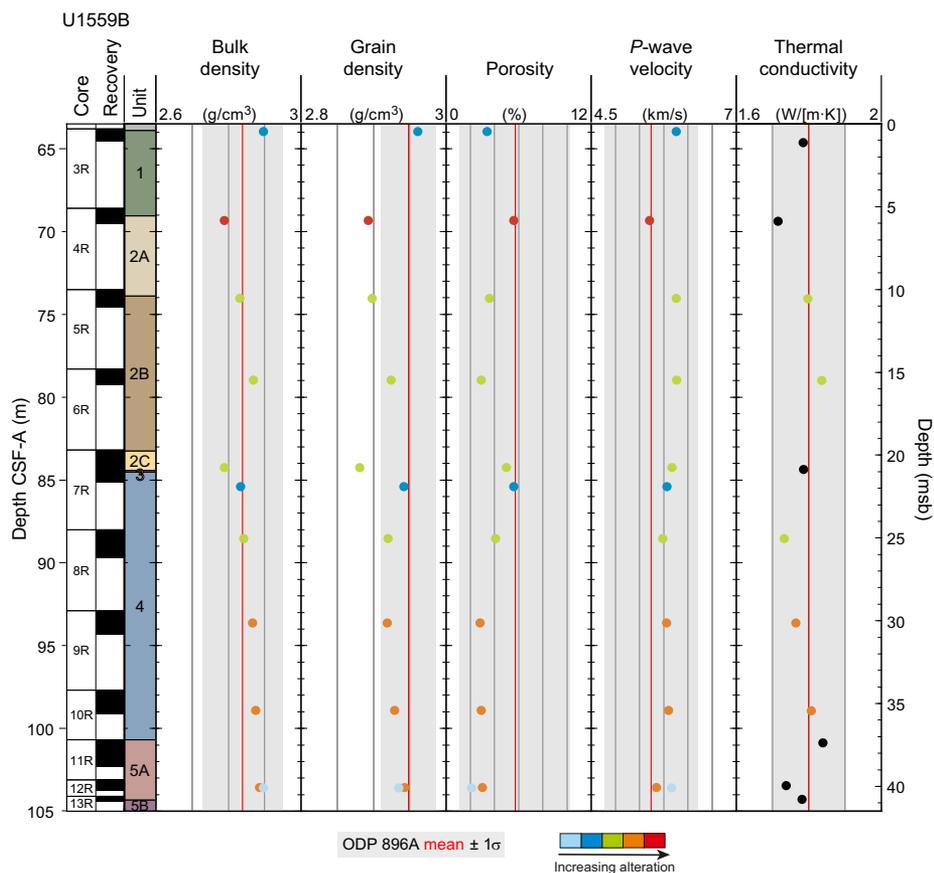

Figure F45. Comparison of physical properties of discrete samples, Holes U1559B and 896A. Range of data from Hole 896A (red line = mean value of each data type, shaded boxes = ±1σ). *V*$_P$ shown is maximum velocity measured for each sample. Symbol colors represent alteration degree, black symbols lack alteration degree description.

limited number of discrete samples (n = 11) from Hole U1559B does not show a clear relationship between alteration level and petrophysical parameters. The average thermal conductivity measured in basement samples was 1.78 ± 0.04 W/(m·K) (Figure **F45**). Together with heat flow estimates from the overlying sediment, this suggests a temperature gradient of about 40°C/km in the shallow basement at Site U1559 if the thermal regime is mostly conductive. These data are similar to measurements from ODP Hole 896A, near the 6.9 Ma ocean crust reference site in Hole 504B (see figure 76 of Shipboard Scientific Party, 1993b).

9.7.3.2.6. Microbiology

Microbiology sampling in basement in Hole U1559B was focused on exploring evidence for life in the sediments and underlying volcanic basement, especially at the sediment/basement interface, using microscopy, culture-based approaches, and culture-independent approaches. In total, eight whole-round samples (5–13 cm long) representative of the different rock types and alteration styles that comprise the volcanic basement stratigraphy of Hole U1559B were collected for shipboard and shore-based microbiological analyses. All eight samples were tested for contamination, but no tracer was detected, most likely the result of the too small amount of rock sample in the test vials. To determine the extent of microbial activity, viral production and ammonium enrichments were established that will be analyzed in laboratories on shore postexpedition.

10. Expedition 390 preliminary scientific assessment

The primary operational objective of the SAT expeditions is to drill a transect of sites along a crustal flow line across the western flank of the southern Mid-Atlantic Ridge, core the uppermost (150–250 m) ocean crust produced between ~7 and 61 Ma at the slow- to intermediate-spreading Mid-Atlantic Ridge, and recover complete sections of the overlying sediments. The SAT was designed to target six primary sites on 7, 15, 31, 49, and 61 Ma ocean crust, which will fill critical gaps in our sampling of intact in situ ocean crust with regard to crustal age, spreading rate, and sediment thickness. These sections are required to investigate the hydrothermal evolution of the aging ocean crust, sediment and basement-hosted microbial community variation with increasing substrate age, paleoceanographic evolution of the South Atlantic Ocean, and deep-ocean and subtropical gyre responses to changing global climate. Expedition 390 was the first of two scientific SAT expeditions, building on the successful operations of engineering Expeditions 390C and 395E that conducted preliminary sediment coring and installed reentry systems cased to basement at five of the primary SAT sites. The primary operational objective of Expedition 390 was to complete the drilling operations at the oldest (Sites U1556 and U1557) and youngest (Site U1559) sites of the SAT.

The SAT operations on 61 Ma crust were hugely successful, with the entire ~290 m thick sediment succession cored twice at Site U1556 and an expanded (~565 m) succession cored at Site U1557 during Expeditions 390C and 390 (Table **T2**; Figure **F15**). These two sites were located close together (6.7 km) in the same fault-bounded localized sedimentary basin to investigate the effects of the significant basement topography and different sediment cover on hydrothermal alteration of the upper crust. The uppermost ~340 and 120 m of basement were cored at Sites U1556 and U1557, respectively. Hitherto, there were no scientific ocean drilling holes that penetrated >100 m into ocean crust formed between 46 and 100 Ma, despite the discernible conductive heat flow deficit out to 65 Ma crust, globally on average, indicating that there is significant advection of heat from the cooling of the oceanic lithosphere out to this age. Basement cores from Sites U1556 and U1557 therefore provide a 61 My time-integrated record of hydrothermal alteration that will enable us to quantify the magnitude and duration of low-temperature chemical exchange with the overlying oceans and investigate the impact of changing ocean conditions on hydrothermal exchange. At Site U1556, the uppermost basement comprises a volcanic sequence of pillow lavas, massive flows, and hyaloclastite breccias, of which ~340 m was cored (Figures **F21**, **F22**). In contrast, at Site U1557 the uppermost ~120 m of basement was found to comprise a basaltic talus breccia consistent with its location in the deeper portion of the localized sedimentary basin adjacent to a fault scarp (Figures **F6B**, **F21**, **F22**). Such breccias are likely a common feature of slow-spreading ridge flanks, which are characterized by fault-bounded basement basins like the one in

which Hole U1557D is located. Breccias from Site U1557 had significant primary porosity, now partially to completely cemented by carbonate and zeolite.

The sediments collected from Sites U1556 and U1557 during Expeditions 390C and 390, along with a ~45 m section cored to basement at Site U1561 during Expedition 395E and described during Expedition 390, capture key paleoclimate intervals from the Paleocene to the Holocene (Figure **F17**). The significant basement topography between these closely spaced sites will allow exploration of the effects of water depth and accommodation space on their sedimentation histories and their records of past ocean conditions and currents. A ~15 My unconformity or condensed interval spanning the early Oligocene to early Eocene at Sites U1556 and U1557, at a depth coincident with a seismic reflector identified by Estep et al. (2020) as representing a regional unconformity, limits investigations of that time interval in this area, but its presence and extent raise further research questions about both global and regional conditions at that time.

Expedition 390 also successfully completed sediment operations at the youngest SAT site (U1559), started during Expedition 390C, with three APC/XCB holes cored to basement in total. The sediment/basement interface was recovered in Holes U1559A and U1559D. The unfortunate failure of the forward drawworks electromagnetic brake after APC/XCB coring was completed prevented deeper basement coring in Hole U1559B. However, the uppermost volcanic rocks recovered in the interface (<2 m) were significantly fresher than the volcanic rocks recovered from 61 Ma Sites U1556, U1557, and U1561, offering a tantalizing glimpse of the effects of crustal aging further revealed by operations completed at Site U1559 and the intermediate age SAT sites during Expedition 393.

Microbiological samples were collected from both sediment and basement in all holes cored during Expedition 390 and were preserved for postexpedition analyses. The high porosity of the 61 Ma basement samples suggests a suitable basement environment for microbes, and sediment chemical profiles of oxygen, manganese, and sulfate concentrations indicate an extended redox gradient that should allow for diverse microorganisms and metabolisms.

The Expedition 393 operations were planned to complete the SAT (Figure **F15B**), allowing integration of results across crustal ages and laterally across the ocean basin. Here, we document progress toward the primary objectives during Expedition 390.

10.1. Objective 1. Quantify the timing, duration, and extent of ridge flank hydrothermal fluid-rock exchange.

With the exception of fresh glass from chilled margins, all volcanic rocks recovered from Sites U1556, U1557, and U1561 are slightly to completely altered. Given that all the samples analyzed are affected by alteration to some degree, the immobile element Zr/Ti ratio was used to discriminate between magma types. Zr/Ti ratios reveal three types of basalts were recovered from Site U1556 (61.2 Ma): OIB, N-MORB, and an intermediate composition (Figure **F22**). Basalt from Site U1561 (61.2 Ma) has OIB-like compositions, whereas only N-MORB composition basalts were recovered from Sites U1557 (60.7 Ma) and U1559 (6.6 Ma).

Our quantitative logging of the variations in the style and extent of alteration of the volcanic rocks recovered at Sites U1556 and U1557 (Figure **F22**) in conjunction with analyses of cores recovered at other crustal ages along the SAT during Expedition 393 will allow us to evaluate hydrothermal contributions to global biogeochemical cycles. Postexpedition analyses will include radiometric dating of hydrothermal minerals to determine the timing and hence duration of hydrothermal exchange.

Hydrothermal alteration of the lavas was shown to affect their physical properties, using analyses of a suite of discrete samples that were representative of the variations in lithology and styles of alteration observed in Hole U1556, classified by the degree of alteration. This classification scheme revealed a robust relationship whereby porosity increases and *P*-wave velocity decreases with alteration extent (Figure **F46**). The observed relationships have important implications for improving interpretations of seismic data and using such data to map variations in hydrothermal alteration and model permeability and hence fluid flow on ridge flanks. Paleomagnetic data will

also contribute to reconstructing alteration history. A negative inclination is expected in 61 Ma lavas if the ChRM has been preserved. However, analyses of the same suite of discrete lava samples from Hole U1556B revealed a normal polarity (positive inclination) overprint of the ChRM that is most strongly developed in samples of hyaloclastite breccia or samples with the greatest extent of alteration (Figure F23).

Expedition 390 benefited from the addition of two nonstandard imaging systems (Figure F24). The DMT CoreScan3 system, loaned by the International Continental Scientific Drilling Program (ICDP), was used to capture high-resolution images of basement core exteriors prior to cutting. The images collected preserve key information about the orientations of contacts and structures in the core that may be lost because of fracturing during core splitting and can be integrated with wireline borehole images during postexpedition analysis to establish a more complete stratigraphy through intervals of low recovery. These data will also allow development of novel computer visualization approaches for automated quantitative core logging. Samples fragmented as part of the basement microbiological sampling were also imaged using the Foldio turntable system prior to breaking them open with a hammer. This system generates a series of 36 images captured at 10° intervals as a core sample is rotated on a stage and will allow scientists to gain insight into the composition and structure of core material removed prior to core description (Figure F24).

Sediment IW chemistry reveals ongoing chemical reactions in the sediment and basement, including mineral dissolution or precipitation, diagenesis, microbial metabolisms, and circulation of basement fluid. Concentration profiles with depth suggest fluid flow between the sediment and basement. IW sulfate normalized to chloride (SO_4^{2-}/Cl) increases toward the basement in Holes U1556A, U1556C, and U1557B, indicating an increase in sulfate below the sulfate reduction zone detected in the upper portions of the sediment (described further in primary Objective 2; Figure F20). Coincident with this change, the decrease in Ca/Mg toward basement suggests the flow of seawater-derived basement fluid into the basal sediments (Figure F20, where depths have been normalized to sediment thickness to make profiles comparable across sites). The dilute seawater sulfate concentrations (SO_4^{2-}/Cl), low Mg concentrations (high Ca/Mg), and excess lithium in Hole U1557B suggest an intriguing interaction between those pore fluids and the basement that can be further studied with Sr isotopes and other geochemical tracers.

10.2. Objective 2. Investigate sediment- and basement-hosted microbial community variation with substrate composition and age.

Samples were collected for postexpedition analysis of cell counts, nucleic acid-based analysis of microbial community composition and function, and lipid-based microbial composition throughout the sediment columns in Holes U1556C, U1556E, and U1559D, as well as from basement cores
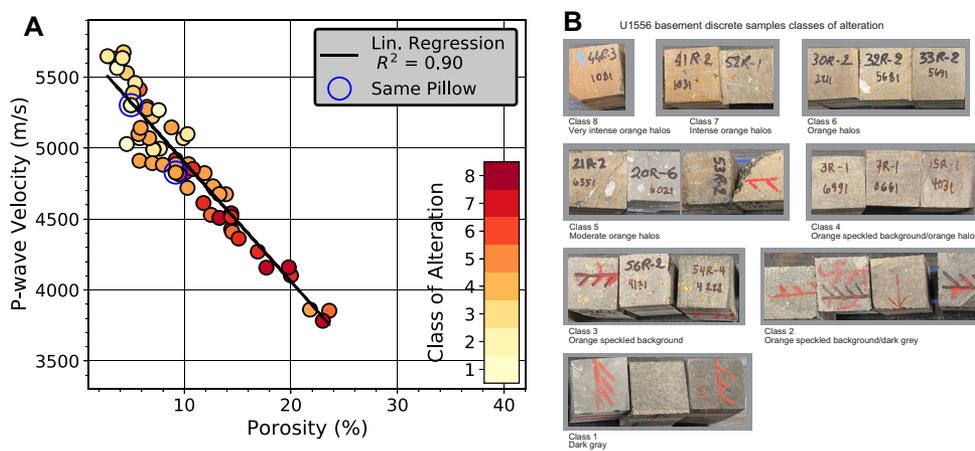

Figure F46. Comparison of porosity, *P*-wave velocity, and alteration for discrete basalt samples, Site U1556. A. *P*-wave velocity vs. porosity by alteration class. B. Basalt cubes illustrating different alteration classes. Class 1 = least altered, Class 8 = most altered. Class descriptions are directly comparable to core alteration description of Site U1556 basement sequence.

from Holes U1556B and U1557D. In addition, incubation experiments targeting uptake of carbon and nitrogen compounds, sulfate reduction rates, and enrichment of anaerobic Archaea were begun on the ship and will be analyzed during shore-based research. Altogether, the work initiated during Expedition 390 will allow postexpedition work to analyze changes in microbial community abundance, composition, function, and activity from the seafloor to the deepest basement sampled.

Pore water chemical profiles of sulfate normalized to chloride (SO_4^{2-}/Cl) and of Mn suggest an intriguing overlap of redox zones with implications for active microbial metabolisms. As commonly observed in reducing sediments, the pore water SO_4^{2-}/Cl decreases with depth, indicating sulfate consumption. Sulfate is not completely reduced at any of the sites visited during Expedition 390. Increased dissolved Mn, indicative of Mn oxide reduction, typically appears above the sediment depths of maximum depletion of sulfate but also appears below the sulfate reduction zone at Site U1556 (Figure **F20**). Postexpedition sulfate reduction rate measurements may better characterize the zones of active microbial activity at these sites.

10.3. Objective 3. Investigate the responses of Atlantic Ocean circulation patterns and the Earth's climate system to rapid climate change, including elevated atmospheric CO$_2$ during the Cenozoic.

The recovery of alternating clay and carbonate intervals in sedimentary units near the top of Sites U1556 and U1557 indicates shoaling and deepening of CCD at these sites from the Oligocene through the Holocene (Figure **F17**). Planktic foraminifera and calcareous nannoplankton were rare or poorly preserved in pelagic clay intervals (Figure **F18**), but the abundant, well-preserved microfossils in carbonate intervals supported the construction of robust age models in combination with magnetostratigraphic reversals for all Expedition 390 sites (U1556, U1557, U1561, and U1559; Figure **F19**). Carbonate dissolution is indicated by high pore water Ca/Mg relative to seawater in the deepwater Holes U1556A, U1556C, and U1557B (Figure **F20**). This finding partially explains poor preservation of calcareous fossils in some intervals at these sites (Figure **F18**). Higher resolution biostratigraphic and isotope studies postexpedition will help to refine age models and calculations for mass accumulation rates, carbonate accumulation rates, and organic carbon accumulation rates that will allow us to answer questions regarding ocean productivity and circulation through the Cenozoic.

We recovered a ~0.8 m clay-rich interval that is characteristic of the PETM in Hole U1557B (Figure **F25**), based on physical properties and sedimentologic evidence as well as the presence of diagnostic *Rhomboaster* nannofossils; however, isotope work postexpedition is required to confirm this interpretation. Recovery of the PETM and other Paleogene hyperthermal events will help to address questions regarding Earth's response to rapid intervals of climate change in a particularly expanded Paleogene stratigraphy (~11.5 cm/ky) from Hole U1557B.

10.4. Operational considerations

The SAT objectives were ambitious but achievable owing to the work done during engineering Expeditions 390C and 395E, new developments in drilling capabilities, and the ingenuity of the crew, staff, and scientists. Expeditions 390C and 395E demonstrated that XCB PDC cutting shoes provide superior recovery of the sediment/basement interface compared to tungsten carbide insert (TCI) cutting shoes, allowing for this critical interval to be sampled multiple times at Sites U1556, U1557, U1561, and U1559. These preliminary engineering expeditions also discovered that the Dril-Quip reentry systems cannot be installed into basement in a single step; when the casing is in basement, weight cannot be removed from the drill string to allow the Dril-Quip release mechanism to operate. To install casing into basement, as planned for the SAT, the hole either needs to be fully drilled out beforehand or a HRT reentry system must be used, which does not allow extension of casing after the initial installation. This finding will aid planning of future expeditions that are considering such installations, which would have cost significant operational time had they been attempted during Expeditions 390 or 393. Having reentry cones with casing installed at five of the six primary SAT sites in advance of Expeditions 390 and 393 expedited basement drilling and allowed for deepening of Hole U1556B beyond the initial target of 250 msb, with

~340 m of basement penetration achieved. Finally, we found that the TransCo C-4 RCB drill bits are more durable than drill bits from previous suppliers, allowing for deeper penetration on a single bit and time savings because fewer pipe trips for bit changes are required. The bit brought back to the rig floor and recovered after 61.0 h and 184.6 m of basement drilling in Hole U1556B had minor damage to the TCI insert and a failed bearing seal but was still coring well. We could not inspect the second bit used in this hole because it was dropped at the bottom of the hole after 78.0 h of coring prior to logging. However, up until coring ended, it was generating good quality core with no sign of a decreasing diameter, which is often the sign of impending bit destruction.

11. Expedition 393 preliminary scientific assessment

The primary operational objective of the SAT expeditions was to drill a transect of sites along a crustal flow line at ~31°S across the western flank of the southern Mid-Atlantic Ridge, core the uppermost (~250 m) ocean crust produced between ~7 and 61 Ma at the slow- to intermediate-spreading Mid-Atlantic Ridge, and recover complete sections of the overlying sediments. The SAT was designed to target six primary sites on 7, 15, 31, 49, and 61 Ma ocean crust that fill critical gaps in our sampling of intact in situ ocean crust with regard to crustal age, spreading rate, and sediment thickness. After more than three decades focusing on the hydrothermal alteration and basement hydrogeology of well-sedimented intact crust formed by intermediate to fast-spreading ridges in the Pacific Ocean (e.g., eastern equatorial Pacific Sites 504, 896, and 1256 and Juan de Fuca Ridge flank ODP Sites 1023–1032 and Integrated Ocean Drilling Program Sites U1301, U1362, and U1363), the SAT marks an overdue pivot back to the Atlantic Ocean and crust formed at slow-spreading rates and ridge flanks with abundant basement outcrops out to beyond 60 My (e.g., DSDP Legs 51–53). Drilling at the SAT sites is required to investigate the hydrothermal evolution of the aging ocean crust, the nature and variation of sediment- and basement-hosted microbial communities with increasing substrate age, the paleoceanographic evolution of the South Atlantic Ocean, and the deep-ocean and subtropical gyre responses to changing global climate.

Expedition 393 was the second of two scientific SAT expeditions, following Expedition 390 (Coggon et al., 2022a), that built on the successful engineering operations of Expeditions 390C and 395E (Estes et al., 2021; Williams et al., 2021) that conducted preliminary sediment coring and installed reentry systems cased to basement at five of the six primary SAT sites. The initial operational goals of Expedition 393 were to complete drilling operations across the middle-aged spread of SAT sites on 15 and 49 Ma ocean crust (Sites U1560 and U1558) and establish a new, not previously occupied site (U1583) on 31 Ma ocean crust. Because of the failure of the forward drawworks electromagnetic brake toward the end of Expedition 390, additional basement drilling, coring, and wireline logging operations at Site U1559 were loaded into the Expedition 393 schedule.

11.1. Operational achievements of Expedition 393

Expedition 393 undertook sediment and basement coring, and when possible, logging operations at four sites to establish a crustal age transect across the western flank of the southern Mid-Atlantic Ridge. Drilling occurred in 12 holes at sites with ages from 6.6 to 49.2 Ma (Tables **T2**, **T3**; Figure **F15**). Legacy cased reentry cones remain at Sites U1559 (6.6 Ma) and U1560 (15.2 Ma) to complement Hole U1557D (60.7 Ma) deepened during Expedition 390. A free-fall funnel honoring Dick Kroon (1957–2022) sits on top of the basement drilled in Hole U1583F at the new site on 31 Ma crust, but poor hole conditions suggest further deepening would be challenging. Volcanic rocks of the uppermost ocean crust were cored to 43 (Hole U1559B), 192 (Hole U1560B), 130 (Hole U1583F), and 220 (Hole U1558B) msb in 6.6, 15.2, 30.6, and 49.2 Ma crust, respectively. More than 1150 m of sediment and basement were cored, recovering >775 m of core with an average recovery rate of >67%. Of this coring, 600 m was into hard rocks, recovering 234 m of core (39% recovery), and more than 550 m of sediment was cored with more than 540 m recovered (>98% recovery). Two holes (U1583F and U1560B) were wireline logged with multiple tool strings (Tables **T2**, **T3**; Figure **F15C**).

Microbiological samples were collected from both sediment and basement in all Expedition 393 holes and preserved for postexpedition analyses. Abundant altered glass, hydrothermal veins, complex breccias, and a wide variety of alteration halos in the volcanic sequences of the uppermost SAT ocean crust suggest myriad environments for microbial activity. Sediment pore water chemical profiles of oxygen, manganese, and sulfate concentrations indicate extended redox gradients from both the seafloor and the sediment/basement interface that may support a diversity of microorganisms and metabolisms.

Expedition 393 operations completed the first operational phase of the SAT and leaves open opportunities for future drilling, logging, and geophysical site characterization operations of the legacy and other sites. Detailed postexpedition integration of results across crustal ages and laterally across the ocean basin will establish a benchmark for understanding the aging of the ocean crust and its interactions with life and the oceans above. Here, we document progress made during Expedition 393 toward the primary objectives.

11.2. Objective 1. Quantify the timing, duration, and extent of ridge flank hydrothermal fluid-rock exchange.

Expedition 393 succeeded in drilling basement at a range of ages across the western flank of the southern Mid-Atlantic Ridge (Figure F47). The progressive influence of the Tristan da Cunha plume on mantle melting at the Mid-Atlantic Ridge over the past ~50 My at this latitude is preserved by the least altered volcanic rocks recovered during Expedition 393 (Figures F47, F48). Although detailed mantle source apportioning will require postexpedition radiogenic isotopic analyses and better characterization of magma fractionation, the progressive changes across the
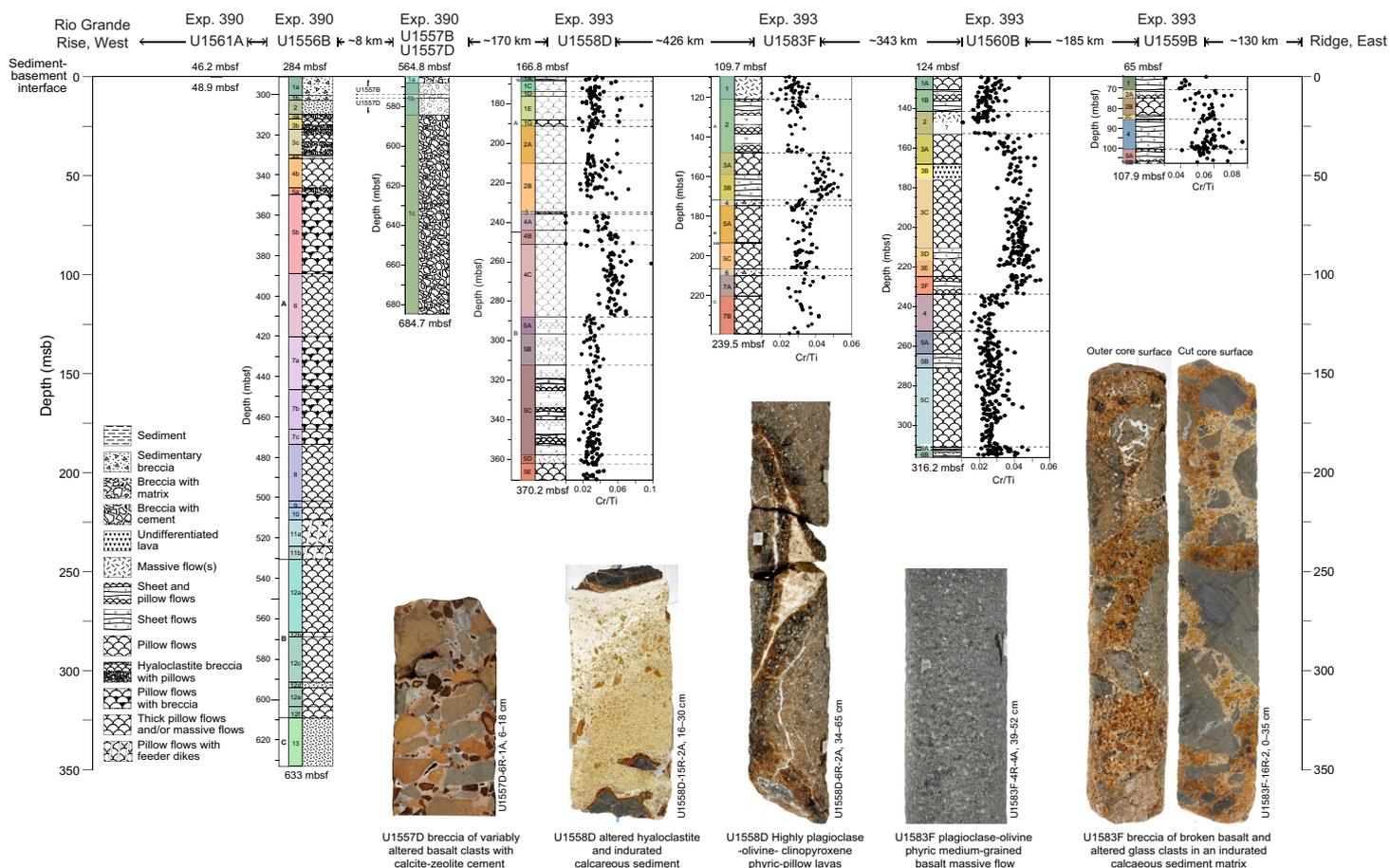

Figure F47. Summary of basement drilling during Expedition 393 across SAT showing examples of basalts, interflow sediments, and breccias. Cr/Ti data were measured directly on split-core surfaces by pXRF.

western flank of the southern Mid-Atlantic Ridge are already apparent from excellent shipboard ICP-AES data and more than a thousand tightly calibrated pXRF measurements directly measured on the split-core surfaces (Figures **F47**, **F48**). Abundant vitreous volcanic glass at all sites and from all volcanic units will provide further opportunities for mantle source definition and description of magmatic processes. Comprehensive postexpedition glass and fresh rock analyses will provide a firm baseline for quantifying the extent of chemical and isotopic hydrothermal exchange through comparison with different styles of more strongly altered materials.

In comparison to the ~61 Ma volcanic rocks recovered during Expedition 390, most volcanic rocks recovered from Sites U1559, U1558, U1560, and U1583 during Expedition 393 are less altered. However, clear differences from the alteration at the ocean crustal reference site Hole 504B are apparent (Alt et al., 1986, 1996). High abundance of iron-stained brown to orange halos and mineralogical and geochemical evidence for alteration, such as the formation of relatively refractory clay minerals, are present. These result from seafloor weathering due to extended exposure to ocean bottom water for millions to perhaps tens of millions of years.

Our quantitative logging of the variations in the style and extent of alteration of the volcanic rocks recovered at Sites U1558, U1559, U1560, and U1583 (e.g., Figure **F28**) in conjunction with analyses of cores recovered at older crustal ages along the SAT during Expedition 390 will allow us to evaluate hydrothermal contributions to global biogeochemical cycles. Postexpedition analyses will include radiometric dating of different hydrothermal minerals (e.g., clay and carbonate minerals) to determine the timing and hence duration of hydrothermal exchange. High spatial resolution elemental and isotopic mapping will illuminate hydrothermal alteration processes and together with XRD and electron beam analyses will allow us to write rigorous reactions and mass balances to quantify the evolving seawater-basalt hydrothermal exchanges. These rocks will provide essential well-characterized samples to better constrain the biogeochemical budgets of a whole suite of traditional (such as O, D, C, S, and ^{87}Sr) and boutique (including Li, B, Mg, K, Ca, and Tl) isotopic tracers. Additionally, they will provide insights into low-temperature hydrothermal exchange and the influence of these processes on global biogeochemical processes and the composition of seawater over the Cenozoic. Our quantitative descriptions and mineralogical studies will provide a reference framework for the changing physical properties of the ocean crust in terms of density, seismic velocity, and thermal conductivity.

Expedition 393 benefited from the addition of two nonstandard imaging systems. The DMT CoreScan3 system, loaned by the International Continental Scientific Drilling Program (ICDP), with transfers supported by Natural Environment Research Council (United Kingdom) IODP (to
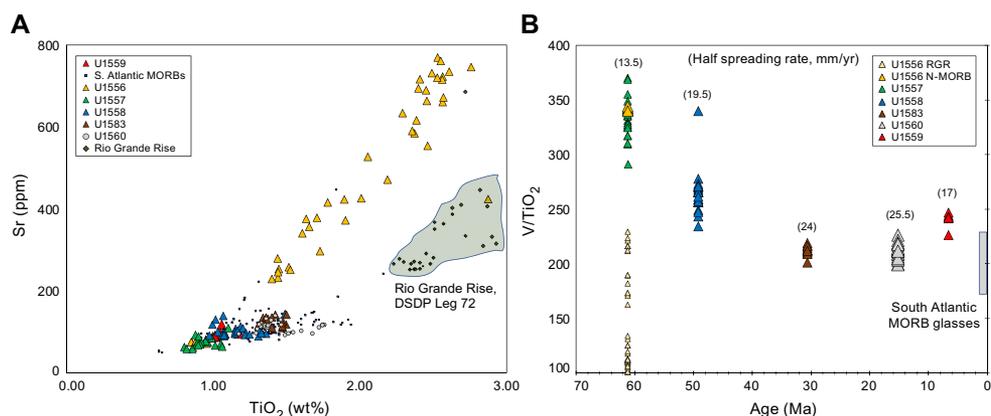

Figure F48. Geochemistry of igneous rocks from across the SAT. A. Shipboard analyses of Sr vs. TiO$_2$ concentrations for basalts showing clustering Expedition 393 analyses (Sites U1558–U1560 and U1583) on top of analysis of fresh glasses from modern South Atlantic Ridge MORB in contrast to analyses from Hole U1556B and the Rio Grande Rise (RGR). B. Basalt V/TiO$_2$ ratios vs. age. Geochemistry of lavas with MORB affinities show irregular progression from compositions with strong influence from Tristan da Cunha plume to V/TiO$_2$ values similar to lavas on modern southern Mid-Atlantic Ridge.

Teagle/Coggon), was used to capture high-resolution images of basement core exteriors prior to cutting. The images collected preserve key information about the orientations of contacts and structures in the core that are lost because of fracturing during core splitting. These presplitting images will be integrated with wireline borehole images to establish a more complete stratigraphy through intervals of low recovery. These data also allow development of novel computer visualization approaches for automated objective quantitative core logging. Samples destroyed as part of the basement microbiological sampling were imaged using the Foldio turntable system prior to breaking them open with a hammer. This system generates a series of 36 images that capture all sides of the core sample and will allow both the microbiologists and other scientists to gain insight into the composition and structure of removed core.

11.3. Objective 2. Investigate sediment- and basement-hosted microbial community variation with substrate composition and age.

Samples were collected for postexpedition analysis of cell counts, microbial community composition and function using molecular approaches, and lipid-based microbial composition from throughout the sediment columns in Holes U1558F, U1560C, and U1583C, as well as from basement cores from Holes U1558D, U1559B, U1560B, and U1583F. In addition, microbial enrichment incubation experiments targeting ammonium oxidizers and viral production and prophage induction experiments were begun on the ship and will be analyzed during shore-based research. Altogether, the work initiated during Expedition 393 will allow postexpedition work to analyze changes in microbial community abundance, composition, function, and activity from the seafloor to the deepest basement sampled.

Knowledge of the microbial communities active in both sediment and basalt environments will be supplemented by geochemical measurements of sediment pore water and other parameters such as heat flow at all sites. These measurements reveal information on diagenetic reactions, elemental diffusion, and the flow of fluids along the sediment/basement interface.

11.4. Objective 3. Investigate the responses of Atlantic Ocean circulation patterns and the Earth's climate system to rapid climate change, including elevated atmospheric CO$_2$ during the Cenozoic.

The recovery of nannofossil oozes with varying amounts of clay at Sites U1558, U1560, and U1583 indicate shoaling and deepening of CCD at these sites from the Oligocene through the Holocene (Figure **F49**). Planktic foraminifera and calcareous nannoplankton are poorly preserved in clay-rich intervals, but the abundant, well-preserved microfossils in carbonate intervals supported the construction of robust age models in combination with magnetostratigraphic reversals for all Expedition 393 sites (U1558, U1560, and U1583; Figure **F49**). Carbonate dissolution is indicated by high pore water Ca/Mg relative to seawater in the deepwater Holes U1558A, U1558F, U1560A, U1560C, U1583C, and U1583E.

Together with Expedition 390, we recovered almost the entire Cenozoic across the SAT. Expedition 393 had excellent recovery of the Oligocene, Miocene, and Pliocene. Based on biostratigraphic and paleomagnetic events, we interpreted a ~6 My hiatus at Site U1583 and two hiatuses at Site U1558 (~18 My at the top and ~7 My before the accumulation of the lowermost sediments), suggesting changes in bottom water masses that resulted in dissolution, low sedimentation rates, and potentially erosion. Despite these hiatuses, the sedimentologic records can be correlated well with sediments of Paleocene and Eocene age recovered during Expedition 390. High-resolution biostratigraphic and isotope studies postexpedition will help to refine age models and calculations for mass accumulation rates, carbonate accumulation rates, and organic carbon accumulation rates that will allow us to answer questions surrounding ocean productivity and circulation through the Cenozoic.

11.5. Operational considerations

The SAT objectives were ambitious but mostly achieved because of the preliminary engineering operations undertaken during Expeditions 390C and 395E, new developments in drilling capabili-

ties, and the ingenuity of the *JOIDES Resolution* crew, Texas A&M University (USA) team, and the Expedition 390/393 science parties. The majority of Expedition 393 operations were successful. More than 600 m of sediments and ~570 m of volcanic rocks were drilled at Sites U1559, U1558, U1583, and U1560 during Expedition 393. Although basement coring at the 7 Ma Site U1559 was challenging and this hole was deepened only ~43 m into basalts, penetrations >130 m were achieved at Sites U1558, U1583, and U1560 and these cores address critical gaps in our sampling of intact in situ ocean crust with regards to crustal age, spreading rate, and sediment thickness.

11.5.1. Casing requirements for basement legacy holes

Reentry cones with casing installed at five of the six primary SAT sites in advance of Expeditions 390 and 393 greatly expedited basement drilling. Most of the basement drilling during Expedition 393 was in holes with reentry cones and casing strings to near the sediment/basement interface. Only the newly occupied Site U1583 did not have legacy infrastructure preinstalled. Unforeseen operational challenges in Hole U1583E resulting in significant time loss precluded the installation of a reentry cone and casing system in the basement of Hole U1583F. Instead, only a free-fall funnel was deployed (the Dick Kroon cone) to allow the RCB bit to be dropped on the seafloor and the hole reentered for wireline logging. The absence of casing in Hole U1583F caused difficulties drilling with abundant fill accumulating at the bottom of the hole between each wireline core run because of the washing out of both sediment and basement cavities and the incomplete removal of these clastic materials from the hole even with large and regular mud-sweeps. Cavities near the sediment/basement interface and within the basement, together with high heave conditions, also complicated our wireline logging operations, leading to incomplete logs and serious damage to one of the FMS tools.

These experiences emphasize the need for reentry systems with casing installed into basement for legacy holes. However, it should be noted that to install casing into basement the hole either needs to be fully drilled out beforehand or a HRT reentry system must be used, which does not allow
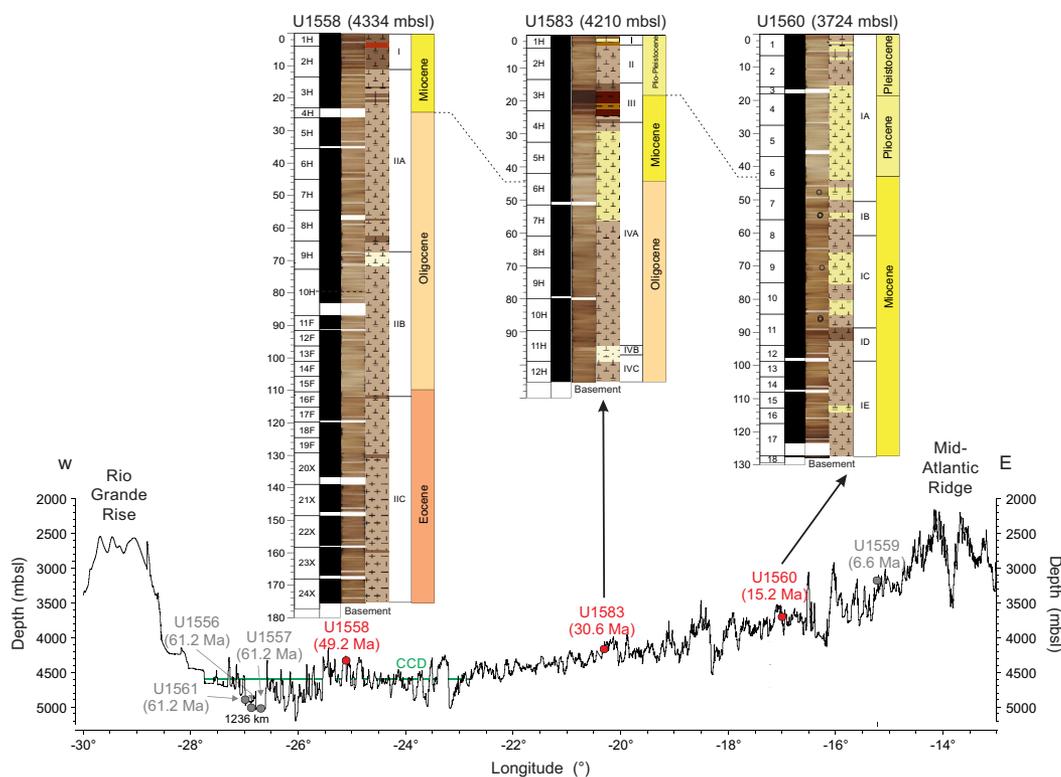

Figure F49. Bathymetric cross section of western flank of southern Mid-Atlantic Ridge at 31°S showing location of sediment coring during Expedition 393 (red) that completes SAT operations initiated during Expeditions 390C, 395E, and 390 (gray). CCD = modern-day CCD.

extension of casing after the initial installation. The preliminary engineering expeditions discovered that the Dril-Quip reentry systems cannot be installed into basement in a single step; when the casing is in basement, weight cannot be removed from the drill string to allow the Dril-Quip release mechanism to operate. This finding from the SAT expeditions will aid planning of future expeditions that are considering such installations.

With the enviable clarity of 20:20 hindsight and knowledge that this phase of the SAT campaign would eventually involve two engineering plus two science expeditions, had the SAT team known that it would have such a generous investment of operational time, SAT operations could have been better optimized. More time could have been dedicated to installing reentry systems cemented into basement, rather than just above basement. Such basement-anchored reentry systems would have improved hole conditions and cleaning, drilling, and wireline logging operations and provided superior legacy sites for future deepening.

11.5.2. TransCo C-4 and C-7 drill bits

Expedition 390 showed that TransCo C-4 RCB drill bits are more durable than drill bits from previous suppliers, and a single C-4 RCB drill bit operated with minimal damage for 65.4 rotational hours to deepen Hole U1558D more than 220 m into basement with reasonable recovery (~46%). Such durability saved a pipe trip and bit change, freeing up time for other operations. However, the C-4 RCB drill bit did not perform well when drilling Hole U1559B into relatively young 6.6 Ma ocean crust on the eastern end of the transect. Basement drilling operations at Site U1559 were slow (<0.5 m/h) with recovery decreasing to 9% and returning undergauge core that showed "elephant-foot" flares on the bottom of some cored pieces. On its return to the ship, the C-4 RCB bit was catastrophically damaged in ways also endured during recent operations drilling young basalts during Expedition 395C in Holes U1562B and U1554F. For future drilling operations in young, less altered ocean crust, a C-7 RCB drill bit should be more suitable than C-4 drill bits in these challenging formations. Any return to deepen Hole U1559B should start with a short-duration C-7 RCB bit run. Sites such as Site U1559 with only thin sediment cover (<<100 m) would benefit from shorter, denser drill collars and bottom-hole assemblages to provide more substantial weight on bit to facilitate making the hole. The TransCo C-7 drill bits used in Holes U1560B and U1583F achieved between 1.8 and 2.8 m of ocean crust penetration per hour on the drill bit, which is just less than the 3.0 m per hour achieved in the deep Hole U1556B during Expedition 390. These TransCo C-7 bits also showed admirable durability (Hole U1583F ~73 hours) that resulted in fewer bit changes and increased science operations.

11.5.3. XCB PDC cutting shoe and APC/XCB PDC bit

As observed during previous SAT expeditions, the XCB PDC cutting shoe provided good recovery of the sediments and basalts during Expedition 393, although a continuous well-preserved sediment/basalt boundary was not recovered at any site during Expedition 393. In addition, an APC/XCB PDC bit allowed us to adapt the operations plan for Site U1560 in response to weather conditions without losing time. Wireline logging was performed in Hole U1560B through the APC/XCB PDC bit, followed by APC/XCB coring of sediments and the critical sediment/basement interface in Hole U1560C without an extra pipe trip.

References

Alt, J.C., 2004. Alteration of the upper oceanic crust: mineralogy, chemistry, and processes. In Davis, E., and Elderfield, H. (Eds.), Hydrogeology of the Oceanic Lithosphere. Cambridge, England (Cambridge University Press), 456–488.

Alt, J.C., Honnorez, J., Laverne, C., and Emmermann, R., 1986. Hydrothermal alteration of a 1 km section through the upper oceanic crust, Deep Sea Drilling Project Hole 504B: mineralogy, chemistry and evolution of seawater-basalt interactions. Journal of Geophysical Research: Solid Earth, 91(B10):10309–10335. https://doi.org/10.1029/JB091iB10p10309

Alt, J.C., and Teagle, D.A.H., 1999. The uptake of carbon during alteration of ocean crust. Geochimica et Cosmochimica Acta, 63(10):1527–1535. https://doi.org/10.1016/S0016-7037(99)00123-4

Alt, J.C., Teagle, D.A.H., Laverne, C., Vanko, D.A., Bach, W., Honnorez, J., Becker, K., Ayadi, M., and Pezard, P.A., 1996. Ridge flank alteration of upper ocean crust in the eastern Pacific: synthesis of results for volcanic rocks of holes 504B and 896A. In Alt, J.C., Kinoshita, H., Stokking, L.B., and Michael, P.J. (Eds.), Proceedings of the Ocean Drilling Program, Scientific Results. 148: College Station, TX (Ocean Drilling Program), 435–450. https://doi.org/10.2973/odp.proc.sr.148.150.1996

Amante, C., and Eakins, B.W., 2009. ETOPO1 1 arc-minute global relief model: procedures, data sources and analysis. NOAA Technical Memorandum NES-DIS NGDC-24. **https://doi.org/10.7289/V5C8276M**

Andrén, T., Jørgensen, B.B., Cotterill, C., Green, S., Andrén, E., Ash, J., Bauersachs, T., Cragg, B., Fanget, A.-S., Fehr, A., Granoszewski, W., Groeneveld, J., Hardisty, D., Herrero-Bervera, E., Hyttinen, O., Jensen, J.B., Johnson, S., Kenzler, M., Kotilainen, A., Kotthoff, U., Marshall, I.P.G., Martin, E., Obrochta, S., Passchier, S., Quintana Krupinski, N., Riedinger, N., Slomp, C., Snowball, I., Stepanova, A., Strano, S., Torti, A., Warnock, J., Xiao, N., and Zhang, R., 2015. Expedition 347 summary. In Andrén, T., Jørgensen, B.B., Cotterill, C., Green, S., and the Expedition 347 Scientists, Proceedings of the Integrated Ocean Drilling Program. 347: College Station, TX (Integrated Ocean Drilling Program). **https://doi.org/10.2204/iodp.proc.347.101.2015**

Antonelli, M.A., Pester, N.J., Brown, S.T., and DePaolo, D.J., 2017. Effect of paleoseawater composition on hydrothermal exchange in midocean ridges. Proceedings of the National Academy of Sciences of the United States of America, 114(47):12413–12418. **https://doi.org/10.1073/pnas.1709145114**

Bach, W., and Edwards, K.J., 2003. Iron and sulfide oxidation within the basaltic ocean crust; implications for chemolithoautotrophic microbial biomass production. Geochimica et Cosmochimica Acta, 67(20):3871–3887. **https://doi.org/10.1016/S0016-7037(03)00304-1**

Barker, P.F., and Thomas, E., 2004. Origin, signature and palaeoclimatic influence of the Antarctic Circumpolar Current. Earth-Science Reviews, 66(1–2):143–162. **https://doi.org/10.1016/j.earscirev.2003.10.003**

Barrera, E., Savin, S.M., Thomas, E., and Jones, C.E., 1997. Evidence for thermohaline-circulation reversals controlled by sea-level change in the latest Cretaceous. Geology, 25(8):715–718. **https://doi.org/10.1130/0091-7613(1997)025<0715:EFTCRC>2.3.CO;2**

Batiza, R., Fox, P.J., Vogt, P.R., Cande, S.C., Grindlay, N.R., Melson, W.G., and O'Hearn, T., 1989. Morphology, abundance, and chemistry of near-ridge seamounts in the vicinity of the Mid-Atlantic Ridge ~26°S. The Journal of Geology, 97(2):209–220. **http://www.jstor.org/stable/30065540**

Beaulieu, S.E., Baker, E.T., and German, C.R., 2015. Where are the undiscovered hydrothermal vents on oceanic spreading ridges? Deep Sea Research, Part II: Topical Studies in Oceanography, 121:202–212. **https://doi.org/10.1016/j.dsr2.2015.05.001**

Becker, K., Fisher, A.T., and Tsuji, T., 2013. New packer experiments and borehole logs in upper oceanic crust: evidence for ridge-parallel consistency in crustal hydrogeological properties. Geochemistry, Geophysics, Geosystems, 14(8):2900–2915. **https://doi.org/10.1002/ggge.20201**

Berner, R.A., Lasaga, A.C., and Garrels, R.M., 1983. The carbonate-silicate geochemical cycle and its effect on atmospheric carbon dioxide over the past 100 million years. American Journal of Science, 283(7):641–683. **https://doi.org/10.2475/ajs.283.7.641**

Billups, K., 2002. Late Miocene through early Pliocene deep water circulation and climate change viewed from the subAntarctic South Atlantic. Palaeogeography, Palaeoclimatology, Palaeoecology, 185(3–4):287–307. **https://doi.org/10.1016/S0031-0182(02)00340-1**

Bohaty, S.M., Zachos, J.C., Florindo, F., and Delaney, M.L., 2009. Coupled greenhouse warming and deep-sea acidification in the middle Eocene. Paleoceanography and Paleoclimatology, 24(2):PA2207. **https://doi.org/10.1029/2008PA001676**

Borrelli, C., Cramer, B.S., and Katz, M.E., 2014. Bipolar Atlantic deepwater circulation in the middle-late Eocene: effects of Southern Ocean gateway openings. Paleoceanography and Paleoclimatology, 29(4):308–327. **https://doi.org/10.1002/2012PA002444**

Broecker, W.S., 1991. The great ocean conveyor. Oceanography, 4(2):79–89. **http://www.jstor.org/stable/43924572**

Bullard, E., Everett, J.E., Gilbert Smith, A., Blackett, P.M.S., Bullard, E., and Runcorn, S.K., 1965. The fit of the continents around the Atlantic. Philosophical Transactions of the Royal Society of London A, Mathematical and Physical Sciences, 258(1088):41–51. **https://doi.org/10.1098/rsta.1965.0020**

Cande, S.C., LaBrecque, J.L., and Haxby, W.F., 1988. Plate kinematics of the South Atlantic: Chron C34 to present. Journal of Geophysical Research: Solid Earth, 93(B11):13479–13492. **https://doi.org/10.1029/JB093iB11p13479**

Christeson, G., and Reece, R., 2020. Bathymetric site survey gridded data in support of IODP Expeditions 390 and 393, South Atlantic Transect (MGL1601, CREST). Interdisciplinary Earth Data Alliance (IEDA). **https://doi.org/10.26022/IEDA/327528**

Christeson, G.L., Reece, R.S., Kardell, D.A., Estep, J.D., Fedotova, A., and Goff, J.A., 2020. South Atlantic transect: variations in oceanic crustal structure at 31°S. Geochemistry, Geophysics, Geosystems, 21(7):e2020GC009017. **https://doi.org/10.1029/2020GC009017**

Coggon, R.M., Christeson, G.L., Sylvan, J.B., Teagle, D.A.H., Estes, E., Williams, T., and Alvarez Zarikian, C.A., 2020. Expedition 390/393 Scientific Prospectus: The South Atlantic Transect. International Ocean Discovery Program. **https://doi.org/10.14379/iodp.sp.390393.2020**

Coggon, R.M., Sylvan, J.B., Teagle, D.A.H., Reece J., Christeson, G.L., Estes, E.R., Williams, T.J., and the Expedition 390 Scientists, 2022a. Expedition 390 Preliminary Report: South Atlantic Transect 1. International Ocean Discovery Program. **https://doi.org/10.14379/iodp.pr.390.2022**

Coggon, R.M., Sylvan, J.B., Teagle, D.A.H., Reece, J.S., Christeson, G.L., Estes, E.R., and Williams, T., 2022b. Expedition 390/393 Scientific Prospectus Addendum: South Atlantic Transect. International Ocean Discovery Program. **https://doi.org/10.14379/iodp.sp.390393add.2022**

Coggon, R.M., and Teagle, D.A.H., 2011. Hydrothermal calcium-carbonate veins reveal past ocean chemistry. TrAC Trends in Analytical Chemistry, 30(8):1252–1268. **https://doi.org/10.1016/j.trac.2011.02.011**

Coggon, R.M., Teagle, D.A.H., Cooper, M.J., and Vanko, D.A., 2004. Linking basement carbonate vein compositions to porewater geochemistry across the eastern flank of the Juan de Fuca Ridge, ODP Leg 168. Earth and Planetary Science Letters, 219(1–2):111–128. **https://doi.org/10.1016/S0012-821X(03)00697-6**

Coggon, R.M., Teagle, D.A.H., Smith-Duque, C.E., Alt, J.C., and Cooper, M.J., 2010. Reconstructing past seawater Mg/Ca and Sr/Ca from mid-ocean ridge flank calcium carbonate veins. Science, 327(5969):1114–1117. **https://doi.org/10.1126/science.1182252**

Coogan, L.A., Parrish, R.R., and Roberts, N.M.W., 2016. Early hydrothermal carbon uptake by the upper oceanic crust: insight from in situ U-Pb dating. Geology, 44(2):147–150. **https://doi.org/10.1130/G37212.1**

Cramer, B.S., Toggweiler, J.R., Wright, J.D., Katz, M.E., and Miller, K.G., 2009. Ocean overturning since the Late Cretaceous: inferences from a new benthic foraminiferal isotope compilation. Paleoceanography and Paleoclimatology, 24(4):PA4216. **https://doi.org/10.1029/2008PA001683**

Davis, A.C., Bickle, M.J., and Teagle, D.A.H., 2003. Imbalance in the oceanic strontium budget. Earth and Planetary Science Letters, 211(1–2):173–187. **https://doi.org/10.1016/S0012-821X(03)00191-2**

Devey, C., 2014. SoMARTherm: the Mid-Atlantic Ridge 13–33°S – Cruise No. MSM25 – January 24–March 5, 2013 – Cape Town (South Africa) – Mindelo (Cape Verde). MARIA S. MERIAN-Berichte, MSM25(80). **https://doi.org/10.2312/cr_msm25**

D'Hondt, S., Inagaki, F., Alvarez Zarikian, C., Abrams, L.J., Dubois, N., Engelhardt, T., Evans, H., Ferdelman, T., Gribsholt, B., Harris, R.N., Hoppie, B.W., Hyun, J.-H., Kallmeyer, J., Kim, J., Lynch, J.E., McKinley, C.C., Mitsunobu, S., Morono, Y., Murray, R.W., Pockalny, R., Sauvage, J., Shimono, T., Shiraishi, F., Smith, D.C., Smith-Duque, C.E., Spivack, A.J., Steinsbu, B.O., Suzuki, Y., Szpak, M., Toffin, L., Uramoto, G., Yamaguchi, Y.T., Zhang, G.-l., Zhang, X.-H., and Ziebis, W., 2015. Presence of oxygen and aerobic communities from sea floor to basement in deep-sea sediments. Nature Geoscience, 8(4):299–304. **https://doi.org/10.1038/NGEO2387**

D'Hondt, S., Pockalny, R., Fulfer, V.M., and Spivack, A.J., 2019. Subseafloor life and its biogeochemical impacts. Nature Communications, 10(1):3519. **https://doi.org/10.1038/s41467-019-11450-z**

Dickens, G.R., Castillo, M.M., and Walker, J.C.G., 1997. A blast of gas in the latest Paleocene: simulating first-order effects of massive dissociation of oceanic methane hydrate. Geology, 25(3):259–262. **https://doi.org/10.1130/0091-7613(1997)025%3C0259:ABOGIT%3E2.3.CO;2**

Engelen, B., Ziegelmüller, K., Wolf, L., Köpke, B., Gittel, A., Cypionka, H., Treude, T., Nakagawa, S., Inagaki, F., Lever, M.A., and Steinsbu, B.O., 2008. Fluids from the oceanic crust support microbial activities within the deep biosphere. Geomicrobiology Journal, 25(1):56–66. **https://doi.org/10.1080/01490450701829006**

Estep, J., Reece, B., Christeson, G.L., Kardell, D.A., and Carlson, R.L., 2021. 70 million years of seafloor spreading and magmatism in the South Atlantic. Earth and Planetary Science Letters, 574:117173. **https://doi.org/10.1016/j.epsl.2021.117173**

Estep, J., Reece, R., Kardell, D.A., Christeson, G.L., and Carlson, R.L., 2019. Seismic Layer 2A: evolution and thickness from 0- to 70-Ma crust in the slow-intermediate spreading South Atlantic. Journal of Geophysical Research: Solid Earth, 124(8):7633–7651. **https://doi.org/10.1029/2019JB017302**

Estep, J., Reece, R., Kardell, D.A., Perez, N.D., Christeson, G.L., and Carlson, R.L., 2020. Intraplate deformation of oceanic crust near the Rio Grande Rise in the South Atlantic. Tectonophysics, 790:228543. **https://doi.org/10.1016/j.tecto.2020.228543**

Estes, E.R., Williams, T., Midgley, S., Coggon, R.M., Sylvan, J.B.,Christeson, G.L., Teagle, D.A.H., and the Expedition 390C Scientists, 2021. Expedition 390C Preliminary Report: South Atlantic Transect Reentry Systems. International Ocean Discovery Program. **https://doi.org/10.14379/iodp.pr.390C.2021**

Expedition 301 Scientists, 2005. Expedition 301 summary. In Fisher, A.T., Urabe, T., Klaus, A., and the Expedition 301 Scientists, Proceedings of the Integrated Ocean Drilling Program. 301: College Station, TX (Integrated Ocean Drilling Program Management International, Inc.). **https://doi.org/10.2204/iodp.proc.301.101.2005**

Expedition 308 Scientists, 2006. Expedition 308 summary. In Flemings, P.B., Behrmann, J.H., John, C.M., and the Expedition 308 Scientists, Proceedings of the Integrated Ocean Drilling Program. 308: College Station, TX (Integrated Ocean Drilling Program Management International, Inc.). **https://doi.org/10.2204/iodp.proc.308.101.2006**

Expedition 309/312 Scientists, 2006. Expedition 309/312 summary. In Teagle, D.A.H., Alt, J.C., Umino, S., Miyashita, S., Banerjee, N.R., Wilson, D.S., and the Expedition 309/312 Scientists, Proceedings of the Integrated Ocean Drilling Program. 309/312: Washington, DC (Integrated Ocean Drilling Program Management International, Inc.). **https://doi.org/10.2204/iodp.proc.309312.101.2006**

Expedition 313 Scientists, 2010. Expedition 313 summary. In Mountain, G., Proust, J.-N., McInroy, D., Cotterill, C., and the Expedition 313 Scientists, Proceedings of the Integrated Ocean Drilling Program. 313: Tokyo (Integrated Ocean Drilling Program Management International, Inc.). **https://doi.org/10.2204/iodp.proc.313.101.2010**

Expedition 325 Scientists, 2011. Expedition 325 summary. In Webster, J.M., Yokoyama, Y., Cotterill, C., and the Expedition 325 Scientists, Proceedings of the Integrated Ocean Drilling Program. 325: Tokyo (Integrated Ocean Drilling Program Management International, Inc.). **https://doi.org/10.2204/iodp.proc.325.101.2011**

Expedition 327 Scientists, 2011. Expedition 327 summary. In Fisher, A.T., Tsuji, T., Petronotis, K., and the Expedition 327 Scientists, Proceedings of the Integrated Ocean Drilling Program. 327: Tokyo (Integrated Ocean Drilling Program Management International, Inc.). **https://doi.org/10.2204/iodp.proc.327.101.2011**

Expedition 329 Scientists, 2011. Expedition 329 summary. In D'Hondt, S., Inagaki, F., Alvarez Zarikian, C.A., and the Expedition 329 Scientists, Proceedings of the Integrated Ocean Drilling Program. 329: Tokyo (Integrated Ocean Drilling Program Management International, Inc.). **https://doi.org/10.2204/iodp.proc.329.101.2011**

Expedition 330 Scientists, 2012. Expedition 330 summary. In Koppers, A.A.P., Yamazaki, T., Geldmacher, J., and the Expedition 330 Scientists, Proceedings of the Integrated Ocean Drilling Program. 330: Tokyo (Integrated Ocean Drilling Program Management International, Inc.). **https://doi.org/10.2204/iodp.proc.330.101.2012**

Expedition 335 Scientists, 2012. Expedition 335 summary. In Teagle, D.A.H., Ildefonse, B., Blum, P., and the Expedition 335 Scientists, Proceedings of the Integrated Ocean Drilling Program. 335: Tokyo (Integrated Ocean Drilling Program Management International, Inc.). **https://doi.org/10.2204/iodp.proc.335.101.2012**

Expedition 336 Scientists, 2012. Expedition 336 summary. In Edwards, K.J., Bach, W, Klaus, A., and the Expedition 336 Scientists, Proceedings of the Integrated Ocean Drilling Program. 336: Tokyo (Integrated Ocean Drilling Program Management International, Inc.). **https://doi.org/10.2204/iodp.proc.336.101.2012**

Fisher, A.T., and Harris, R.N., 2010. Using seafloor heat flow as a tracer to map subseafloor fluid flow in the ocean crust. Geofluids, 10(1–2):142–160. **https://doi.org/10.1111/j.1468-8123.2009.00274.x**

Frank, T.D., and Arthur, M.A., 1999. Tectonic forcings of Maastrichtian ocean-climate evolution. Paleoceanography and Paleoclimatology, 14(2):103–117. **https://doi.org/10.1029/1998PA900017**

Fryer, P., Wheat, C.G., Williams, T., Albers, E., Bekins, B., Debret, B.P.R., Jianghong, D., Yanhui, D., Eickenbusch, P., Frery, E.A., Ichiyama, Y., Johnson, K., Johnston, R.M., Kevorkian, R.T., Kurz, W., Magalhaes, V., Mantovanelli, S.S., Menapace, W., Menzies, C.D., Michibayashi, K., Moyer, C.L., Mullane, K.K., Park, J.-W., Price, R.E., Ryan, J.G., Shervais, J.W., Sissmann, O.J., Suzuki, S., Takai, K., Walter, B., and Rui, Z., 2018. Expedition 366 summary. In Fryer, P., Wheat, C.G., Williams, T., and the Expedition 366 Scientists, Mariana Convergent Margin and South Chamorro Seamount. Proceedings of the International Ocean Discovery Program, 366: College Station, TX (International Ocean Discovery Program). **https://doi.org/10.14379/iodp.proc.366.101.2018**

Fuchs, S., Norden, B., and the International Heat Flow Commission, 2021. The Global Heat Flow Database. GFZ Data Services. **https://doi.org/10.5880/fidgeo.2021.014**

Gillis, K.M., and Coogan, L.A., 2011. Secular variation in carbon uptake into the ocean crust. Earth and Planetary Science Letters, 302(3–4):385–392. **https://doi.org/10.1016/j.epsl.2010.12.030**

Goldberg, D.S., Takahashi, T., and Slagle, A.L., 2008. Carbon dioxide sequestration in deep-sea basalt. Proceedings of the National Academy of Sciences of the United States of America, 105(29):9920–9925. **https://doi.org/10.1073/pnas.0804397105**

Gradstein, F.M., Ogg, J.G., Schmitz, M.D., and Ogg, G.M. (Eds.), 2020. The Geologic Time Scale 2020: Amsterdam (Elsevier BV). **https://doi.org/10.1016/C2020-1-02369-3**

Harris, M., Coggon, R.M., Smith-Duque, C.E., Cooper, M.J., Milton, J.A., and Teagle, D.A.H., 2015. Channelling of hydrothermal fluids during the accretion and evolution of the upper oceanic crust: Sr isotope evidence from ODP Hole 1256D. Earth and Planetary Science Letters, 416:56–66. **https://doi.org/10.1016/j.epsl.2015.01.042**

Harris, M., Coggon, R.M., Teagle, D.A.H., Roberts, N.M.W., and Parrish, R.R., 2014. Laser ablation MC-ICP-MS U/Pb geochronology of ocean basement calcium carbonate veins. Presented at the 2014 American Geophysical Union Fall Meeting, San Francisco, CA, 15–19 December 2014. **https://agu.confex.com/agu/fm14/meetingapp.cgi/Paper/12488**

Homrighausen, S., Hoernle, K., Hauff, F., Wartho, J.A., van den Bogaard, P., and Garbe-Schönberg, D., 2019. New age and geochemical data from the Walvis Ridge: the temporal and spatial diversity of South Atlantic intraplate volcanism and its possible origin. Geochimica et Cosmochimica Acta, 245:16–34. **https://doi.org/10.1016/j.gca.2018.09.002**

Homrighausen, S., Hoernle, K., Zhou, H., Geldmacher, J., Wartho, J.-A., Hauff, F., Werner, R., Jung, S., and Morgan, J.P., 2020. Paired EMI-HIMU hotspots in the South Atlantic—starting plume heads trigger compositionally distinct secondary plumes? Science Advances, 6(28):eaba0282. **https://doi.org/10.1126/sciadv.aba0282**

Houtz, R., and Ewing, J., 1976. Upper crustal structure as a function of plate age. Journal of Geophysical Research, 81(14):2490–2498. **https://doi.org/10.1029/JB081i014p02490**

Hoyer, P.A., Haase, K.M., Regelous, M., O'Connor, J.M., Homrighausen, S., Geissler, W.H., and Jokat, W., 2022. Mantle plume and rift-related volcanism during the evolution of the Rio Grande Rise. Communications Earth & Environment, 3(1):18. **https://doi.org/10.1038/s43247-022-00349-1**

Hutnak, M., Fisher, A.T., Harris, R., Stein, C., Wang, K., Spinelli, G., Schindler, M., Villinger, H., and Silver, E., 2008. Large heat and fluid fluxes driven through mid-plate outcrops on ocean crust. Nature Geoscience, 1(9):611-614. **https://doi.org/10.1038/ngeo264**

Hutnak, M., Fisher, A.T., Zühlsdorff, L., Spiess, V., Stauffer, P.H., and Gable, C.W., 2006. Hydrothermal recharge and discharge guided by basement outcrops on 0.7-3.6 Ma seafloor east of the Juan de Fuca Ridge: observation and numerical models. Geochemistry, Geophysics, Geosystems, 7(7):Q07O02. **https://doi.org/10.1029/2006GC001242**

Inagaki, F., Nunoura, T., Nakagawa, S., Teske, A., Lever, M., Lauer, A., Suzuki, M., Takai, K., Delwiche, M., Colwell, F.S., Nealson, K.H., Horikoshi, K., D'Hondt, S., and Jørgensen, B.B., 2006. Biogeographical distribution and diversity of microbes in methane hydrate-bearing deep marine sediments on the Pacific Ocean margin. Proceedings of the National Academy of Sciences of the United States of America, 103(8):2815–2820. **https://doi.org/10.1073/pnas.0511033103**

Inagaki, F., and Orphan, V., 2014. Exploration of subseafloor life and the biosphere through IODP (2003–2013). In Stein, R., Blackman, D.K., Inagaki, F., and Larsen, H.-C. (Eds.), A Decade of Science Achieved by the Integrated Ocean Drilling Program (IODP). Developments in Marine Geology. R. Stein (Series Ed.), 7: 39–63. **https://doi.org/10.1016/B978-0-444-62617-2.00002-5**

Jungbluth, S.P., Grote, J., Lin, H.-T., Cowen, J.P., and Rappé, M.S., 2013. Microbial diversity within basement fluids of the sediment-buried Juan de Fuca Ridge flank. The ISME Journal, 7(1):161–172. **https://doi.org/10.1038/ismej.2012.73**

Kallmeyer, J., Pockalny, R., Adhikari, R.R., Smith, D.C., and D'Hondt, S., 2012. Global distribution of microbial abundance and biomass in subseafloor sediment. Proceedings of the National Academy of Sciences of the United States of America, 109(40):16213–16216. **https://doi.org/10.1073/pnas.1203849109**

Kardell, D.A., Christeson, G.L., Estep, J.D., Reece, R.S., and Carlson, R.L., 2019. Long-lasting evolution of Layer 2A in the western South Atlantic: evidence for low-temperature hydrothermal circulation in old oceanic crust. Journal of Geophysical Research: Solid Earth, 124(3):2252–2273. **https://doi.org/10.1029/2018JB016925**

Kardell, D.A., Zhao, Z., Ramos, E.J., Estep, J., Christeson, G.L., Reece, R.S., and Hesse, M.A., 2021. Hydrothermal models constrained by fine-scale seismic velocities confirm hydrothermal cooling of 7–63 Ma South Atlantic crust. Journal of Geophysical Research: Solid Earth, 126(6):e2020JB021612. **https://doi.org/10.1029/2020JB021612**

Katz, M.E., Cramer, B.S., Toggweiler, J.R., Esmay, G., Liu, C., Miller, K.G., Rosenthal, Y., Wade, B.S., and Wright, J.D., 2011. Impact of Antarctic Circumpolar Current development on late Paleogene ocean structure. Science, 332(6033):1076–1079. **https://doi.org/10.1126/science.1202122**

Kennett, J.P., and Stott, L.D., 1990. Proteus and proto-oceanus: ancestral Paleogene oceans as revealed from Antarctic stable isotopic results; ODP Leg 113. In Barker, P.F., Kennett, J. P., et al., Proceedings of the Ocean Drilling Program, Scientific Results. 113: College Station, TX (Ocean Drilling Program), 865–880. **https://doi.org/10.2973/odp.proc.sr.113.188.1990**

Kennett, J.P., and Stott, L.D., 1991. Abrupt deep-sea warming, palaeoceanographic changes and benthic extinctions at the end of the Palaeocene. Nature, 353(6341):225–229. **https://doi.org/10.1038/353225a0**

Koppers, A., and Coggon, R. (Eds.), 2020. Exploring Earth by Scientific Ocean Drilling: 2050 Science Framework: San Diego, CA (UC San Diego Library). **https://doi.org/10.6075/J0W66J9H**

Korenaga, T., and Korenaga, J., 2008. Subsidence of normal oceanic lithosphere, apparent thermal expansivity, and seafloor flattening. Earth and Planetary Science Letters, 268(1):41–51. **https://doi.org/10.1016/j.epsl.2007.12.022**

Langseth, M.G., Cann, J.R., Natland, J.H., and Hobart, M., 1983. Geothermal phenomena at the Costa Rica Rift; background and objectives for drilling at Deep Sea Drilling Project Sites 501, 504, and 505. In Cann, J.R., Langseth, M. G., Honnorez, J., Von Herzen, R. P., White, S. M., et al.. Initial Reports of the Deep Sea Drilling Project. 69: Washington, DC (US Government Printing Office), 5–29. **https://doi.org/10.2973/dsdp.proc.69.101.1983**

Langseth, M.G., Mottl, M.J., Hobart, M.A., and Fisher, A., 1988. The distribution of geothermal and geochemical gradients near site 501/504: implications for hydrothermal circulation in the oceanic crust. In Becker, K., Sakai, H., et al., Proceedings of the Ocean Drilling Program, Initial Reports (Part A). 111: College Station, TX (Ocean Drilling Program), 23–32. **https://doi.org/10.2973/odp.proc.ir.111.102.1988**

Lawver, L.A., and Gahagan, L.M., 2003. Evolution of Cenozoic seaways in the circum-Antarctic region. Palaeogeography, Palaeoclimatology, Palaeoecology, 198(1):11–37. **https://doi.org/10.1016/S0031-0182(03)00392-4**

Lee, M.D., Walworth, N.G., Sylvan, J.B., Edwards, K.J., and Orcutt, B.N., 2015. Microbial communities on seafloor basalts at Dorado Outcrop reflect level of alteration and highlight global lithic clades. Frontiers in Microbiology, 6:1470. **https://doi.org/10.3389/fmicb.2015.01470**

Lever, M.A., Rogers, K.L., Lloyd, K.G., Overmann, J., Schink, B., Thauer, R.K., Hoehler, T.M., and Jørgensen, B.B., 2015. Life under extreme energy limitation: a synthesis of laboratory- and field-based investigations. FEMS Microbiology Ecology, 39(5):688–728. **https://doi.org/10.1093/femsre/fuv020**

Lever, M.A., Rouxel, Olivier, Alt, Jeffrey C., Shimizu, Nobumichi, Ono, Shuhei, Coggon, Rosalind M., Shanks, Wayne C., III, Lapham, Laura, Elvert, Marcus, Prieto-Mollar, Xavier, Hinrichs, Kaiwe-Uwe, Inagaki, Fumio, and Teske, Andreas, 2013. Evidence for microbial carbon and sulfur cycling in deeply buried ridge flank basalt. Science, 339(6125):1305–1308. **https://doi.org/10.1126/science.1229240**

Lister, C.R.B., 1972. On the thermal balance of a mid-ocean ridge. Geophysical Journal International, 26(5):515–535. **https://doi.org/10.1111/j.1365-246X.1972.tb05766.x**

Lomstein, B.A., Langerhuus, A.T., D'Hondt, S., Jørgensen, B.B., and Spivack, A.J., 2012. Endospore abundance, microbial growth and necromass turnover in deep sub-seafloor sediment. Nature, 484(7392):101–104. **https://doi.org/10.1038/nature10905**

Mallows, C., and Searle, R.C., 2012. A geophysical study of oceanic core complexes and surrounding terrain, Mid-Atlantic Ridge 13°N–14°N. Geochemistry, Geophysics, Geosystems, 13(6):Q0AG08. **https://doi.org/10.1029/2012GC004075**

Marieni, C., Henstock, T.J., and Teagle, D.A.H., 2013. Geological storage of CO_2 within the oceanic crust by gravitational trapping. Geophysical Research Letters, 40(23):6219–6224. **https://doi.org/10.1002/2013GL058220**

Marty, J.C., and Cazenave, A., 1989. Regional variations in subsidence rate of oceanic plates: a global analysis. Earth and Planetary Science Letters, 94(3):301–315. **https://doi.org/10.1016/0012-821X(89)90148-9**

Mason, O.U., Nakagawa, T., Rosner, M., Van Nostrand, J.D., Zhou, J., Maruyama, A., Fisk, M.R., and Giovannoni, S.J., 2010. First investigation of the microbiology of the deepest layer of ocean crust. PloS One, 5(11):e15399. **https://doi.org/10.1371/journal.pone.0015399**

Matter, J.M., Stute, M., Snæbjörnsdottir, S.Ó., Oelkers, E.H., Gislason, S.R., Aradottir, E.S., Sigfusson, B., Gunnarsson, I., Sigurdardottir, H., Gunnlaugsson, E., Axelsson, H.A., Woff-Boenisch, D., Mesfin, K., de la Reguera Taaya, D.F., Hall, J., Diderikson, K., and Broecker, W.S., 2016. Rapid carbon mineralization for permanent disposal of anthropogenic carbon dioxide emissions. Science, 352(6291):1312–1314. **https://doi.org/10.1126/science.aad8132**

Maxbauer, D.P., Feinberg, J.M., and Fox, D.L., 2016. MAX UnMix: a web application for unmixing magnetic coercivity distributions. Computers & Geosciences, 95:140–145. **https://doi.org/10.1016/j.cageo.2016.07.009**

Meyer, B., Saltus, R., and Chulliat, A., 2017. EMAG2v3: Earth Magnetic Anomaly Grid (2-arc-minute resolution), Version 3. NOAA National Centers for Environmental Information. **https://doi.org/10.7289/V5H70CVX**

Michael, P.J., Forsyth, D.W., Blackman, D.K., Fox, P.J., Hanan, B.B., Harding, A.J., Macdonald, K.C., Neumann, G.A., Orcutt, J.A., Tolstoy, M., and Weiland, C.M., 1994. Mantle control of a dynamically evolving spreading center: Mid-Atlantic Ridge 31–34°S. Earth and Planetary Science Letters, 121(3–4):451–468. **https://doi.org/10.1016/0012-821X(94)90083-3**

Michibayashi, K., Tominaga, M., Ildefonse, B., and Teagle, D.A.H., 2019. What lies beneath: the formation and evolution of oceanic lithosphere. Oceanography, 32(1):138–149. **https://doi.org/10.5670/oceanog.2019.136**

Mottl, M.J., 1989. Hydrothermal convection, reaction, and diffusion in sediments on the Costa Rica Rift flank: pore-water evidence from ODP Sites 677 and 678. In Becker, K., Sakai, H., et al., Proceedings of the Ocean Drilling

Program, Scientific Results. 111: College Station, TX (Ocean Drilling Program), 195–213. **https://doi.org/10.2973/odp.proc.sr.111.125.1989**

Mottl, M.J., 2003. Partitioning of energy and mass fluxes between mid-ocean axes and flanks at high and low temperature. In Halbech, P.E., Tunnicliffe, V., and Hein, J.R. (Eds.), Energy and Mass Transfer in Marine Hydrothermal Systems: Berlin (Dahlem University Press), 271–286.

Mottl, M.J., Druffel, E.R.M., Hart, S.R., Lawrence, J.R., and Saltzman, E.S., 1985. Chemistry of hot waters sampled from basaltic basement in Hole 504B, Deep Sea Drilling Project Leg 83, Costa Rica Rift. In Anderson, R.N., Honnorez, J., Becker, K., et al., Initial Reports of the Deep Sea Drilling Project. 83: 315–318. **https://doi.org/10.2973/dsdp.proc.83.115.1985**

Mottl, M.J., and Gieskes, J.M., 1990. Chemistry of waters sampled from oceanic basement boreholes, 1979–1988. Journal of Geophysical Research: Solid Earth, 95(B6):9327–9342. **https://doi.org/10.1029/JB095iB06p09327**

Mottl, M.J., Lawrence, J.R., and Keigwin, L.D., 1983. Elemental and stable-isotope composition of pore waters and carbonate sediments from Deep Sea Drilling Project Sites 501/504 and 505. In Cann, J.R., Langseth, M.G., Honnorez, J., Von Herzen, R.P., White, S.M., et al., Initial Reports of the Deep Sea Drilling Project. 69: Washington, DC (US Government Printing Office), 461–473. **https://doi.org/10.2973/dsdp.proc.69.121.1983**

Müller, R.D., Roest, W.R., Royer, J.-Y., Gahagan, L.M., and Sclater, J.G., 1997. Digital isochrons of the world's ocean floor. Journal of Geophysical Research: Solid Earth, 102(B2):3211–3214. **https://doi.org/10.1029/96JB01781**

Müller, R.D., Sdrolias, M., Gaina, C., and Roest, W.R., 2008a. Age, spreading rates, and spreading asymmetry of the world's ocean crust. Geochemistry, Geophysics, Geosystems, 9(4):Q04006. **https://doi.org/10.1029/2007GC001743**

Müller, R.D., Sdrolias, M., Gaina, C., Steinberger, B., and Heine, C., 2008b. Long-term sea-level fluctuations driven by ocean basin dynamics. Science, 319(5868):1357–1362. **https://doi.org/10.1126/science.1151540**

Neira, N.M., Clark, J.F., Fisher, A.T., Wheat, C.G., Haymon, R.M., and Becker, K., 2016. Cross-hole tracer experiment reveals rapid fluid flow and low effective porosity in the upper oceanic crust. Earth and Planetary Science Letters, 450:355–365. **https://doi.org/10.1016/j.epsl.2016.06.048**

Norris, R.D., Wilson, P.A., Blum, P., Fehr, A., Agnini, C., Bornemann, A., Boulila, S., Bown, P.R., Cournede, C., Friedrich, O., Ghosh, A.K., Hollis, C.J., Hull, P.M., Jo, K., Junium, C.K., Kaneko, M., Liebrand, D., Lippert, P.C., Liu, Z., Matsui, H., Moriya, K., Nishi, H., Opdyke, B.N., Penman, D., Romans, B., Scher, H.D., Sexton, P., Takagi, H., Turner, S.K., Whiteside, J.H., Yamaguchi, T., and Yamamoto, Y., 2014. Expedition 342 summary. In Norris, R.D., Wilson, P.A., Blum, P., and the Expedition 342 Scientists, Proceedings of the Integrated Ocean Drilling Program. 342: College Station, TX (Integrated Ocean Drilling Program). **https://doi.org/10.2204/iodp.proc.342.101.2014**

O'Connor, J.M., and Duncan, R.A., 1990. Evolution of the Walvis Ridge-Rio Grande Rise hot spot system: implications for African and South American plate motions over plumes. Journal of Geophysical Research: Solid Earth, 95(B11):17475–17502. **https://doi.org/10.1029/JB095iB11p17475**

Olson, P., Reynolds, E., Hinnov, L., and Goswami, A., 2016. Variation of ocean sediment thickness with crustal age. Geochemistry, Geophysics, Geosystems, 17(4):1349–1369. **https://doi.org/10.1002/2015GC006143**

Orcutt, B.N., Bach, W., Becker, K., Fisher, A.T., Hentscher, M., Toner, B.M., Wheat, C.G., and Edwards, K.J., 2011. Colonization of subsurface microbial observatories deployed in young ocean crust. The ISME Journal, 5(4):692–703. **https://doi.org/10.1038/ismej.2010.157**

Orcutt, B.N., LaRowe, D.E., Lloyd, K.G., Mills, H., Orsi, W., Reese, B.K., Sauvage, J., Huber, J.A., and Amend, J., 2014. IODP Deep Biosphere Research Workshop report – a synthesis of recent investigations, and discussion of new research questions and drilling targets. Scientific Drilling, 17:61–66. **https://doi.org/10.5194/sd-17-61-2014**

Orcutt, B.N., Wheat, C.G., Rouxel, O., Hulme, S., Edwards, K.J., and Bach, W., 2013. Oxygen consumption rates in subseafloor basaltic crust derived from a reaction transport model. Nature Communications, 4:2539. **https://doi.org/10.1038/ncomms3539**

Pälike, H., Lyle, M.W., Nishi, H., Raffi, I., Ridgwell, A., Gamage, K., Klaus, A., Acton, G., Anderson, L., Backman, J., Baldauf, J., Beltran, C., Bohaty, S.M., Bown, P., Busch, W., Channell, J.E.T., Chun, C.O.J., Delaney, M., Dewangan, P., Dunkley Jones, T., Edgar, K.M., Evans, H., Fitch, P., Foster, G.L., Gussone, N., Hasegawa, H., Hathorne, E.C., Hayashi, H., Herrle, J.O., Holbourn, A., Hovan, S., Hyeong, K., Iijima, K., Ito, T., Kamikuri, S.-i., Kimoto, K., Kuroda, J., Leon-Rodriguez, L., Malinverno, A., Moore Jr, T.C., Murphy, B.H., Murphy, D.P., Nakamura, H., Ogane, K., Ohneiser, C., Richter, C., Robinson, R., Rohling, E.J., Romero, O., Sawada, K., Scher, H., Schneider, L., Sluijs, A., Takata, H., Tian, J., Tsujimoto, A., Wade, B.S., Westerhold, T., Wilkens, R., Williams, T., Wilson, P.A., Yamamoto, Y., Yamamoto, S., Yamazaki, T., and Zeebe, R.E., 2012. A Cenozoic record of the equatorial Pacific carbonate compensation depth. Nature, 488(7413):609–614. **https://doi.org/10.1038/nature11360**

Palmer, M.R., and Edmond, J.M., 1989. The strontium isotope budget of the modern ocean. Earth and Planetary Science Letters, 92(1):11–26. **https://doi.org/10.1016/0012-821X(89)90017-4**

Parsons, B., and Sclater, J.G., 1977. An analysis of the variation of ocean floor bathymetry and heat flow with age. Journal of Geophysical Research, 82(5):803–827. **https://doi.org/10.1029/JB082i005p00803**

Pearce, J.A., and Norry, M.J., 1979. Petrogenetic implications of Ti, Zr, Y, and Nb variations in volcanic rocks. Contributions to Mineralogy and Petrology, 69(1):33–47. **https://doi.org/10.1007/BF00375192**

Penrose Conference Participants, 1972. Penrose Field Conference: ophiolites. Geotimes, 17:24.

Pérez-Díaz, L., and Eagles, G., 2017a. A new high-resolution seafloor age grid for the South Atlantic. Geochemistry, Geophysics, Geosystems, 18(1):457–470. **https://doi.org/10.1002/2016GC006750**

Pérez-Díaz, L., and Eagles, G., 2017b. South Atlantic paleobathymetry since Early Cretaceous. Scientific Reports, 7(1):11819. **https://doi.org/10.1038/s41598-017-11959-7**

Perfit, M.R., and Chadwick, W.W., Jr., 1998. Magmatism at mid-ocean ridges: constraints from volcanological and geochemical investigations. In Buck, W.R., Delaney, J.A., Karson, J.A. and Lagabrielle, Y., Faulting and Magmatism at Mid-Ocean Ridges. Geophysical Monograph, 106: 59–115. **https://doi.org/10.1029/GM106p0059**

Rausch, S., Böhm, F., Bach, W., Klügel, A., and Eisenhauer, A., 2013. Calcium carbonate veins in ocean crust record a threefold increase of seawater Mg/Ca in the past 30 million years. Earth and Planetary Science Letters, 362:215–224. **https://doi.org/10.1016/j.epsl.2012.12.005**

Reece, R., Christeson, G., Amara, A., Estep, J., Greene, J., Koch, C., Henning, L., Worman, W., and Wright, A., 2016. CREST: Crustal Reflectivity Experiment southern transect South Atlantic multichannel seismic and ocean bottom seismometer experiment, 4 Jan–25 Feb 2016 Cruise Report. **http://www.iris.washington.edu/data/reports/2016/16-003/CREST_2016-01-04-2016-02-25_MGL1601_CruiseReport.pdf**

Reece, R., and Estep, J., 2019. Processed MCS (PSTM) data from the Mid-Atlantic Ridge (MAR) to the Rio Grande Rise, South Atlantic Ocean, acquired by the R/V Marcus G. Langseth in 2016 (MGL1601) **https://doi.org/10.1594/IEDA/500255**

Reese, B.K., Zinke, L.A., Sobol, M.S., LaRowe, D.E., Orcutt, B.N., Zhang, X., Jaekel, U., Wang, F., Dittmar, T., Defforey, D., Tully, B., Paytan, A., Sylvan, J.B., Amend, J.P., Edwards, K.J., and Girguis, P., 2018. Nitrogen cycling of active bacteria within oligotrophic sediment of the Mid-Atlantic Ridge flank. Geomicrobiology Journal, 35(6):468–483. **https://doi.org/10.1080/01490451.2017.1392649**

Ryan, W.B.F., Carbotte, S.M., Coplan, J.O., O'Hara, S., Melkonian, A., Arko, R., Weissel, R.A., Ferrini, V., Goodwillie, A., Nitsche, F., Bonczkowski, J., and Zemsky, R., 2009. Global multi-resolution topography synthesis. Geochemistry, Geophysics, Geosystems, 10(3):Q03014. **https://doi.org/10.1029/2008GC002332**

Sager, W.W., Thoram, S., Engfer, D.W., Koppers, A.A.P., and Class, C., 2021. Late Cretaceous Ridge reorganization, microplate formation, and the evolution of the Rio Grande Rise – Walvis Ridge hot spot twins, South Atlantic Ocean. Geochemistry, Geophysics, Geosystems, 22(3):e2020GC009390. **https://doi.org/10.1029/2020GC009390**

Santelli, C.M., Edgcomb, V.P., Bach, W., and Edwards, K.J., 2009. The diversity and abundance of bacteria inhabiting seafloor lavas positively correlate with rock alteration. Environmental Microbiology, 11(1):86–98. **https://doi.org/10.1111/j.1462-2920.2008.01743.x**

Sarmiento, J.L., Simeon, J., Gnanadesikan, A., Gruber, N., Key, R.M., and Schlitzer, R., 2007. Deep ocean biogeochemistry of silicic acid and nitrate. Global Biogeochemical Cycles, 21(1). **https://doi.org/10.1029/2006GB002720**

Scher, H.D., and Martin, E.E., 2006. Timing and climatic consequences of the opening of Drake Passage. Science, 312(5772):428–430. **https://doi.org/10.1126/science.1120044**

Schmid, F., Peters, M., Walter, M., Devey, C., Petersen, S., Yeo, I., Köhler, J., Jamieson, J.W., Walker, S., and Sültenfuß, J., 2019. Physico-chemical properties of newly discovered hydrothermal plumes above the southern Mid-Atlantic Ridge (13°–33°S). Deep Sea Research, Part I: Oceanographic Research Papers, 148:34–52. **https://doi.org/10.1016/j.dsr.2019.04.010**

Scientific Party, 1970. Introduction. In Maxwell, A.E., et al., Initial Reports of the Deep Sea Drilling Project. 83: Washington, DC (US Government Printing Office), 7–9. **https://doi.org/10.2973/dsdp.proc.3.101.1970**

Sclater, J.G., and McKenzie, D.P., 1973. Paleobathymetry of the South Atlantic. Geological Society of America Bulletin, 84(10):3203–3216. **https://doi.org/10.1130/0016-7606(1973)84<3203:POTSA>2.0.CO;2**

Seton, M., Müller, R.D., Zahirovic, S., Williams, S., Wright, N.M., Cannon, J., Whittaker, J.M., Matthews, K.J., and McGirr, R., 2020. A global data set of present-day oceanic crustal age and seafloor spreading parameters. Geochemistry, Geophysics, Geosystems, 21(10):e2020GC009214. **https://doi.org/10.1029/2020GC009214**

Shipboard Scientific Party, 1983. Site 505: sediments and ocean crust in an area of low heat flow south of the Costa Rica Rift. In Cann, J.R., Langseth, M. G., Honnorez, J., Von Herzen, R. P., White, S. M., et al., Initial Reports of the Deep Sea Drilling Project. 69: Washington, DC (US Government Printing Office), 175–214. **https://doi.org/10.2973/dsdp.proc.69.103.1983**

Shipboard Scientific Party, 1985. Explanatory notes. In Anderson, R.N., Honnorez, J., Becker, K., et al., Initial Reports of the Deep Sea Drilling Project. 83: Washington, DC (US Government Printing Office), 5–11. **https://doi.org/10.2973/dsdp.proc.83.101.1985**

Shipboard Scientific Party, 1993a. Explanatory notes. In Alt, J.C., Kinoshita, H., Stokking, L.B., et al., Proceedings of the Ocean Drilling Program, Initial Reports. 148: College Station, TX (Ocean Drilling Program). **https://doi.org/10.2973/odp.proc.ir.148.101.1993**

Shipboard Scientific Party, 1993b. Site 896. In Alt, J.C., Kinoshita, H., Stokking, L.B., et al., Proceedings of the Ocean Drilling Program, Initial Reports, 148. College Station, TX (Ocean Drilling Program), 123–192. **https://doi.org/10.2973/odp.proc.ir.148.103.1993**

Shipboard Scientific Party, 1997. Introduction and summary: hydrothermal circulation in the oceanic crust and its consequences on the eastern flank of the Juan de Fuca Ridge. In Davies, E.E., Fisher, A.T., Firth, J.V., et al., Proceedings of the Ocean Drilling Program, Initial Reports. 168: College Station, TX (Ocean Drilling Program), 7–21. **https://doi.org/10.2973/odp.proc.ir.168.101.1997**

Shipboard Scientific Party, 2002. Leg 199 summary. In Lyle, M., Wilson, P.A., Janecek, T.R., et al., Proceedings of the Ocean Drilling Program, Initial Reports. 199: College Station, TX (Ocean Drilling Program). **https://doi.org/10.2973/odp.proc.ir.199.101.2002**

Shipboard Scientific Party, 2003a. Leg 201 summary. In D'Hondt, S.L., Jørgensen, B.B., Miller, D.J., et al., Proceedings of the Ocean Drilling Program, Initial Reports, 201. College Station, TX (Ocean Drilling Program), 1–81. **https://doi.org/10.2973/odp.proc.ir.201.101.2003**

Shipboard Scientific Party, 2003b. Leg 206 summary. In Wilson, D.S., Teagle, D.A.H., Acton, G.D., et al., Proceedings of the Ocean Drilling Program, Initial Reports. 206: College Station, TX (Ocean Drilling Program). **https://doi.org/10.2973/odp.proc.ir.206.101.2003**

Shipboard Scientific Party, 2004. Leg 208 summary. In Zachos, J.C., Kroon, D., Blum, P., et al., Proceedings of the Ocean Drilling Program, Initial Reports. 208: College Station, TX (Ocean Drilling Program). **https://doi.org/10.2973/odp.proc.ir.208.101.2004**

Spinelli, G.A., Giambalvo, E.R., and Fisher, A.T., 2004. Sediment permeability, distribution, and influence on fluxes in oceanic basement. In Davis, E.E., and Elderfield, H. (Eds.), Hydrogeology of the Oceanic Lithosphere. Cambridge, UK (Cambridge University Press), 151–188.

Staudigel, H., Hart, S.R., Schmincke, H.-U., and Smith, B.M., 1989. Cretaceous ocean crust at DSDP Sites 417 and 418: carbon uptake from weathering versus loss by magmatic outgassing. Geochimica et Cosmochimica Acta, 53(11):3091–3094. **https://doi.org/10.1016/0016-7037(89)90189-0**

Stein, C.A., and Stein, S., 1994. Constraints on hydrothermal heat flux through the oceanic lithosphere from global heat flow. Journal of Geophysical Research: Solid Earth, 99(B2):3081–3095. **https://doi.org/10.1029/93JB02222**

Stommel, H., 1961. Thermohaline convection with two stable regimes of flow. Tellus, 13(2):224–230. **https://doi.org/10.1111/j.2153-3490.1961.tb00079.x**

Straume, E.O., Gaina, C., Medvedev, S., Hochmuth, K., Gohl, K., Whittaker, J.M., Abdul Fattah, R., Doornenbal, J.C., and Hopper, J.R., 2019. GlobSed: updated total sediment thickness in the world's oceans. Geochemistry, Geophysics, Geosystems, 20(4):1756–1772. **https://doi.org/10.1029/2018GC008115**

Sun, S., and McDonough, W.F., 1989. Chemical and isotopic systematics of oceanic basalts: implications for mantle composition and processes. In Saunders, A.D., and Norry, M.J. (Eds.), Magmatism in the Ocean Basins. Geological Society Special Publication, 42: 313–345. **https://doi.org/10.1144/GSL.SP.1989.042.01.19**

Sylvan, J.B., Hoffman, C.L., Momper, L.M., Toner, B.M., Amend, J.P., and Edwards, K.J., 2015. Bacillus rigiliprofundi sp. nov., an endospore-forming, Mn-oxidizing, moderately halophilic bacterium isolated from deep subseafloor basaltic crust. International Journal of Systematic and Evolutionary Microbiology, 65(6):1992–1998. **https://doi.org/10.1099/ijs.0.000211**

The Shipboard Scientific Party, 1970. Summary and conclusions. In Maxwell, A.E., et al., Initial Reports of the Deep Sea Drilling Project. 3: Washington, DC (US Government Printing Office), 441–471. **https://doi.org/10.2973/dsdp.proc.3.113.1970**

Thomas, D.J., Bralower, T.J., and Jones, C.E., 2003. Neodymium isotopic reconstruction of late Paleocene–early Eocene thermohaline circulation. Earth and Planetary Science Letters, 209(3–4):309–322. **https://doi.org/10.1016/S0012-821X(03)00096-7**

Tobin, H.J., Kinoshita, M., Ashi, J., Lallemant, S., Kimura, G., Screaton, E.J., Thu, M.K., Masago, H., and Curewitz, D., 2009. NanTroSEIZE Stage 1 expeditions: introduction and synthesis of key results. In Kinoshita, M., Tobin, H., Ashi, J., Kimura, G., Lallemant, S., Screaton, E.J., Curewitz, D., Masago, H., Moe, K.T., and the Expedition 314/315/316 Scientists, Proceedings of the Integrated Ocean Drilling Program. 314/315/316: Washington, DC (Integrated Ocean Drilling Program Management, Inc.). **https://doi.org/10.2204/iodp.proc.314315316.101.2009**

Torsvik, T.H., Rousse, S., Labails, C., and Smethurst, M.A., 2009. A new scheme for the opening of the South Atlantic Ocean and the dissection of an Aptian salt basin. Geophysical Journal International, 177(3):1315-1333. **https://doi.org/10.1111/j.1365-246X.2009.04137.x**

Tripati, A., Backman, J., Elderfield, H., and Ferretti, P., 2005. Eocene bipolar glaciation associated with global carbon cycle changes. Nature, 436(7049):341–346. **https://doi.org/10.1038/nature03874**

Vance, D., Teagle, D.A.H., and Foster, G.L., 2009. Variable Quaternary chemical weathering fluxes and imbalances in marine geochemical budgets. Nature, 458(7237):493–496. **https://doi.org/10.1038/nature07828**

Von Herzen, R., 1959. Heat-flow values from the South-Eastern Pacific. Nature, 183(4665):882–883. **https://doi.org/10.1038/183882a0**

Weaver, B.L., Wood, D.A., Tarney, J., and Joron, J.L., 1987. Geochemistry of ocean island basalts from the South Atlantic: Ascension, Bouvet, St. Helena, Gough and Tristan da Cunha. In Fitton, J.G., and Upton, B.G.J. (Eds.), Alkaline Igneous Rocks. Geological Society Special Publication, 30: 253–267. **https://doi.org/10.1144/GSL.SP.1987.030.01.11**

Wegener, A., 1912. Die Herausbildung der Grossformen der Erdrinde (Kontinente und Ozeane), auf geophysikalischer Grundlage. Petermanns Geographische Mitteilungen, 63:185-195.

Westerhold, T., Marwan, N., Drury, A.J., Liebrand, D., Agnini, C., Anagnostou, E., Barnet, J.S.K., Bohaty, S.M., De Vleeschouwer, D., Florindo, F., Frederichs, T., Hodell, D.A., Holbourn, A.E., Kroon, D., Lauretano, V., Littler, K., Lourens, L.J., Lyle, M., Pälike, H., Röhl, U., Tian, J., Wilkens, R.H., Wilson, P.A., and Zachos, J.C., 2020. An astronomically dated record of Earth's climate and its predictability over the last 66 million years. Science, 369(6509):1383–1387. **https://doi.org/10.1126/science.aba6853**

Wheat, C.G., and Fisher, A.T., 2008. Massive, low-temperature hydrothermal flow from a basaltic outcrop on 23 Ma seafloor of the Cocos plate: chemical constraints and implications. Geochemistry, Geophysics, Geosystems, 9(12):Q12O14. **https://doi.org/10.1029/2008GC002136**

Williams, T., Estes, E.R., Rhinehart, B., Coggon, R.M., Sylvan, J.B., Christeson, G.L., and Teagle, D.A.H., 2021. Expedition 395E Preliminary Report: Complete South Atlantic Transect Reentry Systems. International Ocean Discovery Program. **https://doi.org/10.14379/iodp.pr.395E.2021**

Wilson, D.S., Teagle, D.A.H., Alt, J.C., Banerjee, N.R., Umino, S., Miyashita, S., Acton, G.D., Anma, R., Barr, S.R., Belghoul, A., Carlut, J., Christie, D.M., Coggon, R.M., Cooper, K.M., Cordier, C., Crispini, L., Durand, S.R., Einaudi, F., Galli, L., Gao, Y., Geldmacher, J., Gilbert, L.A., Hayman, N.W., Herrero-Bervera, E., Hirano, N., Holter, S., Ingle, S., Jiang, S., Kalberkamp, U., Kerneklian, M., Koepke, J., Laverne, C., Vasquez, H.L.L., Maclennan, J., Morgan, S., Neo, N., Nichols, H.J., Park, S.-H., Reichow, M.K., Sakuyama, T., Sano, T., Sandwell, R., Scheibner, B., Smith-Duque, C.E., Swift, S.A., Tartarotti, P., Tikku, A.A., Tominaga, M., Veloso, E.A., Yamasaki, T., Yamazaki, S., and

Ziegler, C., 2006. Drilling to gabbro in intact ocean crust. Science, 312(5776):1016–1020. https://doi.org/10.1126/science.1126090

Wright, J.D., Miller, K.G., and Fairbanks, R.G., 1991. Evolution of modern deepwater circulation: evidence from the Late Miocene Southern Ocean. Paleoceanography and Paleoclimatology, 6(2):275–290. https://doi.org/10.1029/90PA02498

Wunsch, C., 2002. What is the thermohaline circulation? Science, 298(5596):1179–1181. https://doi.org/10.1126/science.1079329

Yoder, H.S., Jr., and Tilley, C.E., 1962. Origin of basalt magmas: an experimental study of natural and synthetic rock systems. Journal of Petrology, 3(3):342–532. https://doi.org/10.1093/petrology/3.3.342

Zachos, J., Pagani, M., Sloan, L., Thomas, E., and Billups, K., 2001. Trends, rhythms, and aberrations in global climate 65 Ma to Present. Science, 292(5517):686–693. https://doi.org/10.1126/science.1059412

Zachos, J.C., Dickens, G.R., and Zeebe, R.E., 2008. An early Cenozoic perspective on greenhouse warming and carbon-cycle dynamics. Nature, 451(7176):279–283. https://doi.org/10.1038/nature06588

Zachos, J.C., Röhl, U., Schellenberg, S.A., Sluijs, A., Hodell, D.A., Kelly, D.C., Thomas, E., Nicolo, M., Raffi, I., Lourens, L.J., McCarren, H., and Kroon, D., 2005. Rapid acidification of the ocean during the Paleocene-Eocene Thermal Maximum. Science, 308(5728):1611–1615. https://doi.org/10.1126/science.1109004

Zeebe, R.E., Zachos, J.C., Caldeira, K., and Tyrrell, T., 2008. Oceans: carbon emissions and acidification. Science, 321(5885):51–52. https://doi.org/10.1126/science.1159124

Zhang, H., Shi, X., Li, C., Yan, Q., Yang, Y., Zhu, Z., Zhang, H., Wang, S., Guan, Y., and Zhao, R., 2020. Petrology and geochemistry of South Mid-Atlantic Ridge (19°S) lava flows: implications for magmatic processes and possible plume-ridge interactions. Geoscience Frontiers, 11(6):1953–1973. https://doi.org/10.1016/j.gsf.2020.06.007